Advanced Synchronization Techniques for OFDM Systems

Leila Nasraoui

Ministry of Higher Education and Scientific Research
University of Carthage
Higher School of Communications of Tunis
SUP'COM

Advanced Synchronization Techniques for OFDM Systems

A thesis presented in fulfilment of the requirements for the degree of
Doctor of Philosophy in
Information and Communication Technologies

By

Ms. Leïla Nasraoui

Defended on the 4th of April 2015 before the committee composed of:

Chair	Dr. Ridha Bouallegue	Professor at SUPCOM, Tunisia
Reviewers	Dr. Slimane Ben Slimane	Professor at KTH, Sweden
	Dr. Noureddine Hamdi	Professor at INSAT, Tunisia
Examiner	Dr. Ines Kammoun Jemal	Associate professor at ENIS, Tunisia
Supervisor	Dr. Mohamed Siala	Professor at SUPCOM, Tunisia
Co-Supervisor	Dr. Leïla Najjar Atallah	Associate professor at SUPCOM, Tunisia

Academic year: 2014/2015

To my family

Without your support, I would not be the person I am today!

Acknowledgement

I take this opportunity to express my deepest gratitude to my supervisor Prof. Mohamed Siala for sharing his outstanding expertise and knowledge, being a constant source of research ideas and inspiring words in times of needs. I am also extremely grateful to my co-supervisor Dr. Leïla Najjar Atallah for being patient and continuously offering precious advices and help. I learned a lot from her most valuable critique, constructive comments as well as suggestions and feedback to improve the quality of this thesis and my scientific writing in general. I thank them both for their invaluable support and the wholehearted confidence they have shown in me. Without the lengthy discussions and meetings we had and without their constant encouragement and guidance, this thesis would not be the same. I deeply appreciate their understanding of the difficulties I had, trying to balance work and study throughout the duration of my thesis.

I am deeply grateful to all members of the jury for agreeing to read the manuscript and to participate in the defense of this thesis: Prof. Ridha Bouallegue as a Chair, Dr. Ines Kammoun Jemal as external examiner, and Professors Slimane Ben Slimane and Noureddine Hamdi as reviewers, who offered valuable comments to improve the content of this dissertation.

Many thanks go to a group of wonderful colleagues and friends for providing a stimulating and fun environment.

I would like to give my special thanks to my sister Imen for the delicious coffee she used to prepare to me, my sister Ines and my brother Anis. Last but by no means least, I would like to express my deepest gratitude to my parents, to whom I dedicate this work. My every little success would not have been possible without their prayers.

Abstract

The Orthogonal Frequency-Division Multiplexing (OFDM) is a multi-carrier modulation technique in which data symbols are transmitted in parallel over orthogonal sub-carriers. It has been adopted in several broadband wireless communication systems thanks to its numerous advantages, namely, high spectral efficiency, immunity to multipath distortion and simplicity of the receiver architecture to support high data rates and user mobility. However, OFDM systems are very sensitive to synchronization errors, which destroy the orthogonality between sub-carriers resulting in an important performance degradation. Hence, it is important to implement efficient and relevant synchronization algorithm at the OFDM receiver side. In addition to the relevance features, the overhead introduced by the insertion of dedicated synchronization signals and the occasioned computational load should also be considered. This thesis takes an overall look at reduced-complexity data-aided synchronization techniques for OFDM systems, by trading between performance and computational load in possibly fast varying environments of wireless transmissions. In particular, we propose several synchronization techniques, first for single antenna configurations, which we evaluate in existing standards (WiFi and LTE). Then, we consider synchronization problem in multi-antenna OFDM systems.

Exploiting a preamble of two identical parts, we propose a new Brute-Force (BF) single-stage synchronization technique, which carries a differential correlation based metric that provides accurate detection. The metric involves a correlation sequence generated from the preamble sub-sequence and a differentially modulated version of the received signal. Theoretical and experimental studies, achieved to evaluate the performance of the BF technique, ensures its high detection accuracy. However, the differential correlation based treatment results in a huge computational load. To overcome this disadvantage, we propose the Reduced-Complexity (RC) two-stage technique that splits the synchronization processing into two stages. The first stage, based on sliding correlation, determines a short uncertainty interval over which the

second fine stage is carried. The fine stage is indeed based on differential correlation which provides more accurate estimation compared to the first stage, yet it is much more complex. The combined use of sliding correlation characterized by its low complexity and differential correlation which is much more complex, carried over a short interval, results in an overall reduced-complexity approach. The performance study of the RC technique shows that it provides almost the same detection accuracy as in exclusive BF differential correlation based synchronization. Furthermore, it requires a computational load comparable to that of the exclusive sliding correlation based synchronization. To ensure the relevance of both proposed BF and RC approaches, we evaluate them in the standards IEEE 802.11a/g in which the signal structure allows to directly apply the proposed approaches.

For more optimized performance, we study the design of the training sub-sequence defined in the time and frequency domains. The first issue gives an important insight on how the training sub-sequence (length and type) should be chosen in order to achieve a better trade-off between detection performance and complexity. The second issue concerns a further complexity reduction by the quantification of the correlation sequence, for the training sub-sequences generated in the frequency domain, within a QPSK alphabet ($\pm 1 \pm j$). The so optimized sequence then allows replacing the differential correlation operations by simple sign changes. Three schemes are proposed to search the best QPSK sub-optimal sequence in terms of minimizing the performance degradation caused by the quantification. Namely, iterative, deterministic and genetic algorithms based searches are considered.

Furthermore, two new synchronization approaches are proposed, which are based on the transmission of a Zadoff-Chu (ZC) sequence as temporal preamble. These approaches are based on differential correlation and referred to as the Simply-Differential (SD) approach and the Doubly-Differential (DD) approach. Both of the proposed approaches allow accurate detection of the ZC sequence start. Based on the fact that the LTE standard provides dedicated ZC sequences for the primary synchronization, the proposed approaches are successfully adapted and applied to primary synchronization in the LTE standard, which includes symbol start detection and sector identifier search. The DD approach proceeds in two stages, wherein the first stage, a coarse time estimation is achieved, by localizing the ZC sequence within the received signal. In the second stage, cross-correlation of the received signal with the local known ZC sequence candidates is carried to detect the exact synchronization signal start and the sector identifier. The SD approach achieves time synchronization and sector search in a single stage, which is a particular feature compared to the existing detectors and the herein

proposed DD approach. A reduced-complexity implementation of both DD and SD metrics is also proposed to ensure their suitability to be implemented in the standard.

Finally, we propose a new synchronization scheme for 2×1 MISO-OFDM systems, which exploits the full spatial diversity provided by differential Alamouti space-time block coding for non-coherent detection and thus avoids any channel estimation requirement. At the receiver, respecting almost the same framework as in the RC approach, a coarse stage is first carried based on sliding correlation to localize the preamble start. Before carrying the fine stage, differential Alamouti decoding should be achieved to recover the transmitted stream. Then, cross-correlation is calculated during the fine stage, over a short interval around the coarse time estimate, to fine tune the preamble start estimate. To assess the enhancement provided through the spatial diversity and to evaluate the loss compared to a coherent unrealistic scheme where a perfect knowledge of the channel is supposed, we evaluate the proposed scheme in the case of SISO antenna and of coherent space-time block coded MISO configuration.

Keywords: OFDM, Data-Aided Synchronization, Time Synchronization Errors, Frequency Synchronization Errors, PN sequences, Zadoff-Chu sequences, Differential Correlation, MIMO, Differential STBC.

List of Abbreviations

3GPP	3rd Generation Partnership Project
A/D	Analog to Digital
AWGN	Additive White Gaussian Noise
BER	Bit Error Rate
BPSK	Binary Phase Shift Keying
BF	Brute-Force
BLAST	Bell Labs Layered Space-Time
CAZAC	Constant Amplitude Zero Auto Correlation
CDR	Correct Detection Rate
CIR	Channel Impulse Response
CDF	Cumulative Distribution Function
CLT	Central Limit Theorem
CP	Cyclic Prefix
CFO	Carrier Frequency Offset
CSC	Central-Self Correlation
CS	Correlation Sequence
D/A	Digital to Analog
DAB	Digital Audio Broadcasting
DDA	Deterministic Design Algorithm
DMT	Discrete Multi-Tone
DFT	Discrete Fourier Transform

DA	Data-Aided
DD	Doubly Differential
DVB	Digital Video Broadcasting
D-BLAST	Diagonal Bell Labs Layered Space-Time
D-STBC	Differential Space-Time Block Coding
EGC	Equal Gain Combining
EPA	Extended Pedestrian A
ETU	Extended Typical Urban
FDD	Frequency-Division Duplex
FFT	Fast Fourier Transform
FFO	Fractional Frequency Offset
FD	Frequency Domain
FDR	Failure Detection Rate
FO	Frequency Offset
FDM	Frequency Division Multiplexing
GA	Genetic Algorithm
GI	Guard Interval
HSDPA	High Speed Downlink Packet Access
HSUPA	High Speed Uplink Packet Access
ICI	Inter-Carrier Interference
IDA	Iterative Design Algorithm
ISI	Inter-Symbol Interference
IDFT	Inverse Discrete Fourier Transform
IFFT	Inverse Fast Fourier Transform
IFO	Integer Frequency Offset
IMT	International Mobile Telephony
ITU	International Telecommunication Union
IEEE	Institute of Electrical and Electronics Engineers
LAST	LAttice Space-Time
LTE	Long Term Evolution
LOS	Line Of Sight
LS	Least Squares

LMMSE	Linear Minimum Mean Square Error
LO	Local Oscillators
ML	Maximum Likelihood
MCM	Multi-Carrier Modulation
MIMO	Multiple-Input Multiple-Output
MISO	Multiple-Input Single-Output
MLSE	Maximum Likelihood Sequence Estimation
MRC	Maximum Ratio Combiner
MSE	Mean Squared Error
NDA	Non-Data-Aided
NCM	Number of Complex Multiplication
OFDM	Orthogonal Frequency Division Multiplexing
OSTBC	Orthogonal Space-Time Block Coding
PAPR	Peak-to-Average Power Ratio
PCD	Probability of Correct Detection
PDF	Probability Density Function
PM	Precoding Method
PN	Pseudo-Noise
PSS	Primary Synchronization Signal
QAM	Quadrature Amplitude Modulation
QPSK	Quadrature Phase Shift Keying
RC	Reduced-Complexity
SC-FDMA	Single-Carrier Frequency-Division Multiple Access
SC	Schmidl and Cox
SD	Simply Differential
SISO	Single-Input Single-Output
SIMO	Single-Input Multiple-Output
SNR	Signal to Noise Ratio
SINR	Signal to Interference and Noise Ratio
S-ID	Sector Identifier
STBC	Space-Time Block Coding
STC	Space Time Coding

STTC	Space-Time Trellis Coding
SSS	Secondary Synchronization Signal
TD	Time Domain
TDD	Time-Division Duplex
TO	Time Offset
UE	User Equipment
UMTS	Universal Mobile Telecommunications System
V-BLAST	Vertical Bell Labs Layered Space-Time
WCDMA	Wideband Code Division Multiple Access
WLAN	Wireless Local Area Networks
WiFi	Wireless-Fidelity
WiMAX	Worldwide Interoperability for Microwave Access
ZC	Zadoff-Chu
ZP	Zero Padding

Notations

$[.]^{\mathrm{H}}$	Complex conjugate transpose operator (Hermitian)
$[.]^{\mathrm{T}}$	Transpose operator
$(.)^*$	Conjugate operator
$\angle$	Argument of a complex number
$\bigodot$	Element-wise product operator
$\bar{(.)}$	IDFT output
sinc(.)	Cardinal sine function
mod	Modulo operator
$E(.)$	Statistical expectation
$\mathfrak{R}(.)$	Real part
$\mathfrak{I}(.)$	Imaginary part
$\mathbb{N}$	The set of positive integer elements
$\mathbb{C}$	The set of complex elements
$h(t)$	Channel linear transfer function
$H(f)$	Channel frequency impulse response
$s(t)$	Transmitted signal
$r(t)$	Received signal
$s_{l,k}$	Data symbol transmitted on the k^{th} sub-carrier of the l^{th} OFDM block
$\hat{s}_{l,k}$	Demodulated data symbol on the k^{th} sub-carrier of the l^{th} OFDM block
$\hat{r}_d$	The d^{th} decoded received sample (using D-STBC)
$\tau_{\max}$	Channel maximum delay spread

$\tau_{\min}$	Channel minimum delay spread
τ_p	Delay of the p^{th} path
L_H	Length of the channel impulse response
T_b	Sampling period
T_u	OFDM symbol duration
T_g	CP duration
T	CP extended OFDM symbol duration
R_b	Bit rate
BW	Signal bandwidth
τ_{rms}	Root-mean squared (rms) delay spread
B_c	Channel coherence bandwidth
$\upsilon_{\max}$	Maximum Doppler frequency shift
T_c	Channel coherence time
β	spectral efficiency
Δ_f	Sub-carriers spacing
c	Speed of light
v	Speed of the antenna
N_u	FFT size (number of sub-carriers per OFDM symbol)
N_g	CP length
N_s	Total OFDM symbol length
N_{um}	Preamble length
N_{gm}	CP length of the preamble
N_p	Number of effective paths
$\tilde{N}_p$	The set of N_p effective paths
N_t	Number of Transmit antennas
N_r	Number of receive antennas
k	Sub-carrier
f_k	k^{th} sub-carrier frequency
l	OFDM symbol index
$g(t)$	Rectangular pulse shape
$\mathbf{W}$	Normalized IDFT Matrix
$\mathbf{H}$	Channel Matrix

$\mathbf{I}_n$	The identity matrix of size n
η	Additive White Gaussian Noise
σ_η^2	Noise power
σ_s^2	Signal power
ϵ	Time Offset
ξ	Sampling Clock Frequency Offset
Δ_{f_c}	Carrier frequency Offset
K	Integer Frequency Offset
ν	Fractional Frequency Offset
τ	Preamble start
α	Correlation Sequence
$\Delta\tau$	Uncertainty interval
q	Correlation shift
E_s	OFDM symbol energy
E_η	Noise energy
μ_k	Mean of the k^{th} metric element
σ_k^2	Variance of the k^{th} metric element

Contents

List of Figures

List of Tables

Chapter 1

Introduction

1.1 General Context

The evolution in wireless communication systems has accelerated since the beginning of the 1990s with the replacement of the first-generation analogue mobile networks by the current second generation (2G) systems (GSM, IS-95), which opened the door for a fully digital network [1]. The development was continuing with the deployment of the third generation (3G) systems, namely WCDMA/UMTS [2], HSDPA [3], HSUPA [4], and CDMA-2000 [5], which are referred to as IMT 2000. Next, the 3rd Generation Partnership Project (3GPP) Long Term Evolution (LTE) standard, specified in 3GPP Release 8 [6], with significantly higher data rates than in 3G systems, was considered as 3G evolution. With the 3GPP Release 10 [7], new ideas to further push the limits for faster data speeds and better coverage are specified as part of the LTE-Advanced project, to comply with the International Telecommunication Union's (ITU's) IMT Advanced requirements for the fourth generation (4G) wireless networks [8]. The plethora of wireless communication systems is not restricted to mobile cellular networks only, but also includes wireless local area networks (WLANs), which were standardized by the IEEE (Institute of Electrical and Electronics Engineers) in the 802.11 initial specification [9] and followed by various enhancements in latter specifications (IEEE 802.11a/b/g/n). Also, the IEEE 802.16 standard [10], referred to as WiMAX (Worldwide Interoperability for Microwave Access), has been proposed as an alternative wireless broadband network offering different services that have been ameliorated throughout its different specifications (IEEE 802.16a/d/e/f) to support full mobility. Wireless communication has also roofed broadcast systems such as Digital Audio

Broadcasting (DAB) and Digital Video Broadcasting (DVB-T and DVB-H) [11, 12].

In digital wireless communication systems, data is transmitted in the form of electromagnetic wave through wireless channel, which represents the propagation media between transmit and receive antennas. The wireless environment is quite harsh and transmitting high rate information under high mobility conditions generally introduces large delay spreads and strong time variations resulting in a time and frequency selective channel. Also, the spectrum allocation and bandwidth are critical in most of the above-mentioned wireless communication standards because the frequency spectrum is limited. To deal with these problems, systems must be designed to be robust against frequency selective channel behavior, important path losses and large multipath delay spreads and must provide a high spectral efficiency. A promising candidate that provides a robust solution for communication over frequency-selective fading channels is the Multi-Carrier Modulation (MCM) technique [13]. A particular type of MCM that has gained popularity in a number of applications, such as the LTE, LTE-Advanced, WiMAX mobile and the recent WiFi versions (IEEE 802.11n/ac and IEEE 802.22), is the Orthogonal Frequency Division Multiplexing (OFDM).

The OFDM technique avoids the impairments of a frequency-selective fading channel by converting it into several parallel flat-fading sub-channels, which greatly simplifies the receiver structure. The so-obtained flat-fading channels are narrow-band, low-rate, non-frequency-selective, and allow parallel transmission of multiple symbols while maintaining a high spectral efficiency without causing the Inter-Carrier Interference (ICI). By combining multiple low-data-rate sub-carriers, OFDM systems provide a composite high-data-rate with a long symbol duration. This helps to eliminate the Inter-Symbol Interference (ISI), which generally occurs in signals of short symbol duration over multipath channels. In addition to its robustness to multipath fading distortions and narrow-band interferences, the greatest benefit of using OFDM among MCM techniques is its high spectral efficiency due to the orthogonality between sub-carriers. Another key advantage of using OFDM is the efficient and low complexity implementation through the use of Inverse Fast Fourier Transform (IFFT)/ Fast Fourier Transform (FFT) algorithm [14].

In the OFDM link, the sub-carriers remain orthogonal as long as the receiver is perfectly synchronized, which is not generally the case in broadband communication systems. Indeed, the two major problems in broadband communication, which are the main focus of this thesis, are Time Offset (TO) resulting from the propagation delay, and Frequency Offset (FO) resulting

from a mismatch between the transmitter and receiver local oscillators and/or the Doppler effect, in case of moving transmitters and/or receivers. The TO causes both ICI and ISI while the FO causes ICI, which destroy the orthogonality between sub-carriers such that OFDM symbols can no longer be correctly demodulated. For proper demodulation of OFDM signals, two important synchronization tasks, namely symbol timing and frequency synchronization, need to be performed. The timing synchronization determines the symbol start while the frequency synchronization aligns the carrier frequency of the receiver as closely as possible to the carrier frequency of the transmitter. The insertion of a Cyclic Prefix (CP), having a minimum length equal to the channel delay spread, can avoid the interference between symbols and between sub-carriers, only when the symbol start (FFT window) is properly located. To this aim, time estimation accuracy is crucial in the synchronization process to allow maximum tolerance range to multipath channel effects. Indeed, higher accuracy in time estimate means a smaller probability for the channel delay spread to exceed the supported range and a lower risk of data detection error. Obtaining near perfect synchronization is not simple under multipath channel effects, which makes synchronization a very challenging task in OFDM systems.

1.2 Motivation of the Research

A key research challenge in the design of high data-rate communication systems is achieving accurate synchronization. The design of synchronization techniques, to enable such networks to be widely deployed, has been addressed in many works. Depending on whether specific data are used for synchronization purpose or not, synchronization techniques can be split into two main classes: Data-Aided (DA) [15]- [22] and Non-Data-Aided (NDA) or blind synchronization [23]- [29]. Most of the NDA techniques are not totally blind in the sense that some information might be required to assist the synchronization, such as the channel state or the signal to noise ratio. In addition, the performance of blind techniques is severely deteriorated in frequency-selective fading channels. On the contrary, the DA approaches, which require the insertion of known training sequences, are advantageous because they are capable to produce accurate estimates of the synchronization parameters in harsh propagation environments.

The DA approaches in [15]- [22] exploit preambles of specific structures with different polarity patterns, generally for a predefined training sequence class. At the receiver side, metrics tailored to the preamble structure are calculated for synchronization purpose. The calculated

metrics use either sliding correlation, characterized by its low computational load, or differential correlation with higher complexity leading to more accurate detection capacities. The trade-off between complexity and accuracy showed an imbalance in existing approaches and motivated our study on novel DA synchronization algorithms with a particular concern on reducing the computational complexity while keeping good synchronization performance and low overhead. The obtained performance motivated our research on practical synchronization solutions applicable to standardized OFDM systems to allow a maximum of tolerance to the channel impairments. Furthermore, measures that are able to improve the synchronization performance incited us to incorporate them in our research, like the use of multiple antennas at the transmitter and receiver for more reliable reception. Such investment is indeed driven by the great potentials of combining Multi-Input Multi-Output (MIMO) and OFDM techniques, which is actually adopted in most of the wireless communication standards.

1.3 Contributions of the Thesis

In this section, we highlight the contributions of this thesis, which are listed in the following and detailed later

- Brute-Force and Reduced-Complexity synchronization approaches, exploiting random and pseudo-noise sequences, are proposed for OFDM systems.
- Application of both proposed approaches to the IEEE 802.11a/g standard.
- Performance optimization of the Reduced-Complexity approach.
- Simply and Doubly differential synchronization approaches, based on Zadoff-Chu sequences, are proposed for OFDM systems.
- Application of the Simply and Doubly differential approaches to the LTE standard.
- Synchronization in multiple antenna configuration for OFDM systems with space time block coding.

The main purpose of this thesis is to develop synchronization schemes that acquire accurate time and fractional frequency offset estimates over frequency-selective channels with low complexity and low overhead and which can be used in either continuous data stream

transmission, as in broadcast application, or for burst data stream transmission, as in wireless area networks. First, exploiting a single-symbol preamble of two identical parts, we propose a Reduced-Complexity (RC) synchronization technique that proceeds in two stages. Respecting the famous Schmidl and Cox algorithm [15], the proposed technique first carries a sliding-correlation based metric to search for a repetitive pattern (in time domain) and provides a coarse time estimate. Then, a differential-correlation based metric is carried between a differentially demodulated version of the received signal and a Correlation Sequence (CS) generated from the preamble. The fine metric is calculated over a short uncertainty interval centered on the coarse estimate to fine-tune it. The combined use of a coarse stage, with low complexity, carried continuously and a fine stage, with high complexity, carried over a short interval results in an overall reduced-complexity approach with satisfactory accuracy as proved by computer simulations. We also consider the Brute Force (BF) single-stage approach, where differential correlation is exclusively used, resulting in a huge computational load. The evaluation of the proposed techniques is presented in papers [33] and [34] for both the Additive White Gaussian Noise (AWGN) and the multipath channel, which showed the enhancement obtained by the proposed techniques compared to the considered existing benchmarks.

To assess the efficiency of the proposed BF synchronization technique, we conduct a theoretical performance study, which is also valid for the fine stage of the RC techniques. We approximate the BF metric by a Gaussian distribution to derive a closed form expression of the preamble start correct detection probability. Then, the theoretical probability of correct detection is determined and compared to the rate of correct detection given through Monte Carlo simulations. The performance of the proposed synchronization technique is evaluated over AWGN and multipath channels and presented in [36] for the case of OFDM modulation. It is shown that the theoretical probability perfectly agrees with the experimental simulated rate, which from one hand ensures the accuracy of the proposed BF metric and from the other hand validates the theoretical analysis. The evaluation of the proposed technique is also carried in the case of Discrete Multi-Tone (DMT) systems in [41]. The Gaussian distribution approximation in the DMT case is rougher than that of the OFDM case, yet the provided theoretical probability is very close to the experimental rate.

Another component of the thesis work focuses on the adaptation of the proposed synchronization techniques to existing standards. In particular, the IEEE 802.11 standard in which the repetitive structure of the short and long preamble symbols allows a flexible synchronization processing, respecting the proposed techniques that are based on a two identical parts

preamble. The proposed techniques (RC and BF) have shown satisfactory performance that outperforms other well-established methods in the literature and it is published in [39].

As stated above, the proposed synchronization techniques have no further constraint on the preamble than its repetitive structure. To enhance the performance through the preamble choice, we carry an experimental study of the impact of training sub-sequence choice on the detection performance, for the case of binary time domain generated sequences. In addition to randomly generated sequences, pseudo-noise sequences including m-sequences with the specific case of Gold and Kasami sequences are considered. This gives an important insight on how the training symbol should be chosen in order to achieve better detection performance with the same amount of training overhead and computational load. To further reduce the computational load, an optimal choice of the uncertainty interval, over which the fine metric of the RC approach is calculated, can also be adopted. Moreover, we provide an analytical and numerical complexity study to assess the trade-off between performance and complexity. We also compare the computational load of the proposed RC technique to those of existing algorithms as well as the herein proposed BF technique. These contributions have been included in [35, 38].

To further reduce the computational load of the proposed RC technique, we suggest an optimization of the CS which is used during the fine stage in the correlation with a modified version of the received signal. The idea is to replace the differential correlation operations, involved in the fine metric calculation, by simple sign changes. In this way, the encoding sequence must be chosen within a QPSK alphabet ($\pm 1 \pm j$). So, we need to derive the best sub-optimal CS in terms of providing near-optimal performance provided by the initial CS. To this aim, three algorithms are proposed: a deterministic algorithm, an iterative algorithm and a Genetic Algorithm (GA) based search scheme. The same amount of computational load is saved by the three proposed algorithms. Yet, the GA based one provides the better detection performance at the expense of high sequence search complexity. The search of the sub-optimal sequence being carried off-line, completely relaxes the complexity constraints. The classical deterministic and iterative design algorithms are presented in [37] while the GA based design method is presented in [40].

Exploiting the Zadoff-Chu (ZC) sequences, which are known by their good correlation properties well suited for synchronization purpose, we propose two new synchronization approaches which are based on differential correlation and are referred to as Doubly-Differential (DD) [42]

and Simply-Differential (SD) [43]. In both of the proposed schemes, the synchronization process consists of detecting the start of a ZC sequence within the received signal. As these sequences are used in the 3GPP LTE standard, we adapt the proposed SD and DD approaches to the primary synchronization processing, which consists of detecting the Primary Synchronization Signal (PSS), made from ZC sequences, and the sector identifier. The DD approach proceeds in two stages, wherein the first one it provides a coarse time estimate which is refined in the second stage. The sector identifier is also detected during the fine stage through cross-correlation between the received signal and the local known ZC sequence candidates. The SD approach has the particularity of processing both tasks jointly in a sole stage, which to the best of our knowledge, is not the case of existing approaches.

The last part of this thesis is dedicated to the synchronization in multi-antenna OFDM systems. In particular, we propose a new synchronization approach that exploits diversity, through space-time block coding, as a measure to ameliorate the detection performance. To avoid channel estimation requirement in such scheme, we opt for differential Alamouti coding/decoding. Respecting the framework of the RC approach, the herein proposed synchronization processing also exploits a preamble of two identical parts and is split into two stages. The coarse stage is achieved identically to the RC approach. Then, once the received signal is differentially decoded, cross-correlation with the preamble is carried during the fine stage over a short interval centered on the coarse time estimate. Simulations carried over Rayleigh channel show significant enhancement compared to the single antenna systems and a slight loss with respect to MISO coherently decoded systems when a perfect knowledge of channels responses at the receiver is assumed. The results of studies carried in MISO-OFDM systems are presented in [44].

To summarize, in terms of publications, this work led to:

- 11 international conference articles (VTC-Spring 2015, EUSIPCO 2014, IWCMC 2014/2013, ComNet 2014/2012, VTC-Fall 2013/2012/2011, ICECS 2012 and WCNC 2012).
- 1 international journal paper published in the Annals of Telecommunications (May 2013).

The details of publications arising from this thesis are provided in the bibliography [33]- [44].

1.4 Organization of the Dissertation

In this section, we provide an outline of the thesis which organizes the previously detailed contributions on 6 chapters.

Chapter 2 introduces the basic characteristics of radio propagation environment and provides the fundamentals of OFDM technique, which is exploited to cope with severe multipath fading in mobile radio channels. The channel effects on OFDM signal are also analyzed. The chapter ends with a review of the most important properties of the OFDM technique.

Chapter 3 starts with a study of the sensitivity of OFDM systems to the time and frequency synchronization errors. Then, it gives a review on existing synchronization techniques available in the literature. Both blind and data-aided approaches are described with an emphasis on preamble based ones covering different preamble structures.

Chapter 4 presents the two proposed synchronization techniques for OFDM systems. Namely, the reduced-complexity and the brute-force which gain their robustness from the differential correlation based metric. The chapter provides a theoretical performance study of the BF technique whose aim is to validate the detection accuracy performance gotten from Monte Carlo simulations. This study is then carried in the case of DMT technique. The detection accuracy and the computational load of both proposed approaches are also evaluated in this chapter. Finally, the chapter ends with the application of the proposed techniques (RC and BF) to the standards IEEE 802.11a/g.

Chapter 5 is devoted to a deep performance study of the proposed RC technique, which can also be applied for the BF approach. In particular, the effect of the preamble training sub-sequence type/length on performance as well as the effect of the uncertainty interval length on the detection accuracy are analyzed. The optimization of the correlation sequence, for the frequency based preamble training sub-sequence, is also treated in this chapter.

Then, in chapter 6 we investigate synchronization using Zadoff-Chu sequences. In particular, we consider the primary synchronization for 3GPP LTE systems to which we apply the two new simply-differential (SD) and doubly-differential (DD) techniques, followed by a comparison made between the proposed approaches and some existing benchmarks.

Chapter 7 is dedicated to the synchronization in MISO-OFDM systems, where our contri-

bution is based on exploiting diversity in the space and the time through differential space-time block coding for non-coherent synchronization.

Finally, the dissertation is concluded by giving a summary of the contributions, perspectives to the carried work and suggestions for open research subjects.

1.5 Publications Arising from the Thesis

Most of the herein presented work is published or is submitted for publication as journal papers or conference proceedings. These papers are:

Journal articles:

- L. Nasraoui, L. Najjar Atallah, and M. Siala, "Performance Evaluation of an Efficient Reduced Complexity Time Synchronization Approach for OFDM Systems," *Annals of Telecommunications*, vol. 69, pp 321-330, May 2013.
- L. Nasraoui, L. Najjar Atallah, and M. Siala, "Robust Time Synchronization for MIMO-OFDM Systems with Transmit Diversity," submitted to *IEEE Commun. Letters.*

Conference Proceeding:

- L. Nasraoui, L. Najjar Atallah, and M. Siala, "An Efficient Reduced-Complexity Two-Stage Differential Sliding Correlation Approach for OFDM Synchronization in the AWGN Channel," in *Proc. IEEE VTC-Fall*, pp. 1-5, Sept. 2011.
- L. Nasraoui, L. Najjar Atallah, and M. Siala, "An Efficient Reduced-Complexity Two-Stage Differential Sliding Correlation Approach for OFDM Synchronization in the Multipath Channel," in *Proc. IEEE WCNC*, pp. 2059-2063, April 2012.
- L. Nasraoui, L. Najjar Atallah, and M. Siala, "Performance Study of a Reduced Complexity Time Synchronization Approach for OFDM Systems," in *Proc. ComNet,* pp. 1-5, March 2012.
- L. Nasraoui, L. Najjar Atallah and M. Siala, "Analytical Performance Evaluation of an Efficient Reduced-Complexity Time Synchronization Approach for OFDM Systems", in *Proc. IEEE VTC-Fall*, pp. 1-5, Sept. 2012.

- L. Nasraoui, L. Najjar Atallah, and M. Siala, "Encoding Sequence Design for a Reduced Complexity Time Synchronization Technique for OFDM Systems," in *Proc. IEEE ICECS,* pp. 913-916, Dec. 2012.

- L. Nasraoui, L. Najjar Atallah, and M. Siala, "Robust Brute Force and Reduced Complexity Approaches for Timing Synchronization in IEEE 802.11a/g WLANs," in *Proc IWCMC,* pp. 1365-1369, July 2013.

- L. Nasraoui, L. Najjar Atallah, and M. Siala, "Genetic Algorithm Based Optimization of Encoding Sequence for a Reduced Complexity OFDM Time Synchronization Technique," in *Proc IEEE VTC-Fall,* pp. 1-5, Sept. 2013.

- L. Nasraoui, L. Najjar Atallah, and M. Siala, "Performance Study of an Efficient Reduced-Complexity Time Synchronization Approach for DMT Systems", in *Proc. ComNet*, pp. 1-5, March 2014.

- L. Nasraoui, L. Najjar Atallah, and M. Siala, "Robust Doubly Differential Primary Synchronization Approach for 3GPP LTE Systems," in *Proc. IWCMC*, pp. 1069-1074, Aug. 2014.

- L. Nasraoui, L. Najjar Atallah, and M. Siala, "A Simply Differential Low-Complexity Primary Synchronization Scheme for 3GPP LTE Systems," in *Proc EUSIPCO,* pp. 411-415, Sept. 2014.

Chapter 2

Wireless Communications and OFDM Basics

High data rate transmission is a major challenge for wireless communication systems because they require wide bandwidth channels. Indeed, wireless channels have frequency selective fading characteristics which introduce interference between symbols at the receiver end, due to the multipath echoes. Orthogonal Frequency Division Multiplexing (OFDM) has become a popular technique for transmission over wireless channels in many recent applications such as digital audio/video broadcasting, local/metropolitan area networks, vehicle communications and as it is adopted for the 4G LTE, LTE-Advanced and mobile WiMAX mobile (IEEE 802.16e). Also, it is used in recent WiFi versions (IEEE 802.11n/ac and IEEE 802.22) and some digital TV broadcasting standards.

To better understand the communication over wireless channels using OFDM technique, this chapter starts with a presentation of the basic characteristics of radio propagation environment, followed by channel modeling. Then, a thorough description of the fundamentals of OFDM modulator/demodulator, its main parameters and features is provided. We first highlight the OFDM capacity to cope with many constraints in broadband transmissions like spectral efficiency and channel-frequency selectivity. We then underline the OFDM impairment. Later, we present the mathematical modeling of the OFDM signal before and after transmission over wireless communication channels. Through this model, it is shown that the use of a cyclic extension of OFDM transmitted blocks allows an immunity to timing errors up to a certain

level and greatly simplifies the equalization at the receiver side. The chapter ends with a review of the most important advantages and drawbacks of the OFDM modulation scheme.

2.1 Communications over Wireless Channels

There are two fundamental features in wireless communications that make it challenging and interesting. These features are not as significant in wired communications. First, the limited spectrum range available for transmitting data in high bit rate. Second, the variation of the channel gain due to the small-scale effects of multipath propagation, as well as large-scale effects such as attenuation due to the distance and shadowing by obstacles. How to deal with these aspects is paramount in the design of wireless communication systems. In this section, we focus on the characterization of the propagation channel.

2.1.1 Radio Propagation

Radio signals generally propagate according to three mechanisms: reflection, diffraction, and scattering. The appropriate channel model depends strongly on the intended application and different models are used for the different applications such as cellular and WLANs. The channel model directly affects the steps of designing, evaluating, and deploying any wireless system in the objective of ensuring adequate coverage and quality of service. As such, the channel model to be adopted should be wisely chosen.

In mobile radio channels, the transmitted signal undergoes different channel effects which are multipath propagation, Doppler spread, shadowing and path loss [57]:

- Multipath propagation occurs as a consequence of reflections, scattering, and diffraction of the transmitted electromagnetic wave at natural and man-made objects. Thus, at the receive antenna, a multitude of waves arrives from several directions with different delays, attenuations, and phases. The superposition of these waves results in amplitude and phase variations of the composite received signal.
- Doppler spread is caused by moving objects in the mobile radio channel. The changes in the phases and amplitudes of the arriving waves lead to time-variant multipath propagation. Even small movements on the order of the wavelength may result in a totally

different wave superposition. When the signal strength varies due to time-variant multipath propagation, the channel is said fast fading or time selective.

- Shadowing results from the obstruction of the transmitted waves by objects (for example hills, buildings, walls, and trees) along the paths of a signal, which results in more or less strong attenuation of the signal strength. Compared to fast fading, longer distances have to be covered to change the shadowing constellation significantly. The varying signal strength due to shadowing is called slow fading and can be described by a log-normal distribution.

- Path loss indicates how the mean signal power decays with distance between the transmitter and the receiver. In free space Line Of Sight (LOS), the mean signal power decreases with the square of the distance between the transmit and the receive antennas such that the received power, at distance d and for a wavelength λ, decreases proportionally to $\left(\frac{2\pi d}{\lambda}\right)^2$. In a mobile radio channel, where often no line of sight (NLOS) exists, signal power decreases with a power higher than two and typically varies between three and five.

A mobile wireless channel can be characterized by the variations of the channel strength which can be roughly categorized into large-scale fading and small-scale fading. For any given position in the space, the received signal is affected by large scale effects such as path-loss, shadowing, diffraction and rain or foliage attenuation. This is more relevant to issues such as cell-site planning and can be avoided through power control at the transmitter. Small-scale effects are caused by rapid fluctuation of the signal due to multipath propagation and movement of either the transmitter or the receiver. They are more relevant to the design of reliable and efficient communication systems [58].

2.1.2 Frequency Dispersive Channels

As indicated above, the received signal is a superposition of several signals from different directions resulting in a spatial interference pattern. For a moving terminal through this interference pattern with a velocity v, the received signal amplitude fluctuates in time (fading). In the frequency domain, these fluctuations are seen as a superposition of many Doppler shifts corresponding to different directions resulting in a Doppler spectrum instead of a sharp spectral line located at the carrier frequency f_c. The maximum Doppler frequency shift is $\upsilon_{\max} = \frac{\mathrm{v} f_c}{c}$,

where c and v stand respectively for the speed of light and the speed of the antenna. For an angle ϕ between the direction of the received signal and the direction of motion, the Doppler shift is $\upsilon_d = \upsilon_{\max}\cos(\phi)$. The apparent received frequency will be $f_c + \upsilon_{\max}$ if the receiver is moving directly towards the incoming way and $f_c - \upsilon_{\max}$ if it is moving directly away. Thus, the apparent received frequency will always be in the range of $f_c \pm \upsilon_{\max}$ [59, 60].

An example of frequency dispersive channel of two paths is presented in the figure 2.1 showing the effect of time selectivity on both short and long symbols, where $D(f)$ and $r(t)$ respectively denote the Doppler spectrum and the received signal.

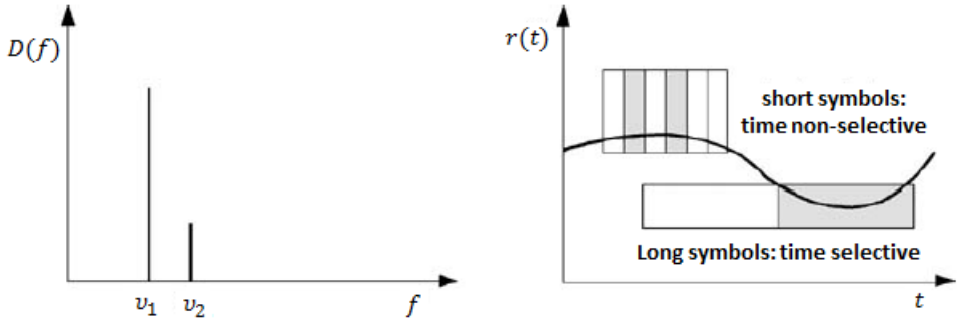

Figure 2.1: Frequency dispersive (time selective) channel and its effects on short and long symbol [60].

For this channel, when neglecting the delay spread between the received signal versions, the baseband signal affected by only the Doppler shift is expressed as

$$r(t) = e^{j2\pi\upsilon_1 t}s(t) + \alpha e^{j2\pi\upsilon_2 t}s(t), \tag{2.1}$$

where $s(t)$ stands for the baseband transmitted signal and υ_1 and υ_2 stand for the Doppler shifts corresponding to the two paths. The Doppler effect introduces two types of distortion to the received signals: signal variation over time and broadened signal spectrum. Let us define channel coherence time as $T_c = \frac{1}{\upsilon_{\max}}$, which corresponds to the period over which the channel remains constant. If the Doppler shift is comparable to the signal bandwidth ($T_c \approx T_s$), the channel is considered as **time-selective (fast-fading)**. On the other hand, when the Doppler shift is insignificant compared to the symbol rate ($T_c \gg T_s$), the channel is considered **time-non-selective (slow-fading)**. An approximation of the coherence time is $T_c = \frac{0.4}{\upsilon_{\max}}$ was presented in [61].

2.1.3 Time Dispersive Channels

The arrival time of scattered multipath signals are inevitably distinct. The impact severity of these delays on the transmitted signal strongly depends on the product of the signal bandwidth with the channel delay spread. The channel can be represented as a linear transfer function $h(t)$. Due to the multipath propagation, the CIR of length L_H is composed of a large number of scattered impulses received over N_p different paths with different propagation delays spanning the time interval $[0, L_H]$ as [60]

$$h(t) = \sum_{p=0}^{N_p-1} \alpha_p(t)\delta(t - \tau_p(t)), \tag{2.2}$$

where α_p and τ_p stand respectively for the attenuation and the time delay of the p^{th} path and $\delta(.)$ is the Dirac delta function which may be time-dependent in the case of non-stationary channels.

Since the multipath delays τ_p are distinct, the frequency response $H(f)$, which is the Fourier transform of $h(t)$, exhibits amplitude fluctuation. Such fluctuation in the frequency domain will distort the waveform of a broadband signal. Specifically, in digital communications, a channel is considered **frequency-selective** if the multipath delays are distinguishable relative to the symbol period $T_s = \frac{1}{BW} < \tau_{max} - \tau_{min}$. On the other hand, if the signal bandwidth (BW) is sufficiently narrow, the channel frequency response within the signal bandwidth can be approximated by a constant. A wireless channel is considered **frequency-non-selective (flat)** if the multipath delays are indistinguishable relative to the symbol period $T_s = \frac{1}{BW} \geq \tau_{max} - \tau_{min}$ [59, 60]. In this case, the interference between symbols can be neglected. An illustration of a time dispersive channel of 3 paths is depicted in figure 2.2 showing the effect of frequency selectivity on both narrowband and broadband signals, where $h(t)$ and $H(f)$ respectively denote the CIR and frequency response.

We define the coherence bandwidth B_c as the range of frequencies, over which the channel gain remains fairly constant. The coherence bandwidth over which the correlation is above 90% and 50% are approximated to respectively $B_{90\%} = \frac{1}{50\tau_{\text{rms}}}$ and $B_{50\%} = \frac{1}{5\tau_{\text{rms}}}$ [61,62], where $\tau_{\text{rms}} = \sqrt{E(\tau^2) - (E(\tau))^2}$ is the root mean square of the delay τ.

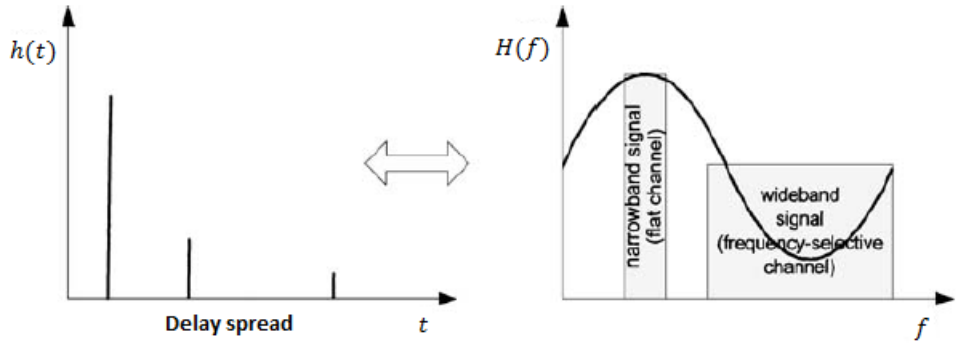

Figure 2.2: Time dispersive (frequency selective) channel and its effects on narrowband and broadband signals [60].

2.1.4 Time-Frequency Dispersive Channels

In practical cases, the wireless channel may be time and frequency dispersive at the same time. Combining the effects described in the two previous sections, the baseband received signal $r(t)$ expresses as

$$r(t) = \int_{-\infty}^{+\infty} h(\tau, t)s(t-\tau)d\tau, \tag{2.3}$$

where

$$h(\tau, t) = \sum_{p=0}^{N_p-1} \alpha_p e^{j\theta_p} e^{j2\pi\upsilon_p t}\delta(t-\tau_p), \tag{2.4}$$

is the time-variant CIR, θ_p and υ_p are the phase offset and Doppler shift of the p^{th} path [59]. Applying the Fourier transform with respect to the delay variable τ to find the time-variant channel transfer function given by

$$H(f, t) = \sum_{p=0}^{N_p-1} \alpha_p e^{j\theta_p} e^{j2\pi\upsilon_p t} e^{-j2\pi f\tau_p}. \tag{2.5}$$

In selective channels, there can be significant variations in the frequency response throughout the bandwidth and there are typically nulls in the frequency response where the channel greatly attenuates parts of the spectrum (deep fading in frequency selective channel), which greatly degrades the transmission performance.

Signals with small bandwidth compared to the channel coherence bandwidth experience flat fading where the channel can be supposed constant. If its response is outside a null, almost

perfect reception is guaranteed. On the other hand, high data rate transmission requires wide bandwidth resulting in a transmission over inevitably selective channels. This may deteriorate the signal at the receiver end, which makes the use of sophisticated reception tasks crucial. Traditionally, channel equalization is utilized to compensate the channel effect. However, since the multipath temporal delay usually spans multiple symbols, the channel equalization is becoming more complicated. In addition, complex adaptive equalizers with feedback loops have to be used to track the channel variations. Alternatively, transferring a broadband signal into parallel narrowband sub-streams allows to overcome the frequency selectivity. We then deal with multi-carrier modulation techniques. In this thesis framework, we are concerned in particular with the OFDM modulation which has become the core of various modern wireless communication systems. OFDM is indeed a parallel data transmission technique that can efficiently mitigate the effects of multipath distortions. Basically, it converts the wideband channel into several narrowband sub-channels, each experiencing flat fading, thus offering multiple advantages over conventional single-carrier modulation techniques.

2.2 OFDM Modulation

The technique of multi-carrier transmission has received wide interest, especially for high data rate applications thanks to their capability to combat hostile frequency-selective fading encountered in mobile communications. Orthogonal Frequency Division Multiplexing (OFDM) is one among the multi-carrier modulation techniques, where a single data stream is transmitted over a number of overlapping lower-rate sub-carriers.

2.2.1 OFDM History

The concept of parallel transmission of data over dispersive channels was first proposed as early as 1957 in the formerly new contribution of Doelz *et al.* [65], while the first OFDM schemes date later in 1960s, when Chang [66] published a paper on the synthesis of bandlimited orthogonal signals for multichannel data transmission. He presented a pioneering principle of transmitting signals simultaneously over bandlimited sub-channels without interference between neither symbols nor channels. Later in 1967, Salzberg analyzed the efficiency of such parallel data transmission systems [67], where he concluded that "strategy of designing an efficient parallel system should concentrate on reducing cross-talk between adjacent channels rather than on

perfecting the individual channels themselves, since the distortions due to the cross-talk tend to dominate".

These systems required banks of sinusoidal sub-carrier generators and demodulators. For a large number of sub-channels, the number of modulators and demodulators are increased proportionally, which results in a high implementation complexity. This drawback limited the application of OFDM to military systems until 1969, when Salzberg and Weinstein proposed a digital system which realized parallel data transmission using Discrete Fourier Transform (DFT) [68]. The transmitted data is the Fourier transform of the original time domain signal and the bank of coherent demodulators was replaced by the Inverse Discrete Fourier Transform (IDFT). Right after, Weinstein and Ebert provided deeper description of the DFT use to perform the baseband modulation and demodulation and investigated the effects of linear channel distortion in [69]. For highly efficient processing, a digital baseband implementation based on the Fast Fourier Transform (FFT) was proposed for computing DFT, which reduced the number of arithmetic operations from N^2 to $N \log_2 N$ (N is the FFT size). The insertion of a guard interval between consecutive symbols helped to eliminate most of the interference but the system could not keep perfect interference immunity over time dispersive channel. This problem was treated in the early 1980s by Peled and Ruiz [70] who suggested to fill the empty guard interval with the cyclic extension of the OFDM symbol, known as Cyclic Prefix (CP). If the CP length is longer than the impulse response of the channel, the interference between symbols can be completely eliminated. Furthermore, the CP acts as if it is performing cyclic convolution with the channel which implies orthogonality between sub-carriers over a time dispersive channel when the CP is longer than the Channel Impulse Response (CIR).

OFDM technique applications were proposed in 1985 by Cimini [71] who investigated the performance of OFDM modems in mobile communication and in 1987 Alard and Lasalle [72] applied OFDM in digital broadcasting systems. Later, with the improvement of its efficiency and low implementation complexity, OFDM technique has found its way into most of the recent wireless systems, such as the Wi-Fi, WiMAX, LTE and DVB as well as DAB broadcast standards [1, 11, 12].

2.2.2 OFDM Basics

2.2.2.1 Principle

The basic idea behind any multi-carrier modulation technique is to divide a high-data rate stream of information units into several parallel lower-rate streams, then each of the obtained data streams modulates one separate carrier (sub-carrier or tone). Hence, the symbol length T_s is increased significantly to counter the channel delay spread and mitigate the ISI effect. The sub-carriers then experience flat-fading since their corresponding sub-channels bandwidth is chosen to be significantly lower than the channel coherence bandwidth, which ensures a robust transmission in frequency-selective channels.

To obtain a high spectral efficiency, the sub-channels relative signals overlap in the frequency domain and are orthogonal to each other. Unlike the traditional Frequency Division Multiplexing (FDM) techniques, in OFDM all the sub-channels have overlapping spectrum but the sub-channels can still be received without adjacent interference as long as the sub-carriers are orthogonal. This overlapping avoids the wasting of bandwidth used to eliminate the ICI in non-overlapping sub-carrier schemes. Indeed, as shown in figure 2.3.a, to implement the conventional parallel data transmission by classical FDM, a guard band must be introduced between adjacent sub-carriers to avoid the ICI. This leads to inefficient use of the rare spectrum resource. For the OFDM technique depicted in figure 2.3.b, the sidebands from one channel become null at the positions corresponding to the other sub-channels. As the sub-carriers are orthogonal to each other, there is no interference between overlapping sub-carriers while achieving almost 50% bandwidth savings.

For simple and reduced complexity pulse forming and modulation, the sub-carrier time pulse is chosen to be rectangular and is truncated to the interval $[0, T_u]$, where T_u is the OFDM symbol duration. The truncation in the time domain implies a cardinal sine (sinc) shape on each sub-channel frequency response with zero at integer multiples of $\Delta_f = 1/T_u$, which is the minimum sub-carrier spacing required for the orthogonality to hold. As sketched in figure 2.4, even though they are overlapping, sub-carriers can be separated from each other since orthogonality guarantees that the interfering "sincs" have null values at the frequency where the "sinc" of interest has a peak.

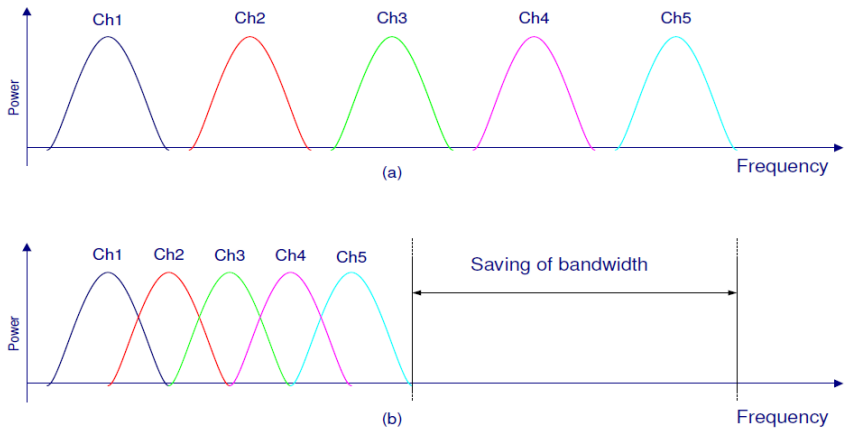

Figure 2.3: Comparison between traditional multi-carrier and OFDM techniques.

2.2.2.2 Block Diagram

A simplified block diagram of an OFDM system is depicted in figure 2.5. As seen, the first stage in the transmitter is the data mapping, which consists in mapping the incoming binary data stream into data symbols using one of the modulation techniques like BPSK (Binary Phase Shift Keying), QPSK (Quadrature Phase Shift Keying), QAM (Quadrature Amplitude Modulation). The resulting complex high bit-rate data stream is split into N_u parallel low-rate streams by using a simple Serial to parallel (S/P) converter to prepare data symbol for alteration to OFDM waveform. The number N_u here corresponds to the sub-carriers number and the FFT size. Then, the N_u-point IFFT is applied to blocks of N_u data symbols, which corresponds to modulating the N_u orthogonal sub-carriers. The obtained samples form an OFDM block samples (temporal signal) which are then serially transmitted over the channel. Usually, N_u is taken as a power of 2 in order to enable the application of the highly efficient (Inverse) FFT algorithms for modulation and demodulation. In some cases, not all the N_u sub-carriers are modulated using the data symbols, some of them are modulated using pilot symbols (symbols known at the receiver) for the purpose of channel estimation. To each OFDM symbol of length N_u, a cyclic prefix of length T_g (N_g samples) that exceeds the maximum delay spread of the multipath propagation channel ($\tau_{max} - \tau_{min}$) is added. Finally, the CP-prepended OFDM symbols are transmitted through the air interface.

At the receiver, the cyclic prefix, which may be corrupted by ISI from the adjacent symbols, is first removed and a serial to parallel conversion is carried to restitute separate OFDM symbols of length N_u each given to the demodulator. This latter is an N_u-point FFT which would give

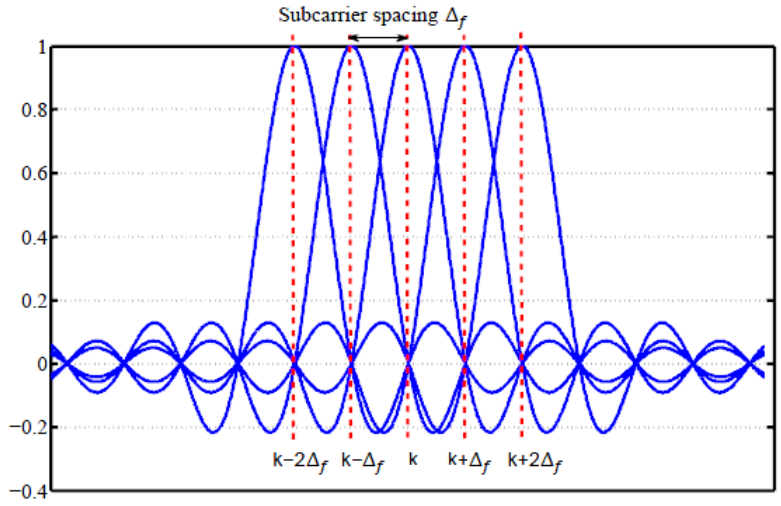

Figure 2.4: The use of overlapping orthogonal sub-carriers in OFDM.

the data symbols back in the frequency domain. Then, the data symbols are demodulated based on the corresponding modulation technique (QPSK, QAM, ...) used at the transmitter to get back an estimate of the transmitted bits stream. In the block diagram, channel coding and interleaving blocks can be incorporated and applied to the input data in order to improve the Bit Error Rate (BER) performance and to reduce the burst symbol error rate of the system, respectively. They are not considered in our system.

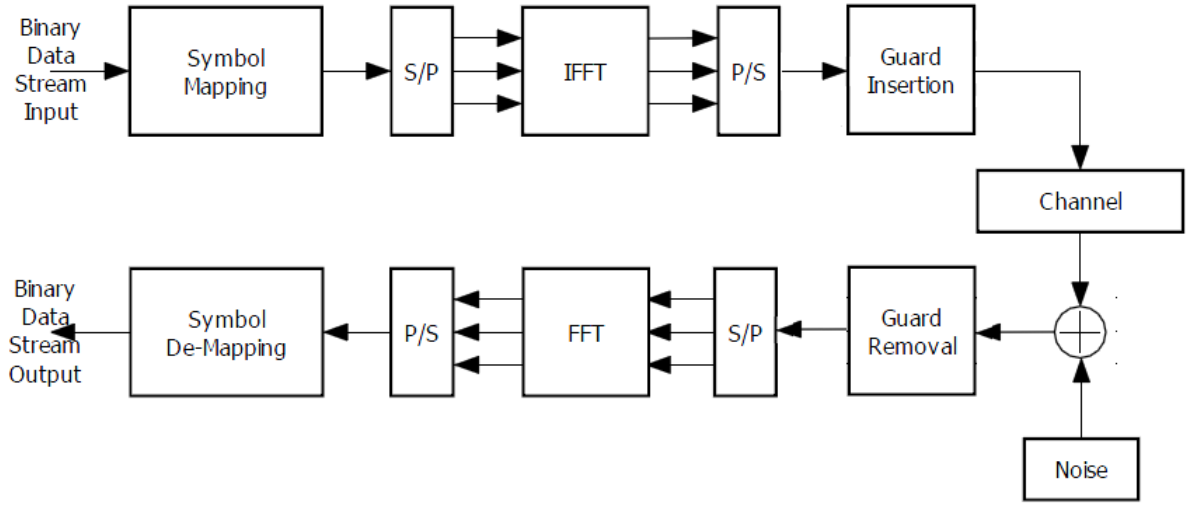

Figure 2.5: Block diagram of the considered OFDM transceiver.

We note that due to the channel distortions, the received symbols will be deteriorated at

the receiver end, which requires sophisticated receiving mechanisms such as equalization and synchronization.

2.2.3 OFDM System Model

The above described features of the OFDM signal generation and demodulation are mathematically derived in this section. This will lead to the conclusion that, using the OFDM principle, data symbols can be transmitted over multipath channels without disturbing each other.

2.2.3.1 OFDM Signal Generation

The continuous OFDM signal is expressed as the sum over time of a number of OFDM symbols. Over the l^{th} OFDM block transmitted on time interval $[lT_u, (l+1)T_u]$, the sum signal resulting from the modulation of sub-carriers $(k = 0, .., N_u - 1)$ by data symbols $s_{l,k}$ is pulse shaped then transmitted. So, the baseband OFDM signal can be represented by

$$s(t) = \sum_{l=-\infty}^{+\infty} \sum_{k=0}^{N_u-1} s_{l,k} g(t - lT_u) e^{j2\pi f_k t}, \tag{2.6}$$

where $f_k = f_c + \frac{k}{T_u}$ stands for the sub-carriers frequencies spaced by $\Delta_f = \frac{1}{T_u}$ and $g(t)$ is the rectangular pulse with length equal to the symbol duration T_u defined as:

$$g(t) = \begin{cases} \frac{1}{\sqrt{T_u}}, & 0 \leq t \leq T_u \\ 0, & \text{otherwise.} \end{cases} \tag{2.7}$$

Assuming an ideal channel (distortion-free), perfect reconstruction of the modulated complex symbols is based on the following orthogonality property:

$$\frac{1}{T_u} \int_0^{T_u} e^{j2\pi f_k t} e^{-j2\pi f_{k'} t} \mathrm{d}t = \begin{cases} 1, & k = k' \\ 0, & \text{otherwise.} \end{cases} \tag{2.8}$$

For the orthogonality between different sub-carriers to be hold, the sub-carrier spacing Δ_f was chosen to be equal to the reciprocal of the symbol duration $\Delta_f = \frac{1}{T_u}$. We recall that the orthogonality will enable the receiver to separate the OFDM overlapping sub-carriers components

without errors. The OFDM transmitted signal (equation (2.6)) discrete formulation using the sampling period $T_b = T_u/N_u$ and $f_c = 0$ (baseband) leads to the OFDM signal $s(t = mT_b)$ denoted by $s(m)$ and expressed as

$$s(m) = \sum_{l=-\infty}^{+\infty} \sum_{k=0}^{N_u-1} s_{l,k} g(m - lN_u) e^{j2\pi \frac{km}{N_u}}. \tag{2.9}$$

The OFDM system can be implemented using banks of modulators and demodulators in the continuous-time analog domain. In practice, however, the entire baseband processing is performed in the discrete-time digital domain. The banks of modulators and demodulators are replaced by DFT which can be implemented either by dedicated hardware or software running on a digital signal processor. As expressed in (2.9), for a given symbol index l, the OFDM signal can be generated through the application of an N_u-point IDFT to the data symbol $s_{l,k}(m)$, $k = 0, \ldots, N_u - 1$ as

$$s_l(m) = \sum_{k=0}^{N_u-1} s_{l,k} e^{j2\pi \frac{km}{N_u}}, \quad lN_u \leq m < (l+1)N_u. \tag{2.10}$$

When substituting m by $m + lN_u$, the expression (2.10) can be rewritten as

$$s_l(m) = \sum_{k=0}^{N_u-1} s_{l,k} e^{j2\pi \frac{km}{N_u}}, \quad 0 \leq m < N_u. \tag{2.11}$$

Reciprocally, the receiver will apply an N_u-point DFT to recover the modulated data as

$$\hat{s}_{l,k} = \sum_{m=0}^{N_u-1} s_l(m) e^{-j2\pi \frac{km}{N_u}}, \quad 0 \leq k < N_u. \tag{2.12}$$

According to the definition provided in (2.11), the transmitted symbol $s_l(m)$ is the IDFT of the data sequence $s_{l,k}$ for $0 \leq k < N_u$. Therefore, the whole transmitted signal $s(m)$ in equation (2.9) corresponds to the concatenation of blocks obtained by performing the IDFT on blocks of N_u data symbols.

In general, N_u is chosen to be a power of 2 so that the DFT can be very efficiently implemented using the FFT algorithm to improve the speed of execution [73]. Indeed, the number of complex multiplications per symbol is reduced from N_u^2 to $N_u \log_2 N_u$, which is especially

important for large number of sub-carriers.

2.2.3.2 Spectral Efficiency

In the OFDM modulation, sub-carrier spacing is carefully selected so that sub-carriers spectrum overlap as shown in figure 2.4. Due to this overlapping, the bandwidth is much more efficiently used than in the classical multi-carrier systems. Let us define the spectral efficiency as the bit rate per unit bandwidth in bits/s/Hz [71]. Considering that each sub-carrier conveys a symbol taken from M-ary constellation ($M = 2^a$, $a \in \mathbb{N}$) over a duration of $T_u = T_b N_u$ seconds. Then, the total bit rate over the N_u sub-carriers for the corresponding M-ary system is $R_b = \frac{a}{T_b}$. Accounting for the fact that the OFDM symbol useful duration T_u is extended with a CP of length T_g. Then, the effective bit rate is given by

$$R_b = \frac{T_u}{T_u + T_g}\frac{a}{T_b} \quad bits/s. \tag{2.13}$$

The frequency spacing between adjacent sub-carriers is $\Delta_f = \frac{1}{N_u T_b}$. Therefore, the total bandwidth occupied by the N_u sub-carriers is

$$BW = N_u \Delta_f = \frac{1}{T_b}. \tag{2.14}$$

Thus, the spectral efficiency of an OFDM system becomes

$$\beta = \frac{R_b}{BW} = \frac{T_u}{T_u + T_g} a \quad bits/s/Hz. \tag{2.15}$$

For an optimal system without guard interval insertion ($T_g = 0$), the spectral efficiency becomes $\beta = a$ bits/s/Hz. Nevertheless, in OFDM mobile communication systems the Guard Interval (GI) is of crucial importance to cope with multipath effects and to maintain the orthogonality between sub-carriers. Hence, in practice an OFDM system will not achieve the maximum bandwidth efficiency.

2.2.3.3 Cyclic Prefix

Although the use of OFDM modulation itself reduces the effect of ISI thanks to the larger symbol duration, OFDM symbols are still not immune to the large channel delay spread. In order

to completely remove the ISI, a guard interval is inserted between consecutive symbols. The required length of the guard interval depends on the channel characteristics and applications. Usually, the GI is selected to have a length of one tenth to a quarter of the symbol period, leading to an SNR loss of 0.5 to 1 dB. To have ISI free transmission, the guard interval length T_g (N_g in its discrete form) should be greater than the delay spread ($T_g \geq \tau_{max} - \tau_{min}$). The complete OFDM symbol of length N_s samples is built up by its useful part generated as in equation (2.11) whose length (in terms of samples) is N_u to which a guard interval of length N_g is prepended ($N_s = N_u + N_g$) as depicted in figure 2.6. The CP added to the useful part of the OFDM signal leads to blocks of length $T = T_u + T_g$ where $T_u = N_u T_b$, $T_g = N_g T_b$ and $T = (N_u + N_g)T_b$.

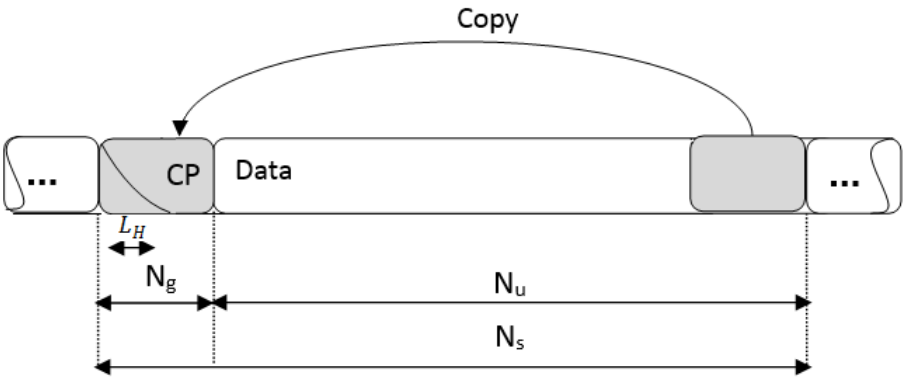

Figure 2.6: An OFDM symbol consisting of a useful part prepended with a cyclic prefix.

The most popular solution is to insert a copy of the last part of the OFDM symbol, referred to as Cyclic Prefix (CP). Due to the CP insertion, the transmitted signal becomes periodic and the effect of the time-dispersive multipath channel is equivalent to a cyclic convolution. Due to the properties of the cyclic convolution, the effect of the multipath channel is equivalent to a pointwise multiplication of the transmitted data constellations by the channel transfer function over each sub-carrier. Hence, the sub-carriers remain orthogonal [48]. If the sub-channel spacing is chosen to be equal to the coherence bandwidth, B_{90} for 90% correlation and the guard interval is chosen to be equal to 5 times the delay spread of the channel, then the length of the guard interval will be 10% of the length of the useful part [50].

It is worth noticing that, as the transmitted blocks contain $N_s = N_g + N_u$ elements instead of N_u, the OFDM signal expression in (2.9) is slightly modified to take into account the CP

insertion as

$$s(m) = \sum_{l=-\infty}^{+\infty} \sum_{k=0}^{N_u-1} s_{l,k} g'(m - l(N_u + N_g)) e^{j2\pi \frac{km}{N_u}}, \tag{2.16}$$

where

$$g'(m) = \begin{cases} \frac{1}{\sqrt{N_u}}, & -N_g \leq m < N_u \\ 0, & \text{otherwise.} \end{cases} \tag{2.17}$$

2.3 Channel Effects on the OFDM Signal

The reason for which the information transmitted over the sub-carriers can still be separated at the receiver is their pairwise orthogonality. Unfortunately, multipath distortion is (almost) unavoidable in radio communication systems, which affects the received signal. In this case, the transmitted signal is received in several delayed versions with different amplitudes and phases. In this section, we study the effect of the mobile propagation channel on OFDM signal.

We here consider the complex baseband-equivalent channel model of the continuous-time channel in (2.4), taken at a given time instant. The discretization affects the continuous time-variant impulse response $h(\tau, t)$ in both τ and t directions at the same time leading to the discrete time-variant CIR denoted by $h(m)$. The received signal is the convolution of the transmitted signal $s(m)$ with the channel impulse response $h(m)$ given by

$$y(m) = h(m)s(m) + \eta(m), \tag{2.18}$$

where $\eta(m)$ denotes a complex Additive White Gaussian Noise (AWGN) with variance σ_η^2.

In the following, matrix notation will be adopted. It is straightforward to show that the OFDM transmitter/modulator can be represented by a simple matrix multiplication. First, let $\mathbf{s}_l = [s_{l,0}, s_{l,1}, \ldots, s_{l,N_u-1}]^T$ be the data sequence of independent complex symbols which modulates the orthogonal sub-carriers during the l^{th} OFDM symbol and $\bar{\mathbf{s}}_l$ its IDFT output. Then, the l^{th} OFDM symbol in expression (2.9) can be written in matrix form as

$$\bar{\mathbf{s}}_l = \frac{1}{\sqrt{N_u}} \mathbf{W}^H \mathbf{s}_l, \tag{2.19}$$

where $\mathbf{W}^{\mathrm{H}}$ and $\mathbf{W}$ represent the N_uxN_u IDFT/DFT matrices given by

$$\mathbf{W} = \frac{1}{\sqrt{N_u}} \begin{pmatrix} 1 & 1 & \cdots & 1 \\ 1 & e^{j\omega} & \cdots & e^{j(N_u-1)\omega} \\ \vdots & \vdots & \ddots & \vdots \\ 1 & e^{j(N_u-1)\omega} & \cdots & e^{j(N_u-1)^2\omega} \end{pmatrix}, \tag{2.20}$$

where $\omega = -\frac{2\pi}{N_u}$. It is worth noticing that $\mathbf{W}$ is a unit matrix, so $\mathbf{W^H W} = N_u \mathbf{I}_{N_u}$ where $\mathbf{I}_{N_u}$ stands for the N_uxN_u identity matrix.

Respecting the matrix notation, after passing through the channel, the received samples form the vector corresponding to $\mathbf{y}$ can be written as

$$\mathbf{y}_l = \mathbf{H}\bar{\mathbf{s}} + \eta, \tag{2.21}$$

where $\mathbf{y}_l = [y_{l,0}, y_{l,1}, \ldots, y_{l,N_u-1}]^T$, $\eta = [\eta_0, \eta_1, \ldots, \eta_{N_u-1}]^T$ (l index relative to the OFDM block is here intentionally dropped) and $\mathbf{H}$ stands for the channel matrix during the l^{th} OFDM block expressed as

$$\mathbf{H} = \begin{pmatrix} h_0 & h_{N_u-1} & \cdots & h_1 \\ h_1 & h_0 & \cdots & \vdots \\ \vdots & & \ddots & h_{N_u-1} \\ h_{N_u-1} & h_{N_u-2} & \cdots & h_0 \end{pmatrix}, \tag{2.22}$$

where $\{h_i\}$, $i = 0, .., N_u - 1$ denote the complex baseband equivalent channel impulse response coefficients.

2.3.1 Time Non-Dispersive Channels

In this section, we consider that the channel in (2.22) is flat-fading with a unique direct path corresponding to an impulse response with one complex constant coefficient which we denote by h_{l_0}. By the property of the Fourier transform, the convolution in time domain is multiplication in frequency domain; that is the convolution of the input signal with the CIR is equivalent to the multiplication of the spectrum of the input signal with the channel transfer function. Thus, all the frequency components in the input signal are simply multiplied by a complex constant h_{l_0}. Assuming coherent demodulation and perfect time/frequency synchronization,

the l^{th} symbol at the demodulator output can be recovered by the application of DFT operation (respecting the expression in (2.12) to the N_u-point block starting from the $(lN_u)^{\text{th}}$ sample and ending at $\big((l+1)N_u - 1\big)^{\text{th}}$ sample as

$$\begin{aligned}\mathbf{r}_l &= \begin{pmatrix} r_{l,0} \\ r_{l,1} \\ \vdots \\ r_{l,N_u-1} \end{pmatrix} = \mathbf{W} \begin{pmatrix} y_{lN_u} \\ y_{lN_u+1} \\ \vdots \\ y_{(l+1)N_u-1} \end{pmatrix} \\ &= h_{l_0}\mathbf{W}\bar{\mathbf{s}}_l + \eta_l' = h_{l_0}\mathbf{W}\mathbf{W}^H\mathbf{s}_l + \eta_l' \\ &= h_{l_0}\mathbf{s}_l + \eta_l',\end{aligned} \tag{2.23}$$

where $\eta_l' = \mathbf{W}\eta_l$ is an additive noise, whose elements are zero mean complex independent Gaussian random variables with variance $\sigma_{\eta'}^2$. Thus, the data symbol can be estimated as $\hat{\mathbf{s}}_l = \frac{\mathbf{r}_l}{\hat{h}_{l_0}}$ on which decision rule should be applied. We note that in the case of flat fading channel, simple channel equalization is sufficient to demodulate the OFDM received symbols.

2.3.2 Time Dispersive Channels

Time dispersive channels result from multipath propagation and frequency selective channels. Such channels are characterized by an impulse response with several coefficients, which causes interference between different OFDM symbols and different sub-channels. Generally, the channel delay spread $\tau_{max} - \tau_{min}$ is lower than the CP extended OFDM symbol period T and only two consecutive symbols may partially interfere with each other. Hence, the elements in the received signal $\mathbf{y}_l$ in equation (2.21) contain elements belonging to both $\bar{\mathbf{s}}_l$ and $\bar{\mathbf{s}}_{l-1}$.

To face the effect of interference between consecutive symbols, a CP of length N_g is inserted before any OFDM block (as a prefix). Thus the l^{th} transmitted OFDM block, denoted as $\bar{\mathbf{s}}$, consists of N_u samples useful part prepended with N_g samples for the CP, having the following structure

$$\bar{\mathbf{s}}_l = [\bar{\mathbf{s}}_{l,N_u-N_g}, \bar{\mathbf{s}}_{l,N_u-N_g+1}, \ldots, \bar{\mathbf{s}}_{l,N_u-1}, \bar{\mathbf{s}}_{l,0}, \bar{\mathbf{s}}_{l,1}, \ldots, \bar{\mathbf{s}}_{l,N_u-1}]^T. \tag{2.24}$$

Its received corresponding symbol is then denoted by

$$\mathbf{y}_l = [\mathbf{y}_{l,-N_g}, \mathbf{y}_{l,-N_g+1}, \ldots, \mathbf{y}_{l,-1}, \mathbf{y}_{l,0}, \mathbf{y}_{l,1}, \ldots \mathbf{y}_{l,N_u-1}]^T. \tag{2.25}$$

Based on the previous expressions and assuming that $N_g > L_H$ so that the channel impulse response samples h_p are zero valued for p indexes higher than N_g ($h_p = 0 \quad \forall p > N_g$), the received signal $\mathbf{y}_l$ then converts into

$$\mathbf{y}_l = \mathbf{H}\bar{\mathbf{s}}_l + \eta, \tag{2.26}$$

where the channel matrix $\mathbf{H}$ is expressed as

$$\mathbf{H} = \begin{pmatrix} h_0 & h_1 & \cdots & h_{L_H-1} & 0 & \cdots & 0 \\ 0 & h_0 & h_1 & \cdots & h_{L_H-1} & \ddots & \vdots \\ \vdots & \ddots & \ddots & \ddots & \ddots & \ddots & 0 \\ 0 & \cdots & 0 & h_0 & h_1 & \cdots & h_{L_H-1} \end{pmatrix}_{\left((N_u+N_g)\mathrm{x}N_u\right)}, \tag{2.27}$$

$\bar{\mathbf{s}}_l$ stands for the l^{th} OFDM symbol with no CP extension and η stands for the noise vector expressed as

$$\eta = \begin{pmatrix} \eta_{l(N_u+N_g)-N_g} \\ \eta_{l(N_u+N_g)-N_g+1} \\ \vdots \\ \eta_{l(N_u+N_g)+N_u-1} \end{pmatrix}. \tag{2.28}$$

As the CP is subject to inter-symbol interference, it is discarded at the receiver side (the first N_g samples of $\mathbf{y}_l$ are discarded). This allows to simplify the received symbol expression in equation (2.26) by omitting the first N_g including the L_H interfering samples from the previous symbol as

$$\mathbf{y}_l = \begin{pmatrix} h_0 & 0 & \cdots & 0 & h_{L_H-1} & \cdots & h_1 \\ h_1 & h_0 & \ddots & \ddots & \ddots & \ddots & \vdots \\ \vdots & \ddots & \ddots & \ddots & \ddots & \ddots & h_{L_H-1} \\ h_{L_H-1} & \cdots & h_1 & h_0 & 0 & \cdots & 0 \\ 0 & \ddots & \ddots & \ddots & \ddots & \ddots & \vdots \\ \vdots & \ddots & \ddots & \ddots & \ddots & \ddots & 0 \\ 0 & \cdots & 0 & h_{L_H-1} & \cdots & h_1 & h_0 \end{pmatrix} \times \begin{pmatrix} \bar{s}_{lN_u} \\ \bar{s}_{lN_u+1} \\ \vdots \\ \bar{s}_{(l+1)N_u-1} \end{pmatrix} + \begin{pmatrix} \eta_{lN_u} \\ \eta_{lN_u+1} \\ \vdots \\ \eta_{(l+1)N_u-1} \end{pmatrix}. \tag{2.29}$$

It can be observed that, thanks to the CP, the circular channel matrix (2.22) preserves its

property in (2.29), in which $\mathbf{H}$ is an $N_u \times N_u$ circular matrix. Hence, there exists a diagonal matrix $\bar{\mathbf{H}}$ generated from the diagonalization of $\mathbf{H}$ by the IDFT/DFT matrices $\mathbf{W^H}$ and $\mathbf{W}$ as

$$\bar{\mathbf{H}} = \mathbf{W}\mathbf{H}\mathbf{W}^H, \tag{2.30}$$

where $\bar{\mathbf{H}}$ is N_uxN_u diagonal matrix whose k^{th} diagonal elements can be expressed as

$$\bar{\mathbf{H}}_{k,k} = \sum_{i=0}^{N_u-1} h_i e^{-j\frac{2\pi k i}{N_u}}. \tag{2.31}$$

Thus, the received vector $\mathbf{y}_l$ can be written as

$$\mathbf{y}_l = \mathbf{W}^H\bar{\mathbf{H}}\mathbf{W}\bar{\mathbf{s}}_l + \eta_l = \mathbf{W}^H\bar{\mathbf{H}}\mathbf{s}_l + \eta_l. \tag{2.32}$$

Hence, the demodulated received symbol $\mathbf{r}$ is recovered as

$$\mathbf{r}_l = \mathbf{W}\mathbf{y}_l = \bar{\mathbf{H}}\mathbf{s}_l + \eta'_l, \tag{2.33}$$

where $\eta'_l = \mathbf{W}\eta_l$. The k^{th} element of the vector $\mathbf{r}_l$, denoted by $\mathbf{r}_{l,k}$, is expressed as

$$\mathbf{r}_{l,k} = \bar{\mathbf{H}}_{k,k}s_{l,k} + \eta'_{l,k}, \tag{2.34}$$

where $s_{l,k}$ and $\eta'_{l,k}$ correspond respectively to the k^{th} elements of $\mathbf{s}_l$ and η'_l. At this stage, when we consider the sole sub-carrier k, we note that each transmitted symbol undergoes an equivalent flat fading channel. Hence, on each sub-channel, we have a propagation affect similar to that of flat fading (2.23) in which a simple one-tap equalization per sub-carrier is sufficient to recover the transmitted data as

$$\hat{\mathbf{s}}_{l,k} = \frac{\mathbf{r}_{l,k}}{\bar{\mathbf{H}}_{k,k}}. \tag{2.35}$$

The equalization consists only in dividing the received data symbol $\mathbf{r}_k$ by the estimated sub-channel transfer function $\mathbf{H}_{k,k}$. The channel can be estimated based on many criteria: Least Squares (LS) or Linear Minimum Mean Square Error (LMMSE) criteria by exploiting pilots or training sequences or using blind approaches.

In the case of non-ISI-free reception, the channel matrix $\mathbf{H}$ can no more be digonalized in a DFT basis as before. Therefore, ICI occur leading to a loss of orthogonality and thus performance deterioration. To overcome this inconvenience, we aim to provide ISI-free recep-

tion through accurate time synchronization which provides a maximum tolerance to channel delay spread. From this point of view, time synchronization remains a very challenging task in OFDM based communications. Time synchronization issues will be later discussed.

2.4 Pros and Cons of OFDM

OFDM systems show much favorable properties suitable for broadband communications such as high spectral efficiency, robustness to channel fading, immunity to interference, capability of handling very strong echoes (multipath fading). However, it exhibits some limitations like sensitivity to synchronization errors and high peak-to-average power ratio (PAPR) which make sophisticated reception techniques mandatory. We here summarize the strengths and weaknesses of the OFDM modulation technique.

a) Advantages

- **Robustness to multipath fading channels**: the multipath fading effect is the most critical limitation in broadband wireless communication. Indeed, if data are transmitted at high rate so that the symbol period is lower than the channel delay spread, each received symbol will spread into adjacent symbols causing ISI. Thanks to the guard interval insertion between successive symbols and if the echoes are shorter than the symbol period, the energy from one symbol only affects the first part of the next symbol which generally corresponds to the guard interval. In other words, if the guard interval is longer than the CIR, the effects of ISI are localized in the useless part of the OFDM signal which corresponds to the guard interval to be eliminated before demodulation.

  Furthermore, by splitting the available channel to several flat sub-channels, OFDM treats each of them as narrow-band channel, hence reducing the overall effect of frequency-selective fading on the data transmission. Hence the ISI can be reduced and even eliminated. This in turn reduces the complexity of the receiver equalizers. In conclusion, the OFDM modulation scheme is robust in a frequency selective fading environment. This is one of the greatest benefit of using OFDM as the modulation scheme in the modern standards in high-speed wireless communication.

- **High Spectral Efficiency**: in classical multi-carrier systems, frequency guard bands

have to be inserted resulting in poor spectral efficiency. By removing the guard bands between adjacent sub-channels, OFDM technique makes efficient use of frequency spectrum. In other words, the sub-carriers have the minimum frequency separation required to maintain orthogonality of their corresponding time domain waveforms, yet the signal spectra corresponding to the different sub-carriers overlap in frequency. The spectral overlapping results in a waveform that uses the available bandwidth with a very high bandwidth efficiency. The orthogonality between sub-carriers will ensure that the receiver can separate the OFDM sub-carriers without errors as there is no mutual influence between sub-carriers.

- **Simple equalization**: as mentioned before, one of the main reasons to use OFDM is its capability to deal with large delay spreads. For a given delay spread, the implementation complexity of an OFDM receiver is significantly lower than that of a single-carrier system with an equalizer [49]. The comparison made in [49] shows that the complexity reduction achieved using OFDM technique is due to the fact that when the bit rate is doubled, an equalizer has to be made twice as long at twice the speed, so its complexity grows quadratically with the bit rate, while the complexity of OFDM grows slightly faster than linear.

  Furthermore, if the bandwidth of each sub-channel is lower than the channel coherence bandwidth, a frequency-flat channel model can be assumed for each sub-carrier and the equalization will be radically simplified. The effect of the multipath channel on each sub-carrier can be represented by a single valued complex number affecting the amplitude and phase of each subcarrier. Hence, the equalization can be carried out by a simple one-tap equalizer operating in the frequency domain.

b) Drawbacks

- **High Peak-to-Average Power Ratio**: an OFDM signal consists of several independently modulated sub-carriers, whose time-domain envelope can be modeled as the superposition of the corresponding sinusoidal signals with different frequencies and phases. When N_u signals are added constructively, they produce a peak power that is N_u times the average power, leading to a high Peak-to-Average Power Ratio (PAPR). A high PAPR ratio brings disadvantages like an increased complexity of the analog-to-digital (A/D) and digital-to-analog (D/A) converters and a reduced efficiency of the radio fre-

quency power amplifier. In other words, the output power amplifier has to maintain high linearity across the entire range of input signal level. Otherwise, the signal will suffer from non-linear distortion resulting in out-of-band emission that causes interference to adjacent sub-channels.

There have been many studies to reduce the peak-to-average power ratio in OFDM systems. A classification into three categories was introduced in [48]. Namely, signal distortion techniques (clipping, peak windowing, and peak cancellation), coding techniques (forward error correction) and scrambling techniques.

- **Sensitivity to synchronization errors**: while OFDM technique solves most of the wideband mobile communication limitations, it introduces new problems itself. By using high numbers of narrow sub-carriers, the system becomes very sensitive to time and frequency offsets. When the time offset (symbol synchronization error) is large, the FFT interval will include a symbol boundary or start in the region of the symbol contaminated by ISI. Thus, the orthogonality is lost and ICI and lSI will occur. Furthermore, the existence of the frequency offset introduces ICI which destroys the orthogonality among the OFDM sub-carriers and leads to performance degradation. Hence, perfect synchronization in time domain and frequency domain is a challenging subject.

  To face these limitations, there have been studies in the literature addressing the time and frequency synchronization. Two classes of synchronization can be distinguished: Blind and Data-Aided. The former approaches exploit the redundancy in the CP, as the work of Van de Beek in [24], which is more suited to continuous flow transmission, such as streaming video. Whereas, data-aided approaches use a preamble before OFDM symbols data transmission, as in [15]. These synchronization methods, cost in terms of bandwidth but are generally more efficient than blind ones, especially for bursty-packet traffic.

In this thesis, we are going to deeply review the sensitivity of OFDM systems to time and frequency synchronization errors. We will also present an overview on existing algorithms and propose several algorithms for the symbol timing and carrier frequency estimation.

Conclusions

This chapter presented the fundamental concepts to understand the main object of the thesis. It started by describing the mobile propagation environment and provided a description of the propagation channel. This latter was characterized by its dispersion that affects transmitted signal in both time and frequency. The mobile radio channel was characterized by time variation and frequency selectivity. To cope with these constraints, we introduced the OFDM transmission technique that is considered as an efficient transmission technique in harsh propagation environment. Indeed, OFDM modulation provides an efficient use of the bandwidth through overlapping orthogonal sub-carriers. The mathematical expression of OFDM signal was given, followed by the effect of propagation channel on it. It was shown that as the cyclic prefix duration is longer than the channel delay spread, it is possible under some conditions (related to synchronization) to completely avoid the interference between symbols and sub-channels. Towards the end of the chapter, the main advantages and disadvantages of the use of OFDM technique were recalled.

Although OFDM technique can guarantee an ISI-free reception if the cyclic prefix is longer than the maximum channel delay spread, accurate symbol start detection is crucial for transmission over frequency selective channel to provide the maximum tolerance to channel multi-path temporal spread effects. Furthermore, any residual frequency offset destroys sub-channels orthogonality and causes ICI, which results in performance degradation at the receiver. These observations highlight the importance of synchronization issues for OFDM systems to make it possible to benefit from their numerous advantages, especially in harsh wideband wireless transmission channels.

Chapter 3

Synchronization in OFDM Systems: State of the Art

The high spectral efficiency offered by the use of OFDM technique is due to the orthogonality between sub-carriers. However, in an OFDM link, it is possible that this orthogonality is destroyed. This can indeed result from several factors such as the Doppler shift resulting from the relative movement between the transmitter and the receiver, the frequency mismatch between the oscillators at two ends, large timing errors and phase noise. Before an OFDM receiver can demodulate the sub-carriers, it has to perform synchronization to maintain the orthogonality among them. At least two tasks are achieved. First, the location of the symbol boundary and the optimal symbol timing must be found (time synchronization) to minimize the effects of ICI and ISI. Second, the carrier frequency offset in the received signal has to be estimated since any frequency offset introduces ICI.

The first part of this chapter provides an analysis of the effect of both timing and frequency synchronization errors on demodulation performance at the receiver. In the second part, we provide a survey on existing synchronization techniques proposed in the literature to mitigate channel impairments. These techniques can be roughly classified in two categories. On the first hand, blind (non-data aided) techniques which exploit either the redundancy in the CP or the statistical properties of the received signal. On the other hand, data-aided techniques which use known training symbols transmitted at the beginning of each frame to achieve synchronization. The training symbols must have specific properties which makes them distinguishable from data

symbols. Data aided techniques generally provide better detection than the blind techniques. Our work is concerned with preamble-based techniques. Hereafter, we give a state of the art od such techniques.

3.1 Effects of Synchronization Errors

In this section, we analyze the effects of imperfect time and frequency synchronization on demodulated OFDM signal. Time offset occurs when transmitter and receiver do not have a common time reference for the same selected IFFT/FFT block, which causes both ISI and ICI. Thus, to properly demodulate the OFDM symbols, the receiver needs to find symbol boundaries. Frequency offset includes carrier/phase and sampling clock errors. The carrier/phase offset is the difference between the frequencies of the transmitter and the receiver local-oscillators, which introduces additional term in the received baseband signal resulting in ICI. The receiver needs to compensate the frequency offset for coherent detection. Symbol clock (sampling frequency) offset results from the difference in sampling clock between the local oscillators of the transmitter and the receiver. This kind of offset results in a gradually growing timing offset and a slightly large sub-carrier spacing. In our work, we mainly focus on time offset effects and give a brief survey on frequency offset.

3.1.1 Effects of Time Synchronization Errors

As mentioned in section 2.2.3, each OFDM symbol is composed of two parts: a guard interval of length N_g and a useful part of length N_u. The useful part consists of the data to be processed by the FFT block, while the guard interval is generally a cyclic extension of the useful part that is removed before passing the received data to the FFT demodulator block. In order to remove the guard interval and align the data window with the useful part, the receiver needs to find the start position of the useful part. Through this criterion, the optimal timing instant will be the boundary between the cyclic prefix and the useful part. Hence, when the data capturing window is placed in this position, the FFT window will cover the useful part only. Furthermore, if the timing offset is large the FFT window will cover the boundary of two adjacent symbols. In this case, the input to the FFT demodulator will be the concatenation of interfering components belonging to different symbols.

As illustrated in figure 3.1, the FFT window can be located at different positions regarding the correct symbol start.

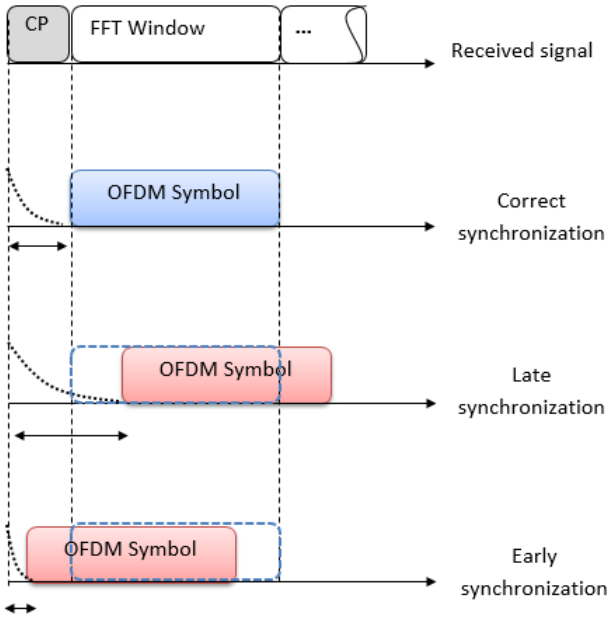

Figure 3.1: Early and late synchronization.

Let us denote the timing offset normalized with respect to the sampling period T_b by ϵ (supposed to be integer), which has no unit and which is equal to the number of samples between the transmitted signal $s(n)$ and the received signal $s(n-\epsilon)$. In case of ideal synchronization, the FFT window will be positioned in the correct time and will exactly be aligned with the useful part of the symbol. Such a case corresponds to a timing offset ϵ equal to zero and the entire guard interval will be discarded thus leading to a correct data demodulation FFT window alignment. In practice, however, due to propagation delay, the time offset ϵ is always non-zero and the start of the FFT is moved away from the optimal start point. The impact of an FFT timing offset at the receiver is widely studied in the literature [48, 49, 74, 75].

In order to understand the effects of the TO, we refer to the mathematical analysis in [74]. We consider a case of non-dispersive AWGN channel and assume that we do not use any kind of guard interval ($N_g = 0$). The demodulated data symbol $\hat{s}_{l,k}$ for the k^{th} sub-carrier and the

l^{th} OFDM symbol after FFT can be written as

$$\begin{aligned}
&\hat{s}_{l,k} = \frac{N_u - \epsilon}{N_u} s_{l,k} e^{j2\pi(\frac{k}{N_u})\epsilon} \\
\text{(ICI)} \qquad &+ \frac{1}{N_u} \sum_{n=0}^{N_u-1} e^{-j2\pi(\frac{n}{N_u})k} \sum_{i=0, i\neq k}^{N_u-1} s_{l,i} e^{j2\pi(\frac{i}{N_u})(n+\epsilon)} \\
\text{(ISI)} \qquad &+ \frac{1}{N_u} \sum_{n=N_u-\epsilon}^{N_u-1} e^{-j2\pi(\frac{n}{N_u})k} \sum_{i=0}^{N_u-1} s_{l+1,i} e^{j2\pi(\frac{i}{N_u})(n-N_u+\epsilon)} \\
\text{(AWGN)} \qquad &+ \eta_{l,k}.
\end{aligned} \tag{3.1}$$

According to the equation above, the TO results in three effects: a phase rotation, ISI and ICI terms. The phase rotation is proportional to the sub-carrier index k and the TO ϵ and it affects the useful part of the demodulated symbol. The ISI term occurs because of the inclusion of samples belonging to the next symbol in the current one. On the other hand, the ICI are inherent to disturbances caused by sub-carriers being adjacent to that of the present symbol (loss of orthogonality). In addition to the TO effects, the demodulated samples suffer from attenuation of their useful part and are affected by an AWGN η of variance σ_η^2 .

Now, extending the study to the case of late synchronization in the presence of a CP ($N_g > 0$). When the synchronization tick is positioned later than the optimal time index, the FFT data window will contain $N_u - \epsilon$ samples from the actual OFDM symbol and ϵ other samples collected from the CP of the next OFDM symbol; if there is no following OFDM symbol, the last samples are filled up with noise.

On the other hand, early synchronization shown in figure 3.2, in this case, has no major effect as long as the CP length is sufficiently high. Indeed, TO results in a misalignment of the FFT window with ϵ samples and the demodulated symbol contains ϵ samples of the current OFDM symbol CP and $N_u - \epsilon$ of its useful part. The symbol timing offset is now equivalent to a time delay in digital sampling. It is a well-known fact that delay in the time domain represents a linear phase shift in the frequency domain. Assuming non-dispersive channel (maximum channel delay spread $\tau_{max} = 0$) and a CP longer than ϵ, then the timing error would result in a simple phase shift, that increases linearly with the sub-carrier index k, without any additional ICI or ISI. The demodulated data in this case becomes

$$\hat{s}_{l,k} = s_{l,k} e^{j2\pi \frac{k}{N_u}\epsilon} + \eta_{l,k}. \tag{3.2}$$

This analysis remains valid as long as the starting position of the data window is within the ISI-free region of the guard interval. The ISI-free region is defined as the time interval in which ϵ is greater than zero but less than $N_g - \tau_{max} + 1$. Here, a number of ϵ samples from the guard interval and $N_u - \epsilon$ samples from the useful part will be selected, which are still free from interference from adjacent symbols.

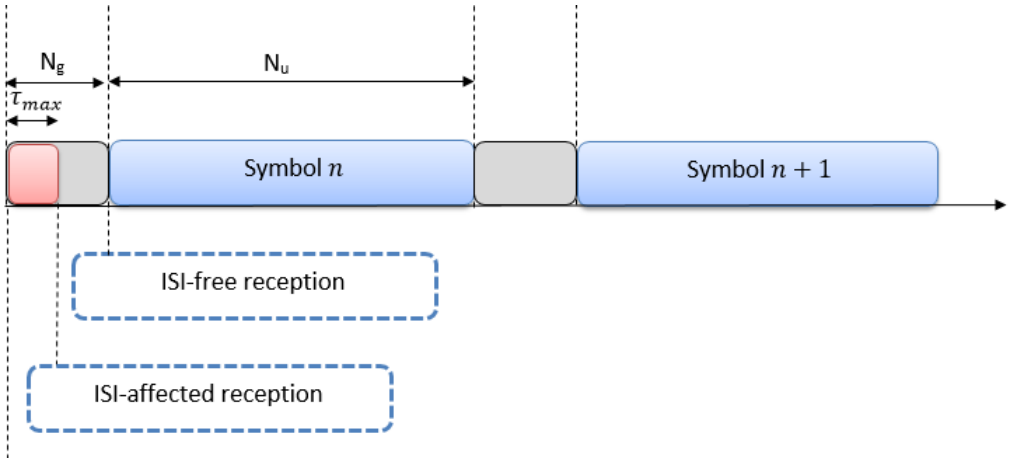

Figure 3.2: Early synchronization: ISI-free reception and ISI-affected reception.

The last case of early synchronization consists in ISI reception where the TO is greater than $N_g - \tau_{max}$. The data window is still within the current symbol boundary. Nevertheless, some samples coming from the CP are corrupted by interference from samples belonging to the preceeding symbol due to the large channel delay spread. Then, the data FFT window will cover two subsets of the received samples taken as:

- ISI Free: $[r_{-Ng+\tau_{max}+1},\ r_{-Ng+\tau_{max}+2},\ldots,r_{N_u-\epsilon-1}]$
- ISI Affected: $[r_{-\epsilon},r_{-\epsilon+1},\ldots,r_{-N_g+\tau_{max}}]$

The third term in equation (3.1) corresponding to the ISI contribution is not zero valued. Hence, the demodulated data is affected by adjacent sub-carriers which are no longer orthogonal to each other. This leads to ICI that may severally affect the orthogonality between the OFDM sub-carriers.

We conclude that a proper cyclic extension with sufficiently long period can be used to effectively cancel the ICI and ISI caused by timing offset. However, to take advantage of spectral efficiency the CP generally does not exceed 20% of the symbol length. For frequency-selective channels with high delay spread, the ISI-free zone is reduced, thus limiting the TO that can be tolerated by the receiver. To face this limitation, accurate time synchronization must be achieved, which makes synchronization one of the biggest challenges of any OFDM communication system. Next, in section 3.2, we provide a survey on some of the existing synchronization approaches and their classification.

3.1.2 Effects of Frequency Synchronization Errors

Compared to single-carrier systems, OFDM systems are much more sensitive to Frequency Offsets (FO), which may result from two kinds of misalignments that are hereafter explained.

Before applying the FFT at the demodulation step, the received analog signal is first sampled at instants determined by the receiver clock T_b', which may be different from the sampling clock of the transmitter T_b. This results in a Sampling Clock Frequency Offset (ScFO), whose normalized version is denoted by $\xi = \frac{T_b' - T_b}{T_b}$. Furthermore, the local oscillators at the transmitter and the receiver do not generate exactly the same oscillator frequency thus leading to a Carrier Frequency Offset (CFO) between them denoted by Δ_{f_c} [74]. In the presence of FO (ScFO or CFO or both), the received signal sampled at time instant nT_b' is affected by a phase rotation $\theta(nT_b')$ given by

$$\theta(nT_b') = 2\pi(1+\xi)\Delta_{f_c} nT_b. \tag{3.3}$$

The sampling clock can be assumed to be close to its actual value, thus with no effect on the result of the FFT output [57]. Also, in [50] it was shown that the oscillators can be accurate to a factor of about 10^{-5} as a relative misalignment. Hence, the difference in sampling rate is typically much lower than one sample per OFDM symbol resulting in much less harmer distortion caused by the ScFO on the FFT output than the CFO.

As mentioned above, Δ_{f_c} is defined as the difference between the transmitter and receiver carrier frequencies. In wireless communications, the CFO comes mainly from the mismatch between oscillating frequencies in the Local Oscillators (LO) of the transmitter and the receiver. It can also result from Doppler effect of the channel due to relative movement between one end

or both ends. For indoor communications, the Doppler effect can be neglected [48].

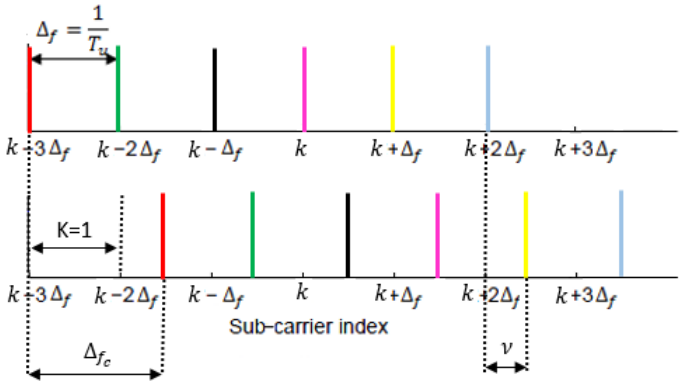

Figure 3.3: Components of total Carrier Frequency Offset.

The CFO is partitioned into two parts (see figure 3.3): the integer part (IFO) multiple of the sub-carrier spacing denoted by K and the remainder fractional part (FFO) ν which is lower than half of the sub-carrier frequency spacing ($-0.5 \leq \nu < 0.5$). The CFO is considered with respect to the sub-carrier spacing as [76]

$$\Delta_{f_c} = (K + \nu)\frac{1}{T_s}. \tag{3.4}$$

In the absence of ISI (correct timing synchronization), the l^{th} demodulated OFDM symbol, under the effect of a normalised CFO Δ_{f_c}, turns into [74]

$$\begin{aligned} \hat{s}_{l,k} &= \left(e^{j\pi a_{k,k}} e^{j2\pi((lN_s+N_g)/N_u)a_{k,k}}\right)\text{sinc}(\pi a_{k,k})s_{l,k} \\ \text{(ICI)} \qquad &+ \sum_{i=0,i\neq k}^{N_u-1}\left(e^{j\pi a_{i,k}} e^{j2\pi((lN_s+N_g)/N_u)a_{i,i}}\right)\text{sinc}(\pi a_{i,k})s_{l,i} \\ \text{(AWGN)} \qquad &+ \eta_{l,k}, \end{aligned} \tag{3.5}$$

with cross-sub-carrier local frequency offset parameter

$$a_{k,i} = \Delta_{f_c} + k - i. \tag{3.6}$$

From (3.5), it is shown that the demodulated signal consists of a rotated and attenuated copy of the desired symbol component $s_{l,k}$ (the first term) and ICI from all the other sub-carriers (the second term), which occur when the frequency offset $\Delta_{f_c} \neq 0$. Generally, the attenuation

factor $\text{sinc}(\pi a_{k,k})$ is very close to 1 and can therefore be neglected. Also, the time-invariant term $e^{j\pi a_{k,k}}$ cannot be distinguished from the channel gain factor (not presented in the equation (3.5)) and is thus incorporated into it.

The effect of the CFO on the spectrum is illustrated in figure 3.4. It is shown in 3.4.a that in the case of perfect frequency synchronization ($\Delta_{f_c} = 0$), the FFT output of the k^{th} sub-carrier will consist only in the signal transmitted on its corresponding sub-carrier without any interference from the neighboring sub-carriers. Nevertheless, it is obvious from figure 3.4.b that in the presence of CFO ($\Delta_{f_c} > 0$), the spectrum will not have single peaks anymore at the k^{th} sub-carrier. Indeed, interference from adjacent sub-carriers will occur and the spectrum is no longer null in its adjacent sub-carrier's frequency.

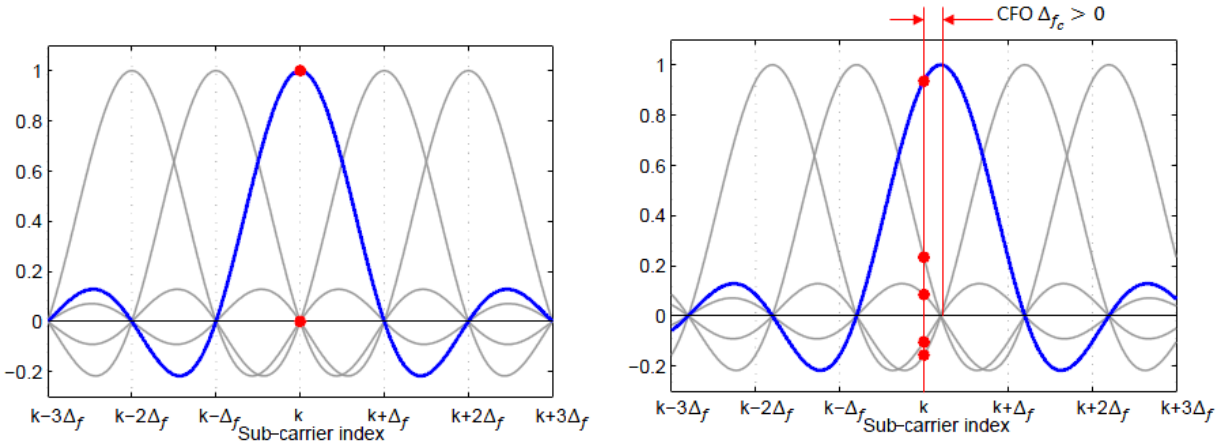

(a) $\Delta_{f_c} = 0$ (b) $\Delta_{f_c} > 0$

Figure 3.4: Effect of CFO on the frequency spectrum of an OFDM signal with 5 sub-carriers.

We also note from figures 3.3 and 3.4 that the IFO K does not affect the OFDM signal spectrum, but only shifts it up or down. If not properly compensated, the FFO ν causes inter-carrier interference at the FFT output, resulting in the sub-carrier orthogonality loss, while the IFO K circularly shifts the sub-carriers away from their original locations in the output of the FFT such that the whole OFDM burst cannot be properly decoded. Consequently, the system performance may be significantly degraded, which makes frequency synchronization critical to the performance of OFDM systems.

Usually, the frequency offset and timing errors are more dominant than the sampling clock error. In the remaining of this thesis, we assume a perfect sampling clock recovery and consider the symbol-timing error normalized with respect to the sampling period T_b as well as the

fractional part of the carrier frequency offset, normalized with respect to the sub-carrier spacing Δ_f and which we denote by ν. Therefore, at time index d and considering a multipath channel (N_p paths), the received sample becomes

$$r_d = e^{j2\pi \frac{d\nu}{N_u}} \sum_{p=0}^{N_p-1} h_p s_{d-\tau_p} + \eta_d, \tag{3.7}$$

where η_d stands for the sample of zero-mean complex Gaussian noise process with variance σ_η^2. Next, we denote the start of the received OFDM symbol by $\tau = t_0 + \epsilon$, where t_0 stands for the transmission start point and ϵ is the time offset in units of OFDM samples. The synchronization process we are focusing on consists in detecting the OFDM symbol start τ and the fractional part of the carrier frequency offset ν. We provide a survey in several time and frequency synchronization approaches in the next section.

3.2 OFDM Synchronization Techniques

The OFDM synchronization techniques can be roughly classified in two main categories: Data-Aided (DA) and Non Data Aided (NDA). These latter, also known as blind techniques, are based on the analysis of the received signal by exploiting either the intrinsic redundancy present in the CP of each OFDM symbol [24, 27] or the statistical properties of the received signal [28,29]. However, these techniques suffer from inaccuracy in the estimation of synchronization offsets. This hints towards severe loss of performance especially in high Doppler environments. The former category of synchronization techniques, on the other hand, exploit special dedicated data that are time and/or frequency multiplexed with the transmitted data as a preamble [15,22]. The preamble generally results in a slight overhead that reduces the spectral efficiency but it greatly enhances the detection accuracy. In this section we take a brief look at some of the synchronization algorithms existing in the literature. Then, we describe DA algorithms, which will serve as benchmarks to evaluate the performance of the techniques that are proposed in this thesis.

3.2.1 Blind Synchronization

Thanks to the CP insertion, the first N_g samples of an OFDM symbol are identical to its N_g last samples. This redundancy is exploited in many works to determine the synchronization parameters. The first CP based techniques were proposed by Van de Beek *et al.* in [24–26]. Even if these estimators provide different estimation performance, they all provide an illustrative view on how a Maximum Likelihood (ML) estimator exploits signal correlation for time and frequency offsets estimation. Considering the example in [24], in which the timing and frequency offsets are jointly estimated through the maximization of the log-likelihood function, initially proposed in [23], as

$$\Lambda(\tau, \Delta_{f_c}) = |\gamma(\tau)| \cos(2\pi\Delta_{f_c} + \angle\gamma(\tau)) - \rho\varepsilon(\tau), \tag{3.8}$$

where $\angle$ denotes the argument of a complex number,

$$\gamma(d) = \sum_{m=0}^{N_g-1} r_{d+m} r^*_{d+N_u+m}, \tag{3.9}$$

corresponds to the correlation of delayed versions of the received signal, with a delay N_u, over a window of N_g samples,

$$\varepsilon(d) = \frac{1}{2} \sum_{m=0}^{N_g-1} |r_{d+m}|^2 + |r_{d+N_u+m}|^2 \tag{3.10}$$

is the energy term, and

$$\rho = \frac{\sigma_s^2}{\sigma_s^2 + \sigma_\eta^2} = \frac{SNR}{SNR+1}, \tag{3.11}$$

where SNR denotes the Signal-to-Noise Ratio and is defined as σ_s^2/σ_η^2 (σ_s^2 and σ_η^2 denote the signal and noise powers respectively). Then, the calculation of the time and frequency offsets ML-estimates $\hat{\tau}$ and $\hat{\Delta}_{f_c}$ are obtained as follows

$$\hat{\tau}_{\mathrm{ML}} = \underset{\tau}{\mathrm{argmax}}\{2|\gamma(\tau)| - \rho\varepsilon(\tau)\}, \tag{3.12}$$

and

$$\hat{\Delta}_{f_{c\mathrm{ML}}} = -\frac{1}{2\pi}\angle\gamma(\hat{\tau}_{\mathrm{ML}}). \tag{3.13}$$

The figure 3.5 presents the timing metric in ideal (noiseless) and dispersive channels evalu-

ated over 9 OFDM symbols. The curves clearly show peaks at the start of each OFDM symbol but the peak amplitude presents significant variation. Recall that the estimator is initially derived under the assumption that the channel distortion consists of only additive noise [23]. The violation of this assumption under frequency selective fading channels may deteriorate severely its performance, which justifies the worsening in figure 3.5.b, where the peak amplitudes show significant variation, and in 3.5.c where some peaks completely disappear.

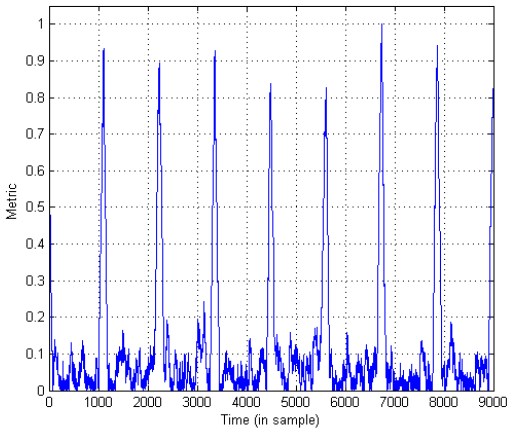

(a) Noiseless case

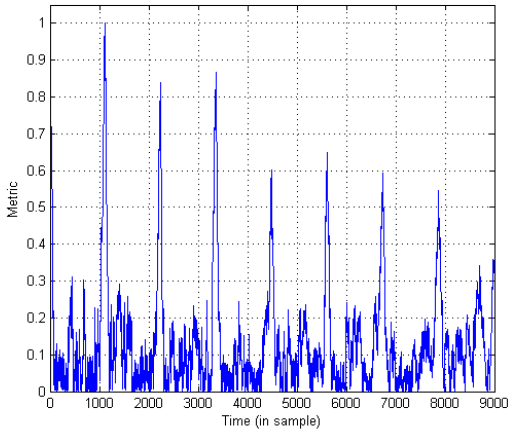

(b) Multipath fading channel (10 dB)

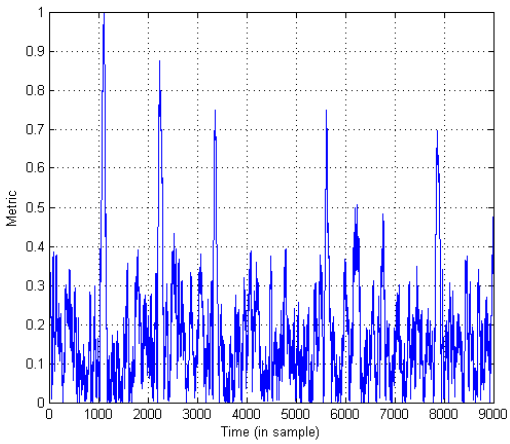

(c) Multipath fading channel (5 dB)

Figure 3.5: Blind ML timing metric of technique [24] for $N_u = 1024$ and $N_g = 102$ samples.

This estimator is attractive because of its low complexity and low overhead, however its performance in fading channels suffers from a severe deterioration. The correlation-based timing metric 3.8, was later adopted for coarse timing synchronization in many standards.

More sophisticated synchronization approaches were later proposed. The estimator in [27]

requires neither the knowledge of the signal-to-noise ratio (SNR) nor the power delay profile of the fading channels and it jointly estimates the TO and FFO. This algorithm is derived by partitioning the received OFDM samples into a few subsets of neighboring uncorrelated entries and treating the channel gains as unknown deterministic variables. Due to this separation, the log-likelihood function, which is based on each subset, is expressed as a function of a parameter associated with channel gains, instead of the channel gains directly. As a result, it does not need the knowledge of the power delay profile of the fading channel. However, the channel maximum delay spread τ_{max} should be known and should be shorter than the CP length N_g. Therefore, this technique can not be considered as totally blind.

By taking advantage of the incurred losses from ISI and ICI which are caused by synchronization errors, the work in [28] proposes a TO estimator based on the maximization of the Signal-to-Interference-and-Noise Ratio (SINR). This estimator does not require neither knowledge of the channel profile nor transmitted data. For complexity reduction, this Maximum SINR based algorithm uses an early-late gate technique which results in a slight performance degradation. The early-late gate technique consists in searching the TO along a limited range instead of the whole one. In [29], the signal statistical information is used to estimate the time synchronization parameters. This estimator is totally blind and it exploits the interference that results due to the loss of orthogonality between sub-carriers. Indeed, the second-order statistics of the resulting interference is proportional to the offset from the optimum sampling point.

Several other blind methods use the cyclostationarity of OFDM signals for time and frequency synchronization. The approach in [30] estimates the TO and the FO either sequentially, by using the cyclic correlation coefficients or independently, by maximizing the cyclic spectrum. This algorithm requires the knowledge of the CIR. This limitation was overcome in the algorithm proposed in [31] where the channel response is modeled by a random process and cyclic correlation is exploited to estimate both TO and FO. In [32], a frequency domain processing is proposed to recover the FO and the TO through power spectrum and spectral correlation computation. This algorithm also does not require any knowledge of the channel state.

To summarize, we highlight that the main advantage of using blind synchronization in OFDM systems is the improvement of the bandwidth efficiency. However, a common problem for most blind synchronization techniques is their sensitivity to multipath distortion. Indeed, most of blind techniques involve significant performance degradation in frequency selective

fading channels, like the estimators proposed in [24], [28] and [29]. Furthermore, information about the SNR and/or CIR might be required in some cases [28, 30].

Since the OFDM technique is the most preferable choice for broadband transmissions over multipath fading channels, the estimation of synchronization parameters should be resilient to multipath distortion. Various methods for time and frequency synchronization are proposed in the literature to enhance the synchronization performance by inserting training sequences, pilots or other types of pre-known data in the transmitted signal. In our work, we address the training sequence based synchronization where specific data are sent at the start of each data frame as a preamble. More specifically, we are concerned with preamble-based methods where a preamble with a priori known structure by the receiver is sent for synchronization purpose. According to the case, the preamble content is not necessarily known to the receiver.

3.2.2 Data-Aided Synchronization

The Data-Aided synchronization techniques are well suited to harsh wireless communication environments for their rapid processing carried in most times directly in time domain without channel knowledge requirement. Furthermore, the use of a specially designed preamble helps the receiver to achieve satisfactory synchronization. Many preamble based synchronization techniques have been proposed to estimate the TO and the FO, either jointly or separately. Hereafter, we address a survey on most used training sequence types for the purpose of synchronization. Then, we investigate the class of existing estimators based on preamble presence for synchronization purpose, which will be relevant as benchmarks for performance comparison with our proposed preamble-based techniques.

3.2.2.1 Training Sequence Types

Training sequences that are used for synchronization generally have common features exploited to provide adequate metric shapes. Their main required property is related to the autocorrelation, which gives the correlation of the sequence with its cyclically shifted versions. For a sequence $B = [b_0, \ldots, b_{N-1}]$, the periodic autocorrelation function R is given by

$$R_{\mathrm{B}}(m) = \frac{1}{N} \sum_{n=0}^{N-1} b_n b_{n-m}^{*}. \tag{3.14}$$

Having sharp correlation peak and very weak out of phase values as is the case for white noise allows more accurate synchronization. Some well-known classes of sequences, such as pseudo random binary sequences, also known as Pseudo-Noise (PN), Constant Amplitude Zero Auto Correlation (CAZAC) sequences, as well as Golay complementary sequences, offering this interesting property are here introduced. It is worth to note that these sequences are widely used in digital communications for a variety of applications such as channel estimation [77] and Direct Sequence Code Division Multiple Access (DS/ CDMA) systems [78].

a) Pseudo-Noise Sequences

A Pseudo-Noise (PN) sequence is a semi-random sequence in the sense that it appears random within the sequence length, fulfilling the needs of randomness, but the entire sequence repeats indefinitely [79]. These sequences have the potential to appear random to the channel but be predictable to the user equipment and are characterized by a large peak to highest side-peak ratio. In the context of synchronization, if the autocorrelation of the sequence used for synchronization presents high side-peaks, the robustness to noise and multipath effect is generally unsatisfactory and the synchronization may miss the first path and in some cases may detect an erroneous path.

M-sequences: as their name indicates, the m-sequences (Maximal length sequences) are the sequences of maximum possible period of $N = 2^m - 1$ where $m \in \mathbb{N}$ [80]. They are obtained from primitive polynomial, using an m-stage binary shift register with linear feedback [81] and can also be generated through shifting an m-sequence [82]. The most interesting property of m-sequences is their two-valued autocorrelation function $(1, -1/N)$. The autocorrelation of an m-sequence B is

$$R_B(m) = \begin{cases} 1 & m = 0, N, 2N, ... \\ -\frac{1}{N} & \text{otherwise.} \end{cases} \tag{3.15}$$

In this respect, for sufficiently long sequences, m-sequences are adequate for synchronization thanks to the absence of side-peaks and low out-of-phase autocorrelation value.

Gold sequences: the Gold sequence class is an important sub-class of m-sequences [83]. They are generated from specific m-sequences, recognized as preferred pairs known to have a minimum value of the out-of-phase cross-correlation. Using gold sequences provides higher peak to highest side-peak ratio which is expected to offer better detection accuracy. It is important to mention that Gold sequences are not defined for m multiples of 4.

Kasami sequences: like the Gold sequences, the Kasami sequences are derived from m-sequences [84] and have the advantage of avoiding the sub-peaks problem in m-sequences. There are two different sets of Kasami sequences: small and large sets. We note that Kasami sequences are defined for only even values of m.

b) CAZAC Sequences

Constant Amplitude Zero Auto-Correlation (CAZAC) sequences are important in waveform design because of their optimal transmission efficiency and tight time localization properties. The first property is guaranteed thanks to the constant amplitude while the second one is guaranteed by the zero autocorrelation of CAZAC sequences. There exists numerous well-known coding sequences among which we can list Chu codes [85, 86], Frank-Zadoff codes [87], generalized Frank sequences [88], and Milewski sequences [89]. The set of CAZAC sequences remains invariant under several operations. For instance, the fast Fourier transform of CAZAC sequence is still a CAZAC sequence [90], which motivates their use in OFDM systems. However, the behavior of side-peaks can differ drastically among the CAZAC families.

c) Golay Complementary Sequences

Golay complementary sequences, also referred to as Golay pairs, have interesting properties that are exploited for synchronization aim. They are characterized by the property that the sum of their autocorrelation functions for the same shift m is zero-valued over all out-of-phase positions.

$$R_b(m) + R_a(m) = 0 \quad m \neq 0. \tag{3.16}$$

Binary Golay sequences are initially defined in [91, 92] for a length of 2^m. This set offers a number of $(2^m m!)$ different sequences. An extension to the case of non-binary sequences was detailed in [93] for number of $(2^{hm} m!)$ different sequences when fixing the constellation size to

h ($2^h PSK$) with $h > 1$.

In addition to the correlation property, Golay sequences are extensively used for the low PAPR value (3 dB) when they are mapped to the OFDM sub-carriers [93, 94].

3.2.2.2 Time Synchronization

The contributions in [15]- [22] exploit preambles of specific structures with different polarity patterns, generally for a predefined sequence type. The receiver, having knowledge of the preamble structure, calculates timing metrics using either sliding autocorrelation, characterized by its low computational load, or differential correlation having higher complexity yet with more accurate detection capacities.

The work proposed by Schmidl and Cox (SC) in [15] uses a training symbol with two identical halves in time domain and estimates the preamble start from the autocorrelation of the received signal. The two halves of the preamble are made identical (in time domain) by transmitting randomly generated sequence on the even frequencies while zeros are transmitted on the odd ones. Transmitted data following the preamble will not be confused with the preamble as all data must contain odd frequencies. Another method to generate the repetitive structure, is to straightforward use an IFFT of half the normal size to generate the time domain sample which has to be repeated (and properly scaled) to form the preamble of two identical parts. The selection of a particular sequence type should not have much effect on the performance of the synchronization algorithm. Instead, the training sequence can be chosen on the basis of being easy to implement or of low PAPR so that there is a little distortion from the transmitter amplifier.

The received signal is affected in magnitude and phase by the frequency selective channel. However, the impact of the channel on both preamble halves is the same, assuming that the channel is constant during the transmission of the preamble (1 symbol duration). Hence, multiplying the samples of the first preamble half with the complex conjugate of the samples of the second half, would cancel the channel effect (phase cancelled and magnitude squared). Therefore, the magnitude of the sum of all the products should be of large value if the summed terms belong to the preamble, whereas the sum output resulting from the data symbols has very low values because of the low correlation between shifted samples not belonging to the

preamble. Let the products sum of each pair of samples be

$$P_{\mathrm{SC}}(d) = \sum_{m=0}^{N_u/2-1} r^*_{d+m} r_{d+m+N_u/2}, \tag{3.17}$$

which, for complexity reduction, can be implemented with the recursive formula

$$P_{\mathrm{SC}}(d+1) = P_{\mathrm{SC}}(d) + r^*_{d+N_u/2} r_{d+N_u} - r^*_d r_{d+N_u/2}. \tag{3.18}$$

We note that d corresponds to the first sample of the observation window. This window slides along in time as the receiver searches for the preamble, hence the name of sliding-correlation. In [15], the window size is fixed to $N_u/2$ samples. The energy of the received second-half preamble is given by

$$R_{\mathrm{SC}}(d) = \sum_{m=0}^{N_u/2-1} \left| r_{d+m+N_u/2} \right|^2, \tag{3.19}$$

which also can be evaluated iteratively as done for the correlation function in equation (3.18). The normalized timing metric can be defined as

$$M_{\mathrm{SC}}(d) = \frac{\left| P_{\mathrm{SC}}(d) \right|^2}{R_{\mathrm{SC}}(d)^2}. \tag{3.20}$$

The SC metric is depicted in figure 3.6 under different channel conditions. This metric exhibits a plateau which has a length equal to that of the CP minus the length of the CIR. Due to the plateau effect, time detection accuracy suffers from uncertainty and large TO estimation variance. To overcome this drawback, Schmidl and Cox propose an averaging method, where two points to the left and right, which are exactly within 90% of the maximum value, are first found. Then, the timing estimate is taken as the middle of these two points. In this way, the preamble start estimate is guaranteed to fall within the plateau, yet the accuracy is still unsatisfactory in terms of providing the maximum tolerance to channel delay spread.

Two timing offset estimators, as modifications of the previous one [15], have been proposed by Minn *et al.* (Minn-A and Minn-B) in [16]. The first method, known as sliding window method (Minn-A), uses the same preamble and proposes two modifications in the timing metric:

- The first modification consists in computing the energy denoted by R_{SWM} over the whole symbol, rather than over the second half in R_{SC} (equation 3.19).
- The second modification is averaging the metric over a window of length $N_g + 1$ instead

of the 90% averaging scheme.

The Modified timing metric is then

$$M_{\mathrm{A}}(d) = \frac{1}{N_g + 1} \sum_{m=-N_g}^{0} M_f(d+m), \tag{3.21}$$

where

$$M_f\left(d\right) = \frac{\left|P_{\mathrm{SC}}\left(d\right)\right|^2}{R_{\mathrm{A}}\left(d\right)^2}, \tag{3.22}$$

and

$$R_{\mathrm{A}}(d) = \sum_{m=0}^{N_u-1} \left|r_{d+m}\right|^2. \tag{3.23}$$

The second method, known as training symbol method (Minn-B), uses a training symbol containing four identical parts of random sequence and inverts the polarity of the two latter ones. The timing metric has the same form as in the previous ones, yet with different correlation function P_{B}

$$P_{\mathrm{B}}\left(d\right) = \sum_{k=0}^{1} \sum_{m=0}^{N_u/4-1} r^*_{d+kN_u/2+m} r_{d+kN_u/2+m+N_u/4}, \tag{3.24}$$

and energy R_{B}

$$R_{\mathrm{B}}\left(d\right) = \sum_{k=0}^{1} \sum_{m=0}^{N_u/4-1} \left|r_{d+kN_u/2+m+N_u/4}\right|^2. \tag{3.25}$$

It is shown in figure 3.6 that the plateau effect disappears in Minn's methods. Nevertheless, the obtained correlation peak is not sufficiently sharp to provide high robustness to noise because of the wide shape in the first modified metric in equation (3.21) and the side-lobes appearing around the main peak of the second metric in equation (3.24).

In [17], Minn extends the previous work (Minn-B) by exploiting a preamble of L identical parts of Golay complementary sequences [91], with certain pattern to give the timing metric a steeper roll-off trajectory at the ideal timing position. Golay complementary sequences are chosen for their specific correlation properties which translate into a low PAPR value (3 dB) when they are mapped to the OFDM sub-carriers [94]. The timing estimation metric is based on the correlation among the L parts of size M samples each. We note that the periodicity of the training symbol equips timing synchronization with robustness against frequency offsets. A larger value of L gives a timing metric trajectory with a steeper roll-off. Some practical L

values that are used are 4, 8 and 16 parts. The timing offset estimation can be improved by designing the signs of the identical parts to give the sharpest possible timing metric trajectory. In this work, both Frequency Domain (FD) OFDM-type preamble and single-carrier-type Time Domain (TD) preamble are investigated.

Based on the previous framework [16,17], a synchronization technique was proposed in [18] by Nasir *et al.*, which uses a preamble of eight identical CAZAC sub-sequences to provide steeper fall off of the timing metric from the strongest correlation point. The choice of CAZAC sequences is justified by having unit PAPR [86]. The creation of the eight identical portions of the preamble is obtained by repeating the FFT of quarter length CAZAC sequence in all the portions. A specific sign pattern is also applied to the eight preamble parts. The timing metric M_{Na} here also corresponds to the correlation function P_{Na} normalized with the energy R_{Na} as

$$M_{\mathrm{Na}}(d) = \left(\frac{L}{L-1} \frac{|P_{\mathrm{Na}}(d)|}{R_{\mathrm{Na}}(d)} \right)^2, \tag{3.26}$$

$$P_{\mathrm{Na}}(d) = \sum_{k=0}^{L-2} b(k) \sum_{m=0}^{M-1} r^*_{d+m+kM} r_{d+m+(k+1)M}, \tag{3.27}$$

and

$$R_{\mathrm{Na}}(d) = \sum_{k=0}^{L-1} \sum_{m=0}^{M-1} |r_{d+m+kM}|^2, \tag{3.28}$$

where $b(k) = p(k)p(k+1)$ for $k = 0, 1, \ldots, L-2$, $p(k)$ for $k = 0, 1, \ldots, L-1$ denote the signs of the repeated parts of the training symbol. As shown in figure 3.6, when compared to Minn's approaches, a steeper fall-off of the timing metric from the strongest correlation point is here provided and side-lobes problem is avoided.

In [19], Chou *et al.* proposed time synchronization technique with Zero Padded (ZP) preambles. Two modified preamble patterns are proposed as modified versions compared to [15] and [16] and using almost the same metrics designed to these preambles. The major benefit of zero padding is to shorten the length of the correlation function for complexity reduction. These preambles have the potentials to reduce the computational complexity without degrading the system performance. Indeed, the N_z padding samples in each repetitive part are not calculated in the correlations function. Therefore, the computation complexity of the estimator can be reduced and the acquiring time of estimation can be decreased. Using the first ZP preamble (based on [15]), the metrics in equations (3.17) and (3.24) are here calculated using a correlation window of size $N_u/2 - N_z$. When inserted in the tail of the preamble, the zero

symbols are duplicated in the CP. If $N_z > N_g$, the CP becomes a full zero block. This property can be exploited to eliminate the effect of the plateau of the initial estimator. It is important to note that very large values of N_z may degrade the system performance in low SNR, while very short values provides almost the same performance as the initial algorithms. An optimum value of N_z is fixed to 10% of the repetitive part size ($N_u/2$ in [15] and $N_u/4$ in [16]). The metric of Chou's approach is drawn in figure 3.6. It is shown that the side-lobes are attenuated and the metric has almost the same shape as in the technique proposed by *Nasir et al.* in [18].

Later, a new Precoding Method (PM) was proposed in [21] and [22] for TO and FFO estimation, operating respectively in the AWGN and multipath channels. The preamble symbol is made from the concatenation of two equal-length sequences $\mathbf{s}_1$ and $\mathbf{s}_2$ related between them through differential modulation as $\mathbf{s}_2 = \mathbf{s}_1 \bigodot \mathbf{c}$, where $\mathbf{c}$ is an adequately designed precoding sequence and $\bigodot$ denotes the element-wise product operator. This structure leads to almost perfect channel autocorrelation profile with sharp in-phase peak and zero out-of-phase correlation. Unlike the approaches [15, 16], the choice of the sequences $\mathbf{s}_1$ and $\mathbf{c}$ is of crucial importance. They must be judiciously chosen such to have an important correlation property to provide good detection performance. The m-sequences [80] known by having specific correlation properties making them suitable for synchronization purpose were considered. The precoding method uses two m-sequences ($\mathbf{s}_1$ and $\mathbf{c}$) to generate the time domain preamble which consists of the concatenation of $\mathbf{s}_1$ and $\mathbf{s}_2$. For a judicious choice, a preferred pair of m-sequences is selected for which the above mentioned correlation property is better verified than arbitrary chosen subsequences. To detect the preamble start, the idea is to search for two strongly correlated symbol halves through the metric

$$M_{\mathrm{PM}}(d) = \frac{|P_{\mathrm{PM}}(d)|^2}{R_{\mathrm{PM}}(d)^2}, \tag{3.29}$$

where

$$P_{\mathrm{PM}}(d) = \sum_{m=0}^{N_{um}/2-1} r^*_{d+m} r_{d+m+N_{um}/2} c^*_m, \tag{3.30}$$

and

$$R_{\mathrm{PM}}(d) = \sum_{m=0}^{N_{um}/2-1} \left| r_{d+m+N_{um}/2} \right|^2, \tag{3.31}$$

where $N_{um} = N_u - 2$ corresponds to the preamble length, which is 2 samples shorter than the OFDM symbols due to the nature of m-sequences whose length is $2^m - 1$ samples. In this case, to keep the same length as for OFDM symbols, the CP is appended with 2 samples and

is denoted by N_{gm}.

The metrics of the previously described DA approaches are illustrated in figure 3.6. It is shown that the SC metric [15] exhibits a plateau of length equal to the CP length minus the channel memory. This plateau disappears in the other methods [16, 18, 19], but some sidelobes appear. Due to the multipath effect, the plateau in the CS metric becomes shorter and the other metrics widen around their maximum, leading to performance degradation and reduced robustness to noise. The approach in [21] presents a metric with a sharp peak at the correct preamble start, which is expected to greatly enhance the time synchronization performance. This peak is attenuated and other side sub-peaks appear in the multipath channel.

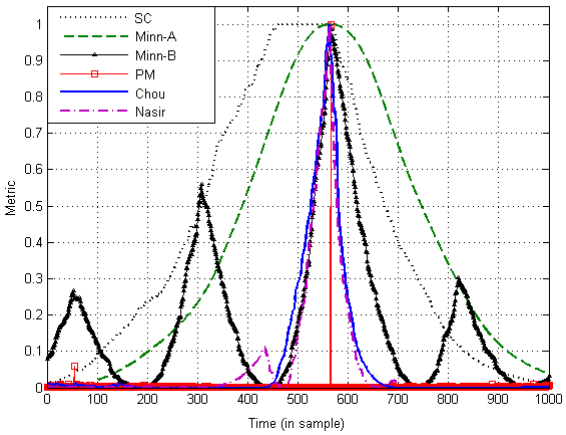

(a) Noiseless case

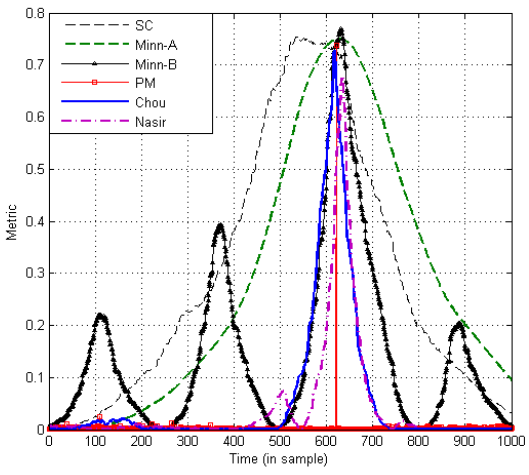

(b) Multipath fading channel (10 dB)

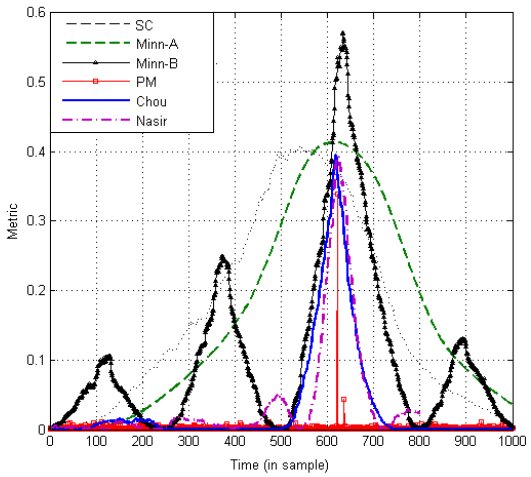

(c) Multipath fading channel (5 dB)

Figure 3.6: Preamble-based timing metrics of techniques [15, 16, 18, 19, 21] for $N_u = 1024$, $N_{um} = 1022$, $N_g = 102$ and $N_{gm} = 104$ samples.

Now comparing the illustrative metric curves in figure 3.6 for preamble based synchronization metrics and figure 3.5 for blind synchronization metric. We observe that in the noiseless case and at relatively high SNR values, both concepts offer distinguishable reference time index, which corresponds to the start of each OFDM symbol in the case of NDA approaches while it corresponds to the preamble start in the DA approaches. Hence, the time synchronization can be achieved with a minimum of required detection accuracy. However, in practical wireless communication selective-channel, the blind metric curve is almost deteriorated resulting in a high symbol start missing rate. In the other hand, data aided metrics always remain able to discern the preamble among the OFDM data symbols, which justifies their suitability to be used in broadband communication systems.

3.2.2.3 Frequency Synchronization

Similarly to the symbol timing synchronization, the CFO estimation can be performed either blindly or exploiting a preamble. It is well known that the blind frequency estimation methods like [24]- [28] suffer from the multipath fading effects, so their performance is usually worse than that of preamble-based methods in realistic wireless communication environments. Some well-known preamble-based CFO estimators are briefly reviewed in this section.

Moose [51] proposed an estimator based on the observation of two consecutive identical symbols. Assuming perfect time synchronization, a ML estimator similar to that in [24] is proposed for the CFO recovery in the frequency domain after applying the FFT on the received signal. The acquisition range is limited to the $\pm\frac{1}{2}$ the sub-carrier spacing. It was shown that it is possible to increase this range through the use of shorter training symbols. For example, using a training symbol of length equal to half the initial one would double the range of carrier frequency acquisition. This scheme works well up to a certain point, where the CFO estimate gets worse as the symbols get shorter. This is produced because the part of the training symbols that is cyclically repeated in the CP should be longer than the CIR in order to avoid ISI, which may deteriorate the step of estimating the frequency offset.

Exploiting the training symbol of two identical parts, Schmidl and Cox [15] showed that the main difference between the two halves is a phase shift equal to

$$\phi = \pi\Delta_{f_c}, \tag{3.32}$$

whose fractional part ν can be calculated exploiting the time estimate in equation (3.20) as

$$\hat{\phi} = \angle(P_{CS}(\hat{\tau})), \tag{3.33}$$

where $\hat{\tau}$ stands for the preamble start estimate. As $|\hat{\phi}|$ can be guaranteed to be lower than π, then the FFO estimate is given by

$$\hat{\nu} = \frac{\hat{\phi}}{\pi}. \tag{3.34}$$

In [52], Morelli and Mengali extended the idea of using repetitive structure exploiting more than two identical parts. This scheme constructs a number of component estimators based on different pairs of the identical parts in the training symbol. Then it combines these components using the Best Linear Unbiased Estimator (BLUE) principle. This makes it possible to achieve better accuracy at the cost of some increase in computational load.

Later, under the assumption of known SNR, Minn *et al.* [53, 54] proposed several methods to take advantage of the SNR knowledge for further performance improvement based on [52]. Frequency domain, post-FFT ML estimators based on optimal training sequences known at the receiver, such as the orthogonal sequences with constant modulus, have been proposed in [55] and [56]. The first estimator assumes perfect time synchronization and knowledge of the CIR to deduce a null subspace based IFO estimator by exploiting the metric below

$$\hat{\nu} = \underset{\tilde{\nu}}{\operatorname{argmin}} \left\{ \left\| \bar{\mathbf{W}}_{N_p+1}^{H} \mathbf{D}_l \mathbf{W} \mathbf{y}_l \right\|^2 \right\}, \tag{3.35}$$

where $\bar{\mathbf{W}}_{N_p+1}$ stands for the null subspace of $\mathbf{W}$ which contains its last $N_u - N_p + 1$ columns, $\mathbf{D}_l = \mathrm{diag}[s_{l,0}, s_{l,1}, \ldots, s_{l,N_u-1}]^T$ and $\tilde{\nu} \in [-0.5, 0.5]$ is the range of the frequency offset ν. To face the strict requirement of perfect time synchronization, this estimator has been reformulated in [56] to perform joint TO and FO estimation. However, an exhaustive search possible combination values of ν and τ is required thus leading to high computational load.

Conclusions

In its first part, this chapter has investigated the effects of time and frequency synchronization imperfections on OFDM signal. The types of synchronization errors considered includes time and frequency offsets. It was shown that time offset introduces interference between adjacent

received symbols and between sub-carriers belonging to the same symbols. These interferences generally result in important performance degradation due to the loss of orthogonality between sub-carriers. Thus, synchronization is considered as one of the biggest challenges in any OFDM communication system.

In the second part, a state of art on existing synchronization approaches to combat time and frequency errors' effects was also provided. Based on the information required for synchronization at the receiver end, a classification of the synchronization techniques into data-aided and non-data-aided was adopted. Non data aided, or blind approaches generally exploit the redundancy in the CP or the intrinsic properties in the received signal to provide the synchronization parameters. Among existing data aided approaches we described some of the preamble based ones. The considered approaches exploit preambles of specific structure of either repetitive parts or parts related between each other. Before describing synchronization approaches, we have made a brief review on different types of sequences that are used for synchronization purpose. All of the above OFDM synchronization methods are associated with one or more of the following limitations or drawbacks: lack of robust detection capability in multipath channel [15], large estimation variance [16], high computational complexity [21, 56], channel and/or SNR knowledge requirement [53]- [55].

To overcome these limitations, we propose in the next chapter an efficient and reduced complexity synchronization approach. Timing synchronization is investigated using one preamble composed of two identical parts made of either random training sequence or specific training sequence with specific properties. As a byproduct, fractional frequency offset will also be estimated respecting the algorithm of Schmidl and Cox [15].

Chapter 4

Simply Differential Synchronization: Average Performance

In this chapter, we propose two new synchronization techniques for OFDM systems which exploit a preamble of two identical randomly generated training sub-sequences. The preamble is sent at the start of the transmission in bursty transmission mode and in a regular manner in continuous transmission mode. The synchronization process, here, focuses on detecting the start of the preamble and estimating the fractional part of the carrier frequency offset.

This chapter starts with a description of the synchronization processing in its two versions: Brute-Force (BF) single-stage and Reduced-Complexity (RC) two-stage proposed in [33, 34]. The BF approach proposes a metric based on differential correlation that exhibits a high sharp peak at the start of the preamble. To evaluate the proposed BF approach, theoretical and experimental performance studies are conducted, first developed in the OFDM modulation [36], and then in the case of DMT modulation [41]. Experimental results are found to agree with the analytical results reasonably well and confirm both the validity of theoretical performance study and the relevance of the proposed method in various MCM techniques and channel conditions.

High detection accuracy is provided by the BF approach at the expense of a huge computational load due to the differential correlation operations. To overcome this disadvantage, we suggest to split the BF synchronization processing into two stages. The first stage, based on sliding correlation metric, provides a coarse time estimate around which an uncertainty

interval is determined. The second stage is based on a differential correlation carried over the uncertainty interval. By limiting the uncertainty interval length, an important reduction in the computational load is realized. The BF single-stage approach, is considered as a benchmark to assess the performance degradation occasioned by the reduction of complexity characterizing the proposed RC two-stage approach.

Furthermore, the fractional part of the frequency offset is derived in both the BF and the RC approaches as an offshoot using the same timing metrics. Its evaluation also shows an enhancement compared to the considered benchmarks.

Later, to concretize the challenging performance reached in the general MCM systems, the proposed RC and BF techniques are applied to the IEEE 802.11a/g standards which incorporate preambles with specific structures allowing the transposition of the proposed method to their signals. The aim of this study is to assess the suitability of the proposed techniques be implemented in the considered standards [39].

4.1 Brute Force Synchronization Approach

The proposed Brute Force (BF) synchronization approach exploits a preamble of length N_u samples having two identical parts, each composed of $L_u = N_u/2$ samples. The preamble is denoted by $\boldsymbol{p} = [p_0, p_1, \ldots, p_{N_u-2}, p_{N_u-1}]$. As its halves are identical, the preamble samples can be denoted as $\boldsymbol{p} = [\boldsymbol{p}_1, \boldsymbol{p}_1]$ with $\boldsymbol{p}_1 = [p_0, p_1, \ldots, p_{L_u-1}]$. Preamble-based synchronization techniques generally use correlation-based metrics to locate the preamble. Different forms of correlation are used; sliding-correlation as in [15, 16] or differential-correlation as in [20–22]. Although differential correlation is costly in terms of computational complexity, it is here chosen for its high accuracy.

4.1.1 Brute Force Metric

The BF metric performs a differential correlation along the whole synchronization process. This processing consists in correlating a differentially modulated version of the received signal, which we denote by Y, with a Correlation Sequence (CS) deduced from the preamble subsequence. The CS, which we denote by α, has a length of L_u samples and it is also generated

through differential correlation respecting a shift q as follows

$$\alpha(d) = p_d^* p_{d+L_u+q} = p_d^* p_{d+q}. \tag{4.1}$$

The CS α is known at the receiver, where the synchronization processing starts by generating the new differentially modulated sequence Y from the received OFDM signal r as

$$Y(d) = r_d^* r_{d+q}. \tag{4.2}$$

Then, it multiplies each d^{th} sample of the differentially modulated sequence Y with the complex conjugate of the $(d \bmod L_u)^{\text{th}}$ sample of the CS α, sums these products and finally takes their squared amplitude normalized by the energy. The BF metric is expressed as

$$M(d) = \left(\frac{|P(d)|}{R(d)} \right)^2, \tag{4.3}$$

where

$$P(d) = \sum_{m=0}^{L_u-1} \alpha^*(m) Y(d+m), \tag{4.4}$$

and

$$R(d) = \sum_{m=0}^{L_u-1} |Y(d+m)|^2. \tag{4.5}$$

The arrival time of the preamble which we denote by τ is defined as $\tau = t_0 + \epsilon$, where t_0 stands for the preamble transmission start time and ϵ is the time propagation delay of the shortest path, and its estimate $\hat{\tau}$ is selected as the argument d that maximizes the metric M in equation (4.3). The choice of the correlation shift q is crucial in the proposed metric. Indeed, for q values equal to 0 or L_u, the metric exhibits a plateau thus penalizing the estimation accuracy. Yet, any other choice of the shift $q \in [1, L_u - 1]$ provides a metric with high sharp peak. The metric curve of the BF approach is depicted in figure 4.1, in which we consider an OFDM signal with $N_u = 1024$ sub-carriers, a guard interval of $N_g = 102$ samples, the correlation shift $q = 1$ and random data of length equal to L_u are sent before the preamble. It is shown that the pronounced peak coincides with the start of the preamble useful part which provides a high detection accuracy. To assess the performance of the BF approach, experimental and theoretical results, in both OFDM and DMT modulations, are carried and presented in the next two sections.

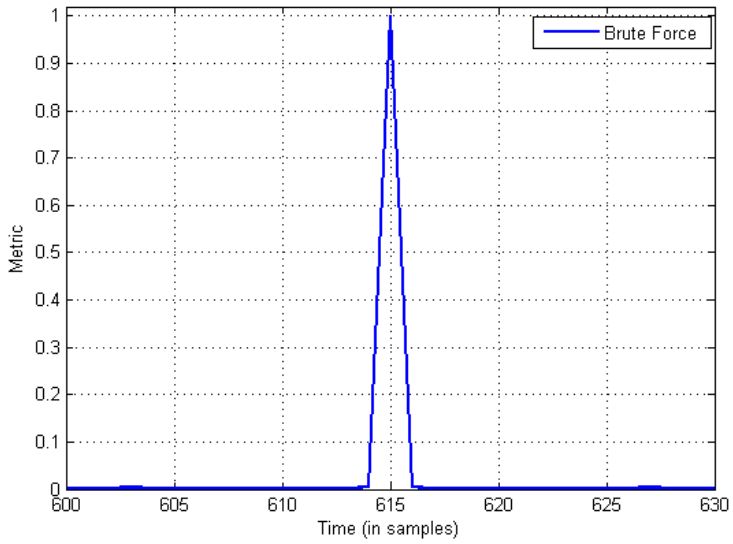

Figure 4.1: Brute-Force timing metric in the noiseless case for $L_u = 512$, $N_g = 102$ and $q = 1$.

4.1.2 Performance Study of the BF Time Synchronization for OFDM Modulation

Since the timing metric is used to determine whether a received sample r_d coincides with the preamble start or not, we evaluate the performance of the preamble start estimator through the criteria of analytical Probability of Correct Detection (PCD) and experimental Correct Detection Rate (CDR). The **PCD** is defined as the probability that, for all values of the time index d, the amplitude of the timing metric $M(d)$ (in equation (4.3)) is lower than that of $M(\tau)$, were τ stands for the correct preamble start. The **CDR**, is determined through Monte Carlo simulations and is defined as the rate of trials where the estimated preamble start $\hat{\tau}$ exactly coincides with the effective preamble start τ (no error tolerance).

4.1.2.1 Probability of Correct Detection

To calculate the PCD of the proposed approach, we first need to model and characterize the timing metric M expressed in (4.3). We do not consider the normalization by the energy in equation (4.5) and we calculate the metric over an interval of width $\Delta\tau$. Substituting (4.1) and (4.2) in (4.4), the BF metric yields

$$M(d) = \sum_{m=0}^{L_u-1} r^*_{d+m} r_{d+m+q} p_m p^*_{m+q}. \tag{4.6}$$

Now, recalling the expression of the received signal r_d in (3.7), in which we consider the effect of a multipath channel of finite impulse response length L_H, assumed to be shorter than the CP length N_g, and coefficients denoted by h_i, $\{i = 0, ..., L_H - 1\}$ (h_i is null for i out of the set of the effective N_p paths' positions). The channel also introduces a zero-mean AWGN with energy E_η. The d^{th} received sample is then expressed as

$$r_d = \sum_{i=0}^{L_H-1} h_i s_{d-i} + \eta_d, \tag{4.7}$$

where s_d belongs to a circular constellation modulating a symbol with energy E_s. In the following, we suppose that the preamble is the first sent symbol, so that $s_d = p_d$ for all values of d in $[0, N_u - 1]$. Inserting (4.7) in (4.6), the metric turns into

$$\begin{aligned} M(d) &= \sum_{m=0}^{L_u-1} \left[\left(\sum_{i=0}^{L_H-1} h_i s_{d+m-i} + \eta_{d+m} \right)^* \left(\sum_{j=0}^{L_H-1} h_j s_{d+m+q-j} + \eta_{d+m+q} \right) s_m s^*_{m+q} \right] \\ &= \sum_{m=0}^{L_u-1} \left(\sum_{i=0}^{L_H-1} \sum_{j=0}^{L_H-1} h^*_i h_j s^*_{d+m-i} s_{d+m+q-j} s_m s^*_{m+q} + \sum_{i=0}^{L_H-1} h^*_i s^*_{d+m-i} \eta_{d+m+q} s_m s^*_{m+q} + \right. \\ &\left. \sum_{j=0}^{L_H-1} h_j s_{d+m+q-j} \eta^*_{d+m+q} s_m s^*_{m+q} + \eta^*_{d+m} \eta_{d+m+q} s_m s^*_{m+q} \right). \end{aligned} \tag{4.8}$$

a) Statistical Analysis

The metric expressed in (4.8) sums up L_u random variables. Assuming the independence between the summed terms and for L_u sufficiently large, the Central Limit Theorem (CLT) enables to approximate $M(d)$ by a Gaussian distribution [95]. Consequently, $M(d)$ can be completely characterized by its mean μ_d and variance σ^2_d, which are hereafter derived.

The mean μ_d corresponds to the expectation of the metric ($E(M(d))$). Since s_d and η_d are mutually uncorrelated and η_d is centered, the second and third terms of (4.8) have zero mean. As η_d is white and $q \neq 0$, the last term in (4.8) is also zero mean. Then, the mean value of

$M(d)$ reduces to

$$\begin{aligned} E(M(d)) &= \sum_{m=0}^{L_u-1} E\left(\sum_{i,j=0}^{L_H-1} h_i^* h_j s_{d+m-i}^* s_{d+m+q-j} s_m s_{m+q}^* \right) \\ &= \sum_{m=0}^{L_u-1} \sum_{i,j=0}^{L_H-1} h_i^* h_j E\left(s_{d+m-i}^* s_{d+m+q-j} s_m s_{m+q}^* \right). \end{aligned} \tag{4.9}$$

The expectation in (4.9) is non zero (and hence the mean μ) only for time index $d = i = j$, where d coincides with an effective path ($h_d \neq 0$). Then, the last expression (4.9) becomes

$$E(M(d)) = \sum_{m=0}^{L_u-1} |h_d|^2 E\left(|s_m|^2 |s_{m+q}|^2 \right) L_u |h_d|^2 E_s^2. \tag{4.10}$$

For all the other values of d, the expectation is zero because the samples s_{d+m-i}^*, $s_{d+m+q-j}$, s_m and s_{m+q}^* are mutually uncorrelated.

Now, to calculate the variance σ_d^2, we first need to determine $E(|M(d)|^2)$. Once again, we use the fact that the samples s_d and η_d are uncorrelated, which leads to a zero valued expectation of the cross terms in $E(|M(d)|^2)$. This latter is then expressed as

$$\begin{aligned} E(|M(d)|^2) = \sum_{m,m'=0}^{L_u-1} \Bigg(& \sum_{i,j,i',j'=0}^{L_H-1} h_i^* h_j h_{i'} h_{j'}^* E\left[s_{d+m-i}^* s_{d+m+q-j} s_m s_{m+q}^* s_{d+m'-i'} s_{d+m'+q-j'}^* s_{m'}^* s_{m'+q} \right] \\ & + \sum_{i,i'=0}^{L_H-1} h_i^* h_{i'} E\left[s_{d+m-i}^* \eta_{d+m+q} s_m s_{m+q}^* s_{d+m'-i'} \eta_{d+m'+q}^* s_{m'}^* s_{m'+q} \right] \\ & + \sum_{j,j'=0}^{L_H-1} h_j h_{j'}^* E\left[s_{d+m+q-j} \eta_{d+m+q}^* s_m s_{m+q}^* s_{d+m'+q-j'} \eta_{d+m'+q} s_{m'}^* s_{m'+q} \right] \\ & + E\left[\eta_{d+m}^* \eta_{d+m+q} s_m s_{m+q}^* \eta_{d+m'} \eta_{d+m'+q}^* s_{m'}^* s_{m'+q} \right] \Bigg). \end{aligned} \tag{4.11}$$

In the case where d coincides with an effective path, the expression (4.11) becomes

$$\begin{aligned} E(|M(d)|^2) = & L_u^2 |h_d|^4 E_s^4 + L_u \sum_{i,j=0}^{L_H-1} |h_i|^2 |h_j|^2 E_s^4 - L_u |h_d|^4 E_s^4 + 2L_u \sum_{i=0}^{L_H-1} |h_i|^2 E_s^3 E_\eta \\ & + L_u E_\eta^2 E_s^2. \end{aligned} \tag{4.12}$$

In the other case, where d falls out of the set of effective paths, it becomes

$$E(|M(d)|^2) = L_u \sum_{i,j=0}^{L_H-1} |h_i|^2 |h_j|^2 E_s^4 + 2L_u \sum_{i=0}^{L_H-1} |h_i|^2 E_s^3 E_\eta + L_u E_\eta^2 E_s^2. \tag{4.13}$$

As mentioned above, for these values of time index d, the mean $\mu_d = 0$. Hence, the variance $\sigma_d^2 = E(|M(d)|^2)$. Otherwise, for d corresponding to an effective path, the variance of the metric yields

$$\sigma_d^2 = L_u \sum_{i,j=0}^{L_H-1} |h_i|^2 |h_j|^2 E_s^4 - L_u |h_d|^4 E_s^4 + 2L_u \sum_{i=0}^{L_H-1} |h_i|^2 E_s^3 E_\eta + L_u E_\eta^2 E_s^2. \tag{4.14}$$

Note that the monopath AWGN channel, reduces to a channel with a single path ($L_H = 1$) whose gain is $h_0 = 1$.

b) Approximated Probability of Correct Detection

The probability of correct detection is defined as the probability that, for all values of the time index d within the interval $\Delta\tau$, the amplitude of the timing metric $|M(d)|$ is lower than that of the correct preamble start $|M(\tau)|$. Let us denote the value of $|M(\tau)|$ (at the correct preamble start) by ε. Now assuming the independence between the different values of $|M(d)|$ and $|M(\tau)|$ for $d \neq \tau$, the probability of correct detection is expressed as

$$\text{PCD} = \int_0^{+\infty} \prod_{d \neq \tau} F_d(\varepsilon) P_\tau(\varepsilon) \mathrm{d}\varepsilon, \tag{4.15}$$

where $F_d(\varepsilon)$ stands for the Cumulative Distribution Function (CDF) of the metric at the time index d and $P_d(\varepsilon)$ stands for the Probability Density Function (PDF) of $|M(d)|$.

For notational convenience, we introduce the random discrete variable X, corresponding to $|M(d)|$. We recall that X is non-uniformly Gaussian distributed. The CDF is calculated for positive values of ε because we consider the metric amplitude. The CDF F_d in the probability expression (4.15) is determined as follows

$$\begin{aligned} F_X(\varepsilon) &= P(X \leq \varepsilon) = P(M(d) \leq \varepsilon) + P(-M(d) \leq \varepsilon) \\ &= \int_0^{\varepsilon} \frac{1}{\sqrt{2\pi\sigma^2}} e^{\frac{-(x-\mu)^2}{2\sigma^2}} \mathrm{d}x + \int_{-\varepsilon}^{0} \frac{1}{\sqrt{2\pi\sigma^2}} e^{\frac{-(x-\mu)^2}{2\sigma^2}} \mathrm{d}x. \end{aligned} \tag{4.16}$$

Applying variable change of x by $x' = \frac{x-\mu}{\sigma}$, we get

$$\begin{aligned} P(X \leq \varepsilon) &= \frac{1}{\sqrt{2\pi\sigma^2}} \int_{\frac{-\varepsilon-\mu}{\sigma}}^{\frac{\varepsilon-\mu}{\sigma}} e^{-\frac{x'^2}{2}} \sigma \mathrm{d}x' \\ &= \frac{1}{\sqrt{2\pi}} \int_{\frac{-\varepsilon-\mu}{\sigma}}^{+\infty} e^{-\frac{x'^2}{2}} \mathrm{d}x' - \frac{1}{\sqrt{2\pi}} \int_{\frac{\varepsilon-\mu}{\sigma}}^{+\infty} e^{-\frac{x'^2}{2}} \mathrm{d}x'. \end{aligned} \tag{4.17}$$

To evaluate the integral in the equation above (eq. (4.17)), we use the Marcum Q function which finds its origin in expressing the performance of digital communication systems [64,101]. It is to be noted that the closed-form expressions in (4.17) deals only with integrands involving the first-order Marcum function in which Q is defined as $Q(x) = \frac{1}{\sqrt{2\pi}} \int_x^{\infty} e^{-\frac{u^2}{2}} \mathrm{d}u$. Hence, the final expression of the CDF turns into

$$P(X \leq \varepsilon) = \mathrm{Q}\left(\frac{-\varepsilon-\mu}{\sigma}\right) - \mathrm{Q}\left(\frac{\varepsilon-\mu}{\sigma}\right). \tag{4.18}$$

Now, we determine the PDF at the correct preamble start τ. To this end, we can derive the CDF expressed in (4.18) that gives

$$P_\tau(\varepsilon) = \frac{1}{\sqrt{2\pi\sigma_\tau^2}} \left(e^{\frac{-(\varepsilon-\mu_\tau)^2}{2\sigma_\tau^2}} + e^{\frac{-(-\varepsilon-\mu_\tau)^2}{2\sigma_\tau^2}} \right), \tag{4.19}$$

where μ_τ and σ_τ^2 stand respectively for mean and variance of the timing metric amplitude $|M(\tau)|$ at the correct preamble start.

4.1.2.2 Numerical and Simulation Results

The performance of the BF synchronization scheme is considered in the AWGN and multipath channels over a practical SNR range. The interval $\Delta\tau$, over which the metric evaluation is carried, is set to N_g. Under the assumption that the samples are modeled as independent Gaussian random variables, the PCD in (4.15) becomes

$$\mathrm{PCD} = \begin{cases} \int_0^{+\infty} \left(F_d(\varepsilon)\right)^{N_g-1} P_\tau(\varepsilon) d\varepsilon, \quad \text{AWGN channel} \\ \\ \int_0^{+\infty} \left(F_{d \notin \tilde{N}_p}(\varepsilon)\right)^{N_g-N_p} \prod\limits_{d \neq \tau} \left(F_{d \in \tilde{N}_p \setminus \tau}(\varepsilon)\right) P_\tau(\varepsilon) d\varepsilon, \quad \text{Multipath channel,} \end{cases} \tag{4.20}$$

where $\tilde{N}_p$ corresponds to the set of N_p effective paths (with non-zero gain). In (4.20), for d out of the set of channel effective paths, F_d can be chosen arbitrarily from any of the time indexes, as they are identically distributed ($d \in \Delta\tau \setminus \tilde{N}_p$).

For the experimental evaluation, we use Matlab simulations and average over 10^4 Monte Carlo trials for an OFDM system with $L_u = 2^9 = 512$, $N_g = 102$ and we set the correlation shift q to 1. The preamble training sequence is generated randomly and, like the data symbols, it is taken from QPSK modulation. We evaluate the approximated PCD (4.20) for the AWGN and multipath channels. The considered multipath channel has 7 paths ($N_p = 7$) uniformly separated by 6 samples and an exponential power delay profile. Consequently, the channel impulse response length is $L_H = 42$ samples. The ratio of the first path to the last path is set to 12 dB with regular adjacent paths gain ratio.

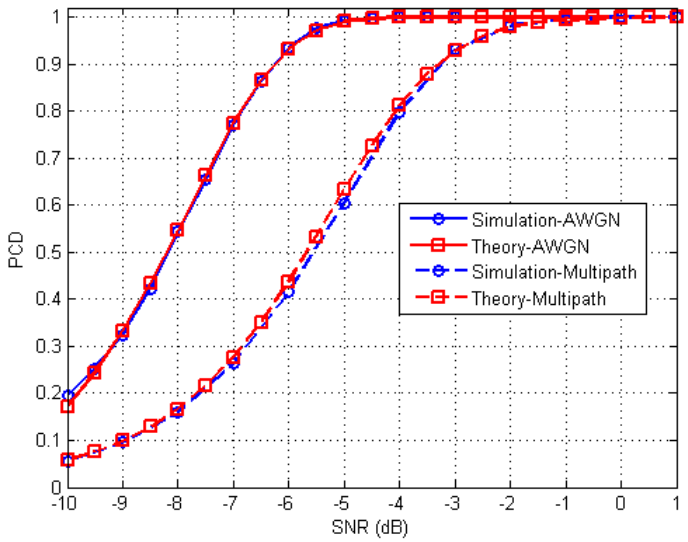

Figure 4.2: Probability/rate of correct detection of the preamble start for OFDM modulation.

Figure 4.2 illustrates the probability of correct detection in the considered channels. As shown in the figure, in the AWGN channel, the analytical probability concords perfectly with the simulated one. In the multipath channel, the experimental curve matches the numerical curve very well for SNR values lower than -6 dB and higher than -3 dB. In between, the theoretically approximated values of the PCD are very close to the experimental values. A very slight gap of about 0.1 dB emerges. This gap may be related to the validity limits of the assumption of independence between the timing metric values, which may be corrupted in the case of multipath channel due to the channel memory. Roughly, the good match obtained

between the theoretical and the experimental results proves that the assumptions made in the analysis are valid and the simulation results confirm the theoretical analysis.

It is worth to note that both of the analytical and the experimental results prove the efficiency of the proposed synchronization technique. Indeed, as shown in figure 4.2, the preamble start detection becomes perfect (PCD= 1 and CDR=1) from SNR values of -5 dB and -1 dB in the AWGN and multipath channels respectively. These results show a very good robustness to noise effects for both channels. This is obtained thanks to the differential correlation which however, as will be shown later, leads to high computational load. The relevance of the BF approach is also assessed in the case of DMT modulation which presents some specificities when compared to the above OFDM case study.

4.1.3 Performance Study of the BF Time Synchronization for DMT Modulation

The Discrete Multi-Tone (DMT) modulation technique is considered as the baseband and wired version of the OFDM technique. Similarly to the OFDM technique, the DMT technique splits the channel into N_u equally spaced sub-channels and transmits data in parallel over these non-overlapped narrow-band sub-channels. If the DMT signal contains $N_u/2$ sub-carriers, the discrete time signal can be obtained from a N_u-point IFFT [97]. Denoting $c_k = a_k + jb_k$ the constellation point that modulates the k^{th} tone, $k = 1, 2, ..., N_u/2 - 1$, during the l^{th} DMT symbol, then s_l is expressed as

$$s_l = \sum_{k=0}^{N_u-1} c_k e^{j2\pi kl/N_u}. \tag{4.21}$$

In order to generate a real signal, the symbols fed to the IFFT must satisfy: $c_{N_u-k} = c_k^*$ on each tone k, $k = N_u/2+1, ..., N_u-1$. For DMT systems, data symbols are also extended with a CP.

The effect of synchronization errors in DMT systems was analyzed in [97], which are almost the same as in the case of OFDM technique. The main difference is that the channel is invariant, thus eliminating the Doppler effects and the transmission is baseband which avoids any frequency offset. Having almost the same properties, DMT systems also require accurate synchronization to obtain satisfactory performance. This issue was studied in many works [98]-[100] either in the general case of the DMT modulation technique or respecting a standard. In

this section, we evaluate the performance of the proposed BF approach for the DMT modulation in terms of probability of preamble start correct detection. Indeed, the closed form analytical expression of the PCD is derived and compared to the experimental CDR.

4.1.3.1 Probability of Correct Detection

We consider the timing metric expressed in (4.6), which sums L_u random variables and with distribution approximated by a Gaussian distribution respecting the CLT, assuming the independence of the metric $M(d)$ L_u summed terms. The same trend as envisaged in the OFDM case is here followed to derive the mean μ_d and the variance σ_d^2 of $M(d)$. Regarding the detailed expression in (4.8), since s_d and η_d are mutually uncorrelated, the second and third terms in (4.8) have zero-mean. As η_d is white and $q \neq 0$, the last term of (4.8) is also zero mean. Then, $M(d)$ reduces to the same expression as in the case of OFDM in equation (4.9). Differently, here for real-valued received signal, the mean μ_d which corresponds to the expectation of the timing metric is expressed as

$$\begin{aligned} E(|M(d)|) &= \sum_{m=0}^{L_u-1} \left(|h_d|^2 \, E(|s_m|^2 \, |s_{m+q}|^2) + |h_{d-q}| \, |h_{d+q}| \, E(|s_m|^2 \, |s_{m+q}|^2) \right) \\ &= L_u E_s^2 \left(|h_d|^2 + |h_{d-q}| \, |h_{d+q}| \right). \end{aligned} \tag{4.22}$$

We note that, like the case of OFDM metric, for the values of d that correspond to an effective path ($d = i = j$), the expectation is not zero-valued. For the other values of d, the expectation is not zero-valued only when their q-shifted indexes also correspond to an effective path. Otherwise, the mean μ_d is null.

To calculate $E(|M(d)|^2)$, we use once again the fact that s_d and η_d are uncorrelated which leads to a zero-valued expectation of the cross terms of $E(|M(d)|^2)$ expressed in (4.11). Exploiting the same properties of uncorrelation between samples and the fact that the noise is centered, $E(|M(d)|^2)$ can be further simplified. Hence, for d values coinciding with an effective

path, $E(|M(d)|^2)$ is given by

$$\begin{aligned} E(|M(d)|^2) =& L_u^2 \left|h_d\right|^4 E_s^4 + L_u \sum_{i,j=0}^{L_H-1} \left|h_i\right|^2 \left|h_j\right|^2 E_s^4 - L_u \left|h_d\right|^4 E_s^4 + \\ & 2L_u \sum_{i=0}^{L_H-1} \left|h_i\right|^2 E_s^3 E_\eta + L_u E_\eta^2 E_s^2 + (L_u^2 - L_u) h_{d-q}^2 h_{d+q}^2 E_s^4. \end{aligned} \tag{4.23}$$

In the other case, where d falls out of the set of paths, $E(|M(d)|^2)$ becomes

$$E(|M(d)|^2) = L_u \sum_{i,j=0}^{L_H-1} \left|h_i\right|^2 \left|h_j\right|^2 E_s^4 + 2L_u \sum_{i=0}^{L_H-1} \left|h_i\right|^2 E_s^3 E_\eta + L_u E_\eta^2 E_s^2 + (L_u^2 - L_u) h_{d-q}^2 h_{d+q}^2 E_s^4. \tag{4.24}$$

Hence, for d corresponding to an effective path, the variance of the metric then expresses as

$$\sigma_d^2 = L_u \sum_{i,j=0}^{L_H-1} \left|h_i\right|^2 \left|h_j\right|^2 E_s^4 - L_u \left|h_d\right|^4 E_s^4 + 2L_u \sum_{i=0}^{L_H-1} \left|h_i\right|^2 E_s^3 E_\eta + L_u E_\eta^2 E_s^2. \tag{4.25}$$

Otherwise, for d values falling out of the set of paths, the variance σ_d^2 reduces to $E(|M(d)|^2)$ in expression (4.24). The PCD is determined respecting the steps in section 4.1.2.1, and the same closed form expression of the PCD in equation (4.20) is then obtained, yet using the new mean and variance formulas' in equations (4.22) and (4.25), respectively.

4.1.3.2 Numerical and Simulation Results

As we consider real-valued signal, the performance is averaged over random preambles taken from BPSK and we consider both AWGN and multipath channels. In addition to the multipath channel used in the evaluation for the OFDM case (channel with 7 paths), we consider another multipath channel with 5 paths uniformly separated by 6 samples. Consequently, the channel impulse response lengths is $L_H = 30$ samples. The power delay profile of the channel is exponential and the ratio of the first path to the last path is set to 12 dB with regular adjacent path gain ratio. The other parameters' values are kept unchanged.

Figure 4.3 illustrates the PCD in the considered channels: AWGN, Chan.I (5 path) and Chan.II (7 path). Again, the proposed BF approach is shown to provide very accurate preamble start detection and can be applied for synchronization in multi-carrier systems with low over-

head. Indeed, simulation results show that in the multipath channels, the detection becomes perfect from SNR values of -3.5 dB and 2 dB in the case of Chan.I and Chan.II respectively. We note that, as for the OFDM case, such good accuracy is obtained at the expense of high computational load, which will be evaluated later. It is also shown in the figure that, in the AWGN channel, the analytical probability concords perfectly with the experimental one and from an SNR of -5 dB, the detection becomes perfect (PCD=1). We note that in both of the multipath channels, the experimental curves match the numerical curves very well, for an SNR lower than -6 dB and higher than -2 dB. In between, the theoretical probability is very close to the experimental rate and a slight gap emerges which becomes a little higher as the channel memory widens. The gap between the analytical and the experimental results may be related to the validity limits of some assumptions such as the independence between the timing metric values for different indexes (used as in the case of OFDM modulation to approximate the PCD expression).

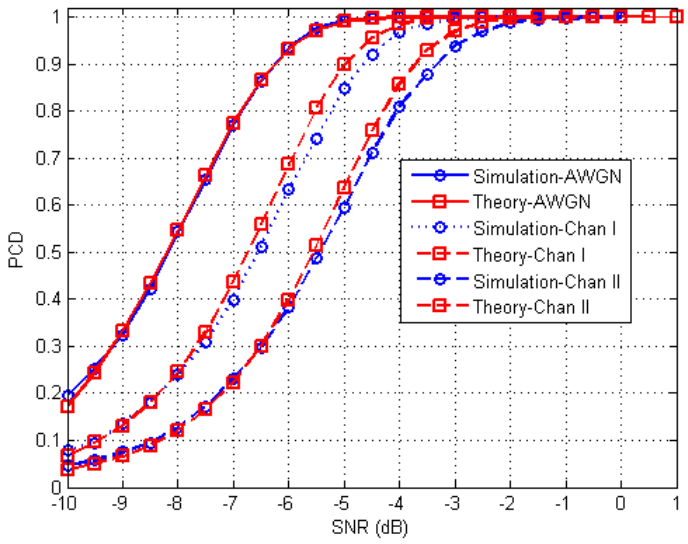

Figure 4.3: Probability/rate of correct detection of the preamble start for DMT modulation.

Thanks to the pronounced peak appearing in the BF metric shape, the preamble start detection is greatly accurate. However, the BF metric is very costly in terms of computational complexity due to the differential correlation operations that require $L_u - 1$ complex multiplications per correlation evaluation. Indeed, in the bursty packet transmission mode, the receiver has to carry synchronization processing continuously, which results in a huge computational load. The continuous transmission mode, in the other hand, allows to reduce the complexity as the preamble is periodically sent such that the synchronization treatment is carried over a

limited interval, intimately related to preamble periodicity. For practical implementation and fast acquisition, the computational complexity must be as low as possible. To take advantage from the accuracy provided by the BF metric while reducing the incurred computational load, we suggest to minimize the number of differential correlation operations carried during the synchronization process. To this end, we propose to proceed into two stages; namely a reduced-complexity coarse stage followed by a high-complexity fine stage, carried over a short interval around the coarse time estimate as described in the next section.

4.2 Reduced-Complexity Synchronization Approach

The purpose of the Reduced-Complexity (RC) two-stage approach is to lessen the complexity of the differential correlation based processing performed in the BF metric. By combining sliding and differential correlations and splitting the synchronization processing into two stages, we show that the computational load can be greatly reduced while keeping high detection accuracy. The first coarse stage requires a preamble of two identical parts and, based on sliding correlation as in [15], it finds out a short uncertainty interval over which the second fine stage is performed based on differential correlation. The combined use of the sliding correlation, characterized by its low complexity (1 complex multiplication per correlation step), and the differential correlation, which is much more complex ($L_u - 1$ complex multiplications per correlation step), carried over a short interval results in an overall reduced complexity approach.

4.2.1 Coarse Synchronization Stage

This stage aims to provide a coarse time estimate $\hat{\tau}_c$ near the true preamble start time τ, which we consider as a reference point around which the uncertainty interval will be set. The uncertainty interval which we denote by $\Delta\tau$ is defined as the interval around which the differential correlation should be carried during second stage, referred to as fine stage.

Similarly to the conventional synchronization algorithms [15, 18, 19], the coarse stage of the proposed RC approach exploits the repetitive structure of the preamble to provide the coarse estimate $\hat{\tau}_c$. Respecting [15], it first operates a sliding correlation, which is computationally simple, with a delay equal to the preamble training sub-sequence length L_u as in equation (3.17). It is obvious in figure 4.4, that the obtained timing metric, drawn for the same system

parameters as in section 4.1.1, is similar to that of [15] and it exhibits a plateau whose length is equal to the CP length N_g minus the channel impulse response time spread $\tau_{max} - \tau_{min}$. To cope with the plateau effect, the middle point d_{opt} of the plateau located at 90% of the absolute metric maximum value is first selected. Then, a time interval of $N_g/2$ is added to the obtained time instant d_{opt} to determine the coarse preamble start estimate ($\hat{\tau}_c = d_{opt} + N_g/2$). To fine tune the coarse estimate, we opt for the second stage, which is based on differential correlation known by its accuracy.

4.2.2 Fine Synchronization Stage

The coarse stage may guarantee that the coarse time estimate $\hat{\tau}_c$ falls within the ISI free part of the preamble, but the tolerance to errors decreases as the channel impulse response widens. To get an estimation with a larger tolerance, we opt for the fine stage which provides a more accurate time estimation. The fine metric is calculated respecting the BF metric as in equation (4.3) which involves the previously introduced correlation sequence α in equation (4.1), generated from the preamble, and the differentially modulated sequence Y in equation (4.2) generated from the received signal.

The main difference between the BF metric and the fine metric of the RC approach is that the latter one is carried over the short-length uncertainty interval $\Delta\tau$ centered on the coarse estimate $\hat{\tau}_c$. Hence, the time index d in equation (4.3) spans the interval $[\hat{\tau}_c - \Delta\tau/2 + 1, \hat{\tau}_c + \Delta\tau/2]$ and in equation (4.2), it varies within the interval $[\hat{\tau}_c - \Delta\tau/2 + 1, \hat{\tau}_c + \Delta\tau/2 + L_u]$. The larger is $\Delta\tau$, the more accurate is the time estimation expected to be more complex is the processing. This implies a trade-off between complexity and accuracy. The interval length $\Delta\tau$ can be chosen either as a function of N_g or related to the standard deviation of $\hat{\tau}_c$ at the worst operating SNR. By choosing an uncertainty interval shorter than the standard deviation of the coarse estimate, the effective preamble start may be missed.

Figure 4.4 illustrates the coarse and fine timing metrics of the proposed RC synchronization technique using the system parameters specified in section 4.1.1 ($N_s = 1126$, $L_u = 2^9 = 512$, $N_g = 102$ and $q = 1$). Obviously, the coarse metric of the RC approach has the same shape as the metric initially proposed by Schmidl and Cox [15] which exhibits a plateau of length equal to N_g (in memoryless channel), while the fine metric of the RC approach is identical to that of the BF approach, thus leading to an accurate preamble start detection.

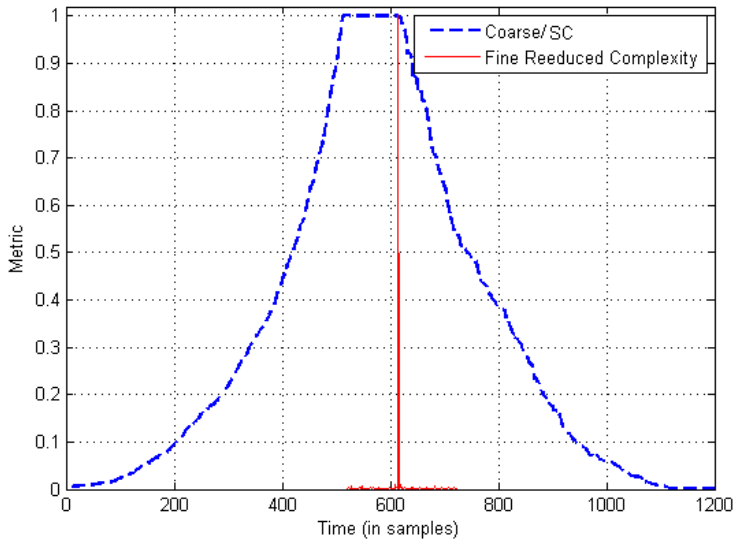

Figure 4.4: Coarse and fine timing metrics of the RC approach in the noiseless case.

4.2.3 Relevance of the RC Time Synchronization: Accuracy and Complexity

The performance of the proposed BF approach was shown to provide satisfactory detection accuracy with high probability of correct detection proved through analytical and experimental studies previously presented in section 4.1.2. As the RC approach uses the BF metric in its fine stage, we expect to get close detection accuracy. To shed light on the performance of the proposed RC approach, we here evaluate it and compare it to existing approaches. We also assess the computational load required to achieve synchronization in the proposed approaches and the considered benchmarks.

4.2.3.1 Detection Accuracy

In this section we evaluate the performance of the proposed RC technique and compare it to the considered benchmarks in the case of monopath AWGN and multipath channels. The BF approach, where differential correlation is exclusively used, is also considered as a benchmark to assess the performance degradation occasioned by the reduction of complexity characterizing the proposed two-stage RC approach. The evaluation is also investigated through Matlab simulations using the same system parameters and channels specified in section 4.1.2.2. The

time estimation performance is evaluated in terms of both Correct Detection Rate (CDR) of the preamble start, as previously defined, and its estimation variance. The variance evaluates the fluctuation of the time estimate $\hat{\tau}$ around the mean value, thus giving a complementary information about the error magnitude. The proposed techniques are compared to the following benchmarks: Schmidl and Cox (SC) [15], Minn-A [16], Minn-B [16], Nasir [18], Chou [19], and the Precoding Method (PM) [21]. In [18], the zero-padding spreads along $7N_u/8$ adjacent samples.

Figure 4.5 illustrates the CDR and estimation variance of the compared approaches in the case of monopath AWGN channel. The CDR (figure 4.5.a) shows that at very low SNR, the PM and the BF methods give the best time detection that attains a CDR of 100% at -6 dB. From a target correct detection rate of 30% to 95%, the RC method presents a slight degradation lower than 1 dB compared to the best benchmark (PM and BF methods), yet with an important reduction in complexity. Beyond an SNR of -6 dB, these three methods provide an almost perfect detection. The SC approach proposed in [15] gives the worst detection rate due to the plateau effect that induces an uncertainty on the preamble start estimate. Thanks to the zero-padding insertion in the preamble of the Chou's method proposed in [19], the preamble start detection is greatly enhanced compared to the SC method. Both of the methods proposed by Minn *et al.* in [16] (Minn-A and Minn-B) outperform it, but the detection accuracy is still lower than the differential correlation based methods (PM, BF and RC).

The variance of the preamble start estimate is depicted in figure 4.5.b. We note that around -10 dB, the variances of all compared estimators are comparable and have high values of about 10^4 squared samples, at the exception of Chou's method which has the highest variance (more than 10^5). For higher SNR values, all estimators' variances decline. The PM, BF and RC methods give the lowest variances that vanish at SNRs of -5 dB, -4 dB and 0 dB, respectively. Consistently with the CDR criterion, the method of SC gives the worst performance and is outperformed by Chou's and Minn's methods.

The performance of the approaches cited above are depicted in figure 4.6 in the case of multipath channel. The preamble start CDR presented in figure 4.6.a shows that the differential correlation based approaches (PM, BF, RC) provide the best CDR which reaches a rate of 100% at an SNR of about 0 dB. We note that the RC approach provides approximately the same time detection performance with an important gain in terms of complexity reduction, compared to the BF approach. For the considered SNR range, the sliding correlation based approaches

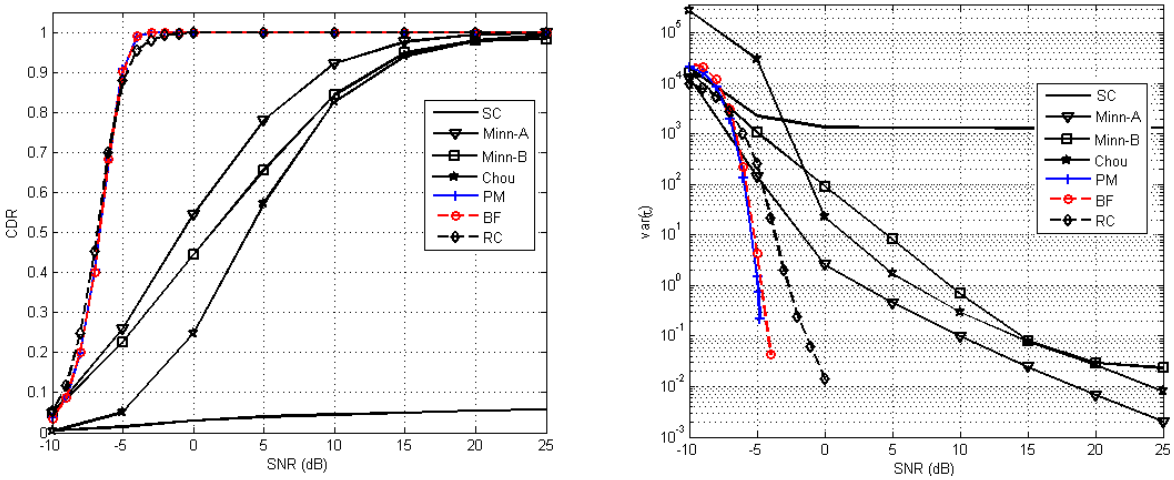

(a) Correct Detection Rate

(b) Preamble start estimation variance

Figure 4.5: Preamble start estimation performance in the monopath AWGN channel.

provide lower rates and saturate well below the 100% best rate. Nasir's method presents a maximum target of correct detection of 64%, Minn-B has a maximum target of about 25%, Minn-A reaches 12%. The SC method gives the worst rate due to the plateau effect as in the case of AWGN channel.

Figure 4.6.b presents the variances of the time estimates. At very low SNR (-10 dB), all estimation variances are comparable with high values between 10^4 and 10^5 squared samples. As shown in the figure, the differential correlation based methods outperform the sliding correlation ones, by providing the lowest estimation variance that vanishes at 4 dB, 1 dB and 4 dB for respectively the BF approach, the PM approach and the RC one. The BF approach gives a slightly lower estimation variance than the RC approach, at the expense of a higher complexity. The difference between the RC and BF curves at SNR values between -5 dB and 0 dB is indeed related to the reduced length of the interval over which the fine stage is performed. In accordance with the previous results, the curves of the sliding correlation based estimators go on declining and present a floor at about 1 squared sample for both Minn's method and 0.1 squared sample for Nasir's one.

The simulation carried in both AWGN and multipath channel showed the robustness of the proposed BF and RC techniques revealed in an important gain in terms of detection accuracy, when compared to conventional approaches. This improvement is mainly due to the use of differential correlation, which results in a huge computational complexity. However, the use of a first computationally simple stage and a second complex one, over a limited interval,

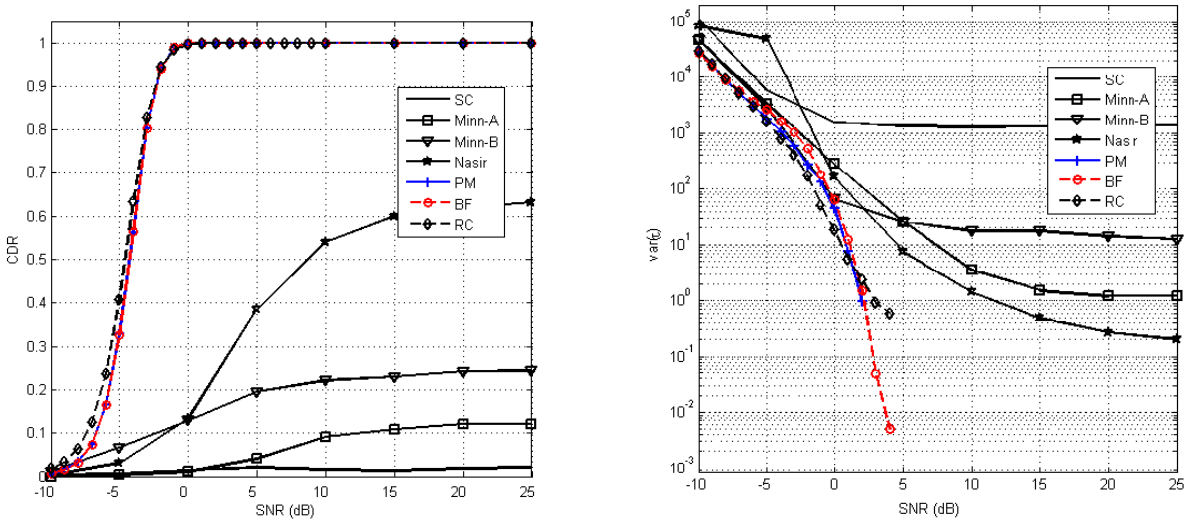

(a) Correct Detection Rate

(b) Preamble start estimation variance

Figure 4.6: Preamble start estimate performance in a multipath channel with 7 paths.

results in an overall simple approach. The proposed RC approach was shown to provide the best tradeoff between complexity and detection accuracy. Indeed, it achieves almost equal performance to the differential correlation based approaches with a much lower complexity, equivalent to that of the sliding correlation based approaches, whose performance are however significantly lower. Next, we evaluate the complexity of the proposed techniques as well as the considered benchmark.

4.2.3.2 Computational Complexity

To shed light on the low complexity of the proposed RC approach, we compare its complexity to the considered benchmarks including the proposed BF. To this aim we assess the total Number of Complex Multiplication (NCM) operations required to achieve synchronization.

In the proposed differential correlation based approaches, we determine the instantaneous NCM required to calculate $M(d)$ in equation (4.3). This latter is the sum of L_u terms involving samples taken from the sequence Y in equation (4.2). Hence, an amount of $L_u - 1$ complex multiplication operations is required for each time index d. The complexity of the metric M rises as the window search widens. For the BF approach, it is calculated continuously in the case of bursty packet transmission mode, while it is calculated over a chosen number of symbols around the expected preamble arrival time in the continuous mode. Whereas, for RC

approach and in both transmission modes, the metric is calculated over the uncertainty interval $\Delta\tau$ of short length, each time the fine metric has to be computed resulting on $\Delta\tau(L_u - 1)$ complex multiplication operations. In the sliding correlation based approach [15], and thanks to the recursive implementation depicted in (3.18), the computational complexity required to calculate the metric in equation (3.20) reduces to 1 complex multiplication. The other approaches [16, 18, 19], respect the same framework yet using different window sizes for the same system parameters resulting in more or less different computational load and detection accuracy.

Let us consider a transmission scenario, for numerical complexity evaluation, in which we aim to derive the NCM carried to detect the first preamble for all the algorithms of interest. The NCM required by the estimation methods considered are presented in table 4.1. The parameter Q denotes the time interval between the processing beginning and the first preamble arrival, M_N denotes the size, in samples, of the repetitive part in the preamble of Nasir's approach [18] and N_z is the size, in samples, of the zero padded part in Chou's approach [19]. The numerical example for the complexities is also given for the same system parameters in section 4.1.2.2. An interval Q of 3 OFDM symbols is chosen, $N_z = N_u/8$ which provides the steepest roll-off of the metric and $M_N = N_u/8$. Table 4.1 shows that the method proposed by Chou *et al.* has the lowest computational load. The PM and the BF methods present the highest complexity. In between, the methods of Schmidl and Cox, Minn, Nasir and the RC approach have a relatively low complexity with an important accuracy enhancement realized by the RC approach as shown in section 4.2.3.1 through simulations.

Table 4.1: Computational complexity comparison among the preamble detection approaches.

Approach	NCM	Numerical example
Schmidl and Cox	$N_u(Q + N_s)$	$4.6\ 10^6$
Minn-A	$\frac{3}{2}N_u(Q + N_s)$	$6.9\ 10^6$
Minn-B	$N_u(Q + N_s)$	$4.6\ 10^6$
Nasir *et al.*	$(2N_u - M_N)(Q + N_s)$	$8.6\ 10^6$
Chou *et al.*	$(N_u - N_z)(Q + N_s)$	$4\ 10^6$
Precoding Method	$\frac{N_u}{2}(1 + \frac{N_u}{2})(Q + N_s)$	$11.78\ 10^8$
Brute Force	$\frac{N_u}{2}(1 + \frac{N_u}{2})(Q + N_s)$	$11.78\ 10^8$
Reduced Complexity	$N_u(\frac{N_g}{2} + Q + N_s)$	$5.1\ 10^6$

Once the first preamble is detected, for the continuous transmission mode (e.g. DVB-

T), the synchronization processing will be performed periodically resulting in an important complexity reduction for all the algorithms. In the case of the bursty packet transmission, where the synchronization processing must continuously be performed (e.g. WiFi), the PM and the BF approaches are penalized by the extremely high complexity. The RC approach provides the best compromise between complexity and performance, as it has a computational load almost equal to that required by the sliding correlation based approaches and an accuracy almost equal to that provided by the other differential correlation based approaches.

4.2.4 Frequency Offset Estimation

For the frequency synchronization, we are interested in only the fractional part of the carrier frequency offset, which is here derived as a byproduct of the fine timing metric, which also corresponds to the BF metric. The conventional approaches which use preambles of repetitive structure, generally exploit the difference between the preamble repetitive parts at the receiver, which may be a sign pattern [17,52] or a phase shift [15], to estimate the FFO. In our work, the FFO estimation can be achieved by evaluating the phase of the correlation function in equation (4.4) at the preamble start estimate $\hat{\tau}_f$, similarly to [15]. When multiplying the conjugate of a sample in the first preamble half to its corresponding sample in the second half, the channel effect is cancelled and the multiplication output corresponds to a phase shift equal to $\pi\nu$. Hence, the FFO estimate is determined as

$$\hat{\nu} = \frac{1}{\pi}\angle P(\hat{\tau}_f), \tag{4.26}$$

where $\angle$ denotes the phase operator. The estimation range allows for the recovery of an FFO up to twice the sub-carriers spacing.

To evaluate the performance of the FFO estimation, we assess its Mean Squared Error (MSE) under the two different AWGN and multipath channel models, previously described, and using the same system parameters as in sections 4.2.3.1 and 4.1.2.2 for the evaluation of the time estimation performance. We recall that the multipath channel has 7 paths and a memory length of 42 samples, thus accumulating an interference till 40% of the CP length of adjacent symbols. The multipath channel has an exponential power delay profile where the ratio of the first path to the last path is set to 12 dB, with a regular adjacent paths gains ratio of 2 dB. The symbol length N_u is of 1024 samples to which a CP of length $N_g = 102$ samples is added.

The FFO value is set to 0.4 sub-carrier spacing. The proposed estimator is evaluated through the RC and the BF schemes and is compared to those of SC [15], Minn-A [16], Minn-B [16], and the PM [21].

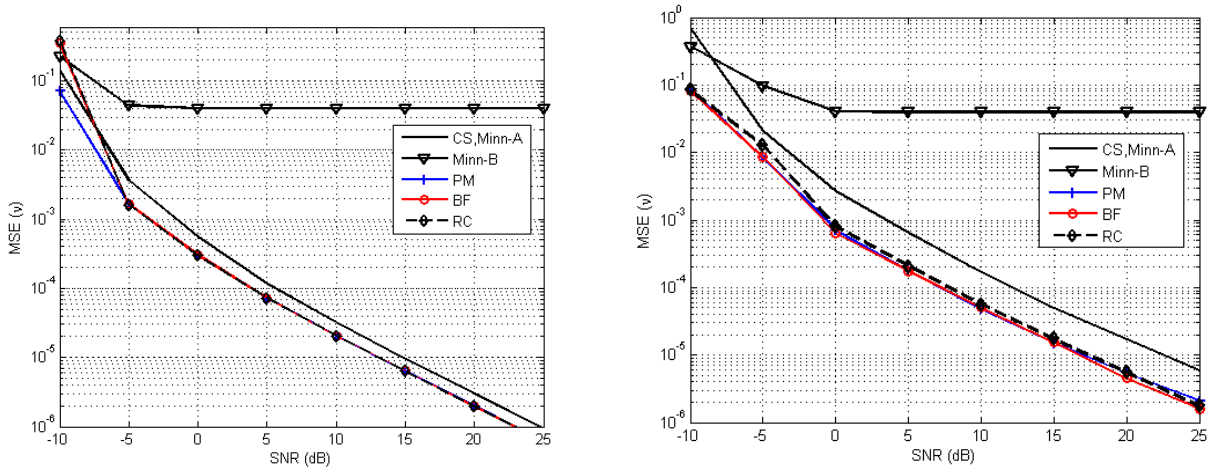

(a) AWGN channel (b) Multipath channel (7 paths)

Figure 4.7: Mean Squared Error of the FFO estimate in the case of SISO OFDM system.

Simulation results, presented in figure 4.7, ensure the robustness of most of the compared estimators in both AWGN and multipath channels. In the AWGN channel, the differential correlation based estimators have almost the same MSE that declines continuously to reach 10^{-6} at an SNR of 25 dB. Below an SNR value of -5 dB, all methods provide close MSE values around 0.1 with slightly higher error for the RC approach. Above an SNR of -5 dB, the PM, RC and BF methods give approximately the same MSE values allowing a slight gain of about 1 dB compared to the sliding correlation based methods (Minn-A and SC). The latter estimators, in the multipath channel, provide worse MSE and achieve a loss of about 3 dB compared to the differential correlation based estimators. This result is expected due to the plateau effect that greatly degrades the detection performance in the multipath channels. The estimator Minn-B gives the worst MSE that presents a floor at an error of about 4 10^{-2} from SNR values equal to -5 dB and 0 dB in the AWGN and multipath channels, respectively.

For both time and the frequency synchronization, the proposed BF and RC techniques were shown to enhance the estimation performance. To provide more insights in the performance of the proposed synchronization techniques, we evaluate their performance for time synchronization in a standardized OFDM system, respecting the IEEE 802.11a/g specifications.

4.3 Application to the IEEE 802.11a/g Standards

One of the most popular standards in use today is IEEE 802.11 and its variations adopted in Wireless Local Area Networks (WLAN). Like all OFDM systems, WLAN receivers require accurate synchronization to demodulate the received symbols. To this aim, the standard specifies a preamble of distinguished repetitive structure. This latter is exploited and adapted to the herein proposed BF and RC synchronization techniques.

4.3.1 State of the Art of Synchronization in the IEEE 802.11a/g

Among the WLAN standards we here study the IEEE 802.11a/g specified in [103] and [104], which support a data rate up to 54 Mb/s and operate in the 5 GHz and 2.4 GHz bands respectively in a bursty transmission mode, are here considered. The synchronization process in IEEE 802.11a/g standards exploits a preamble known at the receiver, The timing synchronization process is split into an initial coarse synchronization stage (packet detection) and a later fine one (frame start detection). A coarse metric, based on autocorrelating the received signal, is used for packet detection. For the frame start detection, a fine metric based on cross-correlating the received signal with the short preamble symbol is carried. In the remaining of this section, we first provide a short description of the preamble used for synchronization. Then, synchronization issues are discussed in existing approaches.

4.3.1.1 Preamble Structure

In order to accomplish synchronized reception, a preamble that has been carefully designed to provide enough information for a good synchronization performance is sent at the beginning of each transmitted packet. It consists of two parts: the first part has 10 short repeated symbols and the second part has two long repeated symbols, as illustrated in figure 4.8. The short training symbols are denoted by t_1 to t_{10}, each of length $D = 16$ samples ($0.8\mu s$ each), whereas T_1 and T_2 denote the long training symbols, of length 64 samples each ($3.2\mu s$ each), preceded by a 32-sample CP ($1.6\mu s$) resulting in a total preamble length of 320 samples ($16\mu s$). The preamble is followed by the signal field and data.

The preamble illustrated in figure 4.8 is dedicated to various reception tasks, including

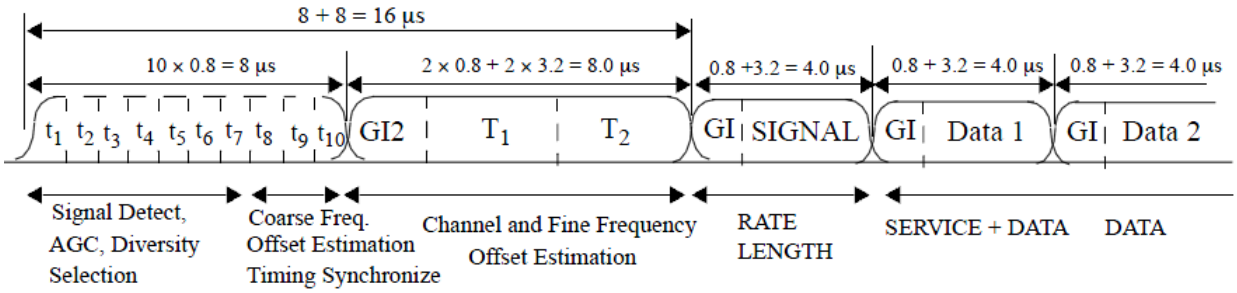

Figure 4.8: IEEE 802.11a/g preamble structure [103].

frame synchronization, Automatic Gain Control (AGC) level setting, carrier frequency offset estimation and symbol timing synchronization and channel estimation [103]. We here focus on time synchronization by exploiting the repetitive structure specificity of either the short training symbols or the long ones.

4.3.1.2 Literature Review of Synchronization in the Standards IEEE 802.11a/g

Many synchronization techniques, originally proposed for general OFDM systems [15]- [17] can be applied to IEEE 802.11a/g WLANs. However, these techniques may lead to unsatisfactory performance especially in the presence of multipath effects. Other techniques that are specifically designed for IEEE 802.11a/g WLANs have been reported in [106]- [109]. In this section, we describe the synchronization processing adopted in the standard and the optimized algorithm proposed in [107], which we hereafter consider as benchmarks.

According to the standards IEEE 802.11a/g, the received signal is first autocorrelated with a delay of D samples to roughly localize the preamble using the metric

$$C\left(d\right)=\left|\sum_{m=0}^{D-1}r_{d+m}^{*}r_{d+m+D}\right|. \tag{4.27}$$

Once the receiver has detected the arrival of a preamble corresponding to the start of a packet, the symbol timing algorithm refines the estimate to sample-level precision. To this aim, the local known repetitive short symbol t (among the 10 short symbols) is used to perform cross-correlation as

$$F\left(d\right)=\left|\sum_{m=0}^{D-1}t_{m}^{*}r_{d+m}\right|. \tag{4.28}$$

Both coarse metric $C(d)$ and fine metric $F(d)$ are normalized by the received signal energy

given by

$$E(d) = \left| \sum_{m=0}^{D-1} r_{d+m+D}^{2} \right|. \tag{4.29}$$

As shown in figure 4.9, the autocorrelation of the received signal in equation (4.27) exhibits a plateau whose length equals the length of 9 short symbols, whereas the cross-correlation with the known short symbol t_1 in equation (4.28) presents peaks at the start of each short symbol. As the first 9 correlation peaks are within the plateau, the last 10^{th} peak is used as the beacon position from which the next symbol starts.

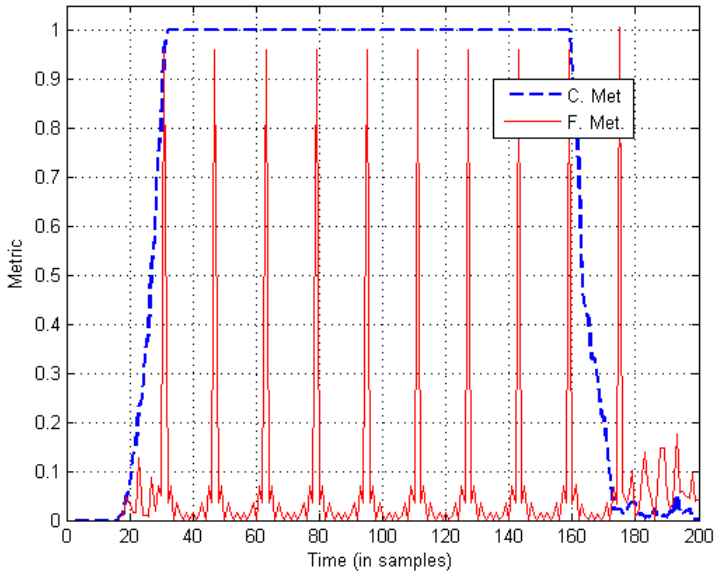

Figure 4.9: Coarse and fine timing metrics of the IEEE 802.11a/g using short symbols under noiseless conditions.

In [107], symbol timing synchronization algorithms for OFDM system based on IEEE 802.11a were put forward. Some of them are based on energy detection and other based on cross-correlation that exploits the repetitive structure of the preamble. Among them, we choose as benchmark an optimized algorithm that uses one period of short training symbol in the IEEE 802.11a preamble. As the real part of the former 8 data and the imaginary part of the latter 8 data in each short symbol t_n are identical [103], the algorithm in [107] decreases the period of short training symbol to 8 sampling points. The metric proposed by this algorithm is given by

$$R(d) = \left| \sum_{m=0}^{7} r_{d-m} \Big(\Im\big(r_{d-m-8}\big) + j\Re\big(r_{d-m-8}\big) \Big)^* \right|, \tag{4.30}$$

where $\Re(x)$ and $\Im(x)$ stand respectively for the real and the imaginary parts of the complex number x. This algorithm can ensure frame synchronization by detecting the first short training symbol.

4.3.2 BF and RC Synchronization in the IEEE 802.11a/g

We here focus on the suitability of the proposed techniques to time synchronization for the standards IEEE 802.11a/g. Indeed, the repetitive structure of the short and long preamble symbols allows a flexible synchronization processing, respecting the proposed techniques which require such structure. Even if the two IEEE 802.11a/g preamble parts (short and long symbols) can be exploited, we consider the first preamble part composed of 10 short symbols to achieve an early time synchronization, thus allowing the processing of the other tasks (carrier frequency offset estimation, channel estimation) that use the second preamble part and must be carried after time synchronization. In this case, depending on the length of the adopted repetitive part L_u and consequently the correlation delay, the coarse metric (3.20) and the BF metric (fine RC) (4.3) exhibit different shapes.

Figure 4.10 illustrates the BF and RC (coarse and fine) timing metrics. We note, in figure 4.10.(a), that using a length $L_u = 5D$ without considering any CP, the coarse metric has a triangular shape exhibiting a single peak. This latter corresponds to the start of the preamble that we consider as a coarse time estimate $\hat{\tau}_c$ around which the fine metric of the RC approach is carried over a limited interval of length $2D$. The fine metric leads to a high sharp peak at the time index $\hat{\tau}_f$, which also corresponds to the time estimate $\hat{\tau}$ of the BF approach. In figure 4.10.(b), we consider the first 2 short symbols as a CP whose length is $N_g = 2D$ and a useful part composed of two identical parts, each of length $L_u = 4D$. The coarse time estimate $\hat{\tau}_c$ is selected as described in section 4.2.1. The estimated time $\hat{\tau}_f$ provided by the peak value of the fine metric here indicates the start of the 3$^{\text{rd}}$ short symbol corresponding to the useful part of the preamble. We notice that, going on calculating the coarse metric, the long symbol also allows a synchronization respecting the proposed techniques for $L_u = 4D$.

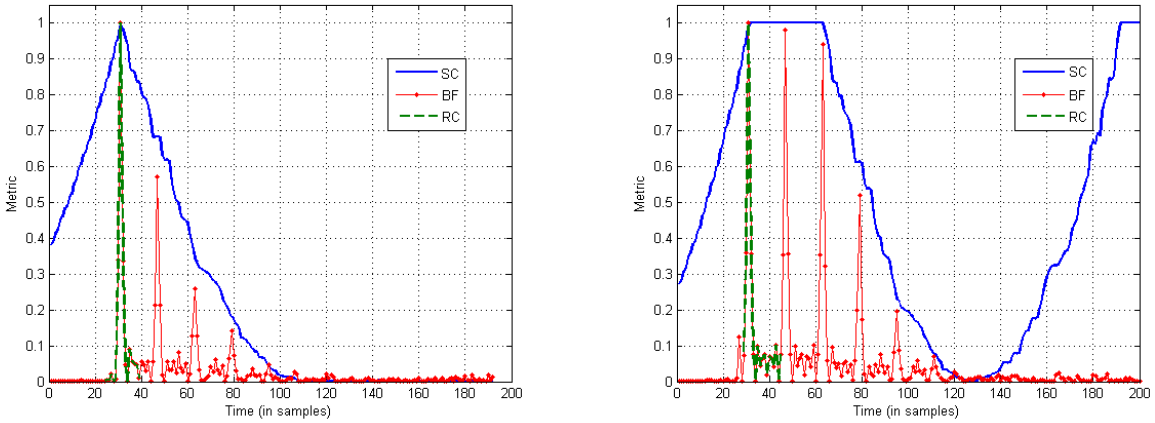

(a) $L_u = 5D$ (b) $L_u = 4D$

Figure 4.10: Coarse and fine timing metric of the RC approach using the short symbols with different correlation delays.

4.3.3 Performance Evaluation of the BF and RC Approaches

The performance of the considered methods are evaluated by computer simulation respecting the Monte Carlo method for 10^4 trials. The parameters of the OFDM system according to IEEE 802.11a/g standards [103] are listed in table 4.2.

Table 4.2: Simulation parameters for the IEEE 802.11a/g systems.

Parameter	value
Number of IFFT points (in sample)	64
Number of used sub-carriers (in sample)	52
Number of data sub-carriers (in sample)	48
Cyclic prefix duration (in sample)	16
Modulation	QPSK

We consider the cases of AWGN and exponential power delay profile multipath channels. Two multipath channels are used, having respectively 4 and 6 uniformly spaced paths with regular normalized path delays of 4 and 2 samples, resulting in a channel memory length of 16 samples for both channels. The ratio of the first path to the last path is set to 15 dB with a constant adjacent path gains ratio. The uncertainty interval $\Delta\tau$ is set to twice the CP length (32 samples). The performance is here evaluated in terms of Correct Detection Rate (CDR), as previously defined ($\hat{\tau}_f = \tau$, no error tolerance). Respecting the proposed arrangement of

the preamble (No CP and two identical parts of length $5D$ each), τ coincides with the start of the second short training symbol as presented in figure 4.10.(a). In addition to the proposed BF and RC approaches, we consider as benchmark the SC algorithm [15] (also corresponding to the coarse synchronization), the IEEE 802.11a/g standards synchronization approach and the optimized algorithm proposed [107], which are recalled in section 4.3.1.2. It is worth to note that in the simulation we tolerate an error of 2 samples for only the SC approach, which has poor detection performance.

Figure 4.11 presents the CDR in the monopath AWGN channel. As in the general case of OFDM systems, the considered BF and RC approaches provide satisfactory detection accuracy and outperform the considered benchmarks. Indeed, even at low SNR (< 0 dB) the detection is good and it becomes perfect (CDR=100%) above an SNR of 1 dB. For SNR values lower than 8 dB, the proposed techniques outperforms the standard and they realize a gain of about 7 dB for a target CDR of about 90%. Compared to the BF and RC approaches, the optimized algorithm provides lower detection rate for all SNR ranges, but for a very low SNR (< -2 dB) it outperforms the standard. The SC approach provides the worst detection rate and its curve stagnates at a target CDR of about 90%, reached from an SNR of 15 dB. We note that the proposed BF and RC approaches are beneficial especially at low SNR values. Yet, the RC approach is more advantageous thanks to its relatively reduced complexity.

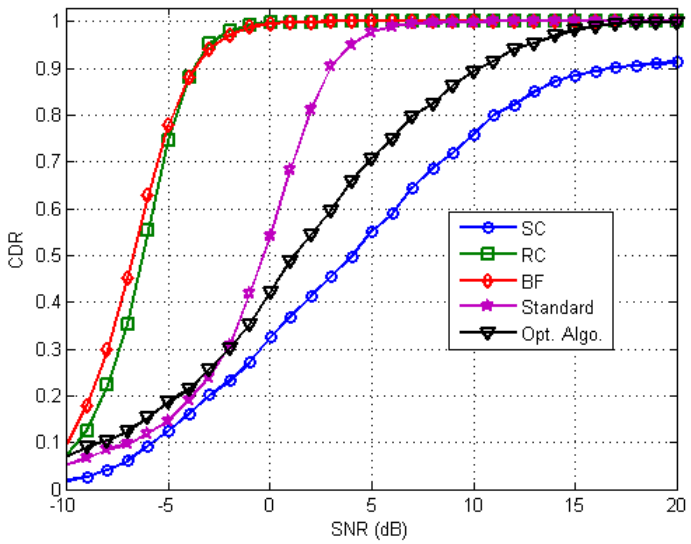

Figure 4.11: CDR of the preamble start in the monopath AWGN channel for the standards IEEE 802.11a/g.

Figures 4.12.a and 4.12.b show the CDR of the previously cited approaches achieved in the multipath channels. We note that, due to the multipath effect, the detection accuracy of all the considered approaches is degraded. Under the same conditions, the RC and BF approaches achieve more or less the same detection performance and outperform the other techniques. The capability of the optimized algorithm is not as satisfactory as the standardized algorithm, but it outperforms the SC approach.

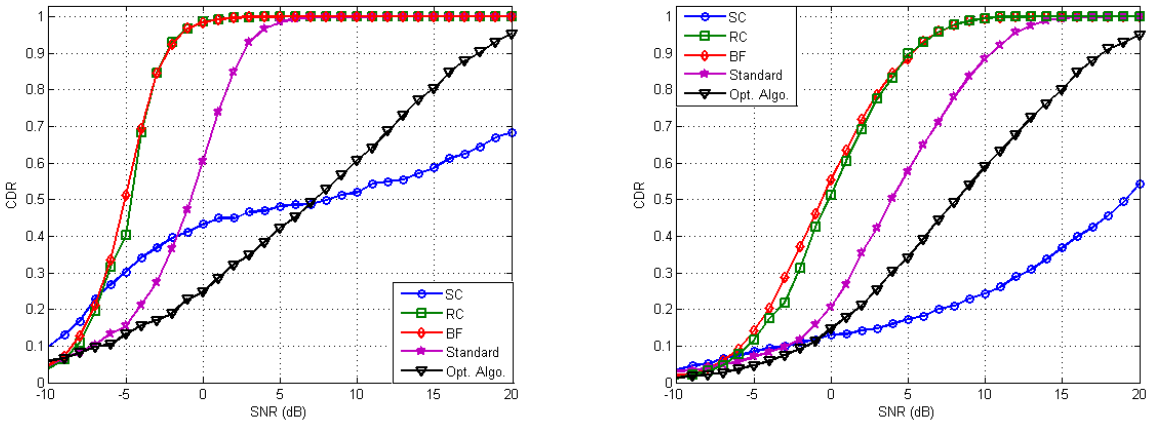

(a) 4-paths channel

(b) 6-paths channel

Figure 4.12: CDR of the preamble start in multipath power delay profile channels for the standards IEEE 802.11a/g.

To shed light on the difference between the proposed BF and RC approaches performance, we draw the probability of missing the preamble start in figure 4.13. We note that the accuracy provided by both approaches is almost the same except for some SNR ranges where a slight gap of about 0.5 dB emerges. It is worth to mention that, in some cases, the RC approach outperforms the BF one, which is not expected. This may be related to the fact that calculating the BF metric over a longer interval (which is the case of the BF approach) results in a higher probability to detect a false peak.

The simulation carried to evaluate the proposed BF and RC synchronization techniques proved their relevance in both AWGN and multipath channels and showed that they outperform the synchronization processing specified by the IEEE 802.11a/g standards and other algorithms considered as benchmark [15, 107]. Moreover, as indicated before, the two-stage RC approach has a low computational load at the expense of a slight accuracy loss, which makes it suitable for fast symbol timing synchronization in bursty IEEE 802.11a/g systems.

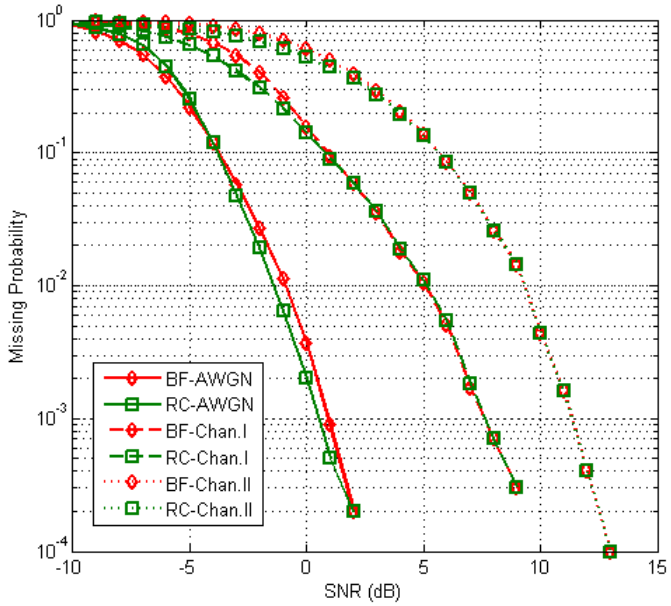

Figure 4.13: Missing probability of the preamble start in the monopath AWGN and multipath channels for the standards IEEE 802.11a/g.

Conclusions

In this chapter, we proposed two efficient preamble-based synchronization approaches for OFDM systems. A brute force single-stage approach based exclusively on differential correlation was first presented. Its analytical performance was provided to assess the detection accuracy and was validated through experimental results. This study was carried for both OFDM and DMT modulation techniques and the performance was improved in both AWGN and multipath channels. The brute force approach was shown to provide very accurate detection performance, yet at the expense of important computational complexity.

To reduce the complexity occasioned by the differential correlation operations, we suggested the two-stage reduced-complexity method, wherein the first stage a sliding correlation, of low computational load, is used to provide a coarse time estimate. Then, a second stage, based on differential correlation carried over a limited range around the coarse time estimate, is used to detect the fine preamble start. This combination yields to an overall reduced complexity approach. The simulation results conducted under various channel conditions confirmed the good performance of the proposed RC approach with respect to existing techniques. This evaluation also covers the computational load. In particular, we evaluated the number of complex

multiplications required to detect the first sent preamble. We have shown that the proposed two-stage reduced-complexity technique offers the best trade-off between complexity and detection performance. Indeed, it provides almost the same detection accuracy of exclusively differential correlation based techniques with a complexity more or less equivalent to that of the sliding correlation based ones. As a byproduct, the fractional frequency offset estimation was also assessed and it was shown to provide satisfactory accuracy.

Finally, by exploiting the repetitive structure of the preamble used in the standards IEEE 802.11a/g, we proved that the proposed techniques are able to work well in these standards and that they outperform the synchronization processing specified by the IEEE 802.11a/g standards and other existing algorithms considered as benchmarks.

Chapter 5

Simply Differential Synchronization: Optimized Performance

This chapter studies two optimization issues of the proposed reduced-complexity synchronization technique described in chapter 4. The first issue concerns the choice of the preamble training sub-sequence, defined in the time domain, and the length of the uncertainty interval. The evaluated training sub-sequences belong to a set of binary m-sequences, Gold and Kasami sequences. We start by analyzing the detection accuracy provided through the use of different binary pseudo-noise sequences. Secondly, we study, for the different envisaged sequence types, the impact of the preamble length on the detection accuracy. This study gives an important insight on how the training sub-sequence should be chosen in order to achieve a better trade-off between detection accuracy and complexity. In fact, with the same overhead, a more or less accurate detection can be achieved depending on the preamble sub-sequence type. Then, an experimental study of the impact of the uncertainty interval width on the detection performance is realized. We show that, above a certain critical width, widening the uncertainty interval results in only more computational load without enhancing the detection performance.

The second issue concerns the choice of the correlation sequence for training sub-sequence defined in the frequency domain. In particular, we study the optimization of the correlation sequence, which is used during the fine stage to carry differential correlation operations. The optimization aims to find the best sub-optimal correlation sequence in terms of providing near optimal performance (provided by the optimal correlation sequence generated from the

preamble). The sub-optimal sequence is chosen among a subset of sequences obtained through the quantification of the original sequence, and whose elements take their values from a finite QPSK alphabet ($\pm 1 \pm j$). The interest of such class is that it allows replacing the differential correlation operations, characterized by its high complexity, by simple sign changes. Hence, the complexity involved for the fine metric calculation is considerably reduced by applying sign change operations instead of complex multiplications. The sub-optimal sequence search is carried off-line, thus relaxing the complexity of the sequence design procedure. Three search algorithms are here developed and evaluated. We first propose two classical optimization schemes and compare their efficiency. Then, we formulate the sequence optimization problem using the genetic algorithm approach. The simulation results show that the use of sub-optimal sequences gives near-best detection performance (which are provided by the optimal correlation sequence) with considerably lower complexity, recording an advantage realized by the genetic algorithm based search over the two other proposed algorithms.

5.1 Training and Correlation Sequences

We recall that similarly to the work in [15], the herein used preamble consists of a single symbol built of two identical training sub-sequences. Both Time Domain (TD) training and Frequency Domain (FD) training are here investigated. The preamble structure is depicted in figure 5.1. We note that, as for OFDM data symbols, the CP-extended preamble has a length of N_s samples. Depending on the training sub-sequence type, the length of the preamble useful part may be equal to that of the OFDM symbol, and thus denoted by $N_u = 2L_u$, or different from the OFDM symbol length and denoted by $N_{um} = 2L_{um}$.

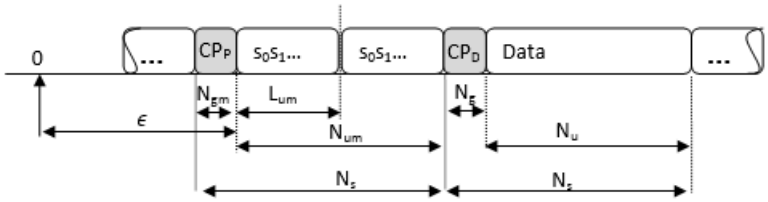

Figure 5.1: Preamble Structure.

In the TD case, the preamble is made repetitive through the concatenation of the two identical training sub-sequences of length $L_{um} = 2^m - 1$ each, and is then sent directly in the

time domain. The choice of such implementation is adopted to preserve the properties of the binary PN training sub-sequences, like m-sequences and Gold sequences, whose properties may be destroyed by the IFFT application. When using randomly generated sequences, the two halves of the preamble are made identical by transmitting data on the even frequencies, while zeros are used on the odd frequencies, followed by the IFFT application as done in [15]. In this case, the FD training sub-sequence length is $L_u = 2^m$ and the IFFT size is $N_u = 2^{m+1}$.

In our work, the training sub-sequence is used to generate the Correlation Sequence (CS) α as in equation (4.1) which can also be defined in TD or FD. Let us recall the expression of the CS generated from the TD training sub-sequence as

$$\alpha_{TD}(d) = p_d^* p_{d+L_{um}+q} = p_d^* p_{d+q}, \quad d \in [0, L_{um} - 1], \tag{5.1}$$

and from the FD training sub-sequence as

$$\alpha_{FD}(d) = p_d^* p_{d+L_u+q} = p_d^* p_{d+q}, \quad d \in [0, L_u - 1]. \tag{5.2}$$

In the former sequence type, as the whole preamble length N_s is kept equal to that of the OFDM symbols, the preamble CP length N_{gm} is appended with $N_s - N_{um}$ samples.

The repetitive structure of the preamble used in our approach allows a coarse time synchronization respecting [15] regardless the sequence type. For fine synchronization, the type of the training sub-sequence used to generate both the preamble and the correlation sequence has an impact on the system performance (as will be shown later). Thus, it is important to build the preamble in such a way to optimize the synchronization performance. It is worth to note that, although the simulations in this chapter are conducted for the RC approach, the study remains available for the BF approach which uses the same fine metric calculated along larger interval.

5.2 Optimization of the Training Sequence

The training sub-sequence can be chosen randomly or respecting specific criterion. During the first coarse stage, the repetitive structure is the sole required condition for successful coarse synchronization, regardless of the training sequence type. However, the fine stage requires

judicious choice of the training sub-sequence such to have an important correlation property. Furthermore, as it is calculated over relatively short uncertainty interval, the fine stage may provide different performance depending on the uncertainty interval width.

In this section, we present simulation results to evaluate the performance of the RC time synchronization approach, using different preamble training sub-sequence types and lengths, under multipath propagation condition. We first evaluate the impact of the preamble sub-sequence type on the metric and thus on the detection accuracy. Then, we assess the impact of both the preamble length and the uncertainty interval length on the detection performance. The measure used to evaluate the performance is the achieved CDR of the preamble start, where the estimated $\hat{\tau}_f$ exactly coincides with the true one τ (no error tolerance). For each SNR value, 10^4 Monte Carlo realizations are averaged, where both noise and sequence are randomly chosen. It is important to mention that preferred pairs of m-sequences, used in Gold sequence generation, do not exist for $m = 4$, 8, 12 and 16. Furthermore, Kasami sequences are defined only for even values of m, which restricts a fair comparison to a few preamble lengths possible values.

5.2.1 Impact of the Training Sequence Type

We note that the required properties of the preamble training sequences are related to their autocorrelation. Indeed, the sequences should be meticulously chosen in such a way to have good correlation properties in terms of minimizing the maximum value of the out-of-phase autocorrelation. The smaller is the out-of-phase autocorrelation of the chosen sequence type, the lower is the number of sub-peaks and the more accurate is the time estimation. In this section, we study the effect of the preamble training sub-sequence type within the set of binary sequences including m-sequences, Gold, Kasami and random sequences. The fine timing metric in equation (4.3) related to these sequence types are presented in figure 5.2 for arbitrary chosen sequence in each of the above mentioned 4 sequence types. More precisely, a random binary sequence of ± 1, two arbitrarily chosen m-sequences (m-sequence 1, m-sequence 2), each generated using a different primitive polynomial. A Gold sequence and a Kasami sequence obtained from m-sequence 2 are also envisaged. The parameter m is set to 6, leading to a preamble of 126 useful samples extended with a CP of length 12 samples. We consider a channel of $N_p = 4$ paths with an exponential power delay profile. Paths are regularly separated by 2 samples and the ratio of the first path to the last path is set to 6 dB. The primitive polynomials

used to generate m-sequence 1 and m-sequence 2 are respectively $P_1 = 1 + x + x^2 + x^5 + x^6$ and $P_2 = 1 + x + x^6$. Random data are sent before the preamble transmission.

As shown in figure 5.2, some side-peaks appear at positions that do not correspond to any path for the choice of m-sequence type. As predicted, this problem is avoided by using one among the Gold or Kasami sequences generated from the considered m-sequence 2. Indeed, the weakness of the m-sequences is that the generated correlation sequence α (5.1) used for the differential correlation coincides with a shifted version of the original training sub-sequence $\boldsymbol{p}_1 = [p_0, p_1, \ldots, p_{L_{um}-1}]$, thus resulting in the appearance of ghost paths in the metric shape for the case of multipath channels. It is worth to note that, for a given multipath channel, certain m-sequences are more adapted than others by avoiding side-peaks effect as depicted in the figure 5.2.a. This dependency is avoided by the Gold and Kasami sequences, which clearly capture the channel profile. The training sub-sequence type has, in this manner, a great impact on the fine timing metric shape thus affecting the detection performance.

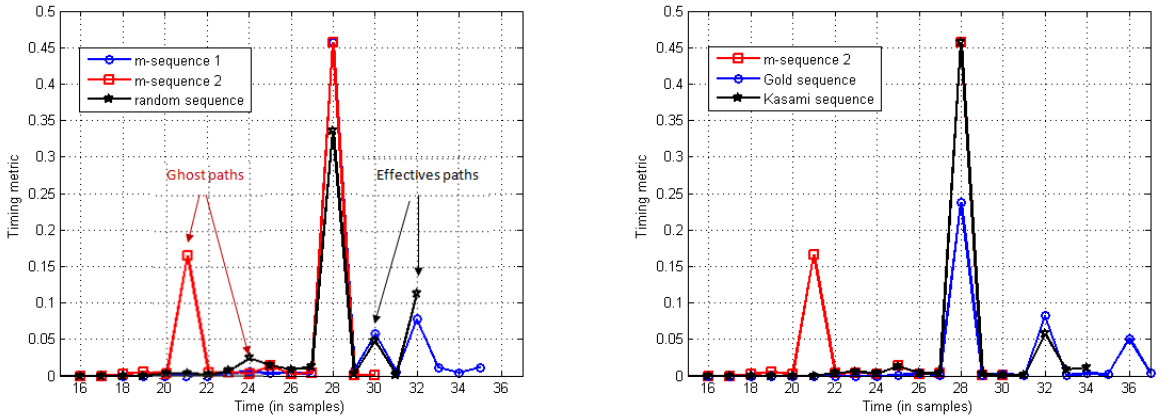

(a) Random sequence and m-sequences

(b) M-sequence, Gold and Kasami sequences

Figure 5.2: RC fine timing metric, using different sequence types, in the case of multipath channel (4 paths, SNR=10 dB)

To assess the impact of the training sequence choice, we evaluate the detection accuracy through the preamble start CDR and its estimation variance criteria. Considering two evaluation scenarios for OFDM systems having different parameters. In the first scenario, we use the same system parameters as in the previous evaluation of section 4.2.3.1 in which $m = 9$ and under the multipath channel with 7 paths. We consider random sequences of ± 1, two m-sequences generated using the primitive polynomials $P_1 = 1 + x^3 + x^4 + x^5 + x^7 + x^8 + x^9$ and $P_2 = 1 + x + x^3 + x^4 + x^5 + x^6 + x^7 + x^8 + x^9$, for which the difference in the performance is

prominent. To overcome this gap, a random choice of an m-sequence realized for each iteration is also considered. Finally, a Gold sequence deduced from the randomly chosen m-sequence is used. The methodology adopted to generate the Gold sequences consists in first finding a preferred pair of primitive polynomials of order $m = 9$. Second, the sequences corresponding to the polynomials are implemented by using a shift register architecture. Then, the L_{um} different phases of one of the generated sequences is used to find each of the $L_{um} + 2$ possible Gold sequences. One among these sequences is randomly picked out to be used in the simulation. We note that in this scenario, the Kasami sequences are not taken into consideration because they are not defined for even values of m.

Figure 5.3.(a) illustrates the CDR of the RC estimator with different sequence types used to generate the preamble. Despite the use of the same sequence type (m-sequences), the detection performance is greatly enhanced through an adequately chosen m-sequence. For a target CDR of 80% a gain of about 2 dB is achieved using m-sequence 1 with respect to m-sequence 2. As can be observed, the random choice of one m-sequence among the 48 defined m-sequences provides a detection rate between the two separately simulated m-sequences and almost equal to the detection rate provided by a random sequence of ± 1. The best detection rate is provided by the use of Gold sequences, especially at very low SNR, which achieves a gain of about 2 dB compared to the other considered sequence types. This enhancement is due to the disappearance of ghost sub-peaks inherent to the m-sequences and problematic especially in the multipath channels.

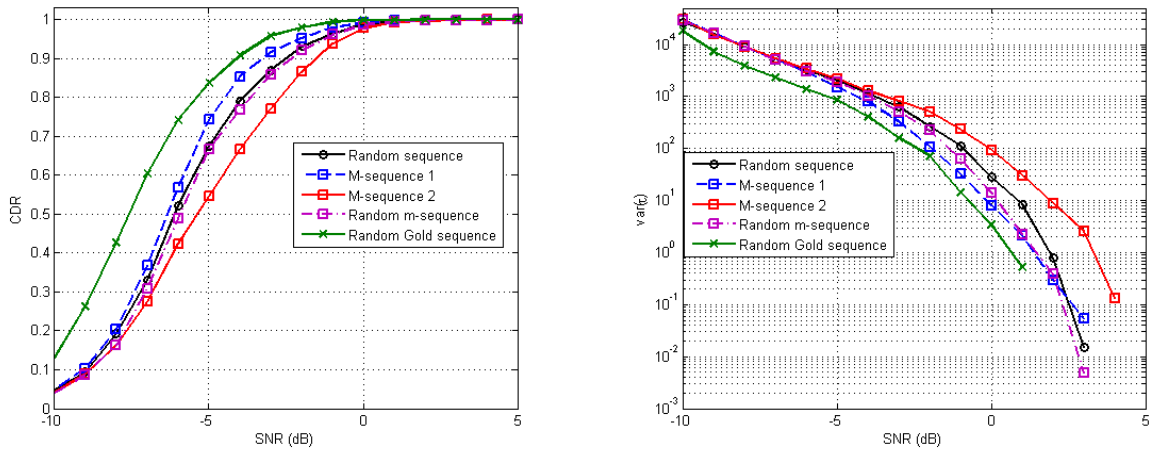

(a) Correct Detection Rate

(b) Preamble start estimation variance

Figure 5.3: Preamble start estimate performance using different TD sub-sequence types in the case of multipath channel (7 paths).

Figure 5.3.(b) shows the variance of the time estimate using the sequences cited above. In concordance with the previous results, the Gold sequences provide the lowest estimation variance, which vanishes at an SNR of 1 dB. The other sequences have almost the same estimation variances with a slight gain realized by m-sequence 1. All the curves vanish at an SNR of about 4 dB, which improves the robustness of the proposed RC approach. The CDR curves show that for SNR higher than 0 dB, all sequence types lead to almost perfect detection. On the contrary, the variance curves show the impact of the sequence choice on the detection accuracy and thus gives a complementary information concerning the detection error (in terms of samples).

The second scenario considers Kasami sequences in addition to the previously evaluated sequence types. To make possible the comparison of all considered sequence types, we set the preamble length to $N_{um} = 2(2^6 - 1) = 126$ to which a CP of length $N_{gm} = 12$ samples is prepended. This choice is justified by the limited values of m for which both Gold and Kasami sequences are defined. The channel used in the present simulation is the same multipath channel used to draw the metrics in the start of this section (4 paths with exponential power delay profile). The curves evaluating the CDR and the preamble start estimation variance are drawn in figure 5.4, in which the choice of the training sub-sequence type impact on the detection performance is clearly shown.

As could be observed in figure 5.4.a, the random sequence of ± 1 provides the worst detection rate while a random choice of an m-sequence among the set of possible sequences gives slightly better detection accuracy. For an SNR value lower than 2 dB, Gold sequences somewhat outperform Kasami sequences. For higher values of SNR, Kasami sequences realize a gain of about 2 dB with respect to Gold sequences for a CDR target of 90%. These two sequence types provide a perfect detection (CDR=100%) for SNR value above 18 dB, which is not the case using m-sequences and random sequences that exhibit a floor effect at a rate of about 97%. Figure 5.4.b shows the variance of the time estimate using the sequences cited above. For an SNR lower than 0 dB, all sequences provide almost the same estimation variance. For higher SNR values, in concordance with the CDR, the Kasami sequences provide the lowest estimation variance, realizing a gain of about 5 dB for 0.3 squared samples, compared to Gold sequences. For this SNR range, all sequence types show floor effect in the variance estimation curves corresponding to an estimation error of about 0.13 for Kasami sequences, 0.3 for Gold sequences, 3 for m-sequences and 3.75 for random sequences.

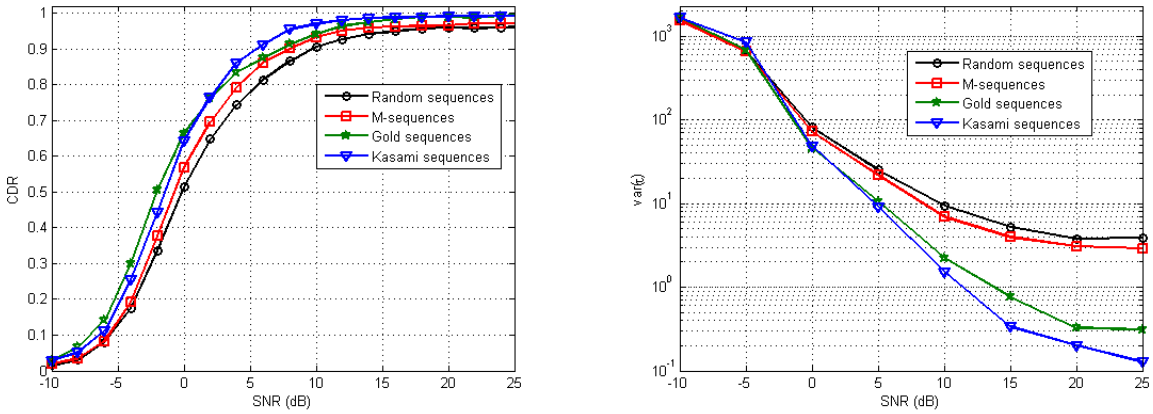

(a) Correct Detection Rate

(b) Preamble start estimation variance

Figure 5.4: Preamble start estimate performance using different TD sub-sequence types in the case of multipath channel (4 paths).

The study conducted here proves the sensitivity of the detection accuracy provided by the RC approach to the training sub-sequence type and choice. It is shown that, at very low SNR, Gold sequences slightly outperform the other sequence types. For moderate SNR values, Kasami sequences provide better detection, while at higher SNR values all sequences offer almost perfect detection. We also note that among the considered types, m-sequences are the most sensitive to the multipath effect that cause potential ghost side-peaks appearing in the fine metric shape.

5.2.2 Impact of the Training Sequence Length

The training sub-sequence length, and hence the preamble length, is one of the most critical parameters to fix synchronization performance. Short preambles are sometimes preferred because they take less time to be processed than long preambles and they minimize the overhead, yet they are not suitable for multipath propagation because the ISI free signal interval used to compute the metric will be reduced. To assess the impact of the preamble length on the detection accuracy, for the different training sub-sequence types, we evaluate the CDR using different preamble lengths. For m-sequences and random sequences, m is set to 5, 6, 7, 8 and 9. As Kasami sequences are defined for only even values of m, we consider the values of 6 and 8. For Gold sequences, which are not defined for m values multiple of 4, we envisage $m = 5$, 6, 7 and 9.

Figure 5.5 shows, for each sequence type, the detection rates using the different possible preamble lengths. It is obvious that independently of the sequence type, the detection accuracy is enhanced with a longer preamble. Under the same propagation conditions and using the same preamble length, the detection accuracy is found to strongly depend on the preamble training sequence type. For preamble lengths lower than 254 samples, the rate provided by m-sequences and random sequences stagnates at 90%. However, using Gold and Kasami sequences, the detection rate reaches 100% for high SNR values (> 10 dB). Using longer preambles, all sequence types provide almost perfect detection at high SNR value.

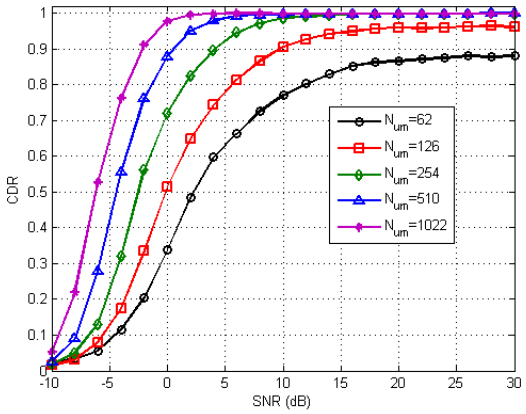

(a) Random sequences

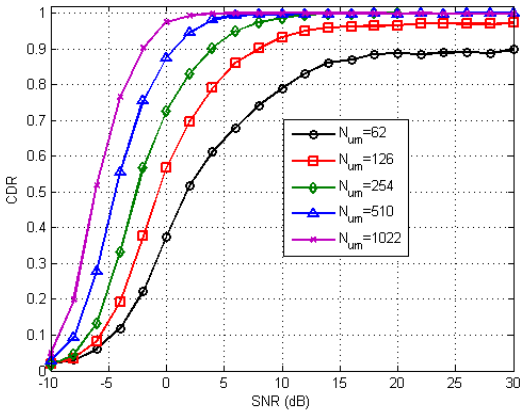

(b) M-sequences

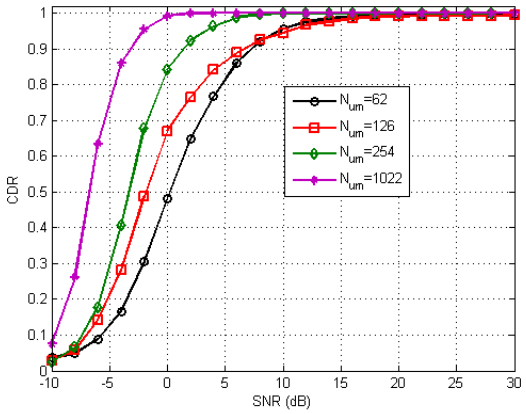

(c) Gold sequences

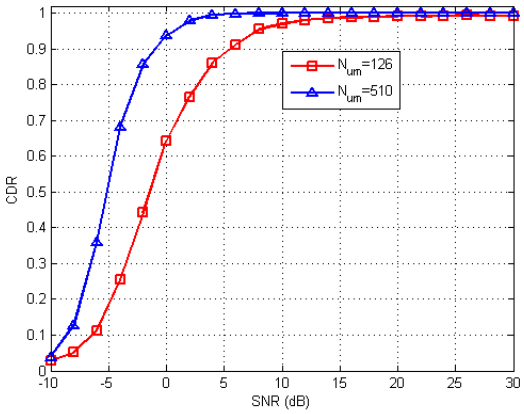

(d) Kasami sequences

Figure 5.5: Correct detection rate using different sub-sequence types for different preamble lengths in the case of multipath channel (4 paths).

To assess the trade-off between the preamble length and the detection accuracy we provide in table 5.1 the minimum required preamble length (in samples) for different targets of correct detection rate for an SNR value of 0 dB. To provide a target correct detection rate more than

60% at an SNR of 0 dB, table 5.1 shows that we require a preamble length ≥ 254 samples using m-sequences and random sequences, whereas using Gold and Kasami sequences we need a preamble of length ≥ 126 samples. Hence, we note that for the same CDR target, it is possible through a judicious choice of training sequence type to reduce the computational complexity to its half. This reduction is possible by using the sequence type for which the CDR is reached with the shortest preamble. We note that even if the Kasami sequences outperform the other considered sequence types, for example for a CDR target of 70%, the lower complexity is obtained using one of the other types because Kasami sequences are not defined for $m = 7$.

Table 5.1: Minimum required preamble length (in term of number of samples) for different CDR target values (SNR= 0 dB).

CDR taget	Random	M-seq	Gold	Kasami
60%	254	254	126	126
70%	254	254	254	510
80%	510	510	254	510
90%	1022	1022	1022	510

5.2.3 Impact of the Uncertainty Interval Width

In this section, we evaluate the impact of the uncertainty interval width ($\Delta\tau$), over which the fine stage is carried, on the detection performance. In particular, we study the trade-off between detection accuracy and computational load. To this end, we assess the CDR of the preamble start estimate for different values of $\Delta\tau$. The same previously considered sequence types are here simulated using a preamble length of $N_{um} = 126$ samples. Simulation results are depicted in figure 5.6 where 5 curves are presented, for each sequence type, corresponding to $\Delta\tau = N_{gm}$, $(4/3)N_{gm}$, $2N_{gm}$, $4N_{gm}$ and $8N_{gm}$. At very low SNR (< -6 dB), the detection performance is almost the same, independently of the sequence type and of the uncertainty interval $\Delta\tau$. Generally, as $\Delta\tau$ value increases, the provided detection rates are enhanced for all the training sub-sequence types. The figure 5.6 shows that above a certain $\Delta\tau$ value ($\Delta\tau = 8N_{gm}$ in this case), the detection accuracy degrades at low SNR, especially for Gold and Kasami sequences. This unpredictable effect comes from the fact that the longer is the search interval, the higher is the probability that a false peak appears, especially at low SNR. For moderate values (< 4 dB) of SNR, the use the same length of $\Delta\tau = 8N_{gm}$ provides lower performance than $\Delta\tau = 4N_{gm}$, for all the envisaged sequence types. Above 4 dB, choosing

$\Delta\tau = 8N_{gm}$ provides the same performance as $\Delta\tau = 4N_{gm}$.

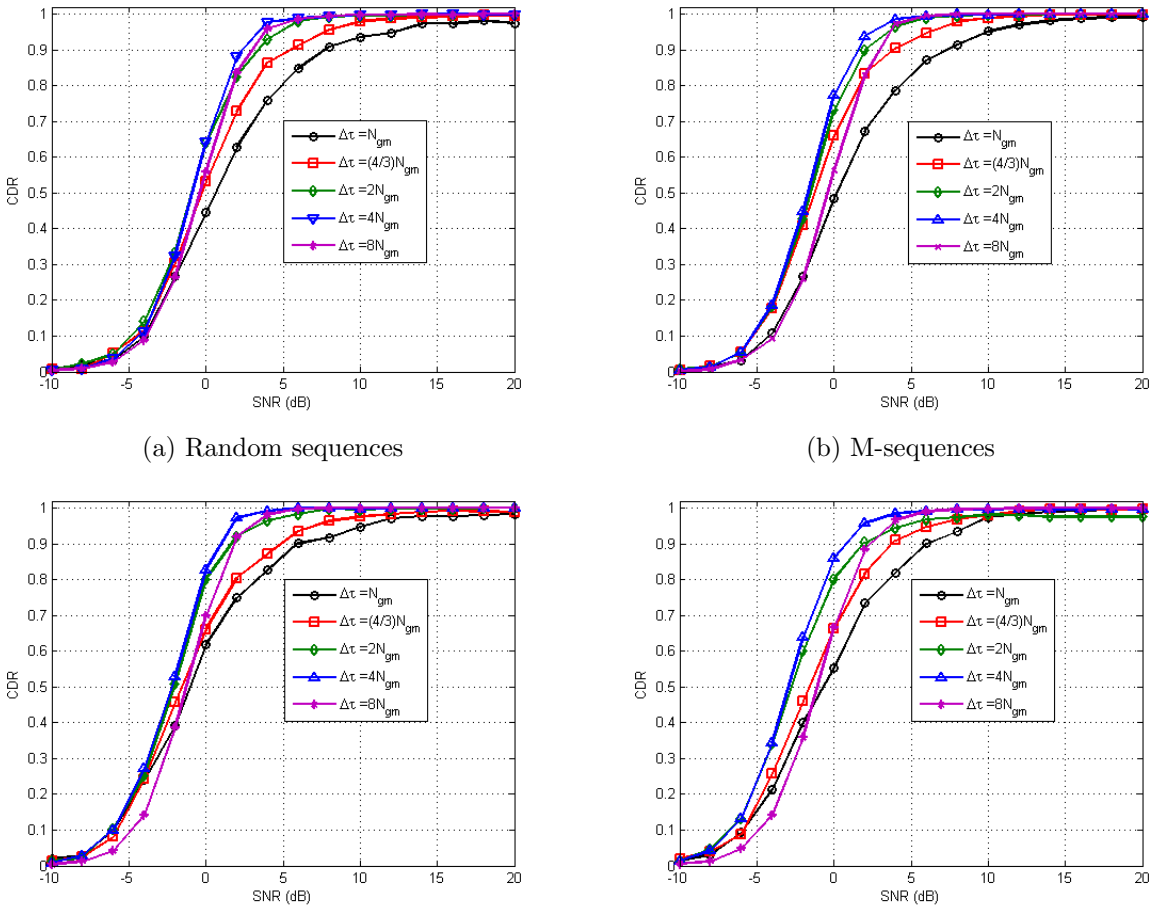

(a) Random sequences

(b) M-sequences

(c) Gold sequences

(d) Kasami sequences

Figure 5.6: Correct detection rate using different sub-sequence types and different values of $\Delta\tau$ in the case of multipath channel (4 paths).

In table 5.2, we present the impact of the uncertainty interval width $\Delta\tau$ on the computational load and the detection accuracy. For an SNR value of 0 dB and a preamble length $N_{um} = 126$, we evaluate the NCM (Number of Complex Multiplications carried to detect the first preamble) as defined in section 4.2.3.2. For each length of the uncertainty interval $\Delta\tau$, we also present the CDR of the preamble start for each training sub-sequence type. It is worth to note that by increasing $\Delta\tau$, the detection performance can be ameliorated up to a specific length ($4N_{gm}$ in this case). Indeed, as shown in the table, the value of $\Delta\tau = 8N_{gm}$ provides a detection rate slightly worse than that provided by $\Delta\tau = 4N_{gm}$, yet with higher computational load.

To summarize, we notice that to optimize the trade-off between synchronization performance

Table 5.2: Trade-off between uncertainty interval width and CDR performance at 0 dB.

$\Delta\tau$	NCM	Rand	M-seq	Gold	Kasami
N_{gm}	$65.3\,10^3$	45%	48%	62%	55%
$(4/3)N_{gm}$	$65.5\,10^3$	54%	65%	66%	68%
$2N_{gm}$	$66\,10^3$	65%	73%	80%	80%
$4N_{gm}$	$67.5\,10^3$	65%	73%	84%	86%
$8N_{gm}$	$70.5\,10^3$	45%	56%	70%	65%

and computational load, a judicious choice of the training sub-sequence type and length as well as of the uncertainty interval width should be accomplished. Indeed, with the same complexity, the detection accuracy can be ameliorated using an appropriate choice of the sequence type. Furthermore, simulation results show that it is possible to enhance the detection accuracy with shorter overhead using well suited training sub-sequence type. Moreover, evaluating the impact of the uncertainty interval length, we notice that it becomes useless to widen the uncertainty interval length up to certain value and this will result in more complexity without enhancing the detection accuracy and for low SNR it even degrades the detection performance.

5.3 Optimization of the Correlation Sequence

The performance analysis realized in the previous section and in section 4.2.3.1 proved the efficiency of the proposed RC approach thanks to the use of differential correlation between α_{FD}, which is generated from the preamble training sub-sequence as in (5.2), and the differentially modulated version of the received signal Y as in (4.2). Although the differential correlation operations have high complexity, by splitting the synchronization processing into two stages, wherein the first stage sliding correlation, characterized by its low complexity is carried while differential correlation is used during the fine stage over a reduced interval, an overall reduced-complexity synchronization is guaranteed.

To further reduce the computational load at the receiver, the idea here is to simplify the differential correlation operations. More precisely, we suggest to replace the differential correlation operations, carried during the fine stage, by simple sign changes. To this aim, we need to derive the best sub-optimal CS in terms of providing near optimal CS performance from a finite QPSK alphabet ($\pm 1 \pm j$). The sub-optimal CS design is carried off-line through different

algorithms. We present three search method for deriving the QPSK sequence, namely the Deterministic Design Algorithm (DDA) [37], the Iterative Design Algorithm (IDA) [37] and the Genetic Algorithm based search [40].

5.3.1 Classic Design Algorithms

The idea of these algorithms is to search for the QPSK sequence leading to the nearest synchronization performance compared to the optimal CS α by searching the sign changes that provide the highest correlation with α.

5.3.1.1 Deterministic Design Algorithm

A deterministic process is here adopted to search the sub-optimal CS. Its aim is to first look for the argument θ that maximizes the metric F_{DDA} defined as

$$F_{DDA}(\theta) = \sum_{k=0}^{L_u-1} |\Re(\alpha(k)e^{-j\theta})| + |\Im(\alpha(k)e^{-j\theta})|, \theta \in [0, \pi/2]. \tag{5.3}$$

The metric F_{DDA} is periodic with period $\pi/2$. Figure 5.7 presents the metric $F_{DDA}(\theta)$ drawn for different gauge of $\Delta\theta$ ($\pi/1000$ and $\pi/50$) using two different randomly generated preamble training sub-sequences $S1$ and $S2$. We note that each scenario provides different maximum values and arguments which may result in different detection performance. Looking at the peaks of each curve, we observe that the maximum value of $F_{DDA}(\theta)$ depends on $\Delta\theta$ and that the maximum argument $\theta_{\max}$ can be missed for large values of $\Delta\theta$.
Secondly, the elements of the sub-optimal CS are then obtained from the sign of the real and imaginary parts of the optimal sequence α when compensated with the phase $\theta_{\max}$ as

$$\beta_k = \text{sign}\left(\Re\left(\alpha(k)e^{-j\theta_{\max}}\right)\right) + j\,\text{sign}\left(\Im\left(\alpha(k)e^{-j\theta_{\max}}\right)\right), \tag{5.4}$$

where $k \in [0, L_u - 1]$.

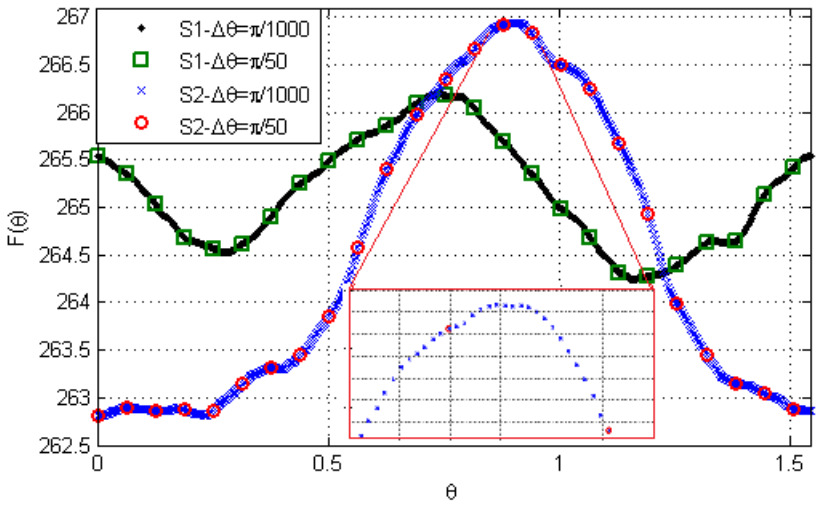

Figure 5.7: Optimization metric of the correlation sequence (F_{DDA} versus θ).

5.3.1.2 Iterative Design Algorithm

The iterative algorithm first defines the metric F_{IDA} operating on a randomly chosen sequence $S = [s(0), s(1), \ldots, s(L_u - 1)]$, from a finite QPSK constellation, written as

$$F_{IDA}(S) = \sum_{k=0}^{L_u-1} \alpha(k)s^*(k) = \rho(S)e^{j\theta(S)}, \tag{5.5}$$

From the initial random sequence S, the algorithm iteratively recalculates the metric F_{IDA} in order to maximize its amplitude ρ. For each iteration i, the metric is compensated by the phase $\theta^{(i-1)}$ of its previous value. At the i^{th} iteration, the IDA can be summarized as follows

1. For the updated sequence $S^{(i)}$ (for $i = 0$, $S^{(0)}$ is the initial randomly QPSK generated sequence), calculate the metric in equation (5.5),
2. Compensate $\alpha^{(i)}$ with the phase $\theta^{(i)}$ resulting from the metric F_{IDA} calculated in step 1, which provides a new sequence $\alpha^{(i+1)}$,
3. Re-compute the new sequence $S^{(i+1)} = \text{sign}\left(\Re\left(\alpha^{(i+1)}\right)\right) + j\ \text{sign}\left(\Im\left(\alpha^{(i+1)}\right)\right)$,
4. Repeat steps 1, 2 and 3 until a stop condition is met.

The stop condition can be set as the convergence of θ value, which is attained when

$\left|\theta^{(i+1)} - \theta^{(i)}\right|$ is below a given threshold, or as the achievement of a parameterized maximum number of iterations. Then, the best sub-optimal correlation sequence β is considered as the last generated sequence $S^{(i_{\max})}$. We note that, for various initial sequences S, the detection performance may be different. This can be proved by trying many random sequences.

5.3.1.3 Comparison of the DDA and IDA Performance

To assess the performance degradation caused by the quantification of the CS, we use the criterion of the preamble start CDR (as previously defined) and its estimation variance. A quantitative evaluation of the complexity gain is achieved to measure the NCM saved thanks to the use of the QPSK sub-optimal sequences. The RC synchronization approach is here evaluated in 4 scenarios using different correlation sequences: the optimal sequence α, a sub-optimal quantified version of α, generated from the sign of α elements as $\alpha' = \text{sign}\left(\Re\left(\alpha\right)\right) + j\text{sign}\left(\Im\left(\alpha\right)\right)$, and the two quantified sequences obtained by the off-line application of the DDA and IDA, denoted respectively by β_{DDA} and β_{IDA}. In the IDA, the stop condition is fixed by a maximum number of iteration set to 10^3. The OFDM system and the channel parameters are the same described in section 4.2.3.1 ($m = 9$, multipath channel with 7 paths).

Figure 5.8 depicts the CDR of the preamble start (a) and its estimation variance (b) in the AWGN channel. The optimal sequence α provides the best performance detection, yet with higher complexity compared to the other sub-optimal CS. The sequence α' provides the worst performance. In between, the new sequences β_{DDA} and β_{IDA} give the same detection performance. For a target CDR of 80%, the sequence α realizes a slight gain of about 0.8 dB, compared to the quantified sequences β_{DDA} and β_{IDA}. Consistently with the CDR, the variance provided using the optimal CS α is the lowest one and its curve vanishes at an SNR equal to -3 dB, thus realizing a gain of about 1 dB compared to the quantified sub-optimal correlation sequences, whose curves vanish at -2 dB.

The previously presented results are shown in figure 5.9 in the case of multipath channel. The same effects are here observed. Indeed, the optimal sequence α outperforms the other quantified sub-optimal sequences. For all considered sequences, the detection becomes perfect (CDR = 100%) above an SNR of about -3 dB and 0 dB respectively in the monopath AWGN and multipath channels.

To compare the computational load involved in the fine stage using the optimal sequence

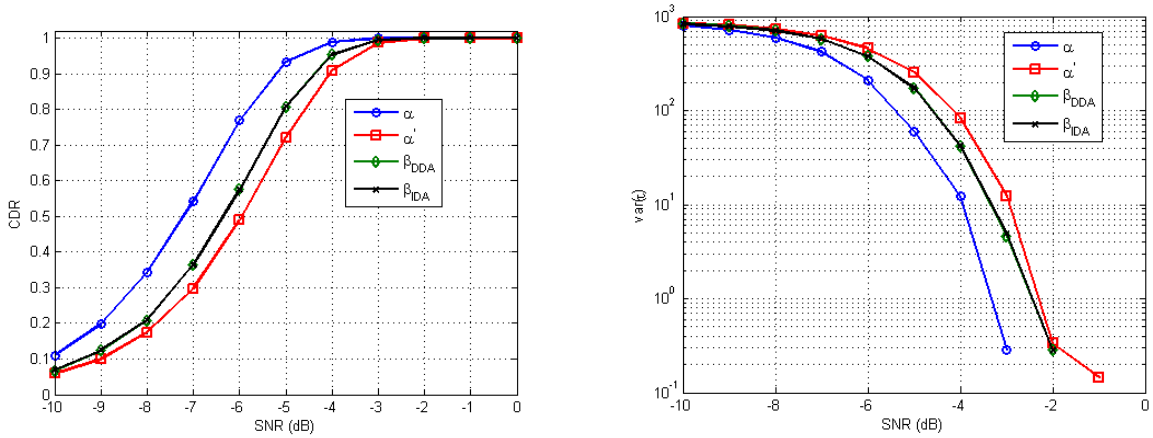

(a) Correct Detection Rate of the preamble start

(b) Time estimation variance

Figure 5.8: Evaluation of the performance degradation occasioned by the CS quantification using classic algorithms in the monopath AWGN channel.

α and the sub-optimal sequences, generated by the mean of the proposed DDA and IDA, we assess the NCM operations carried during the fine stage. We recall that a differential correlation operation (carried using α) costs L_u complex multiplications. Thus, when correlating the received signal with α, the fine metric complexity is of $\Delta\tau L_u$ complex multiplication operations. Whereas, only one sign change operation is required using the quantified sequences β_{DDA}, β_{IDA} and α'. Hence, the complexity of the fine metric calculation can be reduced to $\Delta\tau$ sign change operations, respecting the sign of sub-optimal CS sequences, which is a trifling complexity treatment compared to complex multiplication operations.

To evaluate the performance degradation caused by the CS quantification, we also present the SNR required to reach a target correct detection rate of 70%. We note that the fine metric calculated using all the quantified correlation sequences have the same complexity, as they replace the differential correlation operations by sign changes. As shown in table 5.3, the complexity involved using the optimal sequence α is about $52\ 10^3$, which is much more high than that of the sub-optimal sequence that costs only 102 sign change operations. However, its gain in terms of detection accuracy is slight in both AWGN and multipath channels compared to sub-optimal CS case. Indeed, for a target correct detection rate of 70%, a loss of only 0.8 dB is occasioned by the use of β_{DDA} and β_{IDA}.

From the simulation carried in this section, we note that the use of sub-optimal quantified CS helps to reduce the computational load at the expense of a slight performance degradation. However, even for exhaustive search, over the huge set of CS candidates within sequences

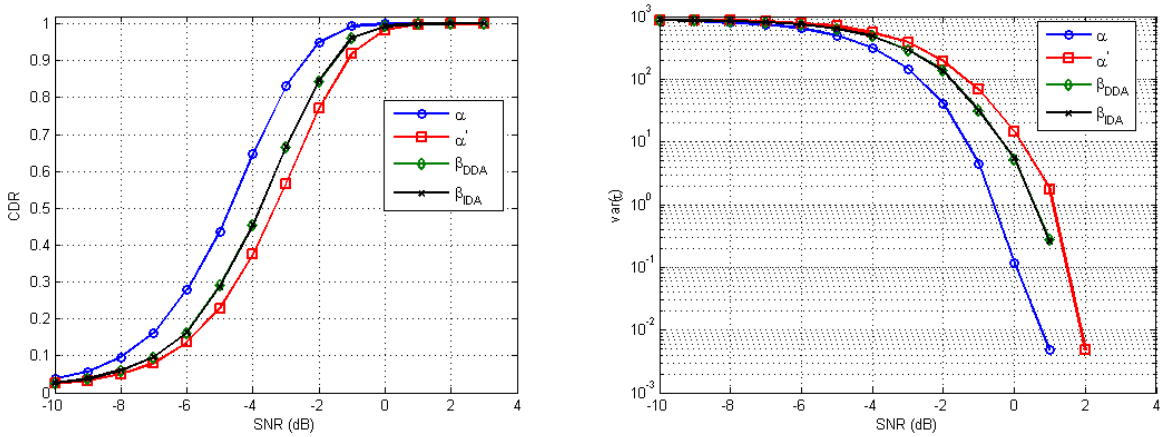

(a) Correct Detection Rate of the preamble start

(b) Time estimation variance

Figure 5.9: Evaluation of the performance degradation occasioned by the CS quantification using classic algorithms in the multipath channel (7 paths).

Table 5.3: NCM carried during the fine stage and SNR required for a target CDR of 70%.

	NCM	SNR for AWGN Chan	SNR for multipath Chan
α	$52\ 10^3$	-6.3 dB	-3.8 dB
α'	-	-5.1 dB	-2.5 dB
β_{DDA}	-	-5.5 dB	-3 dB
β_{IDA}	-	-5.5 dB	-3 dB

taken from QPSK alphabets, the quantified resulting CS may correspond to local sub-optimal sequence, which does not provide the near-best detection performance. As an alternative, we suggest the use a Genetic Algorithms (GA) based search approach to further lessen the performance degradation occasioned by the use of sub-optimal sequences.

5.3.2 Genetic Algorithms Based Design

In the IDA and DDA search techniques, an important complexity reduction was recorded at the expense of a loss in detection accuracy. To minimize this loss, with respect to the optimal CS, we here opt for a genetic algorithms based search to find the sub-optimal quantified CS that leads to near-best CS performance [36]. Indeed, the GA principle provides a powerful tool to efficiently explore a very large space of solutions, which is the case in the present work in which the set of CS candidates is huge. Furthermore, the GA-based search methods have the

advantage of avoiding the sensitivity to initialization, as it is required in the case of the IDA.

The GA [111] search techniques are generally used to find true or approximate solutions to optimization and search problems. They are exploited in different application fields of communication engineering such as sequence generation, cooperative communication and PAPR reduction [112]- [114]. Generally, the optimization using GA allows numerical solution otherwise unfeasible or complicated to be carried by using an by analytical approach. In our case, we exploit the GA search scheme to generate the sub-optimal CS. We note that this processing is done off-line, which relaxes the complexity of the exhaustive search procedure and avoids real-time constraints.

5.3.2.1 Overview of Genetic Algorithms

The genetic algorithms are evolutionary search techniques used to find true or approximate solutions for optimization and search problems [110]. A GA is a random search technique that seeks out the best feature from an evolving available search space known as *population*. This latter comprises a group of *individuals*, each characterized by a set of chromosomes, considered as *candidates* which can be selected as solutions. The individuals of the first population are generated randomly. The search procedure is performed based on an objective function known as *fitness function*. In each iteration, the candidates of a population are evaluated according to their fitness values. Several processes such as *crossing* and *mutation* allow introducing diversity through the successive populations. In crossing, a particular group of well ranked individuals, which are chosen as parents, are used to generate the offspring according to a crossing rule. The fitness of the offspring will also be evaluated in a similar way to their parents. To avoid local optimal problems, randomly generated individuals can be inserted in a new generation. This cycle is repeated until a desired termination criterion is reached (convergence, a predefined number of generations is produced). The best individual in the last population is considered as a solution of the problem.

5.3.2.2 Proposed Genetic Algorithms-Based CS Search

The process of the proposed GA-based search scheme starts with the definition of the coding rule and consequently the population initialization. Then, the sequential reproduction of new populations is carried, based on the chromosomes of individuals (candidates) having the best

goodness (fitness function), until a stop condition is met. Different steps involved in this processing are hereafter described.

a) GA Parameters Definition for the CS Optimization

Coding: Finding a suitable coding of the chromosomes is one of the most tricky and difficult problems in applying GAs. A good choice of representation will make the search easy by limiting the search space, a poor choice will result in a large search space. Various coding types exist (Bit string, real number representation, order-based representation, embedded lists...). We here choose the value encoding method, in which each individual represents a CS defined as an array of L_u chromosomes represented by complex number from QPSK alphabet ($\pm 1 \pm j$).

Population initialization: The initial population is composed of P individuals randomly generated from a QPSK constellation ($\pm 1 \pm j$). Thus, the population is a (P,L_u) matrix of complex elements taken from QPSK alphabet. We note that P must be parameterized depending on the CS length L_u (the longer is L_u, the higher is P) in order to explore a sufficiently large number of the CS candidates space of size L_u^4.

b) GA Processes Definition for CS Optimization

Selection: The selection of the best individuals is here chosen to be based on the evaluation of the fitness function $|F_{IDA}(S)|$, expressed in equation (5.5), which we aim to maximize. Within one generation, the individuals selected as survivors to be preserved in the updated population, are those giving the best fitness function values. There are different possible selection procedures in the GAs depending on how the fitness value is used. Proportional (roulette-wheel), truncation and tournament selections are the most popular selection procedures. We here opt for the truncation selection, where the solution candidates are ordered by fitness value, and a proportion p (e.g. $p = 1/2$, $1/3$, etc) of the fittest individuals is selected as survivors. In this case, the individual of high fitness has an important probability to survive and to create an offspring and thus to transfer its genes to the next population.

Crossover: The first step in the reproduction process is the crossover, in which the chromosomes of the parents P_n and P_m are used to form an entirely new individual. It is a

recombination operator that combines sub-parts of the two parents chromosomes to produce two offspring O_1 and O_2 that inherit some parts of both parents genetic material.
One-point crossover combines two chromosomes with one crossover point. Multi-point crossover combines two individual with several crossover points. Uniform crossover makes a mask formed by a binary sequence and generates two children chromosomes from those of their parents, using this mask. In our work, we choose the multi-point crossover for more diversity. In each iteration, a number of crossover operations c is randomly chosen lower than a maximum fixed crossover point number. The crossover positions are also randomly chosen.

Mutation: The mutation operation prevents the convergence to a locally optimum solution. It is an operation involving changing some chromosomes to introduce variations into the individual. The newly created population (by means of selection and crossover) is later subject to mutation. This operation occurs with small probability P_{mu} and replaces the chosen chromosomes by randomly generated ones.

Note that the crossover and mutation operators are means of large exploration of the solutions space. The higher is the number of crossover points c, the quicker is the introduction of new solutions into the population. However, as c increases the solutions may be disrupted faster. Similarly, the mutation probability P_{mu} also affects the quality of the population. Large values of P_{mu} transform the GA into a purely random search algorithm, while some mutation are required to prevent the premature convergence of the GA to sub-optimal solutions.

After performing the crossover and mutation operations in the current generation, individuals with high fitness are selected to be used in the reproduction of the new population. In our work, to avoid the problem of having a local optimal solution, 10% of each new population is generated randomly. From the new population, based on the fittest fitness values of the individuals, the reproduction procedure is repeated until either the stagnation of the fitness maximum value or a specified maximum number of iterations is reached. The sequence having the highest fitness in the last population is elected as the optimal CS.

5.3.3 Comparison of Classic and GA-Based Search Schemes

In this section, the comparison of the detection accuracy provided by the use of the GA-based quantified CS to the classically generated CS through the DDA and IDA schemes, which provide

almost the same detection accuracy is conducted. To assess the performance degradation occasioned by the used of the differently quantified correlation sequences, the comparison also involves the optimal sequence α.

Three scenarios are here simulated for three different CS lengths L_u. The population size, crossover rate and mutation rate are then chosen depending on $L_u \in \{64, 128, 256\}$. An exhaustive search over all possible QPSK CS involves 16.7 10^6, 26.8 10^7 and 42.9 10^8 candidates respectively for sequence lengths of 64, 128 and 256. This results in a prohibitive complexity thus justifying the GA-based search efficiency. Note that the longer is the CS, the higher are the population size, the crossover and mutation rates. The population size is set to 10^3 for the considered CS lengths of 64 and 128 samples and to 10^4 for the length of 256 samples. In each iteration, the number of crossover points is chosen randomly lower than 10% of L_u and their positions are also picked out randomly. Mutation rate is set to 0.2% of the sequence length L_u. The stop condition for the generation of populations is the stagnation of the maximum fitness value which is defined through simulation. To fix the number of iterations required to reach the stop condition, we evaluate the maximum fitness values for all considered CS lengths. Figure 5.10 shows the evolution of maximum, mean and minimum fitness values for 10^3 iterations (generations) for the considered L_u values. As shown in the figure, the maximum fitness value stagnates after a certain number of generations. Hence, we need to set the maximum number of generations to a best fit number that helps us to find the optimal solution without wasting execution time. Through experimental search, we set the stop condition of the GA-based iterative processing to 200 generations, 500 generations and 1000 generations respectively for CS lengths equal to 64, 128 and 256 samples.

The CP length N_g is set to 5% of the CS length, the correlation shift q is set to 1 and the uncertainty interval $\Delta\tau$ is taken equal to the CP length (N_g). We consider an AWGN monopath channel and an exponential power delay profile 4-path channel of memory $L_H = 12$ samples. The ratio of the first path to the last path is of 12 dB with uniform adjacent path ratio of 3 dB. The 4 effective paths are uniformly spaced with a delay of 3 samples. For all considered scenarios, we use the Monte Carlo simulation method with 10^4 iterations.

Figure 5.11 presents the CDR of the preamble start (a) and its estimation variance (b) in the AWGN channel. We note that the use of the optimal sequence α in equation (5.1) provides the best detection performance. The CS generated through GA-based scheme, within QPSK alphabet, provides slightly lower detection rate with a loss of about 0.2 dB. The sub-optimal

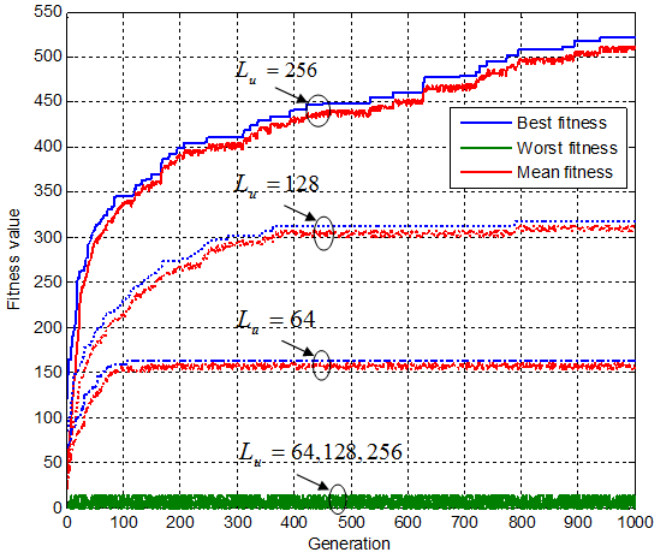

Figure 5.10: Fitness value versus number of generations for CS lengthes of 64, 128 and 256 samples.

quantified CS provided by the IDA (and the DDA) has the worst performance detection. Considering a CS of length 64, for a target CDR of 80%, the optimal sequence α realizes a gain of about 0.2 dB and 2 dB, compared to respectively the GA-based and the IDA-based correlation sequence choices. Both of the sub-optimal CS provide a correct detection (with a rate of 100%) above an SNR of 0 dB.

Figure 5.11.(b) shows that, consistently with the CDR, the variances provided using α and the GA-based searched CS vanish at an SNR equal to -1 dB with a gain of about 1 dB realized by the optimal sequence α for $L_u = 256$ samples. Whereas, the variance corresponding to the CS chosen using the IDA vanishes at an SNR equal to 2 dB. For shorter preamble length $L_u = 64$, the variance values vanish at SNR equal to 4 dB using the optimal sequence and 5 dB using the sub-optimal sequences, yet the GA-based generated sequence provides almost the same detection as the optimal one. Generally, the longer is the CS, the lower is the variance. This behavior is inverted for low SNR values (< -3 dB) where the noise dominates the received signal. This fact is due to the uncertainty interval length which limits the maximum variance value, whose length is here chosen as a fraction of the preamble length.

Figure 5.12 shows the frame start CDR (a) and the time estimation variance (b) of the considered scenarios in the case of multipath channel. As in the previous monopath channel case,

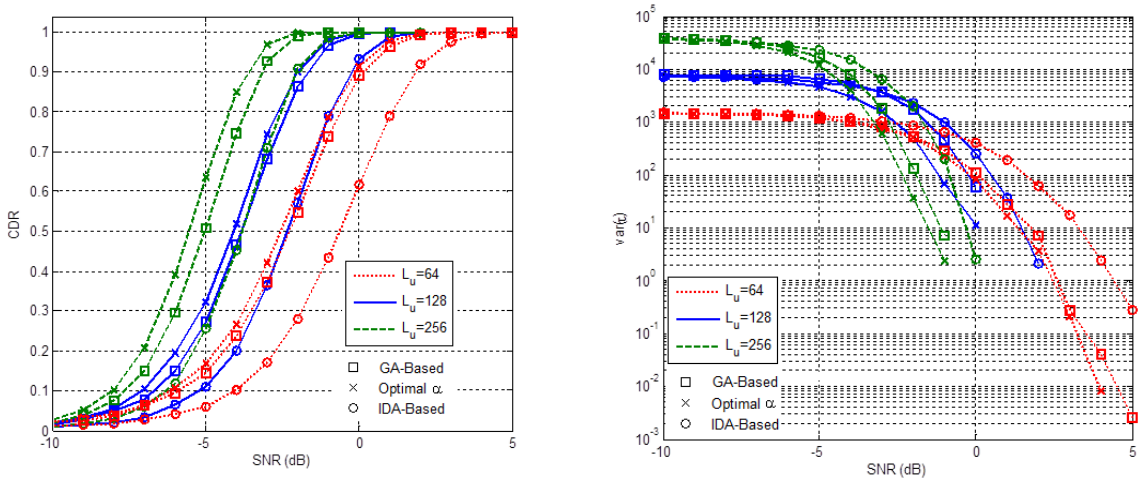

(a) Correct Detection Rate of the frame start

(b) Time estimation variance

Figure 5.11: Evaluation of the performance degradation occasioned by the CS quantification in the monopath AWGN: classic and GA-based search.

the optimal CS α provides the most accurate detection, yet it leads to a high computational load at the receiver. The IDA-based quantified CS provides the worst performance detection. In between, the GA-based CS provides almost the same accuracy as that obtained by the optimal sequence α. The loss resulting from the quantification of the CS slightly rises compared to the case of the monopath AWGN channel. It is also worth to note that as we use the same population size for both sequence lengths $L_u \in \{64, 128\}$, the performance degradation occasioned by the use of the sub-optimal sequence is higher for the longer sequence.

Note that the compared sub-optimal CS design methods (GA-based and IDA-based) provide QPSK ($\pm 1 \pm j$) sequences allowing simple sign changes instead of differential correlation operations. Thus, they have the same reception complexity, which is greatly lower than the complexity resulting from the use of the optimal correlation sequence α. For the execution time of the CS search, the GA-based search takes much more time than the IDA-based search. This is expected since the GA is more computationally complex due to the crossover operations and the number of generations that fix the execution time. However, as the CS choice optimization is carried off-line, the GA-based search higher complexity is not critical and it can be considered as the most appropriate one. It is demonstrated that compared to the iteratively generated CS, the GA-based generated sequence improves the detection accuracy and compared to the optimal CS α, it provides slightly lower detection accuracy with important reduction in the receiver complexity. The advantage of GA over IDA is to avoid local sub-optimal solutions by

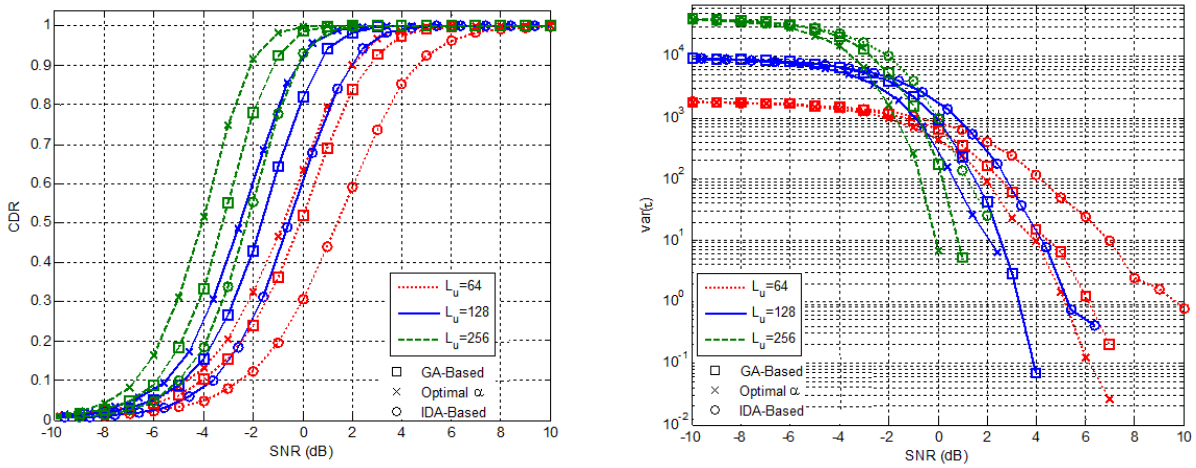

(a) Correct Detection Rate of the frame start

(b) Time estimation variance

Figure 5.12: Evaluation of the performance degradation occasioned by the CS quantification in the multipath channel: classic and GA-based search.

allowing a better exploration of the potential solutions huge set.

Conclusions

In the previous chapter, we have assessed the performance of the RC technique which was shown to provide high detection accuracy with low computational load. To further reduce the computational load of the proposed RC technique, we have studied the optimization of several critical parameters in this chapter. First, for binary time domain generated sequences, the effect of the preamble training sequence choice (type and length) on the detection accuracy was studied. Simulation results, carried in the case of multipath channel and using different sequence types (m-sequence, random, Gold and Kasami sequences), proved that with the same overhead (same complexity) the detection accuracy can be ameliorated using an appropriate sequence type choice. Consequently, it is possible to reduce the computational load by choosing suitable type and shorter training sub-sequence. The optimization of the uncertainty interval width, over which the fine stage is carried, was also studied through simulations. It was shown that, increasing the uncertainty interval width, the detection accuracy can be enhanced up to a certain width above which the detection performance stagnates and may degrades for some training sub-sequence types. Hence, to optimize the trade-off between synchronization performance and computational load, a judicious choice of the training sub-sequence type and

length as well as of the uncertainty interval width should be accomplished.

In the second part of this chapter, we have proposed search algorithms to optimize the correlation sequence choice for frequency domain generated training sub-sequences. The idea behind the CS optimization was to generate a sub-optimal sequence belonging to a finite QPSK alphabet ($\pm 1 \pm j$), which allows to replace the differential correlations carried during the fine stage by simple sign changes. We investigated the sequence search through two classic iterative and deterministic schemes and a genetic algorithm based scheme. The advantage of the GA based search over classic search (deterministic and iterative) schemes is its adequacy to avoid local optimal and its lower sensitivity to the initialization of CS candidates. Simulation results conducted in both monopath AWGN and multipath channels showed the effectiveness of the use of sub-optimal sequence in further lowering the reception computation cost of the RC synchronization technique. Indeed, when compared to the performance obtained using the optimal CS, the GA-based search offers a CS that provides very close detection accuracy, while the sequence generated through classic search algorithms provides 2 dB lower performance. Furthermore, the use of the sub-optimal sequences results in a complexity reduction of L_u complex multiplications per correlation step calculated during the fine synchronization stage.

Chapter 6

Simply and Doubly Differential Synchronization: Zadoff-Chu Sequences

The so far proposed synchronization algorithms use training sequences made of binary elements either in time or frequency domains and do not exploit further characteristics than their good autocorrelation properties. In the present chapter, we consider Zadoff-Chu (ZC) sequences, which have been proposed as training sequences in modern wireless communication systems, and tailor synchronization approaches constructed based on ZC sequences structure, replacing the conventional random and pseudo-random sequences thanks to their perfect autocorrelation properties. ZC sequences are indeed a class of CAZAC sequences, which we have briefly introduced in section 3.2.2, defined for prime lengths. Exploiting ZC sequences in the time domain, we here propose two new synchronization approaches, which are based on differential correlation and are referred to as Doubly-Differential (DD) [42] and Simply-Differential (SD) [43] approaches. Both of the proposed approaches allow time synchronization by detecting the start of a ZC sequence within the received signal. The SD approach carries simultaneous autocorrelation and compensation of the received signal with a frequency shift whose value depends on the sent ZC sequence. The DD approach sums the doubly-differential correlated consecutive samples to detect a ZC sequence pattern regardless of the sent ZC sequence. Both of the proposed differential correlation based approaches (DD and SD) can be implemented in a recursive way, which allows to greatly reduce the incurred computational load.

Recently, ZC sequences have been employed in the 3GPP LTE and LTE-Advanced standards, as frequency domain training sequences, for Uplink (UL) and Downlink (DL) synchronization. It is known that the IFFT of a ZC sequence remains a ZC sequence, yet with different parameters. Hence, the proposed synchronization techniques, based on ZC sequence use in the temporal domain, can be applied with some adaptations to the LTE standard for primary synchronization. This latter consists in detecting the symbol start as well as the Sector Identifier (S-ID) and it exploits the dedicated Primary Synchronization Signal (PSS) which is made from ZC sequences. In this case, the DD approach proceeds in two stages, wherein the first stage a coarse time estimation is achieved by localizing the arrival of a ZC sequence. In the second stage, cross-correlation of the received signal with the local known ZC sequence candidates is carried to detect the exact PSS start and the S-ID. Unlike the conventional methods that perform the cross-correlation over all demodulated OFDM symbols, the DD approach carries it over a short interval centered on the coarse time estimate, which greatly reduces its complexity. The SD approach achieves time synchronization and sector search in a sole stage, which is a particular feature compared to the existing detectors and the herein proposed DD approach, in which the S-ID is always determined by cross-correlation with the local known ZC sequences (or PSS) candidates.

At the end of this chapter, a comparison of the proposed SD and DD approaches to some existing primary synchronization benchmarks is provided for system parameters and channel conditions different from the works in [42] and [43].

6.1 Proposed Synchronization Techniques

This section is devoted to describe the proposed time synchronization approaches based on ZC sequences. We first recall the rule to generate the complex exponential ZC sequence, which we here denote by d_u. The ZC sequence is given by

$$d_u(n) = e^{-j\frac{\pi u n(n+1)}{N_{zc}}},\ 0 \leq n \leq N_{zc} - 1, \tag{6.1}$$

where N_{zc} stands for the sequence length and u refers to the root of the ZC sequence relatively prime to N_{zc}. It was shown in [85] that circular shifted versions of a ZC sequences are uncorrelated from each other which makes them excellent candidates for time synchronization.

6.1.1 Doubly-Differential Approach

The Doubly-Differential (DD) approach achieves time synchronization by localizing the arrival time of a ZC sequence within the received signal, regardless of the sent training ZC sequence. The metric $M_{DD}(d)$ consists in summing the doubly-differential correlated consecutive received samples as

$$M_{DD}(d) = \sum_{l=0}^{N_{zc}-1} \left(r_{d+l} r^*_{d+l-q}\right)\left(r_{d+l-1} r^*_{d+l-1-q}\right)^*, \tag{6.2}$$

where q stands for the correlation shift arbitrarily chosen in the range of [1,$N_{zc}-1$]. Let $m_{DD}(d) = r_d r^*_{d-q} r^*_{d-1} r_{d-1-q}$ denote the correlation output of the d^{th} received sample which will be summed in the metric $M_{DD}(d)$. For weakly correlated samples, the differential correlation output has low value. Whereas, for d values corresponding to samples taken from the ZC sequence, $m_{DD}(d)$ turns into

$$\begin{aligned} m_{DD}(d) &= d_u(d) d^*_u(d-q) d^*_u(d-1) d_u(d-1-q) \\ &= e^{-j2\pi u \frac{d}{N_{zc}}} e^{j2\pi u \frac{(d-q)}{N_{zc}}} \\ &= e^{-j\frac{2\pi u q}{N_{zc}}}. \end{aligned} \tag{6.3}$$

We then note that $m_{DD}(d)$ is independent of d when it includes samples falling within the ZC sequence and it has a constant value equal to $e^{-j\frac{2\pi u q}{N_{zc}}}$. Hence, the metric in equation (6.2) sums constructively and, as shown in figure 6.1, its amplitude $|M_{DD}|$ exhibits a triangular shape that reaches its maximum at the ZC sequence start where it sums over the N_{zc} samples of constant values.

As can be seen through equation (6.2), the metric M_{DD} has a heavy complexity due to differential correlation operations. To decrease its computational load, we propose a reduced-complexity recursive implementation of (6.2) using the following formula

$$M_{DD}(d+1) = M_{DD}(d) - m_{DD}(d) + m_{DD}(d+N_{zc}). \tag{6.4}$$

Using the timing metric expression in (6.2), the calculation of each element requires $3N_{zc}$ complex multiplication operations, which results in a huge computational load. However, only 6 complex multiplication operations are required using the recursive form of the metric (6.4), which allows to save $3N_{zc}-6$ complex multiplication operations per metric evaluation with

2 more complex addition operations, whose computational load is negligible compared to the complex multiplication operations.

6.1.2 Simply-Differential Approach

The Simply-Differential (SD) approach makes the detection faster as it requires lower number of complex multiplications. We here suggest a timing metric in which the received signal is autocorrelated and compensated with a frequency offset whose value depends on the ZC sequence used in the preamble generation.

Let us define λ_l as the differential correlation outcome of the l^{th} received sample with its q-shifted counterpart: $\lambda_l = r_l^* r_{l+q}$. When the received samples belong to the ZC sequence and under noiseless conditions (ideal channel), λ_l becomes

$$\begin{aligned} \lambda_l &= e^{j\pi u l(l+1)/N_{zc}} e^{-j\pi u(l+q)(l+q+1)/N_{zc}} \\ &= e^{-j\pi u(2ql+q^2+q)/N_{zc}}. \end{aligned} \tag{6.5}$$

When compensated with its complex conjugate, λ_l turns into a constant for samples falling within the ZC sequence. We exploit this feature to define the metric M_{SD}^u that sums the compensated elements over N_{zc} samples as

$$M_{SD}^u(d) = \sum_{l=0}^{N_{zc}-1} \lambda_{d+l} e^{j\frac{\pi u}{N_{zc}}\left(2q(d+l)+q^2+q\right)}, \tag{6.6}$$

where u stands for the root of the known ZC sequence which is used in the preamble generation. As shown in figure 6.1, the magnitude of the metric M_{SD}^u provides a triangular shape, similarly to the metric M_{DD}, whose maximum value indicates the start of the ZC sequence. Continuously calculating the metric M_{SD}^u in (6.6) leads to an exhaustive treatment complexity load lower than that of the DD approach, yet it is still high. Hence, for complexity reduction, we propose a recursive implementation of M_{SD}^u as

$$M_{SD}^u(d+1) = M_{SD}^u(d) - m_{SD}^u(d) + m_{SD}^u(d+N_{zc}), \tag{6.7}$$

where

$$m_{SD}^u(d) = \lambda_d e^{\frac{j\pi u}{N_{zc}}(2qd+q^2+q)}. \tag{6.8}$$

In the initial metric (6.6), the computation of each element $M_{SD}^{u}(d)$ requires $2N_{zc}$ complex multiplication operations. However, the expression in (6.7) reduces this number to only 4 with additional 2 complex addition operations whose computational load is trifling compared to that of the complex multiplication operation. Thus, $2N_{zc} - 4$ complex multiplication operations (96%) are saved.

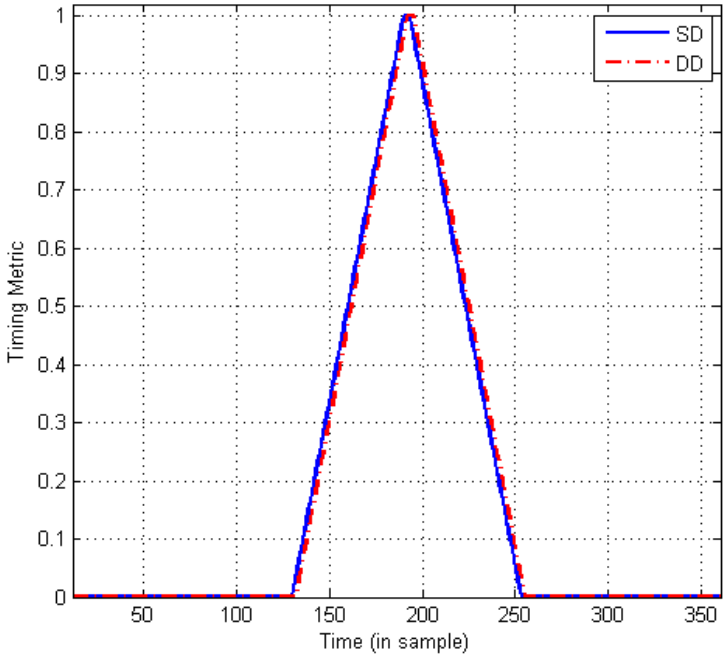

Figure 6.1: The proposed doubly-differential and simply-differential metrics (M_{DD} and M_{SD}) under noiseless conditions.

The timing metrics of the DD and SD approaches are depicted in figure 6.1 for a ZC sequence of length $N_{zc} = 63$ and root $u = 25$. The peaks of the metrics indicate the start of the ZC sequence sent directly in the time domain and which is here preceded by random data.

It was shown in [90] that the IFFT of a ZC sequence maintains its properties and remains a ZC sequence, which makes the herein proposed synchronization techniques available for ZC sequences defined in the time domain extensible to the case of ZC defined in the frequency domain. Hence, they can be applied in numerous existing standards and in particular to the 3GPP LTE standard as explained in the next section.

6.2 Application to the 3GPP LTE Standard

This section is devoted to describe the application of the proposed DD and SD synchronization approaches to the LTE standard for DL primary synchronization. This task includes the detection of the synchronization signal, which is made from ZC sequence, and the sector identifier. To this aim, we first provide a state of the art of the LTE standard and existing synchronization techniques in LTE. Then, the proposed techniques are presented when applied to the considered standard with the incorporation of the required modifications for ZC sequences defined in the frequency domain.

6.2.1 State of the Art of LTE Standard

6.2.1.1 LTE Signal Description

The LTE as defined by the 3GPP is an innovative wireless communication standard which provides peak rates of at least 100 Mbps and 50 Mbps for DL and UL respectively and it supports scalable bandwidth from 1.4 MHz to 20 MHz. The wide range of system bandwidths helps to operate in a large number of different spectrum allocations. LTE also supports both Frequency-Division Duplex (FDD) and Time-Division Duplex (TDD). By offering highly flexible radio interface, LTE suits the needs of different network operators that have different bandwidth allocations. Compared to the traditional communication networks, many innovative techniques are applied to improve the LTE capabilities. Among them, the OFDM which is known by its robustness to frequency-selective channels is used for the DL transmission [116]. For the UL, where the available transmission power is significantly lower than that for the DL, single-carrier transmission based on DFT-precoded OFDM, also referred to as single-carrier frequency-division multiple access (SC-FDMA), is used. Having smaller PAPR than the OFDM, the SC-FDMA technique enables lower complex and/or higher-power terminals [117], which improves coverage and reduces terminal cost and power consumption.

Before a User Equipment (UE) can communicate through an LTE network it has to acquire synchronization to a cell within the network. Precisely, it should accomplish primary synchronization which consists in detecting the PSS start and determining the S-ID. In addition, the secondary synchronization has to be processed, which aims to identify the sub-frame number and the cell group identifier. For the secondary synchronization, the LTE standard uses

the Secondary Synchronization Signal (SSS) which also has a specific structure and is made from m-sequences. There are 504 different physical-layer cell-ID which are grouped into 168 groups identified by a number $N_{ID}^{(1)}$ (ranging from 0 to 167), where each group consists of three identities specified by a number $N_{ID}^{(2)}$ (ranging from 0 to 2). The cell-ID is then determined as

$$C_{ID} = 3N_{ID}^{(1)} + N_{ID}^{(2)}. \tag{6.9}$$

The parameter $N_{ID}^{(2)}$ represents the sector identifier (S-ID) of each cell, which is strongly related to the PSS, whereas the parameter $N_{ID}^{(1)}$ represents the physical-layer group identifier and is sent on the SSS.

a) Downlink Frame Structure

In LTE systems, the transmitted signal is organized into radio frames of $10ms$ duration, each consisting of 10 sub-frames of length $1ms$ which are further divided into two slots of $0.5ms$ each. In case of FDD, all sub-frames of a carrier are used for either DL transmission or UL transmission. On the other hand, in case of TDD, the first and sixth sub-frames of each frame (sub-frame 0 and 5) are always assigned for DL transmission, while the remaining sub-frames can be flexibly assigned to be used for either DL or UL transmissions. We here focus on the former mode, whose frame structure is presented in figure 6.2. We note that depending on whether normal or extended CP is used, a slot contains 7 or 6 OFDM symbols of duration equal to $66.7\mu s$ each. Among them, the LTE system reserves two symbols for the PSS and the SSS. Synchronization signals are sent regularly (in each sub-frame) in the last two OFDM symbols of slot 0 and slot 10. Transmitted data are mapped on a time-frequency resource grid consisting of elementary units, called resource elements, defined as one 15 kHz sub-carrier by one symbol. Resource elements aggregate into resource blocks having dimension of 12 consecutive sub-carriers in the frequency domain over 6 OFDM symbols for extended CP or 7 OFDM symbols for normal CP. The first symbol in each frame has a longer CP with length denoted by N_{g1} [115].

We note that in the case of TDD mode, the PSS is transmitted within the third symbol of sub-frames 1 and 6 while the SSS is transmitted in the last symbol of sub-frames 0 and 5.

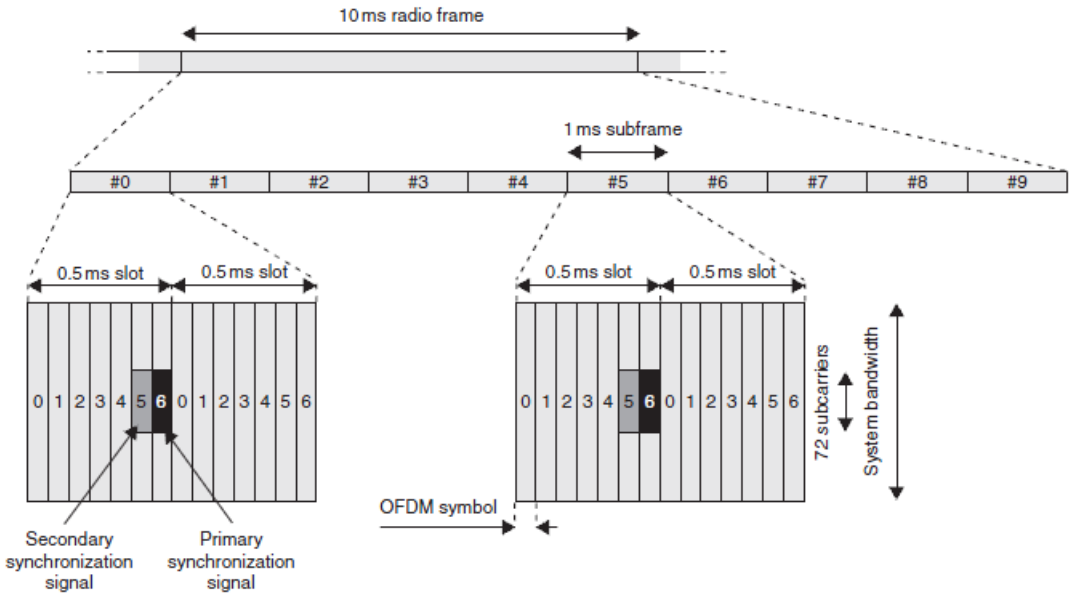

Figure 6.2: LTE frame structure in the FDD mode: 7 OFDM symbols with normal CP [116].

b) Primary Synchronization Signal

In one cell, the two PSSs within a frame are identical. The PSS is generated from one of three known ZC sequences $d_u(n)$ introduced in equation (6.1), with root $u \in \{25, 29, 34\}$ that corresponds to the S-ID ($N_{ID}^{(2)} \in \{0, 1, 2\}$). The ZC sequences have a length of $N_{zc} = 63$ samples and are used in frequency-domain to modulate sub-carriers. The PSS structure is reported in figure 6.3. We note that the 32^{nd} sample is omitted to avoid modulating the DC sub-carrier and only 62 samples of the ZC sequence are mapped on the 62 centered sub-carriers in the transmission bandwidth. Furthermore, the PSS occupies 6 resource blocks which makes 72 sub-carriers for it (five resource elements at each side of the synchronization sequence are set to zero) [115].

The corresponding time-domain signal can be generated using an IFFT of size N_u. The size of the IFFT depends on the system bandwidth. Sub-carriers that are not used for transmission of synchronization signals can be used for data transmission [115].

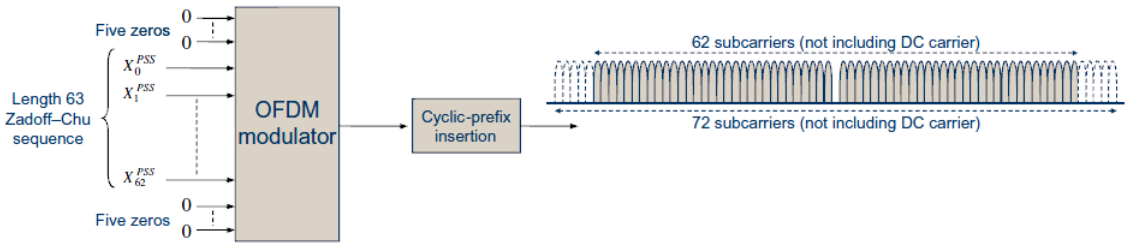

Figure 6.3: Generation of the PSS in the frequency domain [115].

6.2.1.2 LTE Primary Synchronization Literature Review

In LTE systems, the primary synchronization involves symbol start estimation and S-ID determination. We here provide a survey on some existing approaches for each of these tasks. Extensive researches have been done on the primary synchronization in LTE systems. Among them, the methods proposed in [118] and [119] exploit the redundancy in the CP to accomplish symbol start detection in a blind manner. Then, the sector ID is determined through cross-correlating the three local known ZC sequence candidates to the demodulated OFDM symbols. In [119], non-differential correlation as well as differential correlation are used and are found to be more appropriate for long and short channel delay spread respectively, while only non-differential correlation is used in [118]. In [120], the CP based autocorrelation algorithm is also performed to identify the coarse symbol start. Then, the accurate symbol start and S-ID are estimated by cross-correlating the PSS candidates to the received signal over a short interval around the coarse symbol start estimates. The approach proposed in [121] introduces a new concept for coarse timing synchronization which exploits the whole slot to detect the frame start. Accurate detection is provided but a high computational load is required. Low-Complexity synchronization and cell search scheme was proposed in [122], which exploits the central-symmetric property of the ZC sequences to first localize it. Then, the S-ID search can be performed in either time or frequency domains. Analytical descriptions of these approaches are hereafter given.

a) Symbol Start Estimation

Most of the existing time synchronization approaches use the famous blind Maximum Likelihood (ML) estimator which exploits the redundancy induced by the CP in the OFDM signal

structure. Among them, the works in [118] and [119] estimate the symbol start, respecting the algorithm initially proposed for OFDM systems in [24], and which is recalled in section 3.2.1 through equations (3.9), (3.10), (3.11) and (3.12).

The ML symbol start estimator proposed in [120] is derived by maximizing the P-lagged autocorrelation defined as

$$C(d) = \left| \sum_{l=0}^{W-1} r_{d+l}^{*} r_{d+q+l} \right|, \tag{6.10}$$

were q stands for the correlation shift. For a given sliding window size $W = N_g$ and for $q = N_u$, the symbol start estimate turns into the initial estimate in [24] which is also used in [118,119]. An enhancement of this estimator can be achieved by using a total of K OFDM symbols to get an equivalent CP of length KN_g and average out the noise effect.

In [121], a different concept for time synchronization is proposed. The idea therein is to detect the start point of a whole LTE slot instead of one OFDM symbol start. The timing metric is expressed as

$$M(d) = \left(\frac{|P(d)|}{R(d)} \right)^2, \tag{6.11}$$

where

$$\begin{aligned} P(d) = & \sum_{l=0}^{N_{g1}-1} r_{d+l}^{*} r_{d+N_u+l} \\ & + \sum_{i=0}^{5} \sum_{l=0}^{N_g-1} r_{d+N_{g1}+iN_g+(i+1)N_u+l}^{*} r_{d+N_{g1}+iN_g+(i+2)N_u+l}, \end{aligned} \tag{6.12}$$

and

$$\begin{aligned} R(d) = & \sum_{l=0}^{N_{g1}-1} r_{d+l}^{*} r_{d+l} \\ & + \sum_{i=0}^{5} \sum_{l=0}^{N_g-1} r_{d+N_{g1}+iN_g+(i+1)N_u+l}^{*} r_{d+N_{g1}+iN_g+(i+1)N_u+l}. \end{aligned} \tag{6.13}$$

The slot start coincides with the argument d that maximizes the timing metric $M(d)$ in equation (6.11). This latter allows determining the PSS position, as it is known with reference to the slot start, yet it does not enable the S-ID identification. This scheme shows good time detection

performance for AWGN channel. However, its performance is much limited when the received data is deteriorated due to multipath effects.

By exploiting the central-symmetric property of ZC sequences, distinguishing the PSS symbol from the data symbols can be simply achieved by the Central-Self Correlation (CSC) as in [122] which verifies whether a received symbol is central symmetric or not as

$$Z(d) = \left| \sum_{l=0}^{N_u/2-1} r_{d+l}^{*} r_{d+N_u-1-l} \right|. \tag{6.14}$$

Performing the metric above, the UE can quickly know whether a received symbol is a PSS symbol or not by carrying only one self-correlation operation searching for the central-symmetric property of ZC sequences, which always holds regardless of the root u. The PSS start is selected as the time index d that maximizes the metric in equation (6.14).

b) Sector Search

After achieving time synchronization, by detecting either the PSS start (exploiting ZC sequence properties) or other OFDM symbol start (exploiting OFDM symbols structure), which we hereafter denote by $\hat{\tau}$, sector search can be carried in either time domain (before FFT application) or frequency domain (after FFT application). The sector ID strongly depends on the ZC sequence used in the PSS generation. Most of the existing algorithms detect the PSS symbol by exploiting the ZC sequences' near-perfect cross-correlation properties.

The algorithm in [118] cross-correlates the received extracted symbols R (after FFT) with the three local ZC sequences d_u on the 62 centered sub-carriers as

$$Q^u(d) = \left| \sum_{l=0, l\neq 31}^{N_{zc}-1} d_u^{*}(l) R(d+l) \right|. \tag{6.15}$$

The magnitude of the cross-correlator output $Q^u(d)$ corresponding to the correct sector ID provides the highest correlation peak. This is the consequence of orthogonality between ZC sequences used in the PSS generation. Also, the index d that maximizes $Q^u(d)$ indicates the PSS position within the radio frame.

The detector proposed in [119] adapts the metric to the channel delay spread. Indeed, it

uses a non-differential correlation based metric that proceeds as in equation (6.15) for short channels and a differential correlation based metric for long channels as

$$C^u(d) = \left| \sum_{l=0}^{N_{zc}-2} \Big(d_u^*(l)R(d+l)\Big)\Big(d_u^*(l+1)R(d+l+1)\Big)^* \right|. \tag{6.16}$$

Here, the differential correlation is also carried for the extracted middle 62 sub-carriers of each OFDM demodulated symbol. Simulation results provided in [119] show that non-differential correlation works better for short channels whereas differential correlation is more adequate in the case of long memory channels.

The main drawback of the above cited approaches is that the OFDM symbols should be extracted out in frequency domain in advance which may distort the synchronization signals due to synchronization errors. Furthermore, the coarse synchronization is blind, which makes the detection unsatisfactory in the case of multipath fading channels.

The algorithm proposed in [120] performs cross-correlation in time domain with the PSS candidates at all possible symbol starts (previously estimated through blind approach) and neighborhoods. The correlation peak occurs at the effective PSS symbol start, from which a more accurate symbol start can also be obtained. Similarly to the previous algorithms, the cross-correlation is here performed at all symbol start positions which may result in a high computational load. The large amount of computation wasted on the data symbols is avoided in [122] since the PSS acquisition is realized during the coarse time synchronization process. Then, the S-ID search can be performed in either the frequency domain as done in equation (6.15) during one symbol, or in time domain exploiting the central symmetry of the ZC sequences as

$$\Omega^u(d) = \left| D_u(0)r_{\hat{\tau}}^* + D_u(N_u/2-1)r_{\hat{\tau}+N_u/2-1}^* + \sum_{l=1}^{N_u/2-2} D_u(l)\big(r_{\hat{\tau}+l} + r_{\hat{\tau}+N_u-1-l}\big)^* \right|^2, \tag{6.17}$$

where D_u stands for the IFFT of the ZC sequence d_u which is also a ZC sequence. The metric $\Omega^u(d)$ is here carried for each root u. The CSC algorithm avoids the large amount of computation wasted on the data symbols, which dominates the complexity of the S-ID acquisition in the conventional approaches [118]- [120], by detecting the central-symmetric pattern of the PSS during the first synchronization stage. Nevertheless, the complexity of the coarse stage remains high and may not be suitable for fast synchronization in the UE.

For more accurate time detection and lower computational load, we apply the two primary synchronization approaches: the SD approach that proceeds in a single stage for joint PSS start estimation and sector search and the DD approach which provides a coarse PSS start estimate from the first stage and carries a fine stage for fine time estimation and S-ID detection. The principle of the latter approach is similar to the CSC algorithm, yet the coarse stage of the proposed DD approach has much lower computational load.

6.2.2 Application of the Proposed DD Approach

In LTE systems, the ZC sequence is sent in frequency domain (modulates the sub-carriers) and is transformed through IFFT application. We here exploit the duality between ZC sequences in time and frequency domains, which states that the IFFT of a ZC sequence remains a ZC sequence [90]. This property shows the possibility of adapting and applying the previously proposed DD approach, in which ZC sequences are exploited in the time domain, to the LTE system. The primary synchronization is achieved in two stages: a first coarse doubly differential correlation based stage, whose aim is to roughly localize the arrival time of a ZC sequence within the received signal, and a second fine cross-correlation based stage whose aim is to provide the exact ZC sequence start and the S-ID.

Identically to the previous time domain case, the coarse metric $M_{DD}(d)$ in equation (6.2) is here processed onto the received signal, yet with a sum of N_u adjacent samples (not necessarily equal to N_{zc}, corresponding to the oversampled ZC sequence length) given by

$$M_{DD}(d) = \left| \sum_{l=0}^{N_u-1} \left(r_{d+l} r^*_{d+l-q} \right) \left(r_{d+l-1} r^*_{d+l-1-q} \right)^* \right|. \tag{6.18}$$

This expression can also be implemented by a recursive formula similar to that in (6.4) using a shift equal to N_u instead of N_{zc} in the last term. Compared to most of the symbol start detectors described in section 6.2.1.2, the DD approach has the advantage of providing a coarse estimate of the PSS start from the first stage. Hence, the fine search is carried only over one symbol (the PSS). Furthermore, a flexible (time domain or frequency domain) cross-correlation based sector search is now possible. In the time domain based search, cross-correlation is performed between the three local PSS candidates (D_u) and a short-length sequence centered

on the coarse PSS start estimate extracted from the received signal as

$$M_{FDD}^{u}(d) = \left| \sum_{l=0}^{N_u-1} D_u^*(l) r_{d+l} \right|. \tag{6.19}$$

The time index that maximizes the correlation output indicates the PSS start and the candidate D_u that provides the highest peak among the three candidates corresponds to the ZC sequence of root u that identifies the sector. In the frequency domain based search, the coarse PSS start estimate is considered as a trigger FFT point. Once the ZC sequence is extracted after FFT application to the estimated PSS, the cross-correlation is carried as done in [118] and [119] and described in equation (6.15).

6.2.3 Application of the Proposed SD Approach

The previous equations (6.6) and (6.7) are provided for ZC sequences directly sent in time domain, which is not the case in LTE specifications. Once again, we exploit the fact that the IFFT of a ZC sequence preserves its properties and remains a ZC sequence, yet with a modified root u'. Hence, the metric in (6.6) is applicable in the LTE system using the new ZC sequence resulting from the IFFT of the original ZC sequence whose root is u' and length is N_u. In this case, the sum in the metric (6.6) must be carried from 0 to $N_u - 1$ and the compensation term for the d^{th} index becomes $e^{\frac{j2\pi d u' q}{N_u}}$. As u' is unknown, we propose to determine off-line the optimal compensation frequency $\delta = u'q/N_u$, which offers near-best performance, for each of the three possible ZC sequences. To this aim, we use the function below for each initial root u, in order to search the compensation frequency that maximizes the correlation output of the new ZC sequence to its q-shifted counterpart, defined as

$$F^u(\delta, q) = \left| \sum_{l=0}^{N_u-1} D_u(l) D_u^*(l+q) e^{-j2\pi l\delta} \right|. \tag{6.20}$$

In the sequel, we search the couple (δ,q) which maximizes $F^u(\delta, q)$ and hence provides the best compensation (adjustment) frequency δ for each of the three initial ZC sequences. The search of q and δ is achieved through simulation.

6.2.3.1 Search of the Optimal Shift q

The aim of this task is to determine the optimal shift q that provides the highest maximum value of $F^u(\delta, q)$. Hence, for all possible shift values q we sum $F^u(\delta, q)$ throughout $\delta \in \{0, \delta_\tau, 2\delta_\tau, ..., (N_u - 1)\delta_\tau\}$ values as

$$G^u(q) = \sum_{\delta=0}^{(N_u-1)\delta_\tau} F^u(\delta, q),\ q \in [1, N_u - 1]. \tag{6.21}$$

Figure 6.4 shows the curves of the shift search function for the three standardized roots using a step $\delta_\tau = 1$ for $N_u = 2048$. It is shown that each correlation shift q provides different value which, unlike the case of using ZC sequences in time domain, results in different performance. We note that the curves drawn for root values 29 and 34 are superimposed. For each root u, the optimal shift that maximizes the search metric in (6.21), which we denote by q^u_{opt}, is used in the next step to search for the optimal fine compensation frequency δ and is retained to be utilized in the SD metric (6.6) for time synchronization (using new parameters).

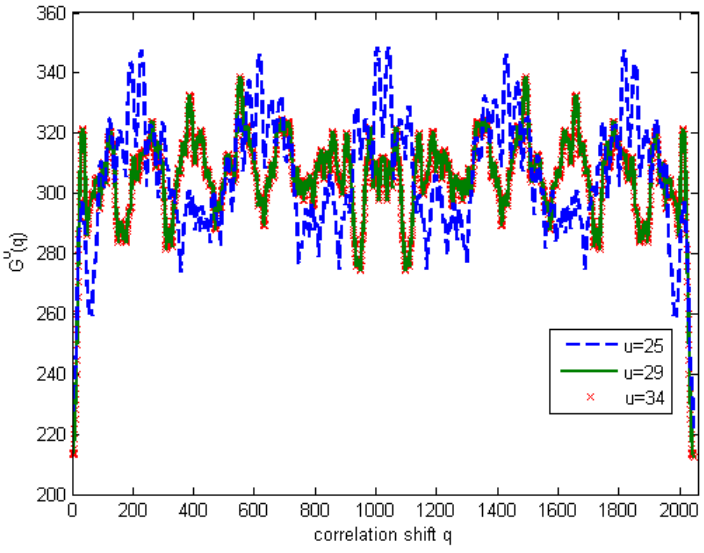

Figure 6.4: The optimal correlation shift search metric for different roots u.

We notice a symmetry in the curves of the function $G^u(q)$, drawn in figure 6.4, which allows its calculation for a range of length $N_u/2$.

6.2.3.2 Search of the Optimal Compensation Frequency δ

For each initial ZC sequence with root u, the search of the best compensation frequency is carried in two phases through the metric $F^u(\delta, q)$ defined in equation (6.20). First a coarse frequency δ_c is determined using a relatively large step δ_τ and the optimized shift q^u_{opt}. Then, $F^u(\delta)$ is refined around δ_c with a very thin step to get a finer compensation frequency δ_f. Figure 6.5 shows the curves of δ_f search around δ_c for the optimal shift values q^u_{opt}.

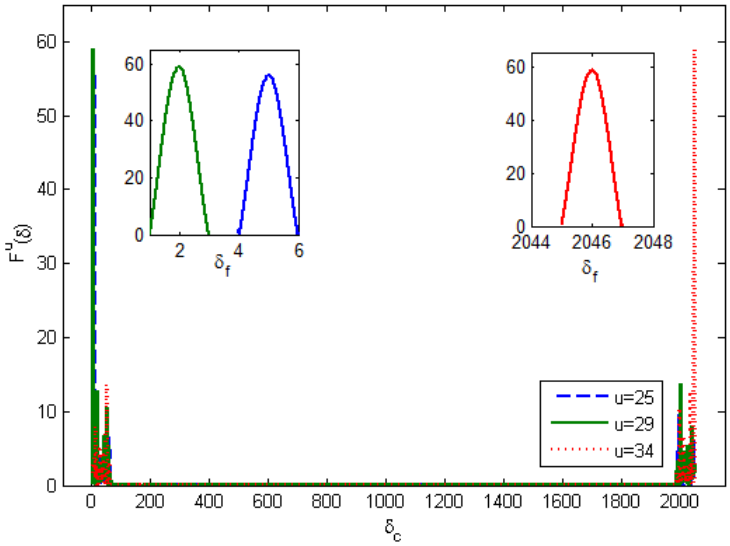

Figure 6.5: The near-best compensation frequency search metric $F^u(\delta, q^u_{opt})$ for different roots u: coarse and fine searches.

The three arguments δ_f (for the three ZC initial roots) which maximize $F^u(\delta, q^u_{opt})$ will be used at the receiver side to calculate the SD timing metric.

6.2.3.3 Application of the SD metric

Once the optimal correlation shift q^u_{opt} and the compensation frequency δ^u_f are determined, the SD metric must be calculated three times (for each defined root $u \in \{25, 34, 39\}$) using the sequence $\lambda_l = r^*_l r_{l+q^u_{opt}}$ corresponding to each root as

$$M^u_{SD}(d) = \left| \sum_{l=0}^{N_u-1} \lambda_{d+l} e^{j2\pi \frac{d\delta^u}{N_u}} \right|. \tag{6.22}$$

The metric $M_{SD}^{u}(d)$ which exhibits the highest maximum among the three calculated metrics is considered for primary synchronization. Indeed, the corresponding root u indicates the S-ID while the argument d that maximizes the metric corresponds to the PSS start. The joint time synchronization and sector search procedures is a particular feature of the SD synchronization approach compared to the herein proposed DD approach and the considered benchmarks. It is worth noting that a recursive implementation of the SD metric respecting the equation (6.7) can further be used to reduce the computational load of the metric calculation.

The figure 6.6 presents the DD and SD coarse metrics drawn in both cases where ZC sequences are defined in time (a) and frequency (b) domains. It is shown in figure 6.6.b that when carrying the metrics onto the LTE signal and for the correct root, the triangular shape is kept with a gap wider than that of the time-domain based metrics and they exhibit a plateau of length equal to the CP length minus the channel memory. As a second fine stage is required in the DD approach, the plateau will be eliminated through the cross-correlation. For the SD approach, we propose two processing to overcome the plateau effect. The first one consists in locating the points to the left and right, which are 90% of the timing metric maximum, average these two values positions and add $N_g/2$ samples to find the PSS start estimate. The second process cross-correlates the estimated PSS to one of the local three known PSS candidates, corresponding to the estimated S-ID.

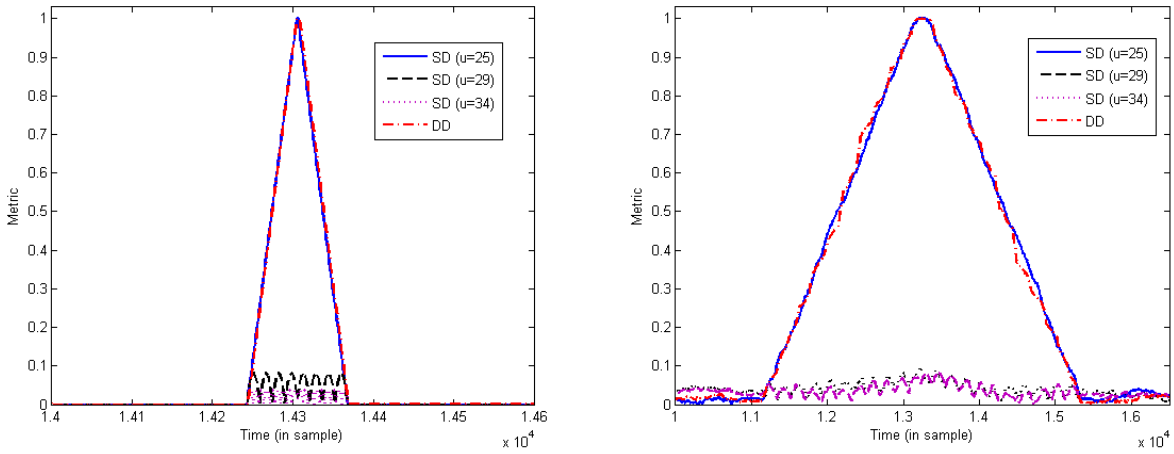

(a) Time Domain (b) Frequency Domain (LTE signal)

Figure 6.6: The proposed coarse DD and SD metrics for time domain and frequency domain based ZC sequences under noiseless conditions.

6.3 Performance Evaluation and Comparison

In this section, we evaluate the performance of the proposed time synchronization and sector search approaches and compare them to the considered benchmarks: Approach 1 proposed in [118], Approach 2 proposed in [119] and the CSC-based PSS detector proposed in [122]. In the SD approach, the refining processing that carries a cross-correlation of the estimated PSS to the local known one is referred to by SD-1 and the processing that selects the middle point of the plateau whose magnitude is of 90% of the absolute maximum is denoted by SD-2. We recall that Approach 1 and 2 use a ML estimator for time synchronization to extract the OFDM symbols. To further improve the time synchronization performance in Approach 1 and Approach 2, averaging processing over the whole slot is adopted as explained in [26]. For sector search and fine PSS start detection, a second stage is carried based on cross-correlating the 62 centered sub-carriers of the extracted OFDM symbols to the local known ZC sequences. Non-differential cross-correlation is used in Approach 1, whereas Approach 2 uses differential cross-correlation based metric. The CSC algorithm exploits the central-symmetric property of the ZC sequence for PSS localization (time synchronization). Then, a time or frequency domain cross-correlation of the estimated PSS with the local known three ZC sequences or their IFFT is carried for sector identification.

Time synchronization performance is evaluated in terms of PSS start Correct Detection Rate (CDR), defined as the percentage of realizations where the estimated time index coincides with the correct PSS start and its estimation variance. Sector search performance is evaluated in terms of S-ID Failure Detection Rate (FDR) defined as the percentage of realizations where the estimated S-ID is erroneous. It is worth to note that in the curves reporting the CDR, we tolerate a mismatch of 2 and 4 samples centered on the correct PSS start in the case of Extended Pedestrian A (EPA) and Extended Typical Urban (ETU) channel models respectively.

6.3.1 Simulation Parameters

Monte Carlo simulation method is here adopted over 10^4 trials. The detailed simulation parameters are given in table 6.1 (specified in [115]).

The parameters of the considered EPA and ETU channel models, with standardized maximum Doppler shifts of 5 Hz and 300 Hz respectively, are specified in TS 36.101 [124] and TS

Table 6.1: Simulation parameters for the LTE system.

Parameter	**value**
Channel bandwidth	20 MHz
Sampling frequency	30.72 MHz
Number of IFFT points, N_u	2048
Cyclic prefix duration, N_g/ N_{g1}	144/ 160
Sub-carrier spacing	15 KHz
Frequency offset	0.7
Number of Tx/Rx antenna	1/1
Channels	EPA-5/ ETU-300
Modulation	4-QAM

36.104 [125] and are presented in table 6.2.

6.3.2 PSS Detection Performance

Figure 6.7 displays the PSS start CDR in the EPA channel (Fig. 6.7.a) and the ETU channel (Fig. 6.7.b) of the compared approaches. The obtained results show that the proposed SD approach outperforms the other approaches in terms of time detection accuracy. Indeed, it is shown in figure 6.7.a that for a target CDR of 80%, it realizes gains of about 1 dB, 1.8 dB and 4 dB compared to the DD approach, the CSC approach and the Approaches 1 and 2 respectively. The DD and CSC schemes provide comparable detection performance with a slight gain of about 0.3 dB realized by the DD scheme at high SNR and by the CSC scheme at low SNR. These two schemes outperform Approaches 1 and 2, which provide almost the same detection accuracy, with gains of about 2 dB and 5 dB respectively for low and high SNR values. We also note that for high SNR values, all the considered benchmarks and the DD approach outperform the SD-1, which uses the averaging technique to determine the PSS start. The CDR curves depicted in figure 6.7.b, for the case of ETU channel, show that consistently with the EPA channel case, the SD approach (SD-1) outperforms the other approaches. These latters (DD, CSC, App.1 and App. 2) provide almost the same detection accuracy for SNR values lower than -4 dB. Beyond this value, the DD and CSC schemes greatly outperform the Approaches 1 and 2 whose maximum CDR stagnates at values lower than 75%. Both of the

Table 6.2: LTE tapped-delay channels' parameters.

Tap	**EPA Channel**		**ETU Channel**	
no.	Tap delay (ns)	Relative Power (dB)	Tap delay (ns)	Relative Power (dB)
1	0	0.0	0	-1.0
2	30	-1.0	50	-1.0
3	70	-2.0	120	-1.0
4	90	-3.0	200	0.0
5	110	-8.0	230	0.0
6	190	-17.2	500	0.0
7	410	-20.8	1600	-3
8			2300	-5
9			5000	-7

proposed detectors and the CSC benchmark provide high CDR of about 98% for SNR values higher than 6 dB.

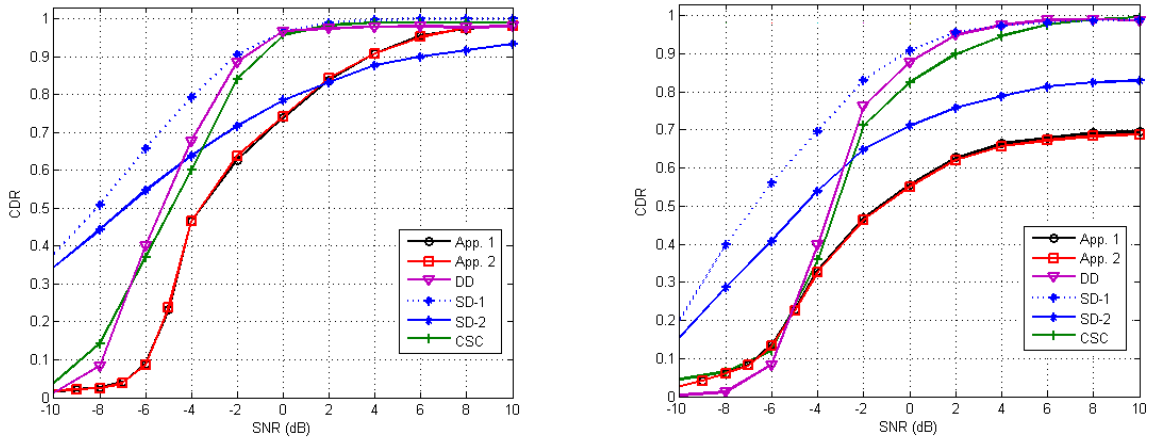

(a) EPA-5 channel

(b) ETU-300 channel

Figure 6.7: Correct Detection Rate of the PSS start.

Figure 6.8 draws the time estimation variance in the EPA channel (Fig. 6.8.a) and the ETU channel (Fig. 6.8.b). The same observations as for the CDR are noticed through the curves of estimation variances. We note, in figure 6.8.a, that the SD approach exhibits low variance compared to all other approaches, but due to the plateau effect, an error of about 5.10^{-3} squared samples remains even at high SNR values. This phenomenon is observed in

all the compared PSS detectors. The DD and CSC approaches are the most sensitive to noise compared to the other approaches and they provide the highest variances at low SNR values. For this SNR range, they provide almost the same detection accuracy, whereas, for higher SNR values, the former scheme outperforms the latter one with a minimum gain of about 2 dB. We also note that the Approaches 1 and 2 provide almost the same detection performance in terms of PSS start detection accuracy and its estimation variance. Consistently with the CDR evaluation and at high SNR, the variance of the scheme SD-2 is the highest one. In figure 6.8.b, it is also proved that the scheme SD-1 is more efficient than the other schemes along the considered SNR range. At very low SNR values (<-2 dB), the DD approach has the highest variance while the considered benchmarks provide slightly lower variances. Beyond this SNR value, the variance of the DD estimator is greatly reduced such to offer an estimation variance comparable to that provided by the SD-1 (a value of 0.1). Moreover, the CSC estimation variance is also improved, yet it stagnates at value higher than 10 squared samples. However, the other approaches (SD-2, App.1 and App.2) are still exhibit high estimation variances.

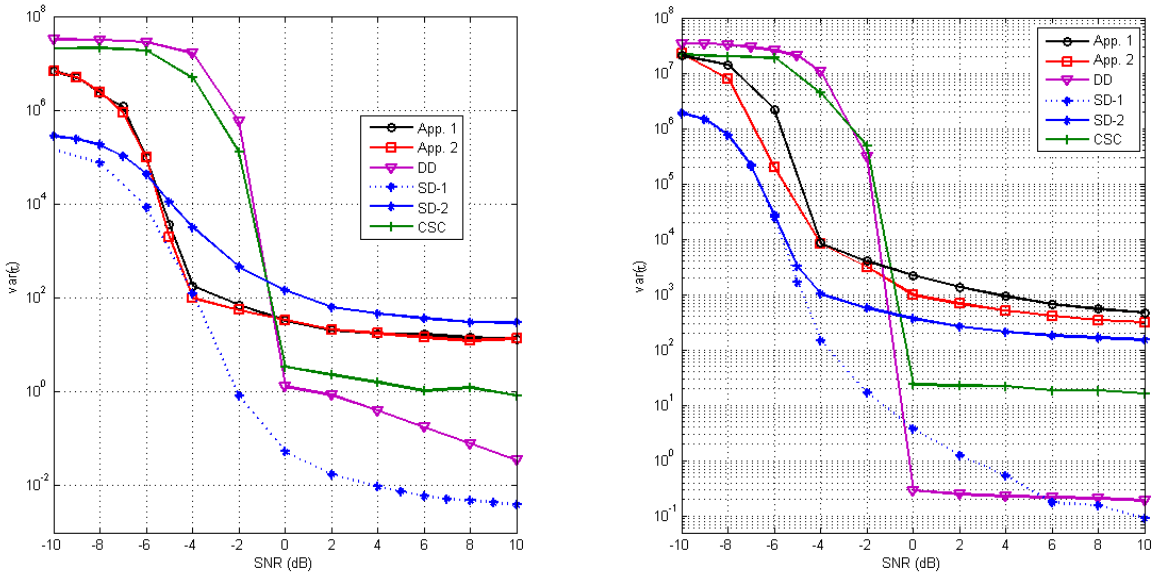

(a) EPA-5 channel

(b) ETU-300 channel

Figure 6.8: PSS start estimation variance.

In both of the considered channel models, the performance provided by Approach 1 and 2 are very close and their limitation is due to the blind coarse time estimation known by its sensitivity to the multipath effect. Indeed, the herein proposed approaches (SD and DD) and the CSC approach, which exploit the ZC sequence properties to first detect the arrival of the

PSS, greatly outperform the other approaches. Although the DD and the CSC approaches have the same principle, the performance provided are almost the same in low SNR, however the DD approach outperforms the CSC approach, for high SNR values. This may be due to the calculation of the fine metric, which is centered on the coarse PSS start for the DD approach while it starts from the coarse estimate in the CSC approach.

6.3.3 Sector ID Search Performance

The sector ID Failure Detection Rate (FDR) is illustrated in figure 6.9. We note that all the compared approaches (Approach 1, Approach 2, CSC and the proposed SD and DD approaches) provide satisfactory detection performance with very low FDR even at low SNR values. In both of the considered channels the SD approach provides the best sector search detection performance, which becomes perfect from SNR values equal to -6 dB and -4 dB in the EPA and ETU channels respectively. In the EPA channel case, reported in 6.9.(a), Approach 2 outperforms the other benchmarks and the DD proposed approach and it realizes slight gains of about 0.5 dB, 1 dB and 1.5 dB compared to respectively Approach 2, the DD and the CSC approaches. In 6.9.(b), the FDR is presented in the case of ETU channel. We here note a perfect sector search achieved from SNR values of -4 dB for the SD approach, -2 dB for the three considered benchmarks and 0 dB for the proposed DD approach, which here provides the highest FDR.

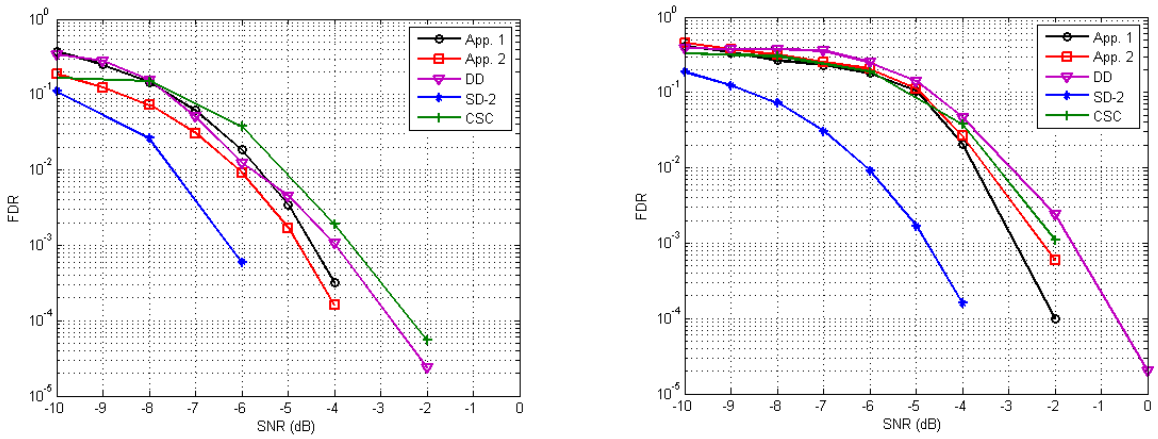

(a) EPA-5 channel

(b) ETU-300 channel

Figure 6.9: Sector Identifier Failure Detection Rate.

6.3.4 Complexity Issues

Computational complexity comparison among the considered benchmarks as well as the proposed DD and SD approaches is here evaluated and presented in table 6.3. The evaluation is assessed in terms of Number of Complex Multiplication operations (NCM) required to accomplish the primary synchronization processing (symbol start detection and sector search) during one slot. We define the slot length as $N_{sl} = 7N_u + 6N_g + N_{g1}$.

Table 6.3: Computational complexity comparison among the PSS detection approaches.

Approach	**NCM**	**Numerical exp.**
App. 1	$2 \times N_{sl} + (N_{zc} - 1)^2 \times 7 \times 3$	11.15 10^4
App. 2	$2 \times N_{sl} + (N_{zc} - 1)^3 \times 7 \times 3$	503.56 10^4
CSC App.	$((N_u/2 - 1) \times N_{sl}) + N_{zc} - 1$	15.7 10^6
DD App.	$N_{sl} + 3 \times N_u \times N_g$	90 10^4
SD App.	$(3 \times 4 \times N_{sl}) + N_g \times N_{zc}$	19.3 10^4

It is observed, in table 6.3, that the non-differential correlation based approach (App. 1) has the lowest computational complexity compared to the other approaches, yet with poor detection performance. Slightly higher NCM is required in the SD approach with a great improvement of the detection performance. Although the differential-correlation based approach (App. 2) is much more costly, its performance are comparable to those of Approach 1 and the DD approach in terms of sector search. Indeed, numbers of 487 10^4 and 72 10^4 complex multiplication operations are saved by Approach 2 and the DD approach, respectively. This latter has much lower computational load than that of Approach 1 and, as presented in the previous simulation results, it greatly outperforms it in terms of PSS detection accuracy. The CSC approach has the highest complexity with better performance, compared to Approaches 1 and 2 whose complexity is reduced thanks to the recursive implementation. The CSC approach was known do decrease the computational load in [122] compared to the conventional approaches (App. 1 and App. 2). However, the recursive implementation of the conventional approaches leads to an important complexity reduction. Although the CSC approach allows PSS localization from the first synchronization task, as in the proposed DD and SD approaches, the recursive implementation of these latter makes them more convenient. Overall, we note that the SD approach provides the best trade-off between the computational complexity and the detection performance.

Conclusions

In this chapter we presented two new synchronization approaches for time synchronization exploiting ZC sequences. These methods are then adapted to be applied in the case of LTE standard, which employs ZC sequences in the frequency domain as a PSS for time synchronization and S-ID search.

The doubly-differential correlation approach proceeds into two stages wherein the first stage a coarse metric of reduced complexity is calculated to detect the pattern of a ZC sequence within the received signal. Then, to exactly locate the PSS start, a fine metric based on cross-correlating the received signal with the three known PSS candidates is carried over a short interval around the coarse time estimate. This process allows determining the PSS start and the S-ID identified by the maximum of the peaks resulting from the three correlation outputs. Unlike the conventional approaches and the herein proposed doubly-differential one, the simply-differential approach has the particularity of combining time synchronization and sector search in a single stage. Indeed, the same metric was used to jointly detect the PSS start and determine the sector ID. Furthermore, its reduced complexity, compared to the considered benchmarks, makes it suitable to working in a high-mobility environment with a frequent handover being performed.

Simulation results, investigated in the EPA and the ETU channels, showed the robustness of the proposed approaches even at very low SNR values. The doubly-differential approach has a computational load comparable to that of the conventional approaches, yet with slight enhancement in the detection accuracy. The simply-differential approach provides the best performance in terms of detection accuracy and computational load, when compared to the benchmarks and to the doubly-differential approach. Moreover, the complexity comparison results showed that, although the PSS localization during the first synchronization stage was treated in former work, the recursive implementation of both proposed approaches greatly relaxes the computational load of the proposed synchronization processing.

Chapter 7

Synchronization in STBC MISO-OFDM Systems

The combination of Multiple-Input Multiple-Output (MIMO) technology with the OFDM modulation technique has been recognized as one of the most promising techniques to provide high data rate through spatial multiplexing, and robust reception through spatial diversity. Configuration with single transmit antenna, known as Single-Input Multiple-Output (SIMO), or single receive antenna, known as Multiple-Input Single-Output (MISO), have also some interesting advantages as the MIMO configuration. Furthermore, MIMO-OFDM technique transforms a frequency selective MIMO channel into a number of flat-fading MIMO channels on each subcarrier, which allows to take advantages from both techniques. Nevertheless, as in the case of single antenna OFDM systems, synchronization errors are still a major problem for MIMO-OFDM systems that cause severe degradation in the system performance. Therefore, residual synchronization errors must be estimated and compensated.

In this chapter, we propose a new synchronization technique for non-coherent MISO-OFDM systems [44]. The proposed scheme exploits a preamble of two identical parts from which different versions are generated and simultaneously transmitted from all transmit antennas. The chapter begins with a brief presentation of the MIMO-OFDM systems with a focus on the MIMO key features: spatial diversity, spatial multiplexing and the tradeoff between them. Then, the proposed synchronization technique is presented. It exploits differential Alamouti space-time block coding/decoding to provide full spatial diversity and to avoid the channel

estimation required in the coherent Alamouti coding scheme. The proposed synchronization technique proceeds in two stages similarly to the RC technique described in chapter 4: an autocorrelation based coarse stage and a cross-correlation based fine stage. The first stage is carried directly using the received signal to roughly localize the preamble. Then, differential Alamouti decoding must be achieved to recover the transmitted signal before calculating the cross-correlation based fine metric to detect the exact preamble start. In the last part of the chapter, to better assess the performance of the proposed synchronization technique, we compare it to the single antenna configuration and to the MISO configuration with Alamouti coding, under the assumption of perfect channel knowledge.

7.1 Basics of MIMO-OFDM systems

Multiple antennas can be employed at the transmitter (N_t) and/or the receiver (N_r) to form an arrangement known as MIMO systems whose special case of N_t transmit antennas equal to 1 and N_r receive antennas also equal to 1 reduces to the traditional Single-Input Single-Output (SISO) systems. Recently, MIMO configuration has become a key technology for wideband communication systems thanks to their potential to achieve higher data rate and provide more reliable reception performance compared to the traditional SISO communication systems [126, 127]. With the advent of MIMO systems, several schemes that benefit particularly well from the added spatial dimensions provided by multiple antennas have been emerged: spatial multiplexing/demultiplexing [129, 130] achieve high spectral efficiency and provide higher bit rate, while antenna subset selection and space-time coding [128] help to increase the reliability of wireless links (spatial diversity).

7.1.1 MIMO Channel

Let us consider the MIMO channel with N_t transmit antennas and N_r receive antennas, then the equivalent channel impulse response between the i^{th} transmit antenna and the j^{th} receive antenna is denoted as $h_{i,j}(t)$. If the MIMO channel is assumed to be linear and time-invariant during one symbol duration, the channel impulse response $\mathbf{H}$ can be characterized by an $N_t \times N_r$ matrix as [57]

$$\mathbf{H} = \begin{pmatrix} h_{1,1} & h_{1,2} & \dots & h_{1,N_r} \\ h_{2,1} & h_{2,2} & \dots & h_{2,N_r} \\ \vdots & \vdots & \ddots & \vdots \\ h_{N_t,1} & h_{N_t,2} & \dots & h_{N_t,N_r} \end{pmatrix}. \tag{7.1}$$

The received signal at each j^{th} antenna considering an AWGN η_j is expressed as

$$r_j(t) = \sum_{i=1}^{N_t} h_{i,j} s_i(t) + \eta_j(t), \quad j = 1, 2, ..., N_r. \tag{7.2}$$

The equation (7.2) can be expressed in a matrix form as

$$\mathbf{r}(t) = \mathbf{H}\mathbf{s}(t) + \eta(t). \tag{7.3}$$

where $\mathbf{r}(t)$ and $\eta(t)$ stand for the received signal and noise vectors in $\mathbb{C}^{N_r \times 1}$, respectively. The vector $\mathbf{s}(t) \in \mathbb{C}^{N_t \times 1}$ stands for the transmitted vector of complex symbols.

As shown in equation (7.2), the received signal consists in summing different replicas of the transmitted signal. These signals experience different channel effects, thus allowing a more reliable recovery than the case of a single received signal. This key feature is known as *spatial diversity*. Furthermore, if different signals are transmitted through each antenna, the spectral efficiency can be greatly enhanced through the so called *spatial multiplexing*.

7.1.1.1 Spatial Diversity

The transmitted signal over broadband wireless channels generally suffers from attenuation due to the detrimental effect of multipath fading, which can severely degrade the reception performance, unless some additional less-attenuated replicas of the transmitted signal are provided. This feature is known as diversity and is the most important factor in achieving reliable communications [57]. Indeed, in a MIMO configuration, the same information can be transmitted from several antennas and received at several antennas simultaneously. Under the assumption that the fading for each link between a pair of transmit and receive antennas is independent from the others, the probability that the information is accurately received is increased when compared to the single link scenario. Apart from the spatial diversity, other forms of diversity are available, namely, temporal diversity and frequency diversity. Time diversity can be

obtained via coding and interleaving where the coded symbols are dispersed over time so that different replicas of the codeword experience independent fades. One can also exploit the frequency diversity if the channel is frequency-selective, where replicas of the transmitted signal are provided to the receiver in the form of redundancy in the frequency domain.

Several mechanisms are used to maximize the spatial diversity. These mechanisms include delay diversity, Space-Time Block-Coding (STBC) [131, 132] and Space-Time Trellis-Coding (STTC) [128]. In the first transmit diversity approach, multiple delayed copies of the same signal are transmitted through the N_t transmit antennas and a Maximum Likelihood Sequence Estimation (MLSE) is used at the receiver to estimate the transmitted sequence. The delay-diversity approach is simple and can be considered as a particular space-time code [14]. The STBC and STTC coding schemes are developed for quasi-static flat fading channels and can provide full spatial diversity for MIMO systems. The STBC utilizes orthogonality property of the used code to achieve full diversity, yet it can not achieve full-rate transmission when the number of transmit antennas is greater than two [128]. On the other hand, the STTC can guarantee full diversity by the use of enough trellis coding, but the decoding complexity increases exponentially with the number of transmit antennas [14, 57].

7.1.1.2 Spatial Multiplexing

It is widely recognized that the capacity of a MIMO system is much higher than that of a SISO system. Indeed, N_t independent data streams can be simultaneously sent, each by a single transmit antenna. This features is known as spatial multiplexing, which has good behavior in environment with high scattering and high SNR. In such environment, the capacity of a MIMO system grows proportionally with $\min(N_t, N_r)$. At the receiver side, spatial multiplexing uses a dedicated detection algorithm to sort out different transmitted signals from the mixed corresponding signal, where at least $N_r = N_t$ receive antennas are needed to ensure non ambiguous recovery [60].

Layered approaches are used to increase capacity through spatial multiplexing including Bell Labs Layered Space-Time (BLAST) schemes. For m-array modulation, the receiver has to choose the most likely signal out of m^{N_t} possible signals in each symbol time interval. Therefore, the receiver complexity grows exponentially with the number of modulation constellation points and the number of transmit antennas. Two basic variants of BLAST are proposed in [129,

133], namely D-BLAST (Diagonal BLAST) and V-BLAST (Vertical BLAST). The difference between them is that in V-BLAST the transmit antenna i corresponds, all the time, to the transmitted data stream i, while in D-BLAST the assignment of the antenna to the transmitted data stream is hopped periodically. In general, the BLAST performance is limited due to the error issued by the multi-stage decoding process. However, the main disadvantage of the BLAST architecture for mobile communications is the need for high numbers of receive antennas (not practical in a small mobile terminal), without guaranteeing the achievement of a full spatial diversity. Furthermore, high system complexity may prohibit the large-scale implementation of such a scheme [57].

7.1.1.3 Diversity-Multiplexing Trade-off

The previous sections highlight two methods for using multiple antennas to improve the performance of wireless communication systems. The first one exploits the different channel responses in order to obtain an optimized version of the transmitted signal through extracting the maximal diversity gain. The second one uses the different channels to increase the data rate by multiplexing different data streams simultaneously onto these channels. However, it is not necessary to use the antennas exclusively for diversity or for multiplexing to enhance the detection performance. Some of the space-time dimensions can be used for diversity gain, while the remaining dimensions used for multiplexing gain. The trade-off between diversity and multiplexing gains has been extensively studied in the literature [135]- [138].

In [135], it is found that both types of gain (spatial diversity and multiplexing) can be simultaneously obtained for a given MIMO channel with the fundamental trade-off between how much gain any coding scheme can extract of each type. Therefore, it is judicious to adapt the diversity and multiplexing gains relative to channel conditions. In particular, more antennas can be used for diversity gain in poor channel states, whereas in good channel states the majority of antennas can be used for spatial multiplexing. In [136, 137], group detection was shown as a key feature in designing schemes that achieve optimal diversity-multiplexing trade-off. First, all transmit antennas are partitioned into G groups over which data is encoded and sent experiencing independent fading. Then, at the receiver group detection should be used to separate and detect the G various groups. In [138], a framework for constructing optimal coding/decoding schemes, which is referred to as LAttice Space-Time (LAST) coding/decoding, is also proposed for achieving the optimal diversity-multiplexing trade-off. More

recently, finite-SNR diversity-multiplexing trade-off for Rayleigh MIMO and spatially correlated Rayleigh MIMO channels is studied respectively in [139] and [140], where dual antennas at the transmitter and/or the receiver are considered. The finite-SNR schemes provided a new insight to design Space Time Codes (STB) for practical MIMO systems optimized at realistic SNRs and propagation environments.

The early research on the MIMO configuration is based on the assumption of flat fading channels. As higher bit rates involve wideband communications, wireless channels become usually frequency selective. To take advantage from diversity and/or spatial multiplexing under frequency selective fading channels, MIMO configuration must be used in conjunction with other techniques that effectively generate one or more flat faded channel. A promising candidate is the multi-carrier technique which divides the frequency-selective channel into several flat fading sub-channels. In particular, the OFDM technique is the most used with MIMO configuration thanks to its high spectral efficiency and capability to cope with multipath effects. Over each frequency, a MIMO flat fading channel model will then be considered.

7.1.2 MIMO-OFDM

Recent and future broadband communication systems should provide high data rate and high performance over wireless channels that are generally frequency selective. The combination of MIMO and OFDM has the potential of meeting this stringent requirement since MIMO can boost the capacity and the diversity while OFDM can mitigate the detrimental effects due to multipath fading [141].

Similarly to the case of SISO OFDM systems, the transmitter here duplicates the same processing to generate the OFDM signal for each transmit antenna as described in section 2.2.3. The blocks s_l^i of N_u complex data samples, which are drawn uniformly from QAM or PSK constellations, are used to modulate the N_u orthogonal sub-carriers during the l^{th} OFDM symbol in the i^{th} transmit antenna as

$$\mathbf{s}_l^i = [s_{l,0}^i, s_{l,1}^i, \ldots, s_{l,N_u-1}^i], \quad i = 1, 2, \ldots N_t. \tag{7.4}$$

The data symbols modulate the N_u sub-carriers using N_u-points IFFT to produce the time

domain symbol $\bar{\mathbf{s}}_l^i = [\bar{s}_{l,0}^i, \bar{s}_{l,1}^i, \ldots, \bar{s}_{l,N_u-1}^i]$ using the IFFT matrix $\mathbf{W}^H$ (in equation (2.20)) as

$$\bar{\mathbf{s}}_l^i = \mathbf{W}^H \mathbf{s}_l^i. \tag{7.5}$$

Then, a time domain CP of N_g samples is inserted at the start of each OFDM symbol of total length $N_s = N_u + N_g$ samples. The serial concatenated symbols are then converted to the analogue domain, up-converted to a radio frequency centered at the carrier frequency f_c, and finally transmitted through the i^{th} antenna. A simplified block diagram of MIMO-OFDM systems is presented in figure 7.1, where space time encoder and decoder are inserted at the start of the OFDM modulator and at the end of the OFDM demodulator, respectively.

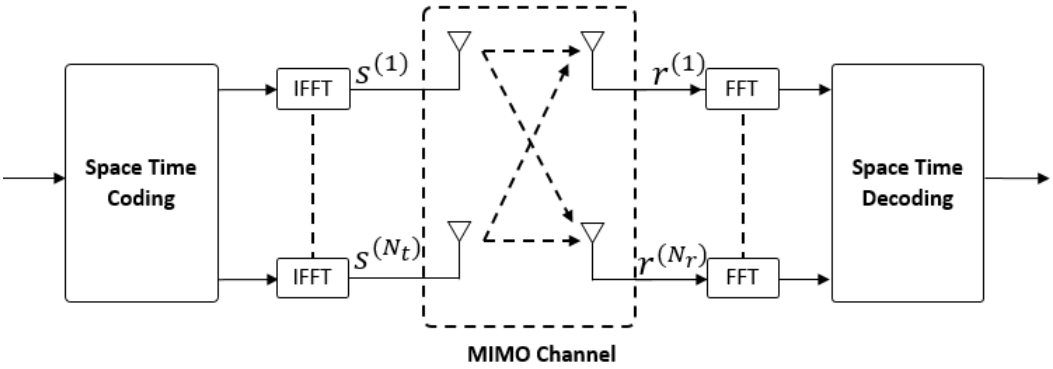

Figure 7.1: MIMO-OFDM simplified block diagram.

At each receive antenna, a superposition of signals from all N_t transmit antennas is received and then down converted to baseband. The signal from each receive antenna at the k^{th} sub-channel of the l^{th} OFDM block can be expressed as

$$r_{l,k}^j = \sum_{i=1}^{N_t} h_{l,k}^{(i,j)} s_{l,k}^{(i)} + \eta_{l,k}^{(j)}, \tag{7.6}$$

where $h_{l,k}^{(i,j)}$ stands for the channel frequency response at the k^{th} sub-channel of the l^{th} OFDM block corresponding to the i^{th} transmit antenna and the j^{th} receive antenna, $s_{l,k}^{(i)}$ stands for the signal sent from the i^{th} transmit antenna and $\eta_{l,k}^{(j)}$ refers to the AWGN at the j^{th} receive antenna.

Similarly to the SISO OFDM case, studied in the previous chapters, the MIMO-OFDM

systems can also tolerate a certain amount of time errors depending on the maximum channel delay spread. However, to prevent ISI and ICI due to the channel impairments, the FFT window should be bounded by the ISI-free region to insure the sub-carriers orthogonality and thus to correctly demodulate the received signal. Spatial diversity, which is known to provide more reliable reception, is expected to enhance the synchronization performance. To benefit from spatial diversity, we opt for coded multi-antenna configuration. In particular, the space time block coding described in the next section.

7.2 Review of Space Time Block Coding

Space-Time Coding (STC) is a transmission technique that uses multiple transmit antennas in an optimized manner. The main goal behind using STC is to extract the total available spatial diversity in a MIMO channel through appropriate construction of the space-time codewords without any channel knowledge at the transmitter. The STC is originally designed for known slow flat fading channels [128,131,132]. However, its combination with the OFDM modulation technique, which is known by its capacity to transform a frequency-selective fading channel into parallel flat-fading sub-channels, allows its application in broadband wireless systems over frequency-selective channels [134]. Among the existing STC schemes, we here present only STBC schemes which we will later exploit to enhance the synchronization performance. In particular, we recall the famous Alamouti STBC [131] for coherent detection and the Differential Alamouti STBC [142] for non-coherent detection.

7.2.1 Alamouti STBC

Alamouti devised a remarkable STBC scheme for transmission with two transmit antennas and N_r receive antennas in [131]. This scheme supports ML detection based on linear processing at the receiver. Let s_1 and s_2 be the two symbols to be transmitted during two successive time intervals. According to Alamouti's scheme, the following data matrix is transmitted through the two transmit antennas during two consecutive time intervals (columns):

$$\mathbf{S_t} = \begin{pmatrix} s_1 & -s_2^* \\ s_2 & s_1^* \end{pmatrix}, \tag{7.7}$$

where s_1 and s_2 are sent respectively from transmit antennas one and two at time t, and $-s_2^*$ and s_1^* are sent respectively from antennas one and two at time $t+1$. It is assumed that the MIMO channel remains constant over the transmission period of $\mathbf{S}_t$. We here consider the example of two-branch transmit diversity with one receiver. At time t, the channel can be modeled by complex multiplicative distortion components h_1 and h_2 for the first and the second transmit antennas, respectively. The received signals can then be expressed as

$$\begin{aligned} r_1 &= r_t = h_1 s_1 + h_2 s_2 + \eta_1, \\ r_2 &= r_{t+1} = -h_1 s_2^* + h_2 s_1^* + \eta_2, \end{aligned} \tag{7.8}$$

where r_1 and r_2 refer to the signals received at time t and $t+1$ and η_1 and η_2 are the complex random variables representing receiver noise and interference. A combining scheme is then applied to generate the following two signals as

$$\begin{aligned} \hat{s}_1 &= h_1^* r_1 + h_2 r_2^* = (|h_1|^2 + |h_2|^2) s_1 + h_1^* \eta_1 + h_2 \eta_2^*, \\ \hat{s}_2 &= h_2^* r_1 - h_1 r_2^* = (|h_1|^2 + |h_2|^2) s_2 - h_1 \eta_2^* + h_2^* \eta_1. \end{aligned} \tag{7.9}$$

These combined signals are then sent to a ML detector which, for each of the signals $\hat{s}_1$ and $\hat{s}_2$, choose s_i respecting the following decision rule

$$(|h_1|^2 + |h_2|^2 - 1)|s_i|^2 + d^2(\hat{s}_l, s_i) \leq (|h_1|^2 + |h_2|^2 - 1)|s_k|^2 + d^2(\hat{s}_l, s_k) \quad \forall i \neq k, \quad l = \{1, 2\}, \tag{7.10}$$

where $d^2(x, y)$ is the squared Euclidean distance between signals x and y calculated as $d^2(x, y) = (x - y)(x^* - y^*)$. In the case of PSK modulation, the decision rule in (7.10) reduces to

$$d^2(\hat{s}_l, s_i) \leq d^2(\hat{s}_l, s_k). \tag{7.11}$$

The Alamouti code was the first Orthogonal STBC (OSTBC) proposed. Later, many schemes have generalized it to higher number of transmit antennas as the work in [128]. This scheme retains the simple ML decoding algorithm of Alamouti, based on only linear processing at the receiver.

STBC schemes are used to provide diversity along both time and space dimensions, which provide more reliable reception. However, the coherent detection of STBC requires perfect channel state information knowledge at the receiver, which requires channel estimation. Furthermore, coherent detection is suitable only for slow fading channels that remain constant for

many symbol durations. Moreover, for low and medium SNR values, the channel estimates are very poor when it is going to be used by the receiver. To overcome this difficulty Differential STBC (D-STBC) may be used.

7.2.2 Differential Alamouti STBC

Differential coding introduces memory in the transmitted data that can be utilized at the receiver to recover the transmitted data without any knowledge of the channel impulse response. This property is important for high speed wireless systems as the channel estimate becomes poor in fast fading conditions. Hence, the differential coding is used in order to avoid the need of channel estimation at the receiver. The differential coding for MIMO systems was first proposed by Tarokh *et al.* in [142] who suggests a differential encoding for MIMO systems employing M-PSK constellation. This scheme is applicable to two transmit antennas and N_r receive antennas. As shown in figure 7.2, the differentially coded elements are then transmitted through Alamouti STB coder.

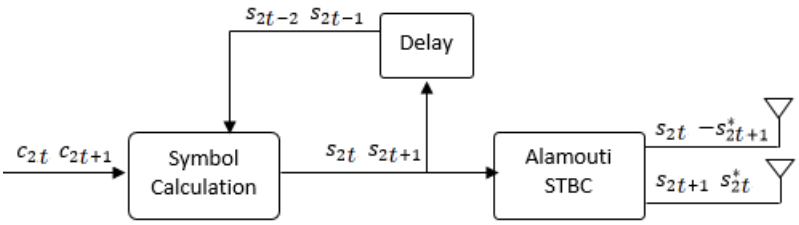

Figure 7.2: Differential Alamouti STBC block diagram.

Tarokh *et al.* define in [142] the following differential coding rule which is applied to the codeword to be sent at time index $2t$ and involves the previous coded block as

$$\mathbf{s}_{2t} = (s_{2t}\ s_{2t+1}) = (c_{2t}\ \ c_{2t+1}) \begin{pmatrix} s_{2t-2} & s_{2t-1} \\ -s^*_{2t-1} & s^*_{2t-2} \end{pmatrix}, \tag{7.12}$$

where c_i are data symbols before encoding and s_i are differentially encoded data. As shown in the block diagram of figure 7.2, once the codeword $\mathbf{s}_{2t}$ is generated, the transmitter then applies the Alamouti's STBC to the differentially coded samples as in (7.7). Hence, at time index $2t$, s_{2t} and s_{2t+1} are sent from antennas one and two respectively, while $-s^*_{2t+1}$ and s^*_{2t} are sent at time index $2t+1$. This process is inductively repeated until the end of the data

to be transmitted. Note that at the start of the encoding process, two samples which do not contain useful data are used to encode the first and the second samples and they will be lost at the receiver during the decoding processing.

Considering a single receive antenna (MISO), the received signal corresponds to the superposition of the transmitted signals affected by the channel coefficients and noise. Assuming a constant channel over two consecutive data symbols (fading conditions can be considered constant), the received signal over two successive symbol intervals can be written as

$$\mathbf{r} = \mathbf{sH} + \eta,\ \mathbf{H} = \begin{pmatrix} h_1 & h_2^* \\ h_2 & -h_1^* \end{pmatrix}, \tag{7.13}$$

where $\mathbf{r} = (r_{2t}\ r_{2t+1}^*)$, $\mathbf{s} = (s_{2t}\ s_{2t+1}^*)$, $\eta = (\eta_{2t}\ \eta_{2t+1}^*)$, η_{2t} and η_{2t+1} are independent AWGN.

At the receiver, the non-coherent differential detection with low complexity is carried to decode the source symbols $(c_{2t}\, c_{2t+1})$, sent from each transmit antenna, as

$$\begin{aligned} \widehat{c}_{2t} &= \left\langle (r_{2t}, r_{2t+1}^*).(r_{2t-2}, r_{2t-1}^*) \right\rangle \\ &= (r_{2t}, r_{2t+1}^*)(r_{2t-2}^*, r_{2t-1})^T \\ &= (|h_1|^2 + |h_2|^2)c_{2t} + \mathcal{N}_1, \end{aligned} \tag{7.14}$$

and

$$\begin{aligned} \widehat{c}_{2t+1} &= \left\langle (r_{2t}, r_{2t+1}^*).(r_{2t-1}, -r_{2t-2}^*) \right\rangle \\ &= (r_{2t}, r_{2t+1}^*)(r_{2t-1}^*, -r_{2t-2})^T \\ &= (|h_1|^2 + |h_2|^2)c_{2t+1} + \mathcal{N}_2, \end{aligned} \tag{7.15}$$

where $\langle \mathbf{a}.\mathbf{b} \rangle$ stands for the inner product of $\mathbf{a}$ and $\mathbf{b}$. The terms $\mathcal{N}_1$ and $\mathcal{N}_2$ incorporate the additive noise and the interference, which are expressed as

$$\begin{aligned} \mathcal{N}_1 =& (s_{2t}\ s_{2t+1})\mathbf{H}(\eta_{2t-2}\ \eta_{2t-1}^*)^* + (\eta_{2t}\ \eta_{2t+1}^*)\mathbf{H}^*(-s_{2t-2}\ s_{2t-1})^* + \\ & (\eta_{2t}\ \eta_{2t+1}^*)(\eta_{2t-2}\ \eta_{2t-1}^*)^*, \end{aligned} \tag{7.16}$$

and

$$\begin{aligned} \mathcal{N}_2 =& (s_{2t}\ s_{2t+1})\mathbf{H}(\eta_{2t-1}\ -\eta_{2t-2}^*)^* + (\eta_{2t}\ \eta_{2t+1}^*)\mathbf{H}^*(-s_{2t-1}^*\ s_{2t-2}^*)^* + \\ & (\eta_{2t}\ \eta_{2t+1}^*)(\eta_{2t-1}\ -\eta_{2t-2}^*)^*. \end{aligned} \tag{7.17}$$

It was shown in [142] that the differential MIMO system works 3 dB poorer than the coherent decoder [131] with perfect channel knowledge. Naturally, it is expected that the performance of this scheme degrades in frequency-selective channels. To adapt this scheme to frequency-selective channels, two procedures were proposed in [134]. The first one operates in the frequency domain where it combines differential Alamouti STBC (as previously described) with the OFDM multi-carrier technique. The second single-carrier scheme operates in the time domain and employs transmit information by encoding over two transmission blocks over which the channel is assumed to be quasi-static. Differential STBC was massively studied for unitary and non-unitary constellation and for MIMO systems with higher order [143]- [146]. Combined with the algorithm of Viterbi at the receiver, the D-STBC schemes proposed in [143] and [144] allow to almost compensate the 3 dB penalty and to reduce it to 0.5 dB loss, respectively.

As mentioned in section 7.1.1, in MIMO systems, the spatial diversity allows to enhance the detection reliability. As a result, it was exploited to ameliorate the receiver performance namely, PAPR reduction [147], channel estimation [148] and synchronization [150]. The use of STBC provides diversity along both the time and space dimensions which is an important challenge, in our work, to improve the synchronization performance.

7.3 Synchronization in MISO-OFDM Systems

Identically to the SISO-OFDM systems, the MIMO-OFDM systems are sensitive to time and frequency synchronization errors [57]. The same synchronization errors' effect study provided in section 2.3 remains valid in the case of MIMO configuration. If not properly compensated, the synchronization errors destroy the orthogonality between different sub-carriers and cause ICI and ISI which consequently cause severe degradation in the reception performance. Therefore, accurate synchronization is crucial for reliable transmission using MIMO-OFDM scheme as in the case of SISO-OFDM.

The time and frequency synchronization problem for MIMO-OFDM systems has been widely investigated in the literature [149]- [154]. The first paper which is interested in MIMO-OFDM time synchronization, to the best of our knowledge, was proposed by Mody in [149]. It uses a simple MIMO extension of Schmidl's synchronization algorithm [15]. Later, most of the proposed synchronization approaches for MIMO-OFDM systems use different preamble training sub-sequences and/or structure for each antenna [151, 152]. At the receiver, a bank of N_t

bandpass filters is used to separate signals coming from different antennas or a combining procedure is carried (Maximum Ratio Combiner (MRC), Equal Gain Combining (EGC)). Other approaches like [153, 154] send unequal period preambles through different antennas. At the receiver, N_t correlators are required for the sake of the synchronization parameters of each individual transmitter or EGC is used. In these techniques, diversity concepts have not been sufficiently explored for performance enhancement. The main novelties are the modification of the preamble structure and/or the training sub-sequence type sent through each antenna without the application of coding schemes that are known to provide full spatial diversity. Exploiting the space time diversity provided through the STBC, we here propose a new time and frequency synchronization technique for MISO-OFDM systems. To avoid the channel estimation requirement in coherent STBC schemes, we opt for differential Alamouti STBC for non-coherent detection [142].

7.3.1 Proposed Non-Coherent Synchronization Technique

The idea of the present work is to benefit from a full spatial diversity transmission to enhance the synchronization performance through differential STBC which is known by its low complexity. As explained in section 7.2, differential STBC is useful since it avoids the need of channel estimation at the receiver end. This presents an important issue in the proposed technique as we focus on non-coherent synchronization. In the following, we assume that the same time and frequency errors emerge through all the propagation channels.

The proposed approach uses a preamble of two identical training sub-sequences as in [15] and carries a treatment similar to that of the RC approach described in chapter 4. The training sub-sequences are made identical in the time domain and the preamble is obtained by the concatenation of these sequences. Respecting the encoding algorithms in [134, 142] for MISO-OFDM systems with dual transmit antennas, two different differentially encoded replicas of the initial training sub-sequence are generated, each duplicated to form the repetitive preamble and sent through a transmit antenna. At the receiver, the repetitive structure first allows a coarse synchronization stage carried by autocorrelating the received signal respecting the algorithm in [15]. Second, the decoding task must be achieved to recover the transmitted signal respecting the scheme in [142]. Then, cross-correlation of the resulting decoded signal with the known non-coded training sub-sequence is performed to fine tune the coarse time estimate. As a byproduct, the fractional part of the frequency offset is also derived using the

same timing metric.

7.3.1.1 Coarse Stage

Coarse time acquisition consists in finding the preamble start over an approximate range of samples. In the considered MISO-OFDM system, the repetitive structure is obtained in the time domain and after D-STBC application. Hence, it will be maintained in the received signal and similarly to the SISO-OFDM case, the coarse synchronization stage is carried by autocorrelating the received signal respecting the algorithm in [15] as

$$M_c(d) = \sum_{m=0}^{N_u/2-1} r^*_{d+m} r_{d+m+N_u/2}. \tag{7.18}$$

The coarse time estimate is chosen as the argument that maximizes $|M_c|$ and is denoted by $\hat{\tau}_c$. Figure 7.3 presents the coarse metric in equation (7.18) for the system parameters used in the SISO case ($N_u = 1024$ and $N_g = 102$). As shown in the figure, the coarse metric exhibits a plateau whose length is equal to that of the CP minus the channel memory. This leads to an uncertainty in the preamble start detection, especially in noisy environments, which requires a second fine stage.

Once the coarse preamble start position is detected, fine time synchronization should be performed to determine the exact starting position of the preamble. The fine metric, which is based on cross-correlation, is carried over a short interval centered on the coarse time estimate.

7.3.1.2 Fine Stage

Fine time synchronization aims to detect the exact preamble start position around the coarse time estimate. We note that at the receiver end, signals from different transmit antennas are superimposed together, and the time estimation algorithm may not work as expected for this stage. Hence the differential decoding must be first achieved to recover the transmitted signal. Once again we refer to the scheme proposed in [142], which is recalled in section 7.2.2, for the reverse decoding treatment. Then, we perform a cross-correlation between the decoded received signal which we denote by $\hat{r}$, whose elements are decoded respecting equations (7.14) and (7.15), with the known initial preamble before D-STBC application. The fine metric is

given by

$$M_f(d) = \sum_{m=2}^{N_u-1} p_m^* \hat{r}_{d+m+N_u}, \tag{7.19}$$

where p_m stands for the m^{th} sample of the preamble. Here, the metric M_f is calculated over a short interval centered on $\hat{\tau}_c$, which allows to reduce the computational complexity of the cross-correlation operations carried during the second stage. The fine preamble start estimate $\hat{\tau}_f$ is chosen as the argument that maximizes the metric amplitude $|M_f|$. It is worth to note that the correlation outputs in the fine metric (7.19) are summed over a window of length $N_u - 2$ because the two first samples of the received signal can not be recovered in the case of D-STBC as they are used to estimate the following samples [142]. As the preamble is sufficiently long ($N_u = 1024$), this will not have an impact on the detection accuracy.

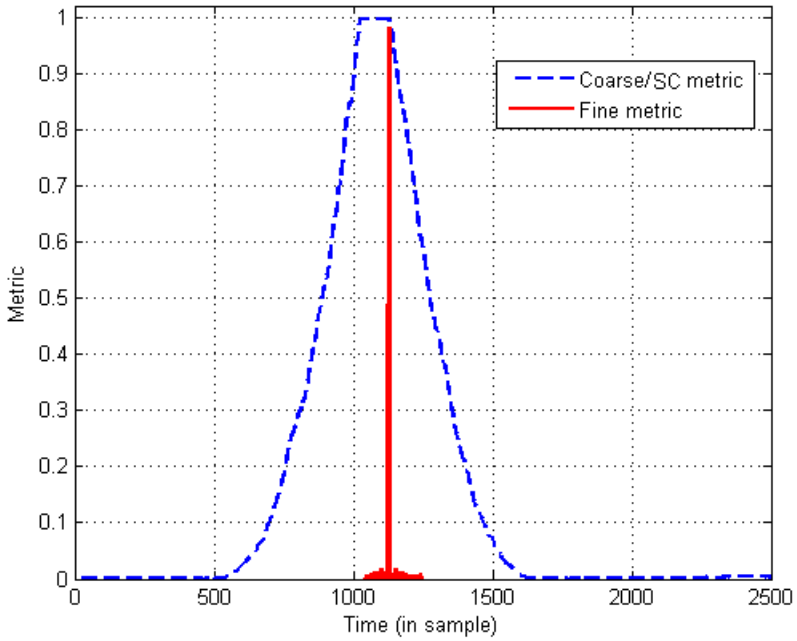

Figure 7.3: Coarse and fine timing metric in MISO-OFDM system under noiseless conditions.

It is shown in figure 7.3 that the fine metric provides extremely high sharp peak compared to the coarse metric, which exhibits a plateau. This peak coincides with the start of the preamble useful part, thus leading to accurate detection.

7.3.1.3 Fractional Frequency Offset Estimation

The FFO estimation is here based on the initial algorithm of Schmidl and Cox [15], which is deduced from the timing metric phase at the preamble start estimate. We recall that the FO causes a shift of the information signal leading to a phase rotation. It then follows that all the terms in the sum of equation (7.18), or in equation (7.19), have a constant phase if the two identical symbol parts are correlated. Hence, we can estimate the FFO by determining the actual phase of either the coarse timing metric M_c, at time instant $\hat{\tau}_c$, or the fine timing metric M_f, at time instant $\hat{\tau}_f$, as

$$\hat{\nu} = \frac{1}{\pi} \angle M(\hat{\tau}). \tag{7.20}$$

As the estimation range of the phase is limited to $[-\pi, \pi]$, the FO estimation range is limited as well to its fractional part only.

7.3.2 Performance Evaluation of the Proposed Synchronization Technique

We use Matlab simulations to evaluate the proposed estimator's performance, showing the Correct Detection Rate (CDR) of the preamble start, the time estimation variance and the MSE of the fractional FO estimate. Simulations are carried out for different SNR values and based on the Rayleigh-fading 2×1 MISO channel model. The system uses $N_u = 1024$ sub-carriers and a CP of length $N_g = 102$ samples. The normalized FFO is set to 0.7 sub-carrier spacing. We use QPSK modulation and 10^4 Monte Carlo trials are run for each SNR value for which 10^4 independent Rayleigh channel realizations are performed.

To assess the impact of the spacial diversity provided by the D-STBC, the proposed synchronization technique is evaluated under three configurations: the SISO-OFDM configuration, the MISO Alamouti STB coded [131] configuration, assuming perfect channel knowledge, and the main proposed differential Alamouti STB coded configuration. It is important to mention that the second configuration (coherent Alamouti), in which we assume perfect channel knowledge, is assessed to evaluate the degradation occasioned by the differential coding on the synchronization performance. This framework has the best synchronization performance that can be provided through STBC. However, it can not be applied in practical system as the channel estimation is required at the receiver end, which results in a degradation due to channel estimation errors. We also consider the synchronization algorithm proposed by Schellmann

et al. in [150] as a benchmark for a MISO configuration.

Figure 7.4 shows the preamble start CDR of the proposed synchronization technique under the considered configurations. As expected, it is obvious that the synchronization becomes significantly more robust if spatial diversity is exploited. The CDR provided in MISO configurations exhibits a minimum gain of about 3 dB compared to the SISO configuration, for SNR values lower than 10 dB. In particular, for a target CDR equal to 90%, we record gains of about 8 dB and 6 dB achieved through MISO configurations with coherent and differential detections respectively. We also note that, for SNR values lower than 5 dB, using the D-STBC scheme the proposed synchronization technique works 2 dB lower than the use of coherent STBC scheme. Yet, in a practical case, the latter scheme requires the channel estimation which is expected to induce errors degrading the synchronization performance. The proposed synchronization framework, that uses D-STBC, provides satisfactory detection accuracy which becomes perfect (CDR=100%) from SNR value equal to 5 dB. We also note that Schellmann's method provides close performance to the proposed one for SNR values lower than -2 dB with a 1 dB loss that rises for higher SNR values. The stagnation of the CDR exhibited in this method is expected as it is based on the SC algorithm whose metric presents a plateau.

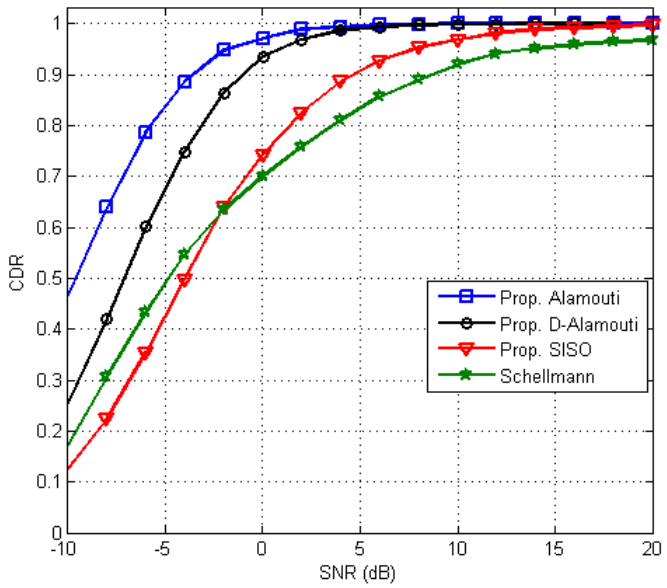

Figure 7.4: Preamble start CDR in the Rayleigh fading channel for MISO-OFDM system.

The preamble start estimation variance is depicted in figure 7.5, where similar observations to the case of CDR evaluation can be concluded. Obviously, the coherent Alamouti coded

estimator (under the assumption of perfect channel knowledge) offers the best synchronization performance in terms of low estimation variance that vanishes at SNR value equal to 14 dB. Throughout the considered SNR range, the differential coded proposed estimator achieves a minimum gain of 5 dB, compared to the single antenna case, and its estimation variance vanishes at SNR value equal to 16 dB. It is worth to note that Schellmann's estimator guaranteed that the preamble start estimate falls within the metric plateau, yet the detection accuracy in terms of CDR remains more or less poor.

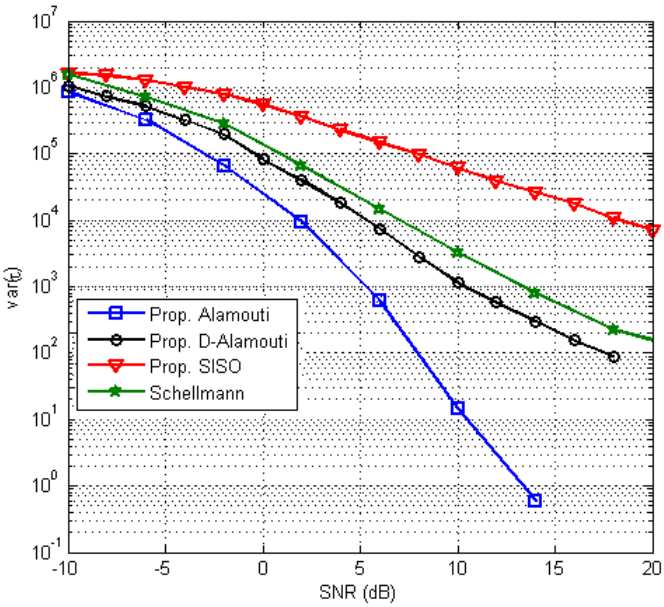

Figure 7.5: Preamble start estimation variance in the Rayleigh fading channel for MISO-OFDM system.

Figure 7.6 presents the mean squared error of the FFO estimate. We note that, unlike the time estimation performance, both coherent and differential estimators provide almost equal performance for the FFO estimation, here deduced from the coarse timing metric. This is unexceptional as the estimation is carried directly on the received signal before the decoding. Schellmann's estimator provides the same accuracy with a slight gain of about 1 dB recorded for SNR values around -10 dB and 10 dB. Evidently, the MISO considered scenarios outperform the single antenna case. Indeed, for the whole considered SNR range, both coherent and differential coding schemes provide a minimum gain of about 5 dB, which becomes higher as the SNR rises. For example, at an error equal to 10^{-4} squared sub-carrier spacing, the use of two transmit antennas provides a gain higher than 10 dB with respect to the case of single transmit antenna.

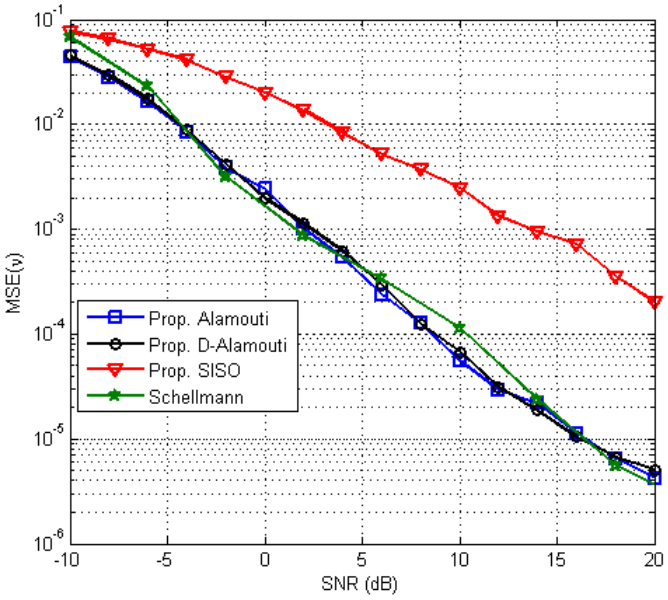

Figure 7.6: MSE of the FFO estimate in the Rayleigh fading channel for MISO-OFDM system.

It shall be noted that, overall, the proposed synchronization technique for D-STBC MISO configuration provides satisfactory detection accuracy. Furthermore, the main advantage is that no channel estimation is required to decode the received signal. Moreover, the provided detection performance are more or less close to those provided by the coherent STBC, in which the channel is assumed to be perfectly known that is not the case in practical implementation.

Conclusions

In this chapter, a new technique for non-coherent time and frequency synchronization for MISO-OFDM systems exploiting differential STBC was presented. The proposed scheme is based on detecting the preamble composed of two identical parts as in the chapter 4, for the case of SISO-OFDM systems. Two different replicas of the same preamble as well as the data symbols are sent through each transmit antenna. To benefit from a full spatial diversity transmission and as neither the transmitter nor the receiver has knowledge of the channel state, D-STBC scheme [142] was applied to generate the dual transmitted signal. The synchronization processing proceeds in two stages. First, exploiting the preamble repetitive structure, a coarse preamble start estimate is achieved respecting Schmidl and Cox algorithm [15]. Secondly, a non-coherent recovery of the transmitted signal, respecting the same D-STBC decoding,

should be achieved before proceeding the second stage. Then, a cross-correlation of the received differentially decoded signal is carried with the known preamble to fine tune the coarse preamble start estimate. The fractional frequency offset was also estimated through the coarse timing metric.

Using Monte Carlo simulations, it was confirmed that the proposed synchronization technique is efficient and robust in Rayleigh fading channels even at low SNR values. The same timing metric was evaluated in the case of SISO and MISO configurations to assess the effect of spatial diversity on synchronization performance. The comparison shed light on the performance improvement provided by the full available spatial diversity, in the considered 2×1 MISO configuration, under unknown channel. For the case of MISO-OFDM systems, the coherent STBC scheme was also considered, under the assumption of perfect channel knowledge, to assess the degradation occasioned in the proposed differential coded synchronization framework.

Chapter 8

Conclusions and Future Work

8.1 Conclusions

Sensitivity to time and frequency synchronization errors is a major drawback in OFDM systems. In this thesis, we proposed reduced-complexity synchronization techniques that provide accurate estimation of the synchronization offsets with reasonable computational load. We started by describing the wireless channel model shedding light on the suitableness of the OFDM technique for such propagation environment, discussing the effects of synchronization errors on OFDM signal, classification of synchronization techniques into data-aided and non-data-aided categories, and reviewing some conventional synchronization algorithms for OFDM systems. Most of the non-data-aided techniques in the literature are not totally blind in the sense that some information might be required to assist the synchronization, such as channel statistical information or SNR. In addition, the performance of most blind techniques is severely deteriorated in frequency-selective fading channels resulting in poor synchronization performance. On the contrary, data-aided techniques are well known by their robustness in such propagation environments. The focus was then on investigating data-aided time synchronization techniques with low overhead and high detection accuracy, which can be used in practical OFDM systems. The recovery of the fractional part of the frequency offset was also considered.

To achieve accurate synchronization with low computational load, we developed a reduced-complexity technique for time and frequency synchronization, using a single-symbol preamble

made of two identical parts. The estimation was performed in two stages. The first stage uses a sliding correlation with a delay equal to half the preamble length, respecting the famous algorithm of Schmidl and Cox, to provide a rough coarse time estimation. The second stage is based on a differential correlation with a delay different from half the preamble length, yielding a metric with high sharp peak. The second stage is carried over a limited range around the coarse time estimate. The combined use of sliding correlation characterized by its low computational load and differential correlation characterized by its high computational load, yet carried over a short interval around the coarse estimate, results in an overall reduced-complexity approach. Furthermore, the training symbol structure was exploited in a single-stage brute-force method where differential correlation is exclusively used, which offered a slightly more accurate detection than the two-stage approach at the expense of an important additional computational burden. Simulation results carried over both AWGN and multipath channels showed the robustness of the proposed techniques which outperform the considered benchmarks for time and frequency synchronization. To ensure the efficiency of the proposed techniques, we provided a theoretical performance analysis of the brute-force approach, which is also valid for the fine stage of the reduced-complexity approach assuming perfect coarse synchronization. Exploiting the central limit theorem, the metric was approximated by a Gaussian distribution and the preamble start probability of correct detection was derived in its closed form expression. Numerical results showed an almost perfect match between the analytical probability and the experimental rate of correct detection, thus validating the analytical performance study for both AWGN and multipath channels. This study was also performed for the discrete multitone modulation, wherein the Gaussian distribution approximation is rougher, yet the provided theoretical probability was very close to the experimental rate.

The proposed synchronization techniques are well suited for practical communication systems. Among them, the standard IEEE 802.11 which provides multiple repetitive training symbols dedicated for synchronization purpose. Indeed, the repetitive preamble structure of the IEEE 802.11 systems allowed a flexible synchronization processing respecting the reduced-complexity and the brute-force proposed approaches, which require a two identical part preamble. Simulation results proved the robustness of the proposed techniques in both AWGN and multipath channels and showed an enhancement in the time synchronization performance compared to some of the existing approaches.

For performance optimization, we studied two issues related to the preamble training subsequence choice. The first issue concerned the choice of the preamble training sub-sequence,

defined in the time domain, and the length of the uncertainty interval. In particular, different sequence types and lengths were assessed in the training sub-sequences. The study showed that it is possible to enhance the detection accuracy using the same computational load and the same overhead by a judicious choice of the preamble training sub-sequence type. Consequently, a reduction in the computational complexity was possible keeping the same accuracy. The second issue concerned the choice of the correlation sequence, for the training sub-sequence defined in the frequency domain. To further reduce the computational load of the synchronization task, the idea was to replace the differential correlation operations, carried during the fine synchronization process, by simple sign changes. To this aim, we had to derive the best sub-optimal correlation sequence, in terms of providing near optimal correlation sequence performance, from a finite QPSK alphabet ($\pm 1 \pm j$). Three search schemes were proposed to find the sub-optimal sequence, namely the deterministic design algorithm, the iterative design algorithm and the genetic algorithm. The sequences generated from both deterministic and iterative search methods provided almost the same performance, which is globally of about 2 dB lower than the optimal performance obtained using the original (non QPSK) sequence. However, much lower performance degradation (0.2 dB) was recorded using the sub-optimal sequence generated through the genetic algorithm based method.

In addition to the wireless local area networks, we focused on synchronization in cellular networks and precisely on primary synchronization in the LTE downlink. Primary synchronization consists in detecting the primary synchronization signal, which is composed of a Zadoff-Chu sequence, and the sector identifier heavily related to that sequence. Two differential correlation based techniques were proposed. Namely, the simply-differential technique, which proceeds in a single stage and has the particularity of jointly achieving the time synchronization and the sector search, and the doubly-differential technique, having a synchronization policy slightly similar to the conventional ones by proceeding into two stages. During the first stage, a coarse time synchronization was achieved to localize the Zadoff-Chu sequence within the received signal. The second stage is dedicated to the fine time synchronization and sector search through cross-correlating of the received signal with the known local Zadoff-Chu sequence candidates. Simulation results, investigated in the Extended Pedestrian A and Extended Typical Urban channel models, showed the robustness of the proposed techniques. The doubly-differential approach realized a slight enhancement in the detection accuracy compared to the best considered benchmark with comparable computational load. The simply-differential approach provided the best trade-off between detection accuracy and computational load, when compared to the

benchmarks and to the doubly-differential approach.

Time and fractional frequency offset estimation was also investigated in the MISO-OFDM systems, employing space-time block coding (STBC) in the last part of the thesis. Like the previous synchronization approaches, we considered non-coherent detection and time domain based synchronization processing. The differential STBC was applied to avoid the recourse for any channel estimation, typically required in conventional coherent STBC. The synchronization processing is carried in two stages wherein the first one the received signal is continuously is autocorrelated to detect the preamble of two identical parts. The second stage starts by decoding the received signal respecting the differential STBC scheme. Then, cross-correlation with the known preamble is calculated over a short interval to fine tune the coarse time estimate. The same metric was also exploited to estimate the fractional part of the frequency offset. The evaluation of the proposed synchronization technique relevance was carried in three different configurations: coherent Alamouti, differential Alamouti and SISO-OFDM cases. The comparison of these configurations showed the improvement realized through spatial diversity, especially at low SNR value when compared to SISO configuration. Furthermore, we showed that the use of differential STBC leads to a loss of 2 dB when compared to the Alamouti coherent scheme. It is worth to note that this latter was considered to compare the proposed differential STBC based synchronization framework to the best performance reached by the coherent STBC scheme, under the assumption of perfect channel knowledge.

8.2 Future Work

This thesis covered several aspects in synchronization for OFDM systems. Yet there are still many remaining and emerging synchronization problems in practical OFDM systems that have not been addressed.

In the first hand, we can envisage the extension to MIMO-OFDM systems by applying the differential STBC based synchronization scheme studied for a 2×1 MISO-OFDM configuration to an $n\times1$ MISO configuration exploiting other coding schemes. The more generalized MIMO configuration can also be treated [45], [46]. Furthermore, an optimal training sequence design, in which a pair of Golay sequences of specific properties is sent through each antenna, can be envisaged to enhance the synchronization performance for both configurations. Moreover, the simply-differential reduced-complexity approach that was developed for a repetitive preamble

structure should be evaluated in the MIMO WLAN systems. In particular, the IEEE 802.11n standard is challenging in synchronization, since it exploits cyclic delay diversity that causes pseudo multipath. By choosing a correlation shift equal to the cyclic delay shift, we expect to avoid the pseudo multipath problem.

In the other hand, to provide a complete insight in synchronization for OFDM systems, we can append the recovery of the integer part of the frequency offset, exploiting the same preamble or a modified version of it.

The synchronization problem considered here is for point-to-point systems. A trivial extension is to study similar problems in OFDMA multiple access communication schemes with more than one user.

Finally, it is worth to study how to adapt the synchronization scheme to deal with the case of uplink LTE where single carrier OFDM is adopted [47].

Bibliography

[1] M. Sauter, *From GSM to LTE an Introduction to Mobile Networks and Mobile Broadband,* John Wiley & Sons, United Kingdom, 2011.

[2] 3GPP (TS 25.401), "UTRAN Overall Description," Technical Specification, Sophia Antipolis, France, 2002.

[3] 3GPP (TS 25.308), "High Speed Downlink Packet Access (HSDPA): Overall Description; Stage 2," Technical Specification, Sophia Antipolis, France, 2004.

[4] 3GPP (TS 25.309), "FDD Enhanced Uplink: Overall Description; Stage 2," Technical Specification, Sophia Antipolis, France, 2006.

[5] TIA/EIA/IS-CDMA-2000, "Physical Layer Standard for CDMA-2000 Spread Spectrum Systems," Aug. 1999.

[6] 3GPP (TS 36.300) "Evolved Universal Terrestrial Radio Access (UTRA) and Evolved Universal Terrestrial Radio Access Network (UTRAN); Overall Description; Stage 2 (Release 8)," Technical Specification, Sophia Antipolis, France, 2007.

[7] 3GPP (TS 36.300) "Evolved Universal Terrestrial Radio Access (E-UTRA) and Evolved Universal Terrestrial Radio Access Network (E-UTRAN); Overall Description; Stage 2 (Release 10)," Technical Specification, Sophia Antipolis, France, 2011.

[8] ITU-R (M.1645), "Framework and Overall Objectives of the Future Development of IMT-2000 Systems Beyond IMT-2000," 2003.

[9] ANSI/IEEE Std 802.11, "Part 11: Wireless LAN Medium Access Control (MAC) and Physical Layer (PHY) Specifications," 1999 Edition (R2003).

[10] IEEE standard 802.16, "IEEE Standard for Local and Metropolitan Area Networks-Part 16: Air Interface for Fixed Broadband Wireless Access Systems," Oct. 2004.

[11] ETSI (ETS 300 401), *Radio Broadcasting Systems; Digital Audio Broadcasting (DAB) to Mobile, Portable and Fixed Receivers,* 2nd ed., 1997.

[12] ETSI (ETS EN 300 744), *Digital Video Broadcasting (DVB); Framing Structure, Channel Coding and Modulation for Digital Terrestrial Television,* V1.1.2, 1997-08.

[13] J. A. C. Bingham, "Multicarrier Modulation for Data Transmission: an Idea Whose Time Has Come," *IEEE Commun. Mag.,* vol. 28, pp. 5-14, May 1990.

[14] Y. Lu and G. Stuber, *Orthogonal Frequency Division Multiplexing for Wireless Communications,* Springer, Atlanta, USA, 2006.

[15] T. M. Schmidl and D. Cox, "Robust Frequency and Timing Synchronization in OFDM," *IEEE Trans. Commun.,* vol. 45, pp. 1613-1621, Dec. 1997.

[16] H. Minn, P. Tarasak, and V. K. Bhargava, "On Timing Offset Estimation for OFDM Systems," *IEEE Commun. Letters*, vol. 4, no. 7, pp. 242-244, July 2000.

[17] H. Minn, V. K. Bhargava, and K. B. Letaief, "A Novel Timing Estimation Method for OFDM Systems," *IEEE Trans. Commun.*, vol. 2, no. 4, pp. 822-839, July 2003.

[18] A. A. Nasir, S. Durrani, and R. A. Kennedy, "Performance of Coarse and Fine Timing Synchronization in OFDM Receivers," in *Proc. ICFCC*, vol. 2, pp. 412-416, May 2010.

[19] C-P. Chou, W-J. Lin, and J-S. Lin, "Timing Synchronization with Insertion of Zero-Padding Preambles for OFDM Systems," in *Proc. ICICS*, pp. 1-5, Dec. 2009.

[20] L. Najjar Atallah and M. Siala, "A New Scheme for Preamble Detection and Frequency Acquisition in OFDM Systems," in *Proc IEEE ICECS,* pp. 1008-1011, Dec. 2009.

[21] L. Nasraoui, L. Najjar Atallah, and M. Siala, "A Very Efficient Time and Frequency Synchronization Method for OFDM Systems Operating in AWGN Channels," in *Proc. ComNet,* pp. 1-5, Nov. 2010.

[22] L. Nasraoui, L. Najjar Atallah, and M. Siala, "An Efficient Synchronization Method for OFDM Systems in Multipath Channels," in *Proc. ICECS,* pp. 1152-1155, Dec. 2010.

[23] J. Gustavsson and P. Börjesson, "A Simultaneous Maximum Likelihood Estimator Based on a Generalized Matched Filter," in *Proc IEEE ICASSP*, vol. 4, pp. 481-484, April 1994.

[24] J. V. Beek, M. Sandell, and P. Börjesson, "ML Estimation of Timing and Frequency Offset in OFDM Systems," *IEEE Trans. Signal Processing,* vol. 45, pp. 1800-1805, July 1997.

[25] J. V. Beek, M. Sandell, M. Isaksson, and P. Börjesson, "Low Complex Frame Synchronization in OFDM Systems," in *Proc. ICUCP,* pp. 982-986, Nov. 1995.

[26] M. Sandell, J. V. Beek, and P. Börjesson, "Timing and Frequency Synchronization in OFDM Systems Using the Cyclic Prefix," in *Proc. International Symposium on Synchronization,* pp. 16-19, Dec. 1995.

[27] R. Mo, Y. Chew, and T. Tjhung, "A New Blind Joint Timing and Frequency Offset Estimator for OFDM Systems Over Multipath Fading Channels," *IEEE Trans. Veh. Technol.,* vol. 57, pp. 2947-2957, Sept. 2008.

[28] W. L. Chin and S. G. Chen, "A Blind Synchronizer for OFDM Systems Based on SINR Maximization in Multipath Fading Channels," *IEEE Trans. Veh. Technol.,* vol. 58, pp. 625-635, Feb. 2009.

[29] A. J. Al-Dweik, "A Novel Non-Data-Aided Symbol Timing Recovery Technique for OFDM Systems," *IEEE Trans. Wireless Commun.,* vol. 1, pp. 37-40, Jan. 2006.

[30] H. Bölcskei, "Blind Estimation of Symbol Timing and Carrier Frequency Offset in Wireless OFDM Systems," in *IEEE Trans. on Commun.,* vol. 49, no. 6, pp. 988-999, June 2001.

[31] B. Park, H. Cheon, E. Ko, C. Kang, D. Hong, "A Blind OFDM Synchronization Algorithm Based on Cyclic Correlation," in *IEEE Signal Processing Letters,* vol. 11, no. 2, pp. 83-85, Feb. 2005.

[32] L. Najjar Atallah, B. Geller, and P. Larzabal, "Blind Estimation of Timing and Carrier Frequency Offsets in OFDM Systems," in *Proc. EUSIPCO,* pp. 358-362, Aug. 2009.

[33] L. Nasraoui, L. Najjar Atallah, and M. Siala, "An Efficient Reduced-Complexity Two-Stage Differential Sliding Correlation Approach for OFDM Synchronization in the AWGN Channel," in *Proc. IEEE VTC-Fall*, pp. 1-5, Sept. 2011.

[34] L. Nasraoui, L. Najjar Atallah, and M. Siala, "An Efficient Reduced-Complexity Two-Stage Differential Sliding Correlation Approach for OFDM Synchronization in the Multipath Channel," in *Proc. IEEE WCNC*, pp. 2059-2063, April 2012.

[35] L. Nasraoui, L. Najjar Atallah, and M. Siala, "Performance Study of a Reduced Complexity Time Synchronization Approach for OFDM Systems," in *Proc. ComNet,* pp. 1-5, March 2012.

[36] L. Nasraoui, L. Najjar Atallah, and M. Siala, "Analytical Performance Evaluation of an Efficient Reduced-Complexity Time Synchronization Approach for OFDM Systems," in *Proc. IEEE VTC-Fall*, pp. 1-5, Sept. 2012.

[37] L. Nasraoui, L. Najjar Atallah, and M. Siala, "Encoding Sequence Design for a Reduced Complexity Time Synchronization Technique for OFDM Systems," in *Proc. IEEE ICECS,* pp. 913-916, Dec. 2012.

[38] L. Nasraoui, L. Najjar Atallah, and M. Siala, "Performance Evaluation of an Efficient Reduced Complexity Time Synchronization Approach for OFDM Systems," Annals of Telecommunications, vol. 69, pp 321-330, May 2013.

[39] L. Nasraoui, L. Najjar Atallah, and M. Siala, "Robust Brute Force and Reduced Complexity Approaches for Timing Synchronization in IEEE 802.11a/g WLANs," in *Proc IWCMC,* pp. 1365-1369, July 2013.

[40] L. Nasraoui, L. N. Atallah, and M. Siala, "Genetic Algorithm Based Optimization of Encoding Sequence for a Reduced Complexity OFDM Time Synchronization Technique," in *Proc IEEE VTC-Fall,* pp. 1-5, Sept. 2013.

[41] L. Nasraoui, L. Najjar Atallah, and M. Siala, "Performance Study of an Efficient Reduced-Complexity Time Synchronization Approach for DMT Systems", in *Proc. ComNet,* pp. 1-5, March 2014.

[42] L. Nasraoui, L. Najjar Atallah, and M. Siala, "Robust Doubly-Differential Primary Synchronization Approach for 3GPP LTE Systems," in *Proc. IWCMC*, pp. 1069-1074, Aug. 2014.

[43] L. Nasraoui, L. Najjar Atallah, and M. Siala, "A Simply Differential Low-Complexity Primary Synchronization Scheme for 3GPP LTE Systems," in *Proc. EUSIPCO,* pp. 411-415, Sept. 2014.

[44] L. Nasraoui, L. Najjar Atallah, and M. Siala, "Robust Synchronization Approach for MIMO-OFDM Systems with Space-Time Diversity,", *IEEE Vehicular Technology Conference (VTC-Spring),* pp. 1-5, May 2015.

[45] L. Nasraoui, L. Najjar, and M. Siala, "Synchronization technique for MIMO-OFDM WLAN systems with space time diversity", in *Proc. International Wireless Communications and Mobile Computing Conference*, pp. 250-255, Aug. 2015.

[46] L. Nasraoui, L. Najjar, and M. Siala, "Reduced-Complexity synchronization technique for MIMO-OFDM WLAN systems", in *Proc. International Conference on Communications and Networking (COMNET)*, pp. 1-5, Nov. 2015.

[47] L. Nasraoui, L. Najjar Atallah, and M. Siala, "Reduced-Complexity Simply/Doubly Differential Approaches for Primary Synchronization in LTE Systems," *Transactions on Emerging Telecommunications Technologies*, vol. 28, pp.1-10, Feb. 2017.

[48] R. Prasad, *OFDM for Wireless Communications Systems,* Artech House, London, 2004.

[49] R. Nee and R. Prasad, *OFDM for Wireless Multimedia Communications,* Artech House, Boston, 2000.

[50] T. M. Schmidl, *Synchronization Algorithm for Wireless Data Transmission Using Orthogonal Frequency Division Multiplexing (OFDM),* Ph.D. dissertation, Stanford University, June 1997.

[51] P. Moose, "A Technique for Orthogonal Frequency Division Multiplexing Frequency Offset Correction," *IEEE Trans. Commun.*, vol. 42, pp. 2908-2914, Oct. 1994.

[52] M. Morelli and U. Mengali, "An Improved Frequency Offset Estimator for OFDM Applications," in *IEEE Commun. Letters,* vol. 3, pp. 75-77, March 1999.

[53] H. Minn, P. Tarasak, and V. K. Bhargava, "OFDM Frequency Offset Estimation Based on BLUE Principle," in *Proc. IEEE VTC-Fall,* vol. 2, pp. 1230-1234, Sept. 2002.

[54] H. Minn, P. Tarasak, and V.K. Bhargava, "Some Issues of Complexity and Training Symbol Design for OFDM Frequency Offset Estimation Methods Based on BLUE Principle," in *Proc. IEEE VTC-Spring,* vol. 2, pp. 1288-1292, April 2003.

[55] Y. Zeng, W. Leon, Y. Liang, and A. Leyman, "A New Method for Frequency Offset and Channel Estimation in OFDM," in *Proc. IEEE ICC,* pp. 4606-4611, June 2006.

[56] J. Chen, Y. Wu, S. Ma, and T-Sang Ng, "ML Joint CFO and Channel Estimation in OFDM Systems with Timing Ambiguity," *IEEE Trans. Wireless Commun.,* vol 7, pp. 2436-2440, July 2008.

[57] K. Fazel and S. Kaiser, *Multi-Carrier and Spread Spectrum Systems,* 2nd ed., John Wiley & Sons, United Kingdom, 2008.

[58] D. Tse and P. Viswanath, *Fundamentals of Wireless Communication,* August, 2004.

[59] H. Schülze and C. Luders, *Theory and Applications of OFDM and CDMA,* John Wiley & Sons, England, 2005.

[60] H. Liu and G. Li, *OFDM-Based Broadband Wireless Networks,* John Wiley & Sons, Canada, 2005.

[61] T. S. Rappaport, *Wireless communications: Principle and Practice,* Prentisse Hall, 1996.

[62] W. C. Y. Lee, *Mobile Cellular Communications Systems,* McGraw-Hill, 1995.

[63] P. A. Bello, "Characterization of Randomly Time-Variant Linear Channels," *IEEE Trans. Commun. Systems*, vol. 11, pp. 360-393, Dec. 1963.

[64] M. Schwartz, W. R. Bennett, and S. Stein, *Communication Systems and Techniques,* McGraw-Hill, New York, 1995.

[65] M. L. Doelz, E. T. Heald, and D. L. Martin, "Binary Data Transmission Techniques for Linear Systems," in *Proc. IRE,* vol. 45, pp. 656-661, May 1957.

[66] R. W. Chang, "Synthesis of Band Limited Orthogonal Signals for Multichannel Data Transmission," *Bell Syst. Tech. J.,* vol. 45, pp. 1775-1796, Dec. 1966.

[67] B. R. Salzberg, "Performance of an Efficient Parallel Data Transmission System," *IEEE Trans. Commun. Technol.,* vol. 15, pp. 805-813, Dec. 1967.

[68] J. Saltz and S. B. Weinstein, "Fourier Transform Communication Systems," in *Proc. ACM Symposium on Problems in the Optimization of Data Commun. Systems,* pp. 99-128, 1969.

[69] S. B. Weinstein and P. M. Ebert, "Data Transmission by Frequency Division Multiplexing Using the Discrete Fourier Transform," *IEEE Trans. Commun. Technol.,* vol. 19, pp. 628-634, Oct. 1971.

[70] A. Peled and A. Ruiz, "Frequency Domain Data Transmission Using Reduced Computational Complexity Algorithms," in *Proc. IEEE ICASSP,* pp. 964-967, April 1980.

[71] L. J. Cimini, "Analysis and Simulation of a Digital Mobile Channel Using Orthogonal Frequency Division Multiplexing," *IEEE Trans. Commun.,* vol. 33, pp. 665-675, July 1985.

[72] M. Alard and R. Lasalle, "Principles of Modulation and Channel Coding for Digital Broadcasting for Mobile Receivers," *EBU,* No. 224, pp. 168-190, Aug. 1987.

[73] J. Cooley and J. Tukey, "An Algorithm for the Machine Calculation of Complex Fourier Series," *Mathematics of Computation,* vol. 19, no. 90, pp. 297-301, April 1965.

[74] M. Speth, S. A. Fechtel, G. Fock, and H. Meyr, "Optimum Receiver Design for Wireless Broad-Band Systems Using OFDM–Part I," *IEEE Trans. Commun.* vol 47, no. 11, pp. 1668-1677, Nov. 1999.

[75] H. Nikookar and M. K. Lakshmanan, "Comparison of Sensitivity of OFDM And Wavelet Packet Modulation to Time Synchronization Error," in *Proc. IEEE PIMRC,* pp. 1-6, Sept. 2008.

[76] J. Lee, H. L. Lou, D. Toumpakaris, and J. M. Cioffi, "Effect of Carrier Frequency Offset on OFDM Systems for Multipath Fading Channels," in *Proc. IEEE GLOBECOM,* vol. 6, pp. 3721-3725, 29 Nov.-3 Dec. 2004.

[77] R. Rodrigues, R. Dinis, and F. Cercas, "Training Sequence Design for Channel Estimation with Nonlinear OQPSK-Type Modulations," in *Proc. IEEE VTC-Fall,* pp. 1-5, Sept. 2012.

[78] B. M. Popović, "Spreading Sequences for Multicarrier CDMA Systems," *IEEE Trans. Commun.,* vol. 47, no. 6, pp. 918-926, June 1999.

[79] R. N. Mutagi, "Pseudo Noise Sequences for Engineers," *Electronic and Commun. Engineering J.,* vol. 8, no. 2, pp. 79-87, April 1996.

[80] S. W. Golomb, *Shift Register Sequences, Holden-Day,* San Francisco, CA, 1967.

[81] A. Mitra, "On the Construction of M-Sequence Via Primitive Polynomials with A Fast Identification Method," *International J. of Computer and Electrical Engineering,* vol. 2, pp. 663-668, Sept. 2008.

[82] M. Rice, S. Tretter, and P. Mathys, "On Differentially Encoded M-Sequences," *IEEE Trans. Commun. Letters*, vol. 49, no. 3, pp. 421-424, March 2001.

[83] R. Gold, "Maximal Recursive Sequences with 3-Valued Recursive Crosscorrelation Functions," *IEEE Trans. Inform. Theory,* vol. 14, no. 1, pp.154-156, Jan. 1968.

[84] T. Kasami, "Weight Distribution Formula for Some Class of Cyclic Codes," *Coordinated Sci. Lab.,* Univ. Illinois, Urbana, April 1966.

[85] D. C. Chu, "Polyphase Codes with Good Periodic Correlation Properties," *IEEE Trans. Inform. Theory*, vol. 18, pp. 531-532, July 1972.

[86] Y. Wen, W. Huang and Z. Zhang, "CAZAC Sequence and Its Application in LTE Random Access," in *Proc. IEEE Inform. Theory Workshop,* pp. 544-547, Oct. 2006.

[87] R. Frank, S. Zadoff, and R. Heimiller, "Phase Shift Pulse Codes with Good Periodic Correlation Properties," *IRE Trans. Inform. Theory,* vol. 8, no. 6, pp. 381-382, Oct. 1962.

[88] P. Kumar, R. Scholtz, and L. Welch, "Generalized Bent Functions and Their Properties," *J. Combinatorial Theory,* vol. 40, no. 1, pp. 90-107, Sept. 1985.

[89] A. Milewski, "Periodic Sequences with Optimal Properties for Channel Estimation and Fast Start-Up Equalization," *IBM J. Res. Develop.,* vol. 27, no. 5, pp. 426-431, Sept. 1983.

[90] D. V. Sarwate, "Bounds on Crosscorrelation and Autocorrelation of Sequences," *IEEE Trans. Inform. Theory,* vol. 25, pp. 720-724, Nov. 1979.

[91] M. J. E. Golay, "Complementary Series," *IRE Trans. Inform. Theory*, vol. 7, no. 2, pp. 82-87, April 1961.

[92] M. J. E. Golay, "Sieves for Low Autocorrelation Binary Sequences," *IEEE Trans. Inform. Theory*, vol. 23, no. 1, pp. 43-51, Jan. 1977.

[93] J. A. Davis and J. Jedwab, "Peak-to-Mean Power Control in OFDM, Golay Complementary Sequences and Reed-Muller Codes," *IEEE Trans. Inform. Theory*, vol 45, no. 7, pp. 2397-2417, Nov. 1999.

[94] R. D. J. van Nee, "OFDM Codes for Peak-to-Average Power Reduction and Error Correction," in *Proc. IEEE GLOBECOM,* vol. 1, pp. 740-744, Nov. 1996.

[95] R. E. Walpole, R. H. Myers, S. L. Myers and K. Ye, *Probability and Statistics for Engineers and Scientists,* 8^{th} ed., Pearson Prentice Hall, 2007.

[96] C. Cole, I. Lyubomirsky, A. Ghiasi, and V. Telang, "Higher-Order Modulation for Client Optics," *IEEE Commun. Magazine,* vol. 51, no. 3, pp. 50-57, March 2013.

[97] T. Pollet and M. Peeters, "Synchronization with DMT Modulation," *IEEE Commun. Magazine*, vol. 37, no. 4, pp. 80-86, April 1999.

[98] T. Pollet and M. Peeters, "A New Digital Timing Correction Scheme for DMT Systems Combining Temporal and Frequential Signal Properties," in *Proc. IEEE ICC,* vol. 3, pp. 1805-1808, 2000.

[99] G. Ke, "A Synchronization Method for DMT Signal Analysis System," in *Proc. ICIMCCC*, pp. 597- 600, Oct. 2011.

[100] A. Lakhzouri and M. Renfors, "Synchronization in DMT Based VDSL Modems," in *Proc. IEEE ICECS*, vol. 2, pp. 761-764, 2001.

[101] M.K. Simon, M.S. Alouini, "Some New Results for Integrals Involving the Generalized Marcum Q Function and Their Application to Performance Evaluation Over Fading Channels," *IEEE Trans. Wireless Commun.*, vol. 2, no. 4, pp. 611-615, July 2003.

[102] A. Nuttall, *Some Integrals Involving the Q-Function,* Naval Underwater Systems Center Technical Report 4297, New London Lab., April 1972.

[103] IEEE standard 802.11a: *Wireless LAN Medium Access Control (MAC) and Physical Layer (PHY) Specifications: High-Speed Physical Layer in the 5 Ghz Band,* Dec. 1999.

[104] IEEE standard 802.11g: *Wireless LAN Medium Access Control (MAC) and Physical Layer (PHY) Specifications: Further Higher Data Rate Extension in The 2.4 Ghz Band,* June 2003.

[105] J. J. Kim, Y. J. Ryu, H. S. Oh, and D. S. Han, "Frame Selection Algorithm with Adaptive FFT Input for OFDM Systems," in *Proc. IEEE ICC,* vol. 1, pp. 187-191, 28 April- 2 May 2002.

[106] E. G. Larsson, G. Liu, J. Liy, and G. B. Giannakis, "Joint Symbol Timing and Channel Estimation for OFDM Based WLANs," *IEEE Commun. Letter* vol. 5, no. 8, pp. 325-327, Aug. 2001.

[107] H. Yuan, X. Hu, and Y. Ling "New Symbol Synchronization Algorithms for OFDM Systems Based on IEEE 802.11a," in *Proc. IEEE ICII*, pp. 186-191, July 2008.

[108] S. Wensheng and Z. Yuanyuan, "A Frame Synchronization and Symbol Timing Synchronization Algorithm in Burst OFDM Communication Based on IEEE 802.11a," in *International Forum in Information Technol. and Applications,* vol. 1, pp. 190-193, May 2009.

[109] C. L. Nguyen, A. Mokraoui, P. Duhamel, and N. Linh-Trung "Time Synchronization Algorithm in IEEE 802.11a Communication System," in *Proc. EUSIPCO,* pp. 1628-1632, Aug. 2012.

[110] D. Whitley, "A genetic algorithm tutorial," *Statistics and Computing,* vol. 4, no. 2, pp. 65-85, June 1994.

[111] K. S. Tang, K. F. Man, S. Kwong, and Q. He, "Genetic Algorithms and Their Applications," *IEEE Signal Processing Magazine,* vol. 13, no. 6, pp. 22-37, Nov 1996.

[112] H. H. Dam, H. J. Zepernick, and H. Luders, "Polyphase Sequence Design Using a Genetic Algorithm," in *Proc. IEEE VTC-Spring,* vol. 3, pp. 1471-474, May 2004.

[113] Z. Sihai, L. Yuan, Z. Ming, and Z. Wuyang, "Improved GA Solution on LNC Coefficient Matrix for Multi-User Cooperative Communication," in *Proc. IEEE PIMRC,* pp. 809-814, Sept. 2012.

[114] M. Lixia, M. Murroni, and V. Popescu, "PAPR Reduction in Multicarrier Modulations Using Genetic Algorithms," in *Proc. OPTIM,* pp. 938- 942, May 2010.

[115] E. Dahlman, S. Parkvall and. J. Skold, *4G LTE/LTE-Advanced for Mobile Broadband,* Academic Press, 2011.

[116] E. Dahlman, S. Parkvall, J. Skold, and P. Beming, *3G Evolution: HSPA and LTE for Mobile Broadband,* Academic Press, 2nd ed., 2008.

[117] D. Astély, E. Dahlman, A. Furuskär, Y. Jading, M. Lindstrom, and S. Parkvall, "LTE: The Evolution of Mobile Broadband," *IEEE Commun. Magazine*, vol. 47, no. 4, pp. 44-51, April 2009.

[118] K. Manolakis, D. M. Gutierrez Estevez, V. Jungnickel, W. Xu and C. Drewes, "A Closed Concept for Synchronization and Cell Search in 3GPP LTE Systems," in *Proc. IEEE WCNC*, pp. 1-6, April 2009.

[119] A. R. Elsherif and M. M. Khairy, "Adaptive Primary Synchronization Signal Detection for 3GPP Long Term Evolution," in *Proc. IWCMC,* pp. 1716-1721, July 2013.

[120] W. Xu and K. Manolakis, "Robust Synchronization for 3GPP LTE Systems," in *Proc. IEEE GLOBECOM*, pp. 1-5, Dec. 2010.

[121] N. Ding, C. Chen, W. Fan, Y. Chen, and Z. Xiaoyang, "An Improved Coarse Synchronization Scheme in 3GPP LTE Downlink OFDM Systems," in *Proc. IEEE ISCAS*, pp. 1516-1519, May 2012.

[122] Z. Zhang, J. Liu, and K. Long, "Low-Complexity Cell Search with Fast PSS Identification in LTE," *IEEE Trans. Veh. Technol.,* vol. 61, No. 4, pp. 1719-1729, May 2012.

[123] 3 GPP (TS 36.211 V8.7.0), *Physical Channels and Modulation,* May 2009.

[124] 3GPP (TS 36.101), *User Equipment (UE) Radio Transmission and Reception,* July 2010.

[125] 3GPP (TS 36.104), *Base Station (BS) Radio Transmission and Reception,* July 2010.

[126] R. D. Murch and K. B. Letaief, "Antenna Systems for Broadband Wireless Access," *IEEE Commun. Magazine,* vol. 40, no. 4, pp. 76-83, April 2002.

[127] S. N. Diggavi, N. Al-Dhahir, A. Stamoulis, and A. R. Calderbank, "Great Expectations: the Value of Spatial Diversity in Wireless Networks," in *Proc. IEEE,* vol. 92, no. 2, pp. 219-270, Feb. 2004.

[128] V. Tarokh, H. Jafarkhani, and A. R. Calderbank, "Space-Time Block Codes from Orthogonal Designs," *IEEE Trans. Inform. Theory,* vol. 45, no. 5, pp. 1456-1467, July 1999.

[129] G. J. Foschini, "Layered Space-Time Architecture for Wireless Communication in a Fading Environment When Using Multi-Element Antennas," *Bell Labs Tech. J.,* vol. 1, no. 2, pp. 41-59, 1996.

[130] G. D. Golden, G. J. Foschini, R. A. Valenzuela, and P. W. Wolniansky, "Detection Algorithm and Initial Laboratory Results Using V-BLAST Space-Time Communication Architecture," *Electronics Letter,* vol. 35, no.1, pp. 14-16, Jan. 1999.

[131] S. M. Alamouti, "A Simple Transmit Diversity Technique for Wireless Communications," *IEEE J. Select. Areas Commun.,* vol. 16, no. 8, pp. 1451-1458, Oct. 1998.

[132] V. Tarokh, N. Seshadri, and A. R. Calderbank, "Space-Time Codes for High Data Rate Wireless Communications: Performance Criterion and Code Construction," *IEEE Trans. Inform. Theory,* vol. 44, no. 2, pp. 744-765, March 1998.

[133] P. W. Wolniansky, G. J. Foschini, G. D. Gloden, and R. Valenzuela, "V-BLAST: An Architecture for Realizing Very High Data Rates Over the Rich-Scattering Wireless Channel,"

in *Proc. International Symposium on Advanced Radio Technol.,* pp. 295-300, 29 Sept.-2 Oct. 1998.

[134] S. N. Diggavi, N. Al-Dhahir, A. Stamoulis, and A. R. Calderbank, "Differential Space-Time Coding for Frequency-Selective Channels," *IEEE Commun. Letters,* vol. 6, no. 6, pp. 253-255, June 2002.

[135] L. Zheng and D. N. C. Tse, "Diversity and Multiplexing: a Fundamental Trade-Off in Multiple-Antenna Channels," *IEEE Trans. Inform. Theory,* vol. 49, no. 5, pp. 1073-1096, May 2003.

[136] V. Tarokh, "Combined Array Processing and Space-Time Coding," *IEEE Trans. Inform. Theory,* vol. 45, no. 4, pp. 1121-1128, May 1999.

[137] S. Sfar, L. Dai, and K. B. Letaief, "Optimal Diversity-Multiplexing Trade-Off with Group Detection for MIMO Systems," *IEEE Trans. Commun.,* vol. 53, no. 7, pp. 1178-1190, July 2005.

[138] H. E. Gamal, G. Caire, and M. O. Damen, "Lattice Coding and Decoding Achieve the Optimal Diversity-Multiplexing Trade-Off of MIMO Channels," *IEEE Trans. Info. Theory,* vol. 50, no. 7, pp. 968-985, June 2004.

[139] A. El Falou, W. Hamouda, C. Langlais, C. A. Nour, and C. Douillard, "Finite-SNR Diversity-Multiplexing Tradeoff for Rayleigh MIMO Channels," *IEEE Commun. Letter,* vol. 17, no. 4, pp. 753-756, April 2013.

[140] A. El Falou, C. Langlais, W. Hamouda, C. A. Nour, and C. Douillard, "Finite-SNR Diversity-Multiplexing Tradeoff for Spatially Correlated Rayleigh MIMO Channels," in *Proc. IEEE ICC,* June 2014.

[141] W. Zhang, X.-G. Xia, and K. B. Letaief, "Space-Time/Frequency Coding for MIMO-OFDM in Next Generation Broadband Wireless Systems," *IEEE Wireless Commun.,* vol. 14, no. 3, pp. 32-43, June 2007.

[142] V. Tarokh and H. Jafarkhani, "A Differential Detection Scheme for Transmit Diversity," *IEEE J. Select. Areas Commun.*, vol. 18, no. 7, pp. 1169-1174, July 2000.

[143] E. Ben Slimane, S. Jarboui, and A. Bouallegue, "An Improved Differential Space-Time Block Coding Scheme Based on Viterbi Algorithm," *IEEE Commun. Letters,* vol. 17, no. 9, pp. 1707-1709, Sept. 2013.

[144] E. Ben Slimane, S. Jarboui, and A. Bouallegue, "Differential Orthogonal Space-Time Block Codes for Four Transmit Antennas," *IEEE Electro. Letters*, vol. 50, no. 3, pp. 180-182, Jan. 2014.

[145] Jinan Leng, Lei Xie, Huifang Chen, and Kuang Wang, "Optimized Differential Space Time Block Code without Constellation Expansion," in *Proc. IEEE VTC-Fall*, pp. 1-5, Sept. 2013.

[146] G. Bauch and A. Mengi, "Non-Unitary Orthogonal Differential Space-Time Modulation with Non-Coherent Soft Output Detection," in *Proc. IEEE VTC-Fall*, pp. 977-981, Sept. 2005.

[147] P. S. Kumar, M. G. Sumithra, M. Sarumathi, and E. P. Kumar, " Performance Analysis for PAPR Reduction Using SLM Technique in 2×1 and 2×2 Differential STBC MIMO RS OFDM Systems in Rayleigh Fading Channel," in *Proc. ICGCE*, pp. 287-290, Dec. 2013.

[148] H. Minn, Dong In Kim, and V. K. Bhargava, "A Reduced Complexity Channel Estimation for OFDM Systems with Transmit Diversity in Mobile Wireless Channels," *IEEE Trans. Commun.*, vol. 50, no. 5, pp. 799-807, May. 2002.

[149] A. N. Mody and G. L. Stüber, "Synchronization for MIMO OFDM Systems," in *Proc. IEEE Globecom,* vol. 1, pp. 509-513, Nov. 2001.

[150] M. Schellmann, V. Jungnickel, and C. von Helmolt, "On the Value of Spatial Diversity for the Synchronisation in MIMO-OFDM Systems," in *Proc. IEEE PIMRC,* pp. 201-205, Sept. 2005.

[151] H. C. Wang and C. L. Wang "A Compact Preamble Design for Synchronization in Distributed MIMO OFDM Systems," in *Proc. IEEE VTC-Fall,* pp. 1-4, Sept. 2011.

[152] Y. Wen, and D. Lemoine, "A Postfix Synchronization Method for OFDM and MIMO-OFDM Systems," in *Proc. IEEE WCNC,* pp. 1-6, April, 2008.

[153] A. R. Elsherif and M. M. Khairy, "A Novel Timing Synchronization Method for Distributed MIMO-OFDM System," in *Proc. IEEE VTC-Spring,* vol. 4, pp. 1933-1936, May 2006.

[154] E. Zhou, X. Zhang, H. Zhaou, and W. Wang, "Synchronization Algorithms for MIMO OFDM Systems," in *Proc. IEEE WCNC,* vol. 1, pp. 18-22, March 2005.